NONLINEAR 3-D BEAM/CONNECTOR FINITE ELEMENT WITH WARPING FOR A GLULAM DOME

by

Sandeep A. Kavi

Thesis submitted to the Faculty of the

Virginia Polytechnic Institute and State University

in partial fulfillment of the requirements for the degree of

Master of Science

in

Civil Engineering

APPROVED

S. M. Holzer, Chairman

J. R. Loferski

J. D. Dolan

D. A. Garst

October 1993

Blacksburg, Virginia

C.2

LD
5655
V855
1993
K384
C.2

Nonlinear 3-D Beam/Connector Finite Element with Warping for a Glulam Dome

by

Sandeep A. Kavi

Committee Chairman: Dr. S. M. Holzer

Civil Engineering

(ABSTRACT)

The main objectives of the present study are to incorporate Saint-Venant's torsion solution in the analysis of a glulam dome with ABAQUS to include warping of rectangular beams, and to model the nonlinear beam/decking connectors (nails) of the dome in order to develop an effective finite element model of the glulam dome for investigating its ultimate load capacity. The shear modulus is modified to include warping of the beams. The nonlinear connector is defined through a user-coded FORTRAN subroutine UEL. Results from the thorough testing of these two capabilities are presented.

A convergence study of the solution in the nonlinear analysis of the dome cap with ABAQUS is performed. The effect of variation in parameters such as the nonlinear material law and the stiffness of hinge-connector elements on the dome cap model is examined. A dome cap model with 16 nailed joints for each beam is analysed. Dome models with nailed joints at truss bracing points (i.e., the end nodes of the truss bracing elements) and with 16 nailed joints for every beam are analyzed. The results of these models are compared with the models with and without truss bracing. Finally, conclusions based on this study and recommendations for future research are presented.

Acknowledgments

I take this opportunity to express my sincere appreciation and gratitude to my advisor Dr. S. M. Holzer for his patience, continued support, and encouragement throughout this study. It has been a pleasure working with Dr. J. R. Loferski and Dr. J. D. Dolan, whom I thank for their enthusiastic participation, help, and advice during the present study. I am very grateful to Professor D. A. Garst for his help and excellent teaching during the course of my study and also for serving on my committee.

I am very thankful to my fellow students Niket Telang, Samruam Tongtoe, Raul Andruet, Jacem Tissoui, and Moses Tsang for their suggestions and help. Special thanks to Scott Gutshall of Wood Science Department for guidance and help in performing experimental tests on the nailed connections.

I am extremely grateful to my family for their constant encouragement and moral support during my education. My heart goes to my parents and my grandfather S. B. Kavi to whom I dedicate this thesis and thank them for their patience, love, and everlasting support.

TABLE OF CONTENTS

1. INTRODUCTION 1

1.1 General 1

1.2 Research Background 3

2. CONVERGENCE AND MESH REFINEMENT STUDY FOR THE DOME ANALYSIS

2.1 Introduction 5

2.2 Constitutive Modeling in ABAQUS using the User Subroutine UMAT 6

2.2.1 Linear Material Law 6

2.2.2 Nonlinear Material Law 11

2.3 Cap Rib Model 18

2.3.1 Nonlinear Analysis Procedure 20

2.3.2 Results for the Nonlinear Analysis of the Cap Rib Model 20

2.3.3 Effect of Mesh Refinement 23

2.4 Convergence and Mesh Refinement Study of the Dome Cap 25

2.4.1 Load Discretization 25

2.4.2 Analysis of Dome Cap for Full and Half Snow Load Cases 29

2.5 Analysis of Full Dome for Full and Half Snow Load Cases 44

3. PARAMETRIC STUDIES OF THE DOME CAP MODEL

3.1 Introduction 49
3.2 Modified Dome Cap Model 49
3.3 Variation in the Area of Tension Ring 50
3.4 Variation in the Nonlinear Constitutive Law 53
3.6 Effect of Joint Flexibility 59

4. APPLICATION OF SAINT-VENANT'S TORSION SOLUTION IN DOME ANALYSIS

4.1 Introduction 68
4.2 Review of Torsion Theory 68
4.2.1 Navier's Solution for Elastic Circular Sections 69
4.2.2 Saint-Venant's Semi-Inverse Method 71
4.2.3 Torsion of Rectangular Bars 78
4.3 Application of Saint-Venant's Solution in Analysis with ABAQUS 82
4.4 Test Cases on Steel Cantilever Beams 83
4.5 Analysis of Dome Cap Model with Warping of Beam Cross sections 93
4.6 Analysis of Dome with Warping of Beam Cross sections 95

5. FORMULATION AND TESTING OF NONLINEAR BEAM/CONNECTOR ELEMENTS

5.1 Introduction 97
5.2 Load-Deflection Curve for Nails 99
5.3 Formulation of 2D and 3D Connector Stiffness Matrices 109
5.3.1 Connector Stiffness Matrices for the Beams in Dome 120
5.4 User Subroutine UEL to Define Nonlinear Connector Elements 120

5.4.1 Defining the User Elements in ABAQUS 122
5.4.2 User Subroutine UEL 122
5.4.3 Contribution of User Elements Defining b/c Model 123
5.5 Test Cases on the Nonlinear Connector Element 130
5.5.1 A Single Nonlinear Spring with Two Nodes 130
5.5.2 Testing of 2D Nonlinear b/c Elements 134
5.5.2.1 Linear Analysis 134
5.5.2.2 Nonlinear Analysis 140
5.5.3 Testing of 3D Nonlinear b/c Elements 145
5.5.3.1 Linear Analysis 145
5.5.3.2 Special Case 147
5.5.3.3 Nonlinear Analysis 147
5.5.4 Subroutine UEL for the Dome Cap and Dome Models 149

6. ANALYSIS OF DOME CAP AND DOME WITH 3D B/C ELEMENTS

6.1 Introduction 156
6.2 Modification in the Input File for the Model with b/c Elements 156
6.3 Analysis of Dome Cap Models 157
6.4 Analysis of Dome Models 162
6.5 Analysis of Dome Model with Nonlinear Material Law 168

7. CONCLUSIONS AND RECOMMENDATIONS

7.1 Conclusions 177
7.2 Recommendations 179

REFERENCES 181

APPENDIX A 184

APPENDIX B 197

APPENDIX C 201

APPENDIX D 205

APPENDIX E 207

APPENDIX F 216

APPENDIX G 224

APPENDIX H 227

VITA 229

LIST OF FIGURES

Figure 2.1 : Axially loaded beam 7
Figure 2.2 : Dome cap rib: 2 element mesh 7
Figure 2.3 : Cap rib: load-deflection path for 2-element mesh model 22
Figure 2.4 : Cap rib: load-deflection paths for refined mesh models 24
Figure 2.5 : Options for shell loading in ABAQUS 26
Figure 2.6 : Shell arrangements for the 4-element mesh model of sector of dome cap ... 28
Figure 2.7 : Shell arrangement for 8-element mesh model of cap sector 30
Figure 2.8 : Dome cap: 2-element mesh model 33
Figure 2.9 : Dome cap: 16-element mesh model 34
Figure 2.10 : Dome cap: 2-element mesh model with connector elements 35
Figure 2.11 : Material laws, a) linear law 1, b) linear law 2, c) bilinear law 36
Figure 2.12 : Nonlinear material law for wood ,Connors' model SG = 12%, MC = 0.52 37
Figure 2.13 : Dome cap model, full snow load, nonlinear material law, Original subroutine UMAT 38
Figure 2.14 : Dome cap model, full snow load, nonlinear material law, Modified subroutine UMAT 40
Figure 2.15 : Dome cap model, half snow load, nonlinear material law, Modified subroutine UMAT 41
Figure 2.16 : Dome cap model, full snow load, refined mesh model with hinge elements 42
Figure 2.17 : Dome model with truss bracing a) plan view, b) side view 45
Figure 2.18 : Buckling mode for the dome model with truss bracing : full snow 47
Figure 2.19 : Buckling mode for the dome model with truss bracing : half snow 48
Figure 3.1 : Modified dome cap model, full snow load case 51
Figure 3.2 : Modified dome cap model, half snow load case 52
Figure 3.3 : Dome cap model, different areas of tension ring, full snow load 54
Figure 3.4 : Dome cap model, different areas of tension ring, half snow load 55

Figure 3.5 : Nonlinear material law for wood, Connors' segmented model, MC = 12 % 57
Figure 3.6 : Nonlinear material law for wood, Connors' segmented model, MC = 14 % 58
Figure 3.7 : Dome cap model, full snow load, variation in material law 60
Figure 3.8 : Dome cap model, half snow load, variation in material law..... 61
Figure 3.9 : Varax beam-to-beam joint..... 64
Figure 3.10 : Stiffness reduction of hinge elements..... 64
Figure 3.11 : Dome cap model with hinge elements, full snow, variation in stiffness of hinge elements 66
Figure 3.12 : Dome cap model with hinge elements, half snow, variation in stiffness of hinge elements 67
Figure 4.1 : Equilibrium and compatibility of circular shaft..... 70
Figure 4.2 : Twisting of a shaft with non-circular cross section 73
Figure 4.3 : Stresses in a cross section of shaft..... 79
Figure 4.4 : Rectangular cross section..... 79
Figure 4.5 : Circular cantilever subjected to torque at free end 85
Figure 4.6 : Rectangular cantilever subjected to torque at free end 85
Figure 4.7 : Circular beam in space, default integration points..... 89
Figure 4.8 : Rectangular beam in space, default integration points..... 89
Figure 4.9 : Circular beam with varying cross section..... 92
Figure 4.10 : Rectangular beam with varying cross section..... 92
Figure 5.1 : Tongue-and-groove decking of the dome..... 98
Figure 5.2 : Foschi's load-deflection curve 101
Figure 5.3a : Nailed connection for the lateral load test..... 102
Figure 5.3b : Dimensions of the wood samples in the tests on the nailed connections.... 103
Figure 5.4 : Experimental setup for the lateral load tests on the nailed connections..... 104
Figure 5.5 : Load-deflection curves for the test samples with Southern Pine wood 107
Figure 5.6 : Bilinear elastic-plastic load-deflection curve assumed for the 16-d nailed connection in Southern Pine wood..... 108
Figure 5.7 : Plane beam element with an attached connector 112
Figure 5.8 : DOF for plane beam and plane frame element 112
Figure 5.9 : Local space beam element..... 114
Figure 5.10 : 3D beam/connector assembly..... 114
Figure 5.11 : Nailed connection between decking and beams..... 115
Figure 5.12 : Relationship between nail deflection and nodal deflections of the beam.... 115

Figure 5.13 : 3D beam/connector assembly for the inclined main beams of the dome.... 119
Figure 5.14 : 3D beam/connector assembly for a) vertical, b) inclined nails on the edge beams of the dome..... 121
Figure 5.15 : Truss model to verify the use of global stiffness matrix in user element option in ABAQUS 125
Figure 5.16 : Nonlinear analysis: Newton/Raphson option..... 127
Figure 5.17 : Nonlinear analysis: a) Riks, b) modified-Riks methods..... 129
Figure 5.18 : N/R scheme for bilinear load-deflection curve 131
Figure 5.19 : Test case of a single spring, a) nonlinear spring with 2 DOF, b) load-deflection curve for the spring..... 133
Figure 5.20 : N/R iteration for the nonlinear spring model..... 135
Figure 5.21 : 2D b/c assembly for linear analysis 137
Figure 5.22 : Spring energy for a constant spring stiffness..... 137
Figure 5.23 : Bilinear load-deflection curve for 2D and 3D test cases..... 142
Figure 5.24 : 2D b/c assemblies with a) 3 and b) 15 connectors..... 142
Figure 5.25 : Spring energy for the second segment of bilinear load-deflection curve.... 144
Figure 5.26 : 3D b/c assembly, a) with user element, b) with SPRING2 elements for the connectors, c) beam cross section 148
Figure 5.27 : 3D beam/connector assembly, a) 3 connectors, b) 15 connectors..... 150
Figure 5.28 : Dilfferent boundary conditions used in the test cases on the b/c element . 151
Figure 5.29 : 3D b/c model with vertical beam 155
Figure 5.30 : 3D b/c model with two b/c elements..... 155
Figure 6.1 : Load-deflection paths for dome cap models with, without truss bracing and with b/c elements, full snow load 158
Figure 6.2 : Load-deflection paths for dome cap models with, without truss bracing and with b/c elements, half snow load..... 159
Figure 6.3 : Dome sector: nails at bracing points..... 163
Figure 6.4 : Sector of the dome 165
Figure 6.5 : Load-deflection paths for various dome models, full snow load case 166
Figure 6.6 : Load-deflection paths for various dome models, half snow load case..... 167
Figure 6.7 : Buckling mode for the dome model without truss bracing: full snow 173
Figure 6.8 : Buckling mode for the dome model with b/c elements: full snow..... 174
Figure 6.9 : Buckling mode for the dome model without truss bracing: half snow..... 175
Figure 6.10 : Buckling mode for the dome model with b/c elements: half snow 176

Figure A.1 : Geometry of the dome 186
Figure A.2 : Convention for the local axes: (a) beam in ABAQUS, (b) connector..... 186
Figure A.3a : The local axes orientation for the vertical main beams..... 189
b : The local axes orientation for the inclined main beams 189
Figure A.4 : The local axes orientation for the edge beams..... 190

LIST OF TABLES

Table 2.1 Nonlinear Analysis for the Beam in Tension, Linear Material 13
Table 2.2 Nonlinear Analysis for the Beam in Compression, Linear Material 13
Table 2.3 Nonlinear Analysis of the Beam in Tension, Nonlinear Material Law 16
Table 2.4 Nonlinear Analysis of the Beam in Compression, Nonlinear Material Law..... 17
Table 2.5 Results for the Cap Rib Refined Mesh Models..... 21
Table 2.6 Results for the Cap Rib models with Extra Nodes on Curved Arch of the Cap Rib 25
Table 2.7 Nodal Reactions for the Cap Sector Models with Different Arrangements of Shell Elements 31
Table 2.8 Results for the Dome Cap Models with and without Corrections in UMAT 39
Table 2.9 Results for the Dome Cap Models with Mesh Refinement, Full Snow Load..... 43
Table 2.10 Results for the Dome Cap Models with Mesh Refinement, Half Snow Load..... 43
Table 3.1 Proportional Limit and Ultimate Stresses for Nonlinear Material Law..... 59
Table 3.2 Results for Variation in Nonlinear Material Law : Full Snow Load 62
Table 3.3 Results for Variation in Nonlinear Material Law : Half Snow Load..... 62
Table 3.4 Hinge Element Dimensions for Reduced Stiffness..... 63
Table 3.5 Results for Reduced Stiffness for Full Snow 65
Table 3.6 Results for Reduced Stiffness for Half Snow 65
Table 4.1 Saint-Venant's Coefficients for Rectangular Sections..... 82

Table 4.2 Results for the Dome Cap Model with and without Warping of Beams : Full Snow 94
Table 4.3 Results for the Dome Cap Model with and without Warping of Beams : Half Snow 95
Table 5.1 Results for the 2D b/c Test Models 146
Table 5.2 Results for the 3D b/c Test Models : B. C. #1 152
Table 5.3 Results for the 3D b/c Test Models : B. C. #2 153
Table 6.1 Results for the Different Dome Cap Models 160
Table 6.2 Proportional Limits and Ultimate Stresses for Different Material Laws 161
Table 6.3 Results for Different Dome Models 168
Table 6.4 Locations of Maximum Nail Deflections in Dome: Full Snow 169
Table 6.5 Locations of Maximum Nail Deflections in Dome: Half Snow 169
Table 6.6 Results for the Dome Models with Nonlinear Material Law 171
Table 6.7 Maximum Nail Deflections in the Dome: Nonlinear Law 171
Table H.1 Critical Pressure on the Dome 227
Table H.2 Stresses in the Beam Elements and Nail Deflections at Critical Pressures: Full Snow 228
Table H.3 Stresses in the Beam Elements and Nail Deflections at Critical Pressures: Half Snow 228

Chapter 1

Introduction

1.1 General

The primary objectives of this study are to develop a 3-D beam/connector finite element for a glulam dome with nonlinear connectors (nails) to model the beam/decking connections, and to incorporate warping of rectangular beams in the analysis of the dome. This model is analyzed using the finite element program ABAQUS and the results are compared with those of finite element models with truss bracing to simulate the decking. The geometry of a glulam dome built in Raleigh, NC, is used to construct the models of the dome.

The dome model with truss bracing for decking was analyzed by Telang (1992) using a nonlinear material law for wood developed by Connors (1989). The material law is supplied through user subroutine UMAT. Convergence problems were experienced in the analyses with the nonlinear law for the refined mesh cap models and the dome model. The factors affecting the convergence of the solution using the modified Riks method for geometrically nonlinear analysis are studied in Chapter 2. Coding of the nonlinear material law in UMAT, the tolerance specifications PTOL and MTOL in the RIKS option and the degree of mesh refinement are some of the factors considered. For this purpose, test cases of a single beam element with a concentrated load at one end and a dome cap rib model are analyzed first. The dome cap and dome models are later analyzed to confirm the results obtained in these test cases regarding the factors influencing the convergence. Mesh refinements are performed on the dome cap rib and dome cap models to investigate the precision of the solution. The refined mesh models are created graphically using I-DEAS. The input file for the analysis with ABAQUS is obtained from I-DEAS and is modified to include additional information such as beam orientations, boundary conditions, STEP definition cards, material properties, and dead and live loading. The finite elements and boundary conditions are the same as those used by Telang (1992) and Tsang (1992) in order to have a common basis for comparing the results. For each refined mesh model, a linear analysis is performed to test the accuracy of the finite element model created by I-

DEAS by checking the equality of loads and reactions and the symmetry of reactions for the full snow load case.

The dome cap model is modified to make it conform to the cap of the full dome by using inclined base beams and using appropriate beam orientations. This model is analyzed in Chapter 3 with varying factors such as the area of tension ring, nonlinear material law, and joint flexibility. The purpose is to study the effect of these factors on the solution.

The beams in the present study are rectangular and therefore are subjected to warping of the cross section. Warping is included in the analysis by modifying the shear modulus as described in Chapter 4. Saint-Venant's torsion theory for rectangular bars is used. This is because Saint-Venant's isotropic torsion solution can accurately represent the linear torsional response of southern pine glulam beams (Davalos, et al., 1991). A comprehensive review of the theory of torsion of bars is presented in order to develop the background for the scheme of including warping in the analysis with ABAQUS. The results for the test cases of propped cantilever beams with circular and rectangular cross sections are checked with Navier's solution and the solution obtained with Saint-Venant's torsion theory. These tests are done to check the feasibility of using the above scheme in the analysis with ABAQUS. The dome cap and dome models with truss bracing are analyzed with a modified shear modulus to include warping.

The potential of the beam/connector (b/c) model to simulate the effect of the decking was demonstrated by Tsang (1992) in the analysis of the dome cap. Linear connectors (nails) were used in the b/c model. It was felt necessary to use nonlinear connectors since the nail deflections for the cap model were in the nonlinear range. The nonlinear connector is defined using a user coded subroutine UEL in ABAQUS. The connector deflections are checked in this subroutine and the stiffness matrix and force contributions of the connector are updated.

The nonlinear load-deflection model for 16-d nails used in the glulam dome is used to define the connectors in UEL. This model is based on the model by Foschi (1974) which was later modified by Dolan (1989) to take into account the decrease in the capacity of nails after a specified deflection. The load-deflection curve adopted in the analysis of the

dome is obtained from averaging the test results on the nailed connections in southern pine wood. A bilinear elastic-plastic load-deflection curve is assumed for the analysis.

The user subroutine UEL is thoroughly tested in Chapter 5 with different test problems such as for a single nonlinear spring, 2-D and 3-D b/c models, and the dome cap model before analyzing the full dome. Two types of 3-D b/c models are analyzed in Chapter 6 to check the subroutine for two different loading and boundary conditions. The dome cap model is analyzed for full and half snow load conditions with a linear material law (E = 1.8 E06 psi, G = 1.6 E05 psi). The results are compared with those for the model with and without truss bracing. Finally, the dome model is analyzed with linear and nonlinear material laws and with full and half snow load conditions. Two main types of b/c models for the dome are used in the analysis. In the first type, the nails are attached at the centroids of beam elements (rigid link length, h = 0), first at all nodes and then at the locations (nodes) where the truss bracings are connected to the beam elements. These are comparatively simpler and cost-effective models and can be used to model the decking effectively. The second model has 16 connectors attached to the top of the beams. Though this is the most precise model, it is also the most expensive. The results of these models are compared with the models with and without truss bracing. The equilibrium paths, critical loads, and maximum stresses are presented for all these models. The nail deflections are computed for the b/c models at the critical loads to study the status of nails at the point where instability occurs.

Conclusions based on the present study and recommendations for future research are presented.

1.2 Research Background

Singly and doubly curved structural space frames belong to the type of structures in which the axial forces in the members mainly resist the applied loading. The members undergo large elastic deformations as a result of this. The geometrically nonlinear analysis of these types of structures is important because elastic instability may occur before they exhibit any nonlinear material behavior (Meek and Loganathan, 1989). The prebuckling behavior of lattice domes exhibit large joint displacements and large member rotations, and the nonlinear effects must be included to predict the response accurately (Wu, 1991).

Bathe (1982) gives a comprehensive review and formulation of finite elements for linear and nonlinear analysis of structures.

The most valuable background information for the development of a finite element method of analysis for glulam lattice domes is provided by Holzer and Loferski (1987). Also, a complete review of finite element methods that are used to investigate the stability of spatial structures is presented by Holzer, Davalos, and Huang (1989).

Wind and snow loads are two important design loads for lattice domes. Most U.S. codes specify design requirements for these two types of loads. However, Wu (1991) showed conclusively that wind load is not a critical factor in the design of the dome analyzed in the present study. It was also shown that the half snow load case is more critical as far as maximum element stresses are concerned.

There are few constitutive models to predict the entire stress-strain curve for wood. Also, there are no analytical models that can predict the complete 3-D response of straight or curved beams up to failure (Davalos, 1989). However, torsional response of glulam beams was tested experimentally by Davalos et al. (1991). The experimental results showed the transverse isotropic behavior of southern pine beams. The results also showed that Saint-Venant's torsion can accurately represent the linear torsional response of southern pine glulam beams. The shear moduli, G, of rectangular and circular glulam samples were computed from torsion tests and Saint-Venant's isotropic torsion solution. A constitutive law for Yellow Poplar, based on specific gravity and moisture content, was developed by Connors (1989), and it is used as the nonlinear material law for wood in the present study.

Chapter 2

Convergence and Mesh Refinement Study for the Dome Analysis

2.1 Introduction

The dome model used in this study was analyzed by Telang (1992) using a nonlinear material law for wood based on a constitutive model developed by Connors (1989) with segmented strain-stress curves. The purpose of including the nonlinear material law in the analysis was to incorporate the material properties of wood beyond the proportional limit in the finite element model of the dome for determining its ultimate load capacity. The analysis of the dome cap and dome models with selective mesh refinement using connector (hinge) elements at the joints had experienced difficulty in converging after passing through the limit point. This problem was attributed to the combined effect of the size and number of the connector elements and the inelastic material law (Telang, p110).

In this chapter, an attempt is made to look into the factors affecting the convergence of the solution in the nonlinear analysis using the modified Riks-Wempner method in ABAQUS. For this purpose, the user subroutine option in ABAQUS is tested in section 2.2 for a case problem by specifying different constitutive equations to model material laws in tension and compression. In section 2.3, a model of one rib of the dome cap is tested to verify the findings in section 2.2 and also to investigate the influence of other parameters on the convergence of the solution. This model is also analyzed for different mesh sizes to study the effect of mesh refinement on the accuracy of results and also on the convergence of the solution. The above mentioned nonlinear material law for wood is used in the analysis.

The earlier models of the dome cap and the dome had meshes composed of 2 elements, 4 elements, and two elements with connector (hinge) elements at beam-to-beam joints for every real beam in the actual structure. The connector elements were beam elements, of 6 in. length, used at the location of all the nodes in the finite element model. They are created to model the joints between various members of the structure. The dome

cap is analyzed for further mesh refinements to study the level of accuracy relative to successive mesh refinements. The accuracy of the solution is also studied with respect to the findings in sections 2.2 and 2.3. The full and half snow load conditions are used, and the results for the same are presented in the section 2.4. Finally, results from full dome model analyses with the Riks method are studied in section 2.5.

2.2 Constitutive Modeling in ABAQUS using the User Subroutine UMAT

This section deals with testing of the User Subroutine option in ABAQUS for specifying various linear and nonlinear constitutive equations, both in tension and compression. A beam modeled with one B23 plane beam element from the ABAQUS library of elements is analyzed using the RIKS option for nonlinear analysis (Figure 2.1).

*STEP,NLGEOM

*STATIC,PTOL= --- ,MTOL= --- ,RIKS

A concentrated force of 10 kips is applied at one end, as shown, to induce tension or compression in the beam. The direct user control method can also be employed by using the DIRECT parameter on the *STATIC card instead of the RIKS parameter. The user specifies a constant load increment when DIRECT parameter is used. The material properties of the beam are varied to test its response. A linear law in tension and compression is specified first with the *ELASTIC option in ABAQUS and then using the User Subroutine option. Material laws with nonlinear terms in the constitutive (stress-strain) equations for tension and compression are used next in the above model.

2.2.1 Linear Material Law

A linear material law for axial stress

$$\sigma(\varepsilon) = E\,\varepsilon \tag{2.1}$$

where

$\sigma(\varepsilon)$ = Axial stress (as a function of strain)

ε = Axial strain

E = Proportionality constant (Young's modulus)

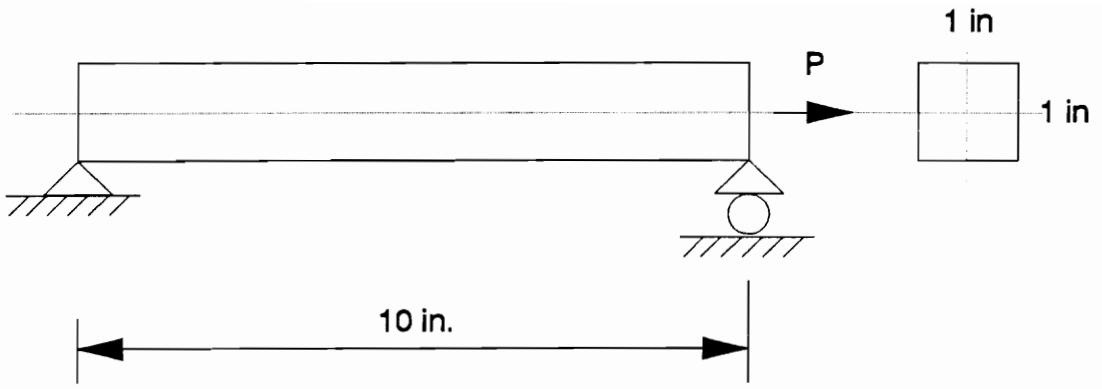


Figure 2.1 Axially loaded beam

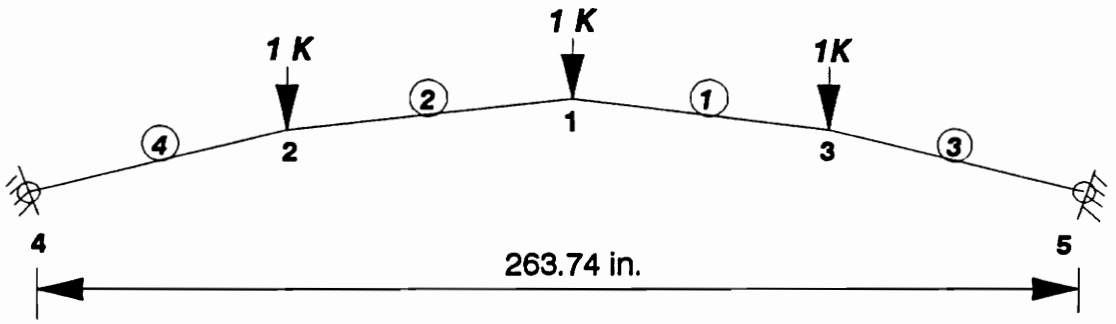


Figure 2.2 Dome cap rib : 2 element mesh

can be specified in ABAQUS using the *ELASTIC option as follows. For a value of E equal to 2.9×10^7 psi and Poisson's ratio (ν) of 0.3, the above law can be given as

*ELASTIC

2.9E07,0.3

The shear modulus (G) is automatically calculated by the program using

$$G = \frac{E}{2(1+\upsilon)} \tag{2.2}$$

ABAQUS limits the value of ν to 0.5 (Telang, 1992). The user subroutine option must be used if the value of G is such that the value of ν required in Eq. (2.2) to specify G is greater than 0.5. The FORTRAN code for the material model is written in the subroutine UMAT. It is called by the main program at each material calculation point for which the *MATERIAL definition includes the *USER MATERIAL option, and it is used to define the mechanical constitutive behavior of the material (sec.8.18.1, ABAQUS). The primary task of UMAT is to define the Jacobian matrix of the constitutive model and the stress tensor for the user specified constitutive model. The stress tensor array STRESS (NTENS) is passed in the subroutine at the beginning of an increment in the nonlinear analysis and must be updated at the end of the increment. In the arrays corresponding to stress and strain tensors and the Jacobian matrix, the direct and shear stress components are stored consecutively as defined in sec. 6.6.1 of ABAQUS User's manual. The stress/strain components that are always zero are omitted from the storage. Thus the size of the arrays depends on the number of non-zero stress/strain components for a particular type of element. There are 'NDI' and 'NSHR' number of direct stress and shear stress components, respectively for any type of element in the ABAQUS element library. These can be determined from the general description of all elements available in the ABAQUS element library. For example, for the beams in space (sec. 3.3.5, ABAQUS), the subscripts of the stress/strain components are

11 Axial stresses

12 Shears caused by torsion

The components of the stress tensor for a fully anisotropic material are given below. The above implies that out of these components only σ_{11} and τ_{12} are required.

$$\begin{pmatrix} \sigma_{11} \\ \sigma_{22} \\ \sigma_{33} \\ \cdots\cdots \\ \tau_{12} \\ \tau_{13} \\ \tau_{23} \end{pmatrix}$$

Therefore, for the beam in space, the values of NDI and NSHR are both equal to 1 and the linear elasticity matrix becomes

$$\begin{pmatrix} \sigma_{11} \\ \tau_{12} \end{pmatrix} = \begin{bmatrix} D_{1111} & D_{1112} \\ D_{1112} & D_{1212} \end{bmatrix} \begin{pmatrix} \varepsilon_{11} \\ \gamma_{12} \end{pmatrix} \tag{2.3}$$

It follows from this that the Jacobian matrix of any constitutive model for a beam in space must also be a 2×2 matrix given as (Telang, 1992)

$$J = \begin{bmatrix} J_{11} & 0 \\ 0 & J_{22} \end{bmatrix} \tag{2.4}$$

The Jacobian matrix array in UMAT is DDSDDE(I,J) and defines the change in the Ith stress component at the end of the time increment caused by an infinitesimal perturbation in the Jth component of the strain increment array. Therefore, we get

$$\begin{aligned} J_{11} &= \frac{\partial \Delta\sigma_{11}}{\partial \Delta\varepsilon_{11}} \\ J_{22} &= \frac{\partial \Delta\tau_{12}}{\partial \Delta\gamma_{12}} \end{aligned} \tag{2.5}$$

For an increment in the strain of value $\Delta\varepsilon$, the stress value from the Eq. (2.1) becomes

$$\begin{aligned} \sigma(\varepsilon+\Delta\varepsilon) &= E\,(\varepsilon+\Delta\varepsilon) \\ &= E\,\varepsilon + E\,\Delta\varepsilon \\ &= \sigma(\varepsilon) + \Delta\sigma(\varepsilon) \end{aligned} \tag{2.6}$$

where $\Delta\sigma$ represents the increment in the stress corresponding to an increment $\Delta\varepsilon$ in the strain ε. From Eq. (2.6)

$$\Delta\sigma(\varepsilon) = E\,\Delta\varepsilon \tag{2.7}$$

From Eqs. (2.5) and (2.7)

$$J_{11} = E \tag{2.8}$$

Thus, J_{11} in Eq. (2.4) is the proportionality constant E, or the Young's modulus. Similarly, J_{22} is equal to the shear modulus G. Equations (2.1), (2.7), (2.6) and (2.8), respectively are coded in the subroutine as

```
STRESS(1) = E * STRAN(1)
DSTRESS(1) = E * DSTRAN(1)
STRESS(1) = STRESS(1) + DSTRESS(1)
DDSDDE(1,1) = E
```

Alternatively, the above relations can also be coded as

```
TS = STRAN(1) + DSTRAN(1)
STRESS(1) = E * TS
DDSDDE(1,1) = E
```

It should be noted that STRAN(NTENS) and DSTRAN(NTENS) represent the array of the total and incremental strain components respectively, and are 'passed in' the subroutine for information only. It is required that the variables passed in the subroutine for information only should not be modified in the subroutine and redefining them may cause severe problems (sec 8.1.0, ABAQUS). For this reason, the new variable 'TS' is defined to represent the incremented strain value.

An important aspect in coding the subroutine is that the constitutive equations (as used in the spreadsheets for graphical presentation) are usually written assuming the positive values for stress (σ) and strain (ε), either in tension or compression. However, in the finite element analysis programs, these values are negative in compression. Therefore it becomes necessary to modify these equations in compression so as to get the appropriate

negative values of stresses for the negative values of strains. In the case of the constitutive law in Eq. (2.1), the positive or negative values of strain would appropriately give positive or negative values of stresses, respectively. Thus in this case it is not necessary to modify the constitutive equation for compression. However, if higher order terms are present in the equation as in case of nonlinear material law, it is necessary to write different equations in tension and compression as discussed in the next section.

The beam in Figure 2.1 was analyzed with the *ELASTIC option and also with the *USER MATERIAL option with the subroutine UMAT coded as described earlier. The E value of 2.9×10^7 psi was used. Both analyses gave the same results as given in Table 2.1 for the beam in tension and Table 2.2 for the beam in compression. Note that the user coded material law is satisfied for every increment.

2.2.2 Nonlinear Material Law

A nonlinear constitutive equation as given in Eq. (2.9) can be coded in the subroutine UMAT in a similar way as described in the last section.

$$\sigma(\varepsilon) = E\,\varepsilon + E\,\varepsilon^2 \tag{2.9}$$

For the strain increment $\Delta\varepsilon$, Eq. (2.9) becomes

$$\begin{aligned} \sigma(\varepsilon+\Delta\varepsilon) &= E\,(\varepsilon+\Delta\varepsilon) + E\,(\varepsilon+\Delta\varepsilon)^2 \\ &= E\,\varepsilon + E\,\varepsilon^2 + E\,(\Delta\varepsilon + 2\,\varepsilon\,\Delta\varepsilon + \Delta\varepsilon^2) \\ &= \sigma(\varepsilon) + \Delta\sigma(\varepsilon) \end{aligned} \tag{2.10}$$

where

$$\Delta\sigma(\varepsilon) = E\,(\Delta\varepsilon + 2\,\varepsilon\,\Delta\varepsilon + \Delta\varepsilon^2) \tag{2.11}$$

Eqs. (2.5) and (2.11) give

$$\begin{aligned} J_{11} &= E\,(1 + 2\,\varepsilon + 2\,\Delta\varepsilon) \\ &= E + 2E\,(\varepsilon + \Delta\varepsilon) \end{aligned} \tag{2.12}$$

Eqs. (2.9) through (2.12) can be used in the subroutine as

```
STRESS(1) = E * (STRAN(1) + STRAN(1)**2)
DSTRESS(1) = E * DSTRAN(1) * (1 + 2.*STRAN(1) + DSTRAN(1))
STRESS(1) = STRESS(1) + DSTRESS(1)
DDSDDE(1,1) = E * (1 + 2. * (STRAN(1) + DSTRAN(1)))
```

The above can also be coded alternatively as

```
TS = STRAN(1) + DSTRAN(1)
STRESS(1) = E * (TS + TS ** 2)
DDSDDE(1,1) = E * (1+2 * TS)
```

Note that both the stress and the Jacobian of the constitutive equation contain the incremental strain value. In the subroutine UMAT used by Telang (1992) to code the Connor's nonlinear material law, an erroneous expression for Jacobian was used. STRAN(1) was used instead of TS in the two statements containing the Jacobian. The DDSDDE(I,J) array must be defined accurately if rapid convergence of the overall Newton scheme in a geometrically nonlinear analysis is to be achieved. In most cases, the accuracy of this definition is the most important factor governing the convergence rate (ABAQUS, p. 8.18.1-4). Thus, it can be concluded that a potential cause of the convergence problem was the error in the expression for the Jacobian.

The Eqs. (2.9) through (2.12) are written for the positive values of strains and corresponding stress values and are correct for tension in the beam since the strain values are positive in tension in the analysis with ABAQUS. Therefore, the coding described above is correct only in case of tension. Since the strain/stress values in compression in the analysis with ABAQUS are always negative and the Eq.(2.9) is written for positive values of strains and corresponding positive stresses, care must be taken in coding it for the analysis with ABAQUS. Note that the STRAN and DSTRAN values passed in the subroutine are negative if the beam is in compression. We must modify the constitutive equation such that the absolute values of ε are used so as to make them positive in the equation. The corresponding calculated stress values will be positive. Then we apply a negative sign to the right hand side of the equation in order to make the stress values negative as desired by the main program. Thus the Eq. (2.9) can be coded in the subroutine for compression as follows.

Table 2.1

Nonlinear Analysis for the Beam in Tension, Linear Material

Increment	P (lb)	Deflection in the direction of P (in.)	Axial stress, S11	Axial strain, E11
1	1000	3.45 E-04	1000	3.45 E-05
2	2000	6.89 E-04	2000	6.89 E-05
3	3500	1.20 E-03	3500	1.20 E-04
4	5751	1.98 E-03	5750	1.98 E-04
5	9127	3.15 E-03	9125	3.15 E-04
10	7.60 E04	2.61 E-02	7.59 E04	2.61 E-03
20	4.8 E06	1.372	4.25 E06	0.1466
25	1.67 E07	3.602	1.23 E07	0.4250

Table 2.2

Nonlinear Analysis for the Beam in Compression, Linear Material

Increment	P (lb)	Deflection in the direction of P (in.)	Axial stress, S11	Axial strain, E11
1	-1000	-3.50 E-04	-1000	-3.50 E-05
2	-2000	-6.90 E-04	-2000	-6.90 E-05
3	-3500	-1.20 E-03	-3500	-1.20 E-04
4	-5749	-1.98 E-03	-5750	-1.98 E-04
5	-9123	-3.15 E-03	-9125	-3.14 E-04
10	-7.60 E04	-2.62 E-02	-7.60 E04	-2.62 E-03
20	-3.80 E06	-1.719	-4.60 E06	-0.1571
25	-4.50 E06	-6.465	-1.27 E07	-0.4375

$$\sigma(\varepsilon) = -(E\,Abs(\varepsilon) + E\,(Abs(\varepsilon))^2)$$

$$= -(E\,Abs(\varepsilon) + E\,\varepsilon^2) \qquad (2.13)$$

For negative values of ε, $-E\,Abs(\varepsilon) = E\,\varepsilon$. The Eq. (2.13) then becomes

$$\sigma(\varepsilon) = E\,\varepsilon - E\,\varepsilon^2 \qquad (2.14)$$

For Eq. (2.14), we get

$$\sigma(\varepsilon+\Delta\varepsilon) = E\,(\varepsilon+\Delta\varepsilon) - E\,(\varepsilon+\Delta\varepsilon)^2$$

$$\Delta\sigma(\varepsilon) = E\,(\Delta\varepsilon - 2\,\varepsilon\,\Delta\varepsilon - \Delta\varepsilon^2) \qquad (2.15)$$

$$J_{11} = E\,(1 - 2\,(\varepsilon + \Delta\varepsilon))$$

The Jacobian J_{11} can be expressed alternatively as $E\,(1 + 2\,(Abs(\varepsilon + \Delta\varepsilon))$, since both ε and $\Delta\varepsilon$ values are negative in compression. The coding for the beam in compression is given below.

```
STRESS(1) = E * (STRAN(1) - STRAN(1)**2)
DSTRESS(1) = E * DSTRAN(1) * (1 - 2.*STRAN(1) - DSTRAN(1))
STRESS(1) = STRESS(1) + DSTRESS(1)
DDSDDE(1,1) = E * (1 - 2. * (STRAN(1) + DSTRAN(1)))
```

or alternatively,

```
TS = STRAN(1) + DSTRAN(1)
STRESS(1) = - E * (Abs(TS) + (Abs(TS)) ** 2)
DDSDDE(1,1) = E * (1+2 * Abs(TS))
```

The beam in Figure 2.1 was tested in compression with the coding done in the two alternative ways given above. Both the analyses gave exactly the same results, as will be discussed later.

In general, for a constitutive law

$$\sigma(\varepsilon) = A + B\varepsilon + C\varepsilon^2 + D\varepsilon^3 + ...$$

with positive stress/strain values assumed, the expressions for stress and the Jacobian of the constitutive equation in the subroutine can be written as follows.

Constitutive law :

In tension (σ & ε are positive) $\sigma(\varepsilon) = A + B\varepsilon + C\varepsilon^2 + D\varepsilon^3 + ...$ (2.16)

In compression $\sigma(\varepsilon) = -(A + B\,Abs(\varepsilon) + C\,(Abs(\varepsilon))^2 + D(Abs(\varepsilon))^3 + ...)$

(σ & ε are negative) $= -A + B\varepsilon - C\varepsilon^2 + D\varepsilon^3 - .....$ (2.17)

Jacobian :

In tension $J_{11} = B + 2C\,(TS) + 3D\,(TS)^2 + ...$ (2.18)

In compression $J_{11} = B + 2C\,(Abs(TS)) + 3D(Abs(TS))^2 + ...$

$= B - 2C\,(TS) + 3D(TS)^2 - .....$ (2.19)

If Eq. (2.17) is to be used, it is advised to check the constitutive equation in compression to be sure that it is written assuming the positive values of σ and ε.

The beam in Figure 2.1 was analyzed for the constitutive material law in Eq.(2.9) with appropriate modification for compression. The beam was analyzed first with the erroneous Jacobian expression containing STRAN(1) and then with the one containing the incremental strain TS. These two analyses gave distinct results, both for the beam in tension and compression. These are given in Tables 2.3 and 2.4 for the beam in tension and compression, respectively. Values for a few increments only are presented.

It can be observed that the results in tension and compression, respectively, are the same in both cases for the first few (about 15) increments but differ substantially for the later increments. The runs with the Jacobian term using TS seem to converge rapidly, which is evident from the fact that higher values of loads and deflections are obtained in each of the later increment. It is also observed that in both cases the constitutive law is followed exactly. This is expected because in both cases the same expression for the stress-strain relationship is used. From these observations it can be concluded that the accuracy of the Jacobian matrix term is reflected in the rate of convergence as stated

Table 2.3

Nonlinear Analysis of the Beam in Tension, Nonlinear Material Law

Increment	P (lb)	Deflection in the direction of P (in.)	Axial stress, S11	Axial strain, E11
Jacobian with STRAN				
1	1000	3.50 E-04	1000	3.50 E-05
5	9128	3.15 E-03	9127	3.15 E-04
10	7.61 E04	2.60 E-02	7.60 E04	2.60 E-03
15	5.96 E05	0.196	5.85 E05	1.98 E-02
16	8.02 E05	.2593	7.82 E05	2.63 E-02
17	1.01 E06	0.3215	9.80 E05	3.27 E-02
18	1.22 E06	0.3827	1.18 E06	3.90 E-02
19	1.43 E06	0.4429	1.37 E06	4.53 E-02
20	1.68 E06	0.502	1.57 E06	5.15 E-02
25	2.76 E06	0.7839	2.55 E06	8.14 E-02
Jacobian with TS				
1 to 15	Same as above			
16	9.06 E05	0.2905	8.80 E05	2.95 E-02
17	1.38 E06	0.4280	1.32 E06	4.37 E-02
18	2.11 E06	0.6247	2.00 E06	6.44 E-02
19	2.87 E06	0.8110	2.65 E06	8.44 E-02
20	3.64 E06	0.9875	3.30 E06	0.1036
25	7.72 E06	1.7510	6.60 E06	0.1904

Table 2.4

Nonlinear Analysis of the Beam in Compression, Nonlinear Material Law

Increment	P (lb)	Deflection in the direction of P (in.)	Axial stress, S11	Axial strain, E11
Jacobian with STRAN				
1	-1000	-3.45 E-04	-1000	-3.45 E-05
5	-9124	-3.14 E-03	-9127	-3.15 E-04
10	-7.60 E04	-2.60 E-02	-7.60 E04	-2.60 E-03
15	-5.96 E05	-0.196	-5.85 E05	-1.98 E-02
16	-8.67 E05	-0.3042	-8.95 E05	-2.99 E-02
17	-1.15 E06	-0.4069	-1.20 E06	-3.98 E-02
18	-1.43 E06	-0.5104	-1.50 E06	-4.97 E-02
19	-1.72 E06	-0.6146	-1.83 E06	-5.96 E-02
20	-2.00 E06	-0.7197	-2.15 E06	-6.90 E-02
25	-3.34 E06	-1.2590	-3.80 E06	-0.1180
Jacobian with TS				
1 to 16	Same as above			
17	-1.29 E06	-0.4586	-1.36 E06	-4.48 E-02
18	-1.93 E06	-0.6933	-2.10 E06	-6.70 E-02
19	-2.85 E06	-1.054	-3.20 E06	-9.98 E-02
20	-4.15 E06	-1.618	-4.95 E06	-0.1487
25	-7.50 E06	-4.962	-1.50 E07	-0.3731

earlier. Also, the error in the Jacobian does not affect the accuracy of the results for this particular case, as far as the stress/strain values and corresponding deflections are concerned.

2.3 Cap Rib Model

A rib of the dome cap shown in Figure 2.2 was analyzed with the RIKS option in ABAQUS. The purpose was to investigate the causes of the convergence problem. Two types of rib models were tested. The first was a two-dimensional (2D) model with B23 plane beams and second was a three-dimensional (3D) model with B33 space beams. The boundary conditions used are pin connections for both models, as shown in Figure 2.2. The nonlinear material law for wood, developed by Connors, was used in the analysis. The detailed description of this material model and the user subroutine UMAT for the same are given in the thesis by Telang (1992). Some of the statements in this subroutine were modified as noted in the previous section and are given below.

Tension Zone :
DDSDDE(1,1) = BETA2 + 2. * BETA3 * (TS) ..... (for TS > AK1)
Compression Zone :
DDSDDE(1,1) = BETA2 + 2. * BETA3 * ABS(TS) ..... (for AK1C > TS > AK2C)

The initial input file for the 3D model containing the nodal coordinates element connectivity was created using I-DEAS. The file was then modified to include the nodal loads, beam orientations, boundary conditions, the step definition, and the output request cards. The graphical model of the cap rib in I-DEAS was created from the dome cap model by deleting the extra nodes and elements of the dome cap. The input file for the 2D model was created next from the input file for 3D model by making the following changes.

- The nodal X and Y coordinates in the 2D model correspond to the nodal X and Z coordinates in the 3D model. This is because the 2D model, for which only X and Y coordinates are required, lies in the XZ (global 1-3) plane defined in ABAQUS for the 3D model. The Y-coordinates in the input file of the 3D model are deleted and only X and Z coordinated are retained for the input file of the 2D model. These now represent the X and Y coordinates in the 2D model.

- The element type is changed from B33 to B23.
- In case of the plane beams, the direction cosines of the normalized n_1 vector as given in the *BEAM SECTION card (refer to Appendix A) should be specified as (0, 0, -1). Therefore, it is not necessary to specify different direction cosines for all the beams in the 2D model as done for the 3D model.
- The nodes other than the boundary nodes in the 3D model are fixed in the 2-direction in order to support them laterally. This is necessary because in the case of the pinned boundary condition, the 3D model is unstable in the lateral direction unless supported in that direction.
- For the pinned support, the boundary nodes are fixed in the 1 and 2 directions for the 2D model and the 1 through 3 directions for the 3D model.
- The direction of the nodal loads for the 3D model is Z (global 3) and Y (global 2) for the 2D model.

Both models were analyzed with mesh refinements. The finite element meshes of 2, 4, 8, and 16 elements for every real beam were used in the analyses. The 2 element mesh models with hinge-connector elements of 6 inch length at the beam-to-beam joint and also at the pinned ends were also analyzed. As stated earlier, the initial input files are created with I-DEAS. The Y-coordinates in case of the cap rib model are all zeros, since the rib lies in the global XZ plane. However, some of the Y-coordinates created with I-DEAS are not exactly zero but have very small finite values as shown below for the 4-element mesh model. Those errors are caused during the creation of the ABAQUS input file from the graphical model using the Pearl-Database menu in I-DEAS, since the nodal coordinates in the graphical model have these values.

1, 0.0000E+00, 0.0000E+00, 2.1234E+02
2,-1.3232E+02,**-1.5018E-04**, 2.0686E+02
3, 1.3232E+02, 0.0000E+00, 2.0686E+02
4,-2.6374E+02, **7.5092E-05**, 1.9046E+02
5, 2.6374E+02, 0.0000E+00, 1.9046E+02
6, 6.6161E+01, 0.0000E+00, 2.0960E+02
7,-6.6161E+01,**-7.5092E-05**, 2.0960E+02
8, 1.9803E+02, 0.0000E+00, 1.9866E+02
9,-1.9803E+02,**-3.7546E-05**, 1.9866E+02

It was found that this small error in the Y-coordinates was affecting the convergence of the solution. The analysis stopped a few increments after passing through the limit point. The analysis with the input files having corrected Y-coordinates had no such problem. The results in both the cases were exactly same except the convergence problem.

2.3.1 Nonlinear Analysis Procedure

The cap rib model in this section and the dome cap and dome models in the later sections are analysed with geometrically nonlinear analysis procedure. In this analysis, the strain-displacement relationship is nonlinear and equilibrium is satisfied for the deformed state. The nonlinear analysis methods used in this study are Newton-Raphson and modified Riks-Wempner methods. These methods are discussed briefly in Chapter 5.

The loading on the cap rib, the dome cap and the dome models is applied in two steps in the nonlinear analysis with ABAQUS as follows:

1. The Newton-Raphson method is used in the first step to load the dome upto its full dead load (16 psf).
2. The Riks method is used in the second step to apply the snow load upto the limit load and trace the equilibrium path beyond the limit point.

The total pressure at any instant is given by (Holzer, Wu, Tissoui, 1991)

$$p = p_D + \lambda p_L \tag{2.20}$$

where

p = total load pressure
p_D = dead load pressure (16 psf)
p_L = dead load pressure (20 psf)
λ = load proportionality factor (referred as L.P.F. hereafter)

2.3.2 Results for the Nonlinear Analysis of the Cap Rib Model

The load-deflection paths of node 1 (see Figure 2.2) for the 3D model is shown in

Figures 2.3. For the load condition in Figure 2.2, the critical load proportionality factors (L.P.F.) and the corresponding deflection of node 1 for all models are given in Table 2.5.

Table 2.5
Results for the Cap Rib Refined Mesh Models

3D model				
Mesh size	Critical L.P.F.	Vertical deflection (in.)	Maximum L.P.F.	Vertical deflection (in.)
2-element	7.116	1.557	22.03	9.019
4-element	6.971	1.660	20.66	8.792
8-element	6.901	1.670	20.41	8.503
16-element	6.868	1.667	20.38	8.324
2D model				
Mesh size	Critical L.P.F.	Vertical deflection (in.)	Maximum L.P.F.	Vertical deflection (in.)
2-element	19.57	5.40	22.02	9.027
4-element	18.31	5.5	20.66	8.795
8-element	17.88	5.418	20.41	8.505
16-element	17.72	5.351	20.38	8.326

Following observations were made in the analysis of the two models.

- The corrections in the nodal Y-coordinates had a pronounced effect on the convergence of the solution. For the small out of plane eccentricities of some of the nodes, the nonlinear analysis procedure abruptly stops a few increments after passing through the limit point for all models except the 2-element mesh model. The analysis proceeds normally for any number of increments specified if the Y-coordinate values are corrected to zero.
- Modification in the subroutine for the corrected Jacobian had no effect on results. The analyses with or without the correction converged, however, the one with the corrections converged more rapidly. The reason the analyses without corrections also converged may be the comparatively small size of the model. However, the complex models with a large

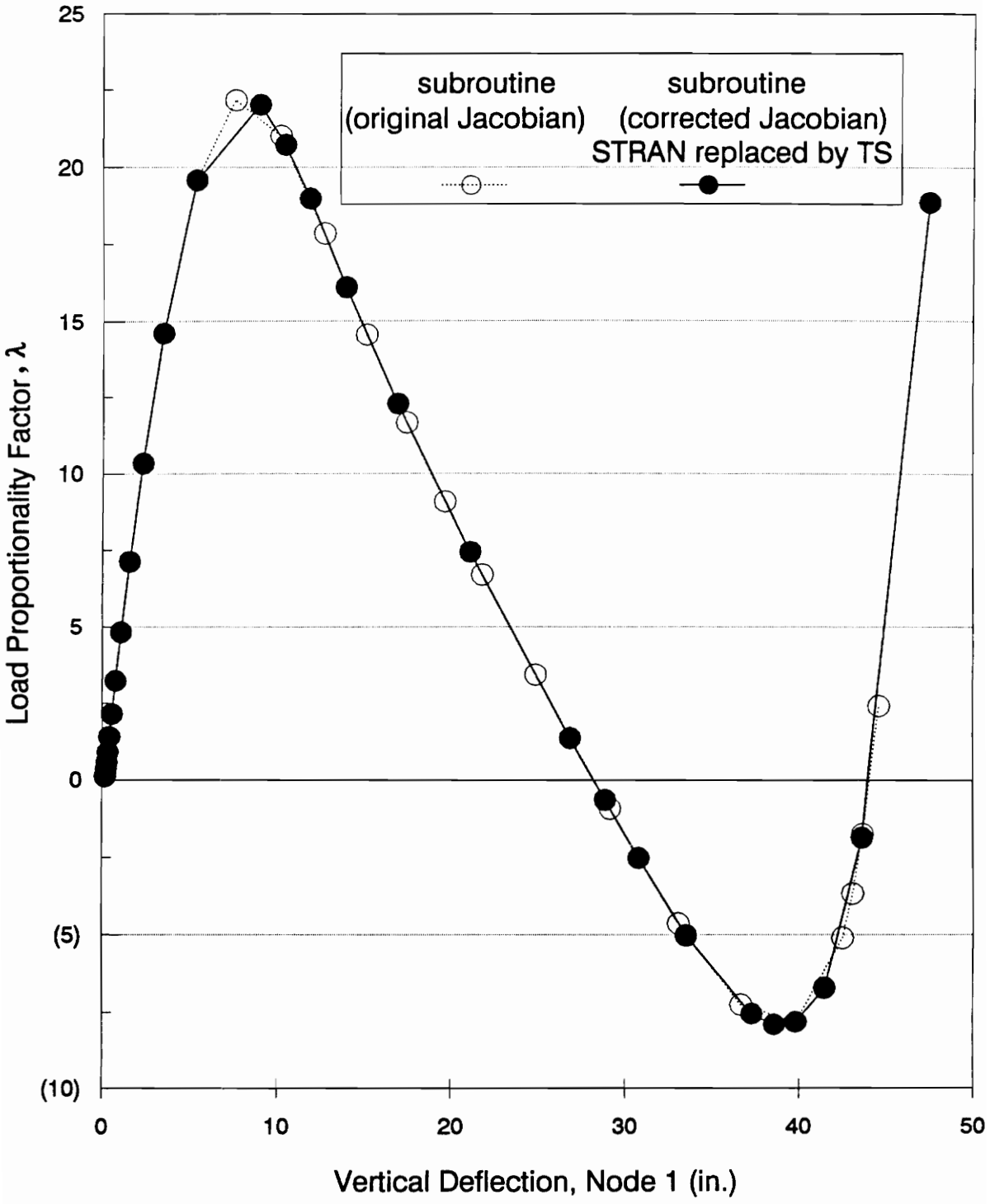


Figure 2.3 Cap Rib, Load-Deflection Path for 2-Element Mesh model

number of nodes and elements show difficulty in convergence, as discussed in the next section for the analysis of the dome cap models with various mesh sizes.

- The tolerances PTOL and MTOL have a major effect on the convergence as the mesh is refined. They are required to be relaxed successively to get convergence for bigger mesh sizes. The PTOL value in the range of 10^{-3}-10^{-4} of the maximum load on the structure should be specified according to section 7.3.12, ABAQUS. However, in case of the refined mesh models, much higher tolerances are required as given below. For the maximum load of 10^4 pounds, the tolerance values are

2 & 4 Element mesh : PTOL = 0.1 lb., MTOL = 1.0 lb-in

8 & 16 Element mesh : PTOL = 1.0 lb., MTOL = 10.0 lb-in

2 Element mesh, (hinge) connector elements :

PTOL = 100.0 lb., MTOL = 1000.0 lb-in

Even though the convergence depended on the tolerances, the values of L.P.F. and deflections obtained for any of the above tolerance values were the same at all the load increments.

From the above observations, it can be concluded that the convergence problem seems to be arising out of the numerical difficulty experienced by the Riks algorithm in getting a convergent solution in the post-buckled zone. This is caused by factors such as the inaccuracies in the nodal coordinates and the constitutive equations and also depends on the degree of mesh refinement. These factors are, however, found to have little or no effect on the solution accuracy itself.

The buckling modes of the cap rib models were studied with I-DEAS. It was found that the cap rib snaps through completely at the critical load.

2.3.3 Effect of Mesh Refinement

One of the objectives of analyzing the cap rib model was to study the effect of mesh refinement. It can be seen from Table 2.5 that for both models (2D and 3D), the difference in the maximum load proportionality factor between the 2-element and 4-element mesh is 6.2 percent. This difference drops down to 1.2 and 0.2 percent for the refinement from 4 to 8-elements and from 8 to 16-elements, respectively. Figure 2.4 shows the load-deflection path of node 1 for the 3D models with uniform mesh refinement

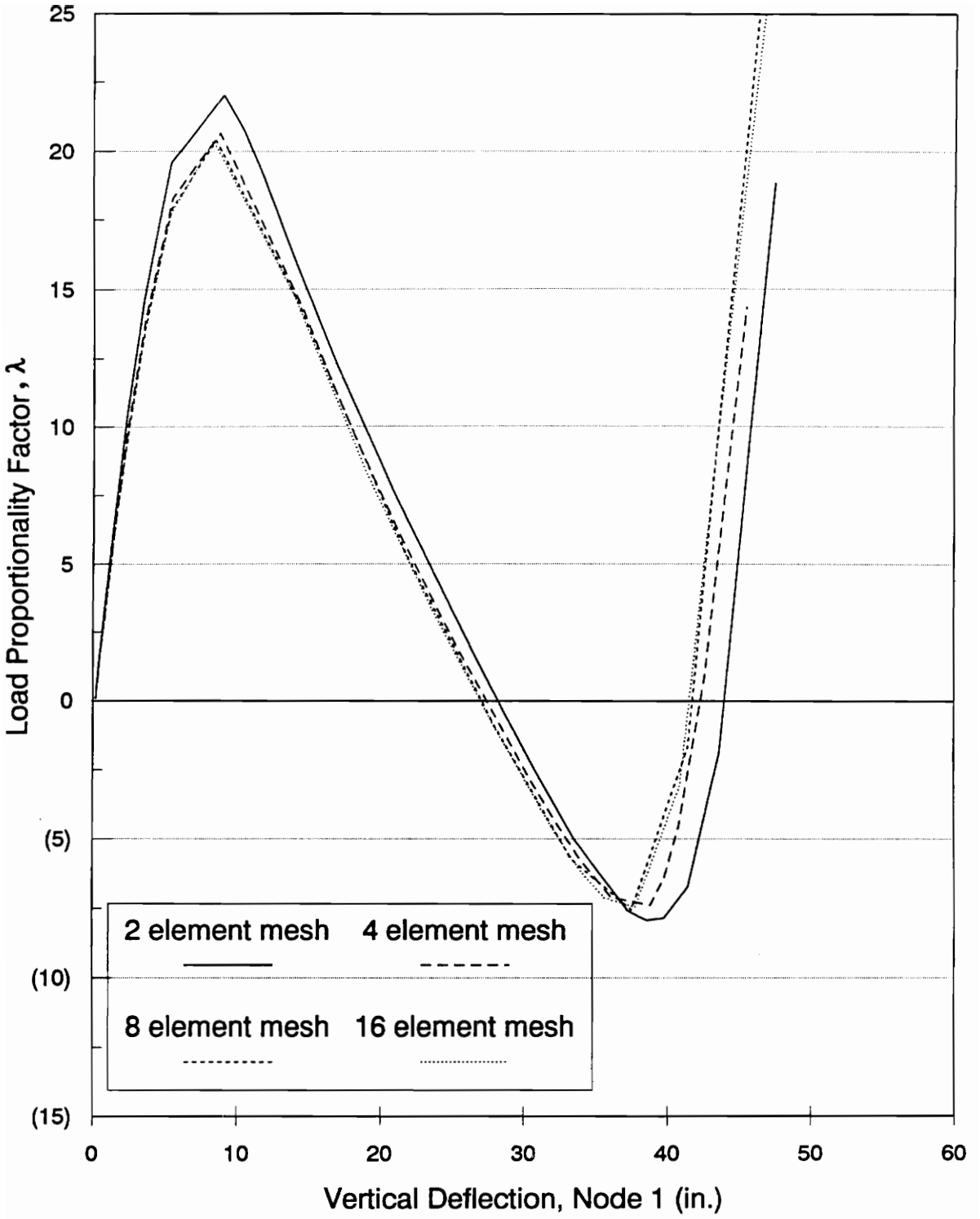


Figure 2.4 Cap Rib : Load-Deflection Paths for Refined Mesh Models

It is important to mention that in the successive mesh refinements after the 2-element mesh, the extra nodes were created on the elements of the 2-element mesh rather than on the curved arch rib lying on the surface of the dome cap. Also, the beams B23 or B33 are linear and not curved as in case of the beams in the actual dome cap. Two cap rib models having 4 and 8-element mesh sizes with all the extra nodes lying on the curved arch rib were created with I-DEAS and analyzed. The 3D models with B33 beam elements gave the results given in Table 2.6.

Table 2.6

Results for the Cap Rib models with Extra Nodes on Curved Arch of the Cap Rib

Mesh size	Critical L.P.F.	U2 (in.)	Maximum L.P.F.	U2 (in.)
4-Element	7.02	1.64	20.11	8.97
8-element	6.96	1.63	20.14	8.61

Comparing with the values in Table 2.5, the difference in the above L.P.F. and deflection values are about 2-3 percent of the values for the 4 element mesh model with nodes not on the curved arch and 1 percent for the 8-element mesh model. Note that these differences are true only for this model and may vary for other models with different span to height ratios and load conditions. Also, they may vary for the more complex models such as the dome cap and the full dome.

2.4 Convergence and Mesh Refinement Study of the Dome Cap

The dome cap model similar to the one used by Telang (1992) is analyzed for studying the convergence with respect to the observations in the last sections. Also, the finite element mesh is refined to get an estimate of the accuracy of the solution and the mesh required for a fairly accurate solution.

2.4.1 Load Discretization

An important concern in the refined mesh models is the discretization of the uniformly distributed load on the dome cap into equivalent nodal loads. The nodal loads are found

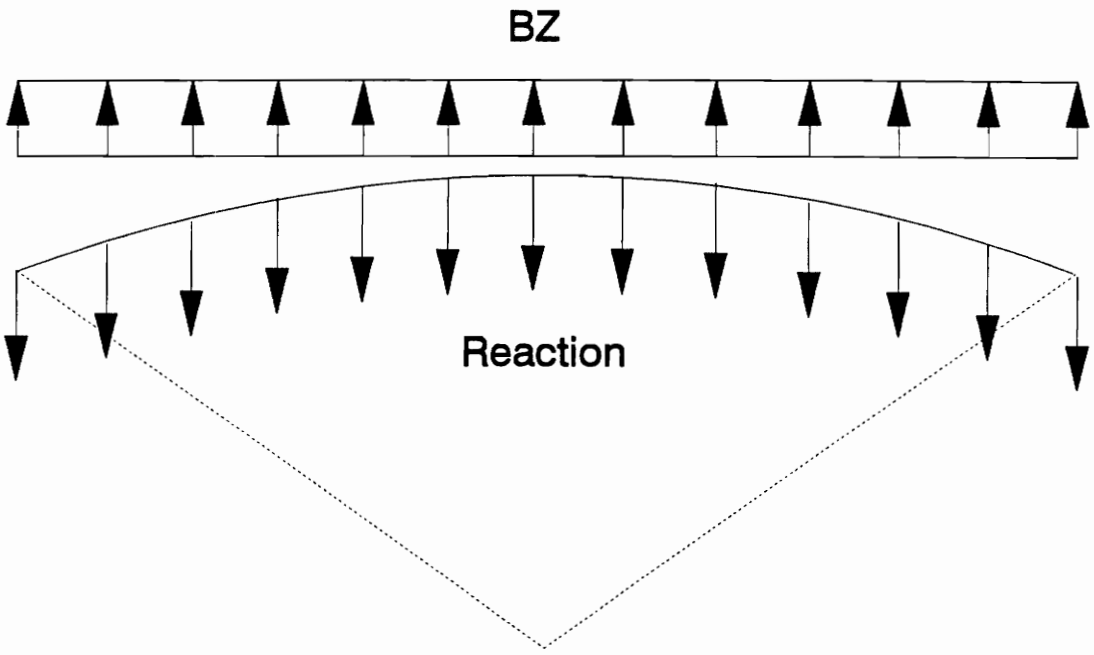


Figure 2.5 Shell Loading in ABAQUS to obtain Equivalent Nodal Loads

from the linear analysis of the dome cap with ABAQUS. The input file for this analysis consists of triangular and rectangular shell elements and no beam elements. The shell elements are used to specify the distributed dead and live (snow) loads in the upward (positive Z) directions. All the nodes in the finite element model are fixed in the Z-direction. This is done so that the downward (negative Z-direction) reactions obtained from the analysis represent the equivalent nodal loads.

The load on the shell elements can be specified in two different ways. It can be specified either as surface pressure (lb/in^2) on the shell elements or alternatively as the body weight (lb/in^3) of the shell elements. For example, the distributed load of 0.1 psi can be specified in ABAQUS as body weight (Figure 2.5) in following way.

```
*SHELL SECTION, ELSET=SHELL
0.001,3
*DLOAD
SHELL, BZ, 100.0
```

The thickness of the shell elements is given as 0.001 in., therefore to get a distributed load of 1.0 psi, the BZ must be equal to

$$\frac{0.1 \text{ psi}}{0.001 \text{ in}} = 100.0 \text{ lb/in}^3$$

The dead load must be given by the BZ loading since it truly represents the body weight of the dome members. The snow load to be specified on the dome, according to American National Standards Institute (ANSI) code, acts on the plan area rather than the surface area of dome. Therefore, the nodal snow load also is calculated using the BZ loading option. For the dome loading, the dead and snow loads of 16 psf (0.1111 psi) and 20 psf (0.1388 psi) are specified as 111.111 lb/in^3 and 138.888 lb/in^3 , respectively. The BZ option is used in the input files for linear analyses for finding the equivalent nodal loads.

For the refined mesh dome cap models, the uniformly distributed dead and live loads must be discretized into the nodal loads as uniformly as possible. To achieve this, the arrangement of the shell elements must be chosen carefully. Note that as the mesh is

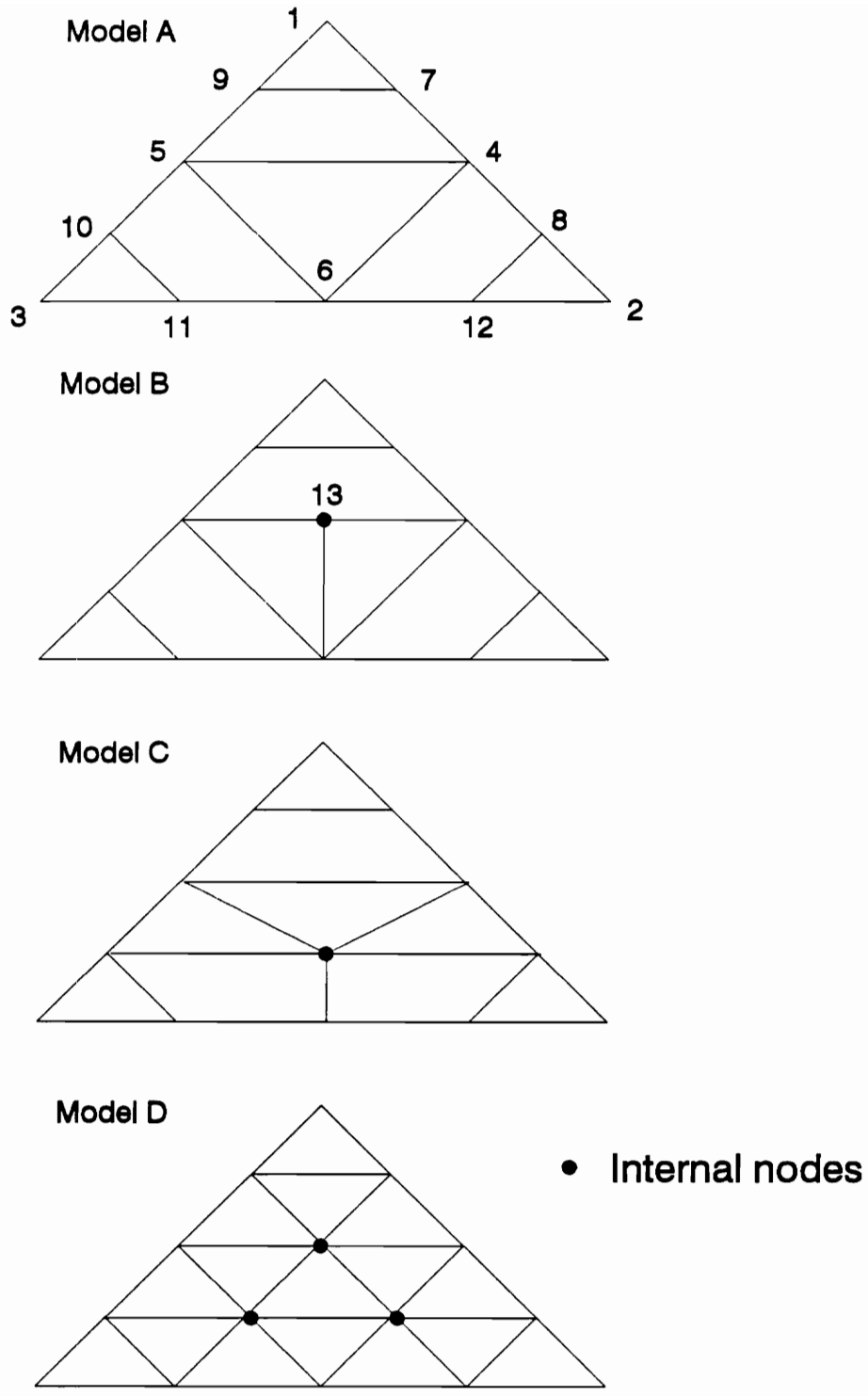


Figure 2.6 Shell Arrangements for the 4 Element Mesh Model of Sector of Dome Cap

refined, extra nodes created will also carry loads since the load discretization becomes more uniform and resembles the uniformly distributed load more closely.

Different configurations of the triangular and rectangular shell elements, as shown in Figure 2.6 for the 4-element mesh, were tried to discretize the load as uniformly as possible on a sector of the dome cap. The cases other than Case A require additional nodes to be created inside the sector in order to define the shell elements. These nodes are not fixed in the Z-direction in the linear analysis to find the nodal loads since these nodes do not exist in the actual finite element model and therefore do not carry any nodal loads. The reactions at the fixed nodes obtained from the linear analyses of these models are given in Table 2.7.

It can be seen from Table 2.7 that in case of the models with internal nodes, all the reactions do not have negative values. The values for node 6 are positive for these cases indicating upward reaction. This is not desirable since all the nodal loads in the finite element models must act downward if the distributed load is acting downward. For this reason, we cannot use the models with internal nodes. The model in Case A gives reasonably uniform distribution of nodal loads, therefore, this and the models with similar shell arrangements are used for the dome cap models for load discretization. For example, Figure 2.7 shows the shell arrangement for the 8-element mesh model. In future studies, the purlin can be modeled as beam elements instead of the truss elements so that extra nodes can be created on the purlin as the mesh is refined. These nodes can be fixed in Z-direction in that case so as to get negative reactions at all the nodes. For example, if the internal node 13 in Case B (Figure 2.6) is fixed in Z-direction, the reaction values as given in Table 2.8 are obtained.

2.4.2 Analysis of Dome Cap for Full and Half Snow Load Cases

The successive mesh refinements in the cap models were done such that the additional nodes required were created on the beam finite elements in the 2-element mesh and not on the great circles on which the actual beams of the dome cap lie.

Truss elements similar to the ones in the full dome model are created at the base of the dome cap for modeling the stiffening effect on the dome cap due to the rest of the dome.

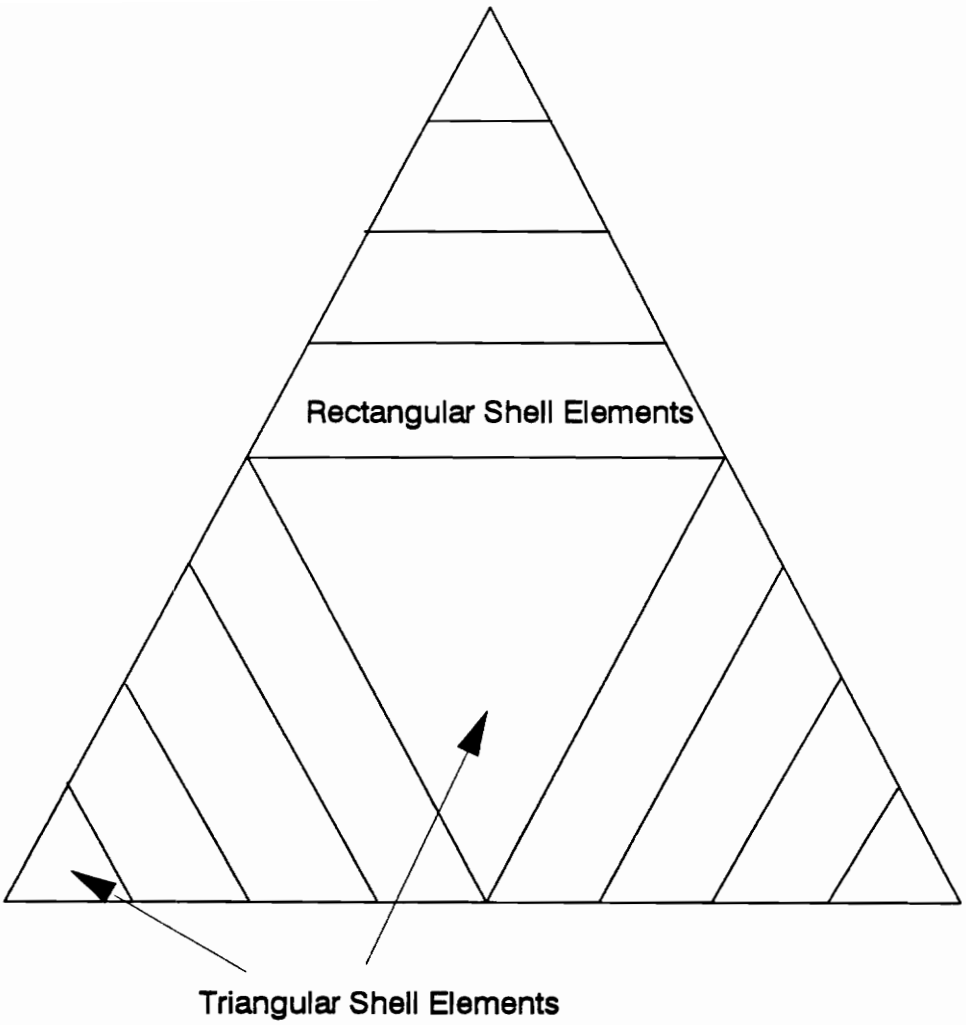


Figure 2.7 Shell Arrangement for 8 Element Mesh Model of Dome Cap Sector

Table 2.7

Nodal Reactions for the Cap Sector Models with Different Arrangements of Shell Elements

Node	MODEL A	MODEL B	MODEL B (node 13 fixed)	MODEL C	MODEL D
1	-63.25	-63.25	-63.25	-63.25	-63.25
2	-63.25	-63.25	-63.25	-63.25	-63.25
3	-63.24	-63.24	-63.24	-63.24	-63.23
4	-570.2	-3369.	-443.2	-203.8	-967.6
5	-570.2	-3372.	-443.2	-203.8	-967.6
6	-570.2	5030.	-570.2	17.66	251.1
7	-189.8	-189.8	-189.8	-189.8	-97.05
8	-189.8	-189.8	-189.8	-452.9	-205.9
9	-189.8	-189.8	-189.8	-189.8	-97.05
10	-189.8	-189.8	-189.8	-452.8	-205.9
11	-189.8	-189.8	-189.8	-586.9	-279.6
12	-189.8	-189.8	-189.8	-586.8	-279.7
13	-	0	-253.9	-	-

The cross sections of the base beams of the dome cap are made vertical (Figure A.4) so that $n_1 = (0 \;\; 0 \;\; \pm 1)$. This is done in order to simulate the full dome in which the base beams also have vertical cross sections. Refer to Appendix A for the discussion on the direction cosines of the beam local axes. Note that in the complete dome these beams are inclined so that the n_1 axis is tangent to the dome surface (Figure A.3b).

Also, the base beam dimensions are the same as the dimensions of the base beams in the full dome, even though the dimensions of all the beams are same in this region of the dome.

Main beams	11.0 " × 6.75 "
Base beams	12.25 " × 3.0 "

The dome cap with inclined base beams and with the same dimensions for all the beams is analyzed in the next chapter.

The boundary conditions are similar to the ones used by Telang (1992). The 6 base nodes 2, 3, 7, 10, 13, and 14 are restrained in the Z-direction for all the refined mesh models, i.e., the extra nodes created in the refined models are not restrained. This is because the boundary conditions in the unrefined and refined models must remain the same in order to analyze the same problem for the mesh refinement.

The details of the refined mesh cap models are as follows:

- Uniform mesh refinement :
  - 2 element mesh (Figure 2.8)
  - 4 element mesh
  - 8 element mesh
  - 16 element mesh (Figure 2.9)

- Selective mesh refinement :
  - 2 element mesh with hinge elements (Figure 2.10)
  - 4 element mesh with hinge elements
  - 8 element mesh with hinge elements

In the models with selective mesh refinement (Figure 2.10), the hinge elements are created at the real joints only, i.e., at the beam-to-beam joints with the Varax steel hub connector. The material laws used in the analysis are as follows.

- Linear laws (Figure 2.11):
  1. $E = 1.8 \times 10^6$ psi, $G = 1.6 \times 10^5$ psi
  2. $E = 2.2 \times 10^6$ psi, $G = 1.6 \times 10^5$ psi
- Bilinear law (Figure 2.11, and Figure 2.12):
  $E_t = 1.8 \times 10^6$ psi, $G = 1.6 \times 10^5$ psi
  $E_c = 2.2 \times 10^6$ psi,
- Nonlinear material law, Connors' model (Figure 2.12)

The analyses' results showed similar characteristics as the results of the cap rib model.

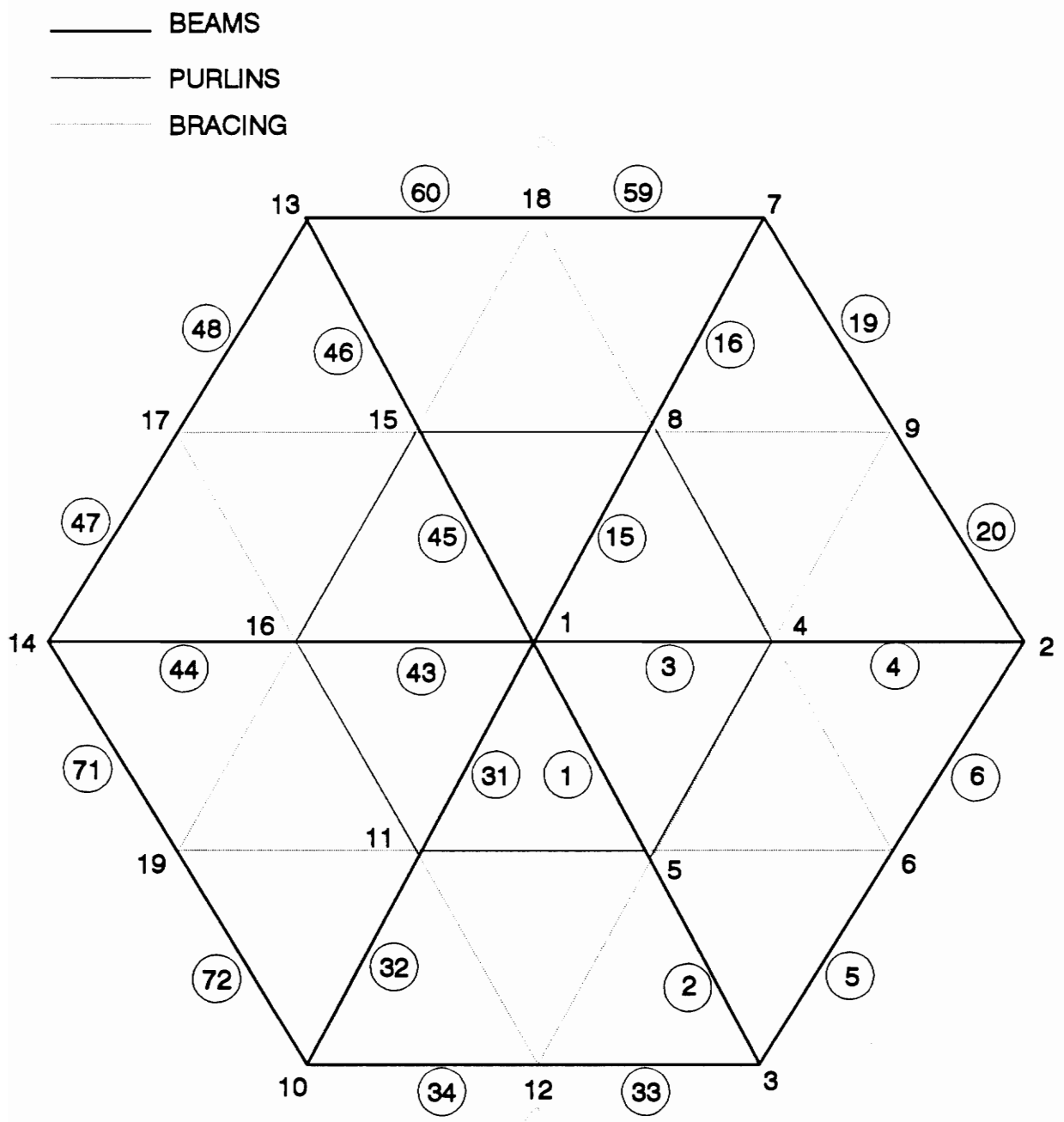


Figure 2.8 Dome Cap : 2 Element Mesh Model

✳ NODE

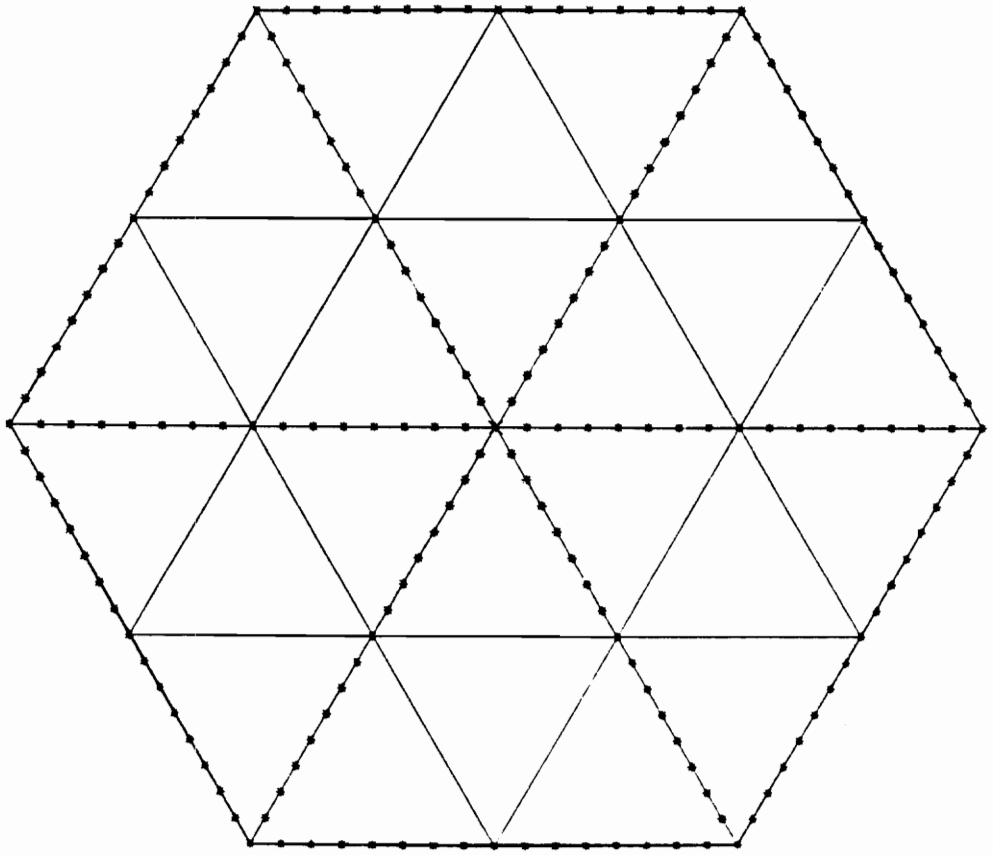


Figure 2.9 Dome Cap : 16 Element Mesh Model

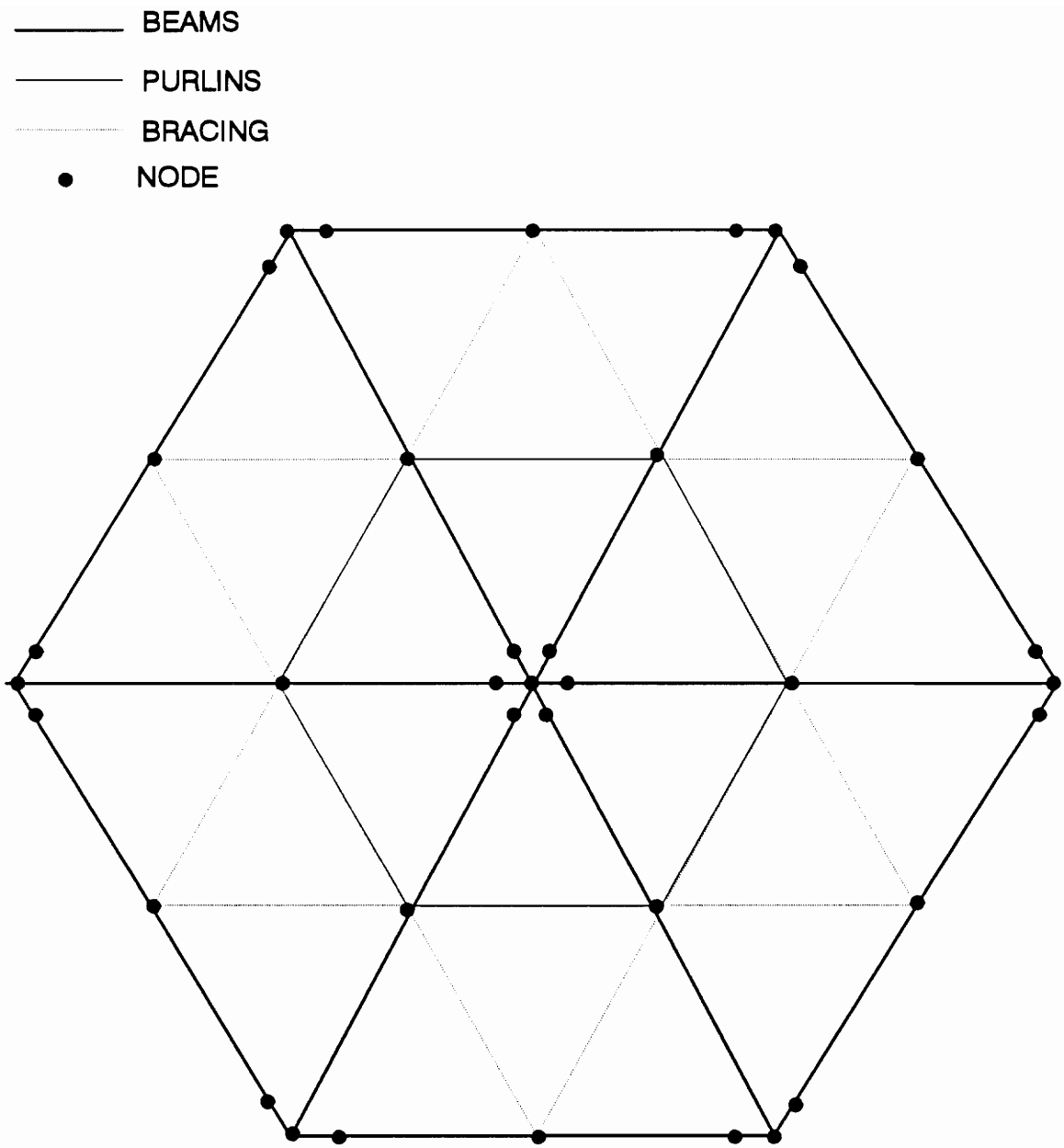
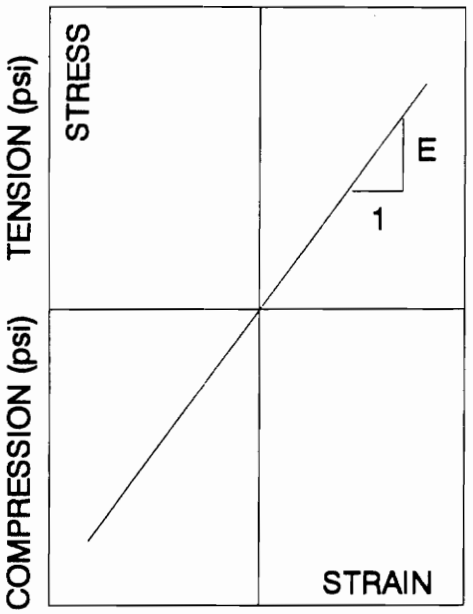
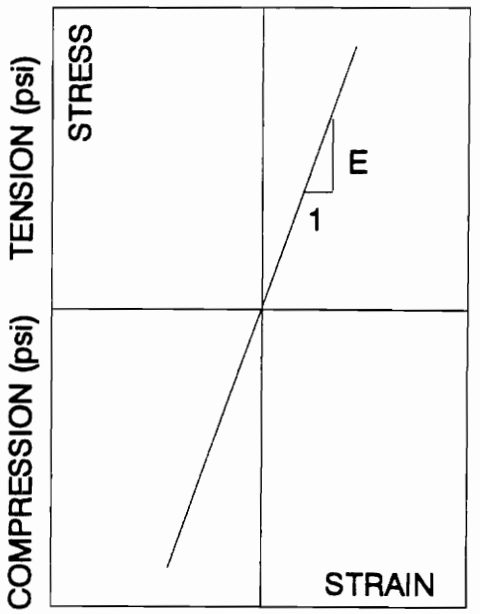


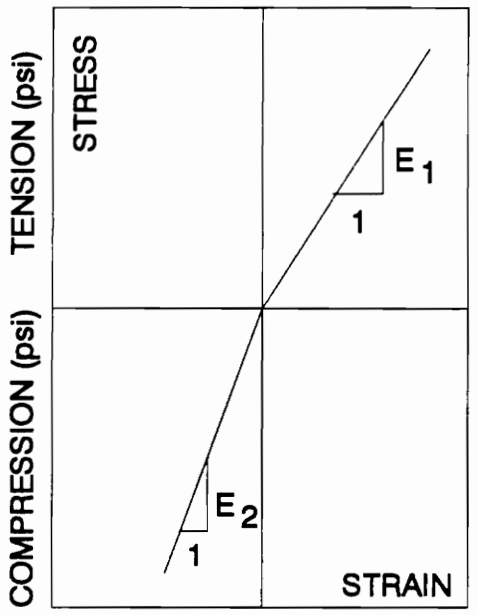
Figure 2.10 Dome Cap : 2 Element Mesh Model with Connector Elements



a) E = 1.8 E06 psi



b) E = 2.2 E06 psi



c) E_1 = 1.8 E06 psi, E_2 = 2.2 E06 psi

Figure 2.11 Material laws, a) Linear law 1, b) Linear law 2 c) Bilinear law

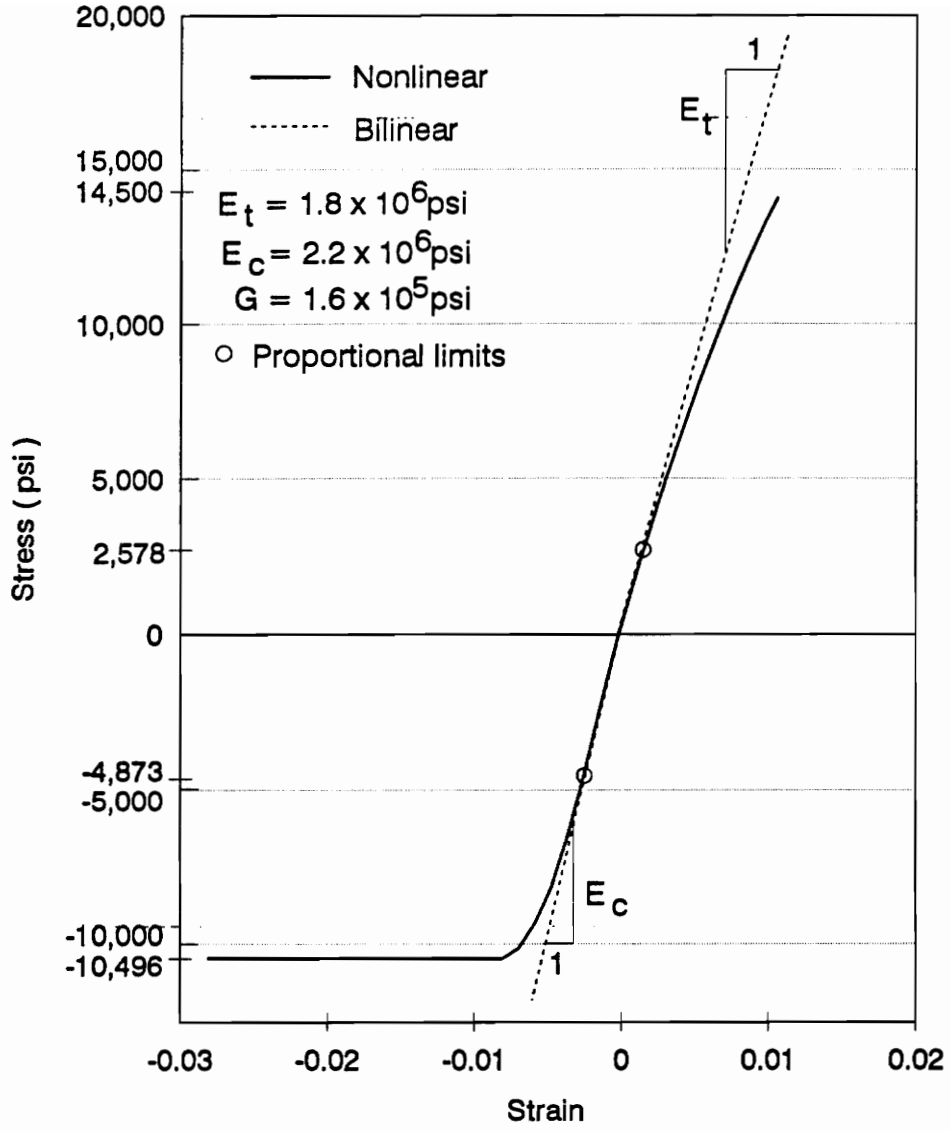


Figure 2.12 Nonlinear Material Law for Wood
Connors' Model, MC = 12 %, SG = 0.52

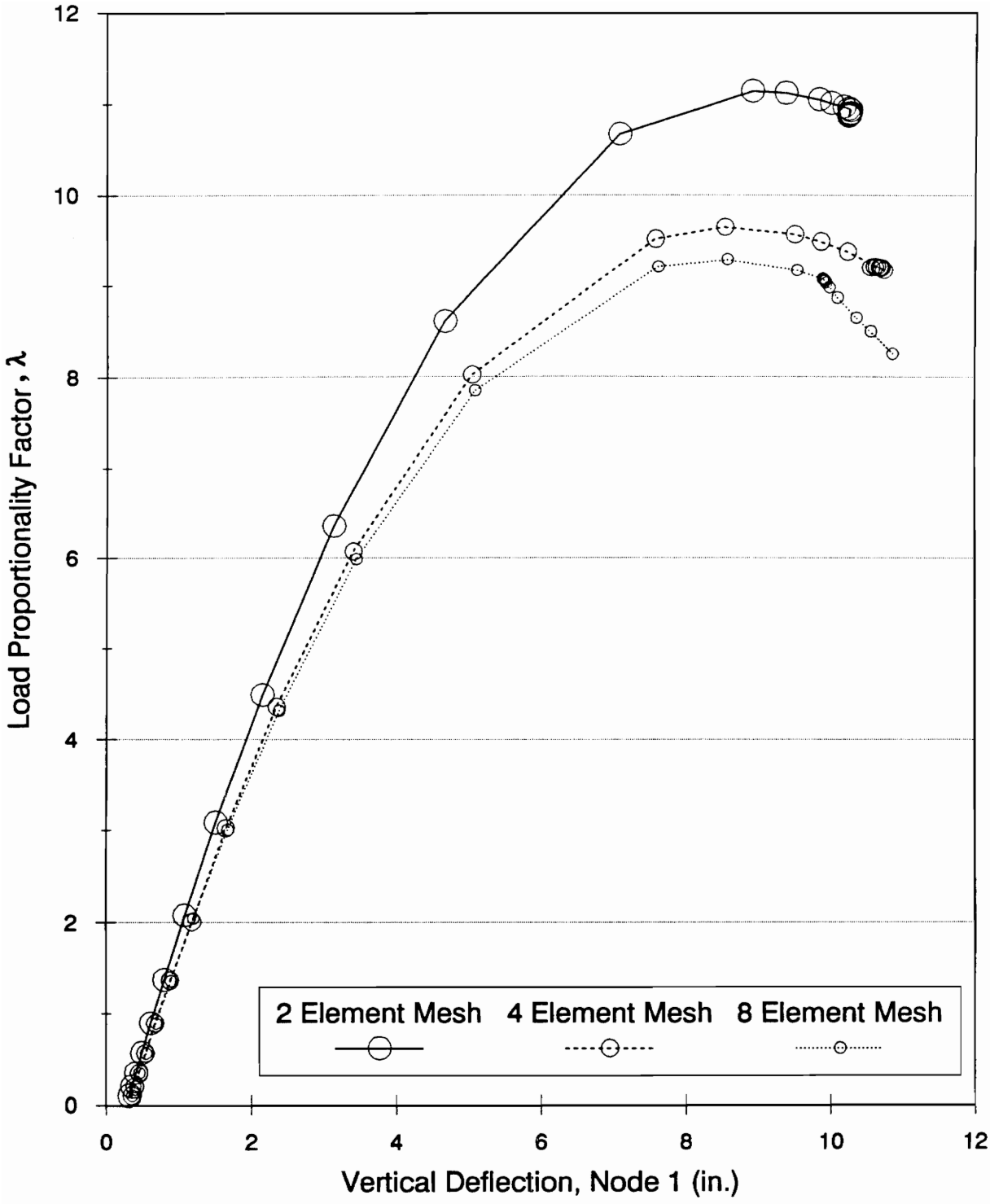


Figure 2.13 Dome Cap Model, Full Snow Load
Nonlinear Material Law, Original Subroutine UMAT

- In the analysis with the nonlinear material law using Telang's Jacobian formulation, convergence problem was encountered in all refined mesh models for both the full (Figure 2.13) and half snow load conditions. However, the analyses with the corrected Jacobian expression and nodal coordinates had no difficulty in converging (Figures 2.14 and 2.15). It was also observed that these corrections had little effect on the precision of the solution itself.

Table 2.8 shows the critical and maximum load proportionality factors (L.P.F.) and corresponding deflections of the apex node (node 1) for some of the models with and without the corrected Jacobian and nodal coordinates. Note that lower values of maximum L.P.F. but higher corresponding deflection values are obtained in the corrected models.

Table 2.8

Results for the Dome Cap Models with and without Corrections in UMAT

Mesh size		Model without corrected Jacobian		Models with corrected Jacobian	
		L.P.F.	Deflection (in)	L.P.F.	Deflection (in)
2	critical	10.67	-7.08	10.68	-7.08
	maximum	11.14	-8.91	10.76	-10.77
2 + Conn.	critical	10.19	-7.37	10.20	-7.37
	maximum	10.68	-9.94	10.46	-11.23
16	critical	9.13	-7.59	9.13	-7.59
	maximum	9.21	-8.54	9.13	-7.59

- The tolerance values specified in PTOL and MTOL need to be relaxed (increased) as the mesh is successively refined.

The critical L.P.F. and vertical deflection of the apex node (node 1) for all the dome cap models are given in Table 2.9 and 2.10 for full and half snow load conditions, respectively. It can be seen that, as the mesh is refined uniformly from 2 to 16 elements per beam, the differences in the critical load values for the full snow load case are 11 percent, 3.5 percent and 0.7 percent between the successive refined mesh models as

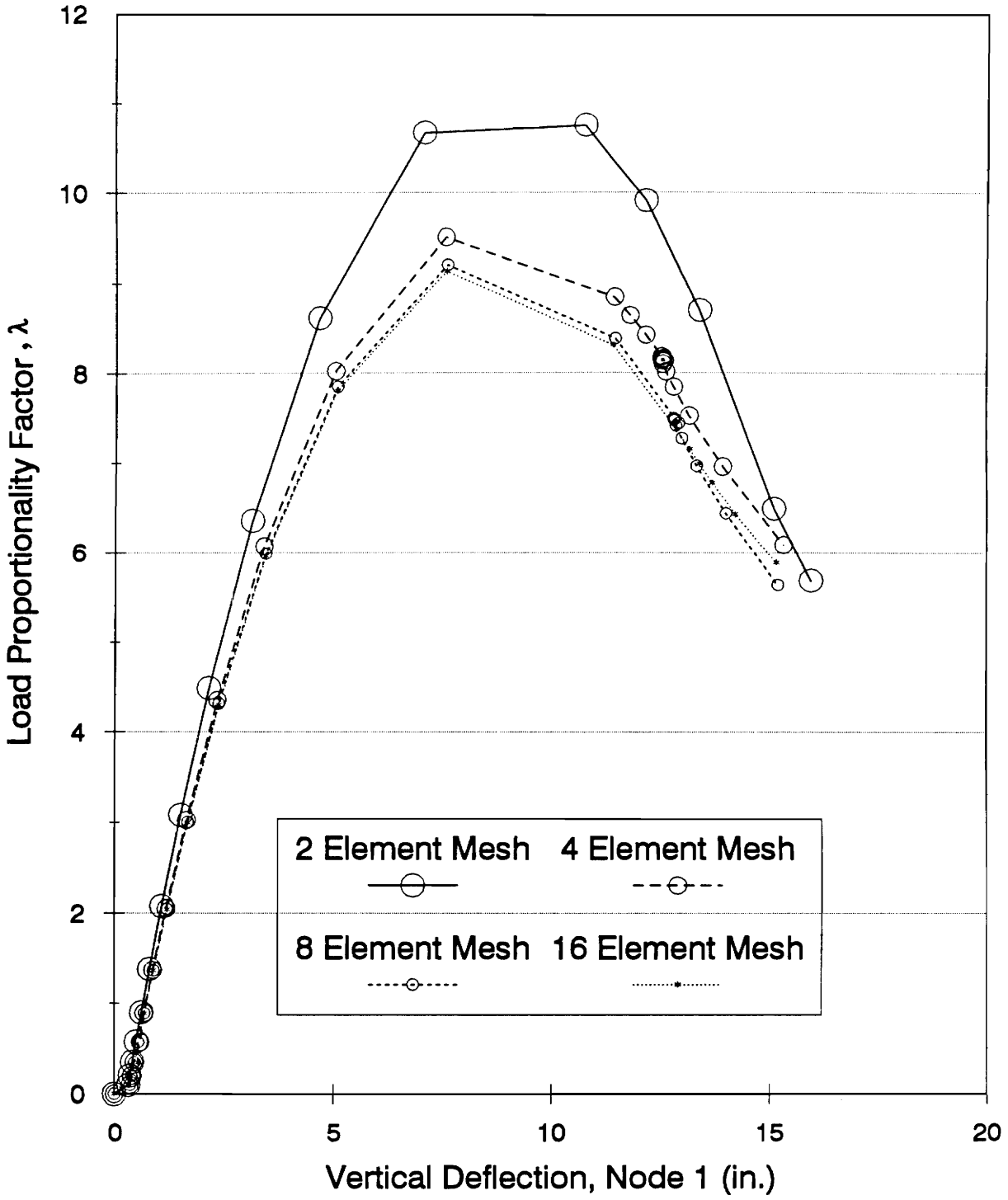


Figure 2.14 Dome Cap Model, Full Snow Load Nonlinear Material Law, Modified Subroutine UMAT

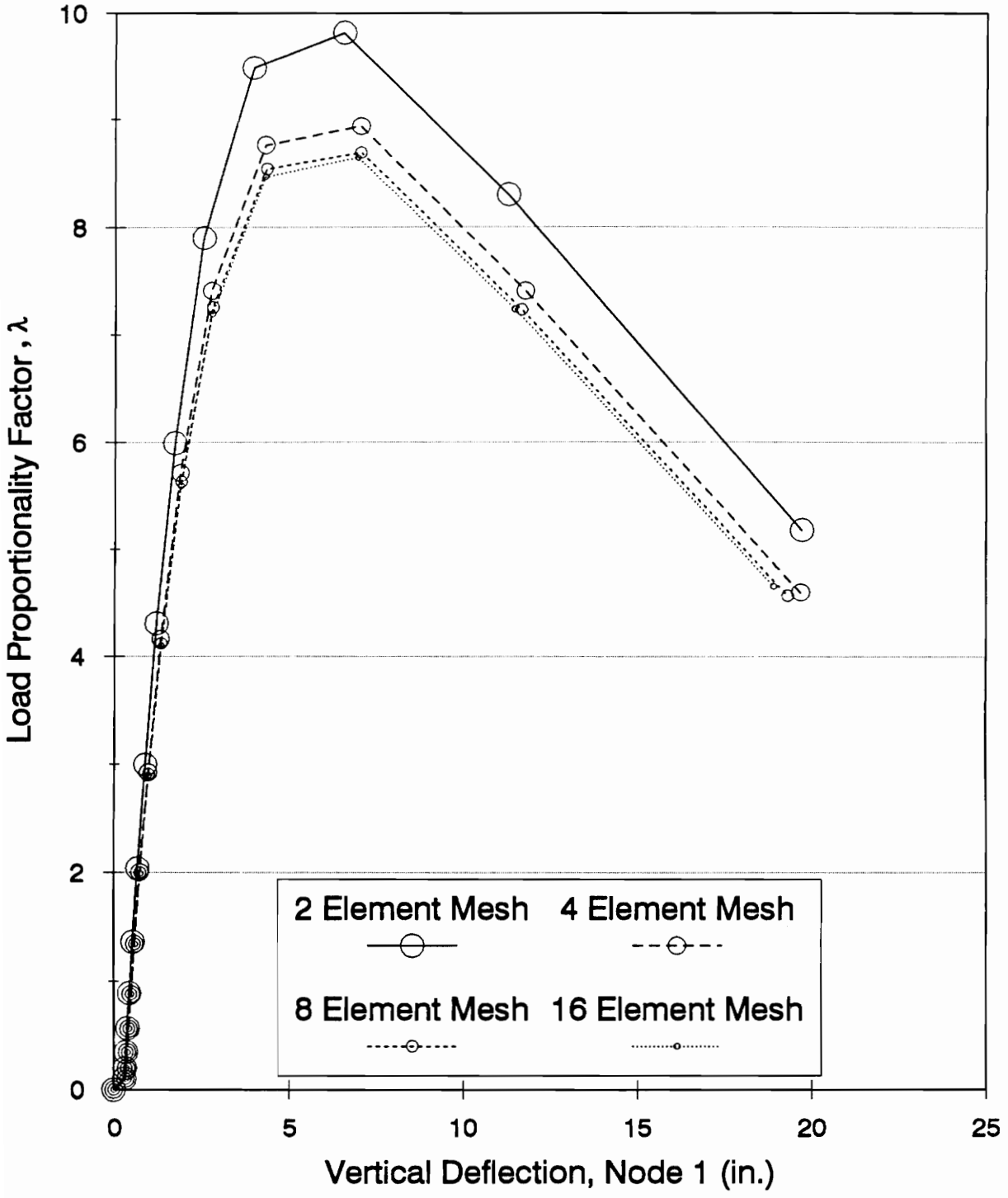


Figure 2.15 Dome Cap Model, Half Snow Load Nonlinear Material Law, Modified Subroutine UMAT

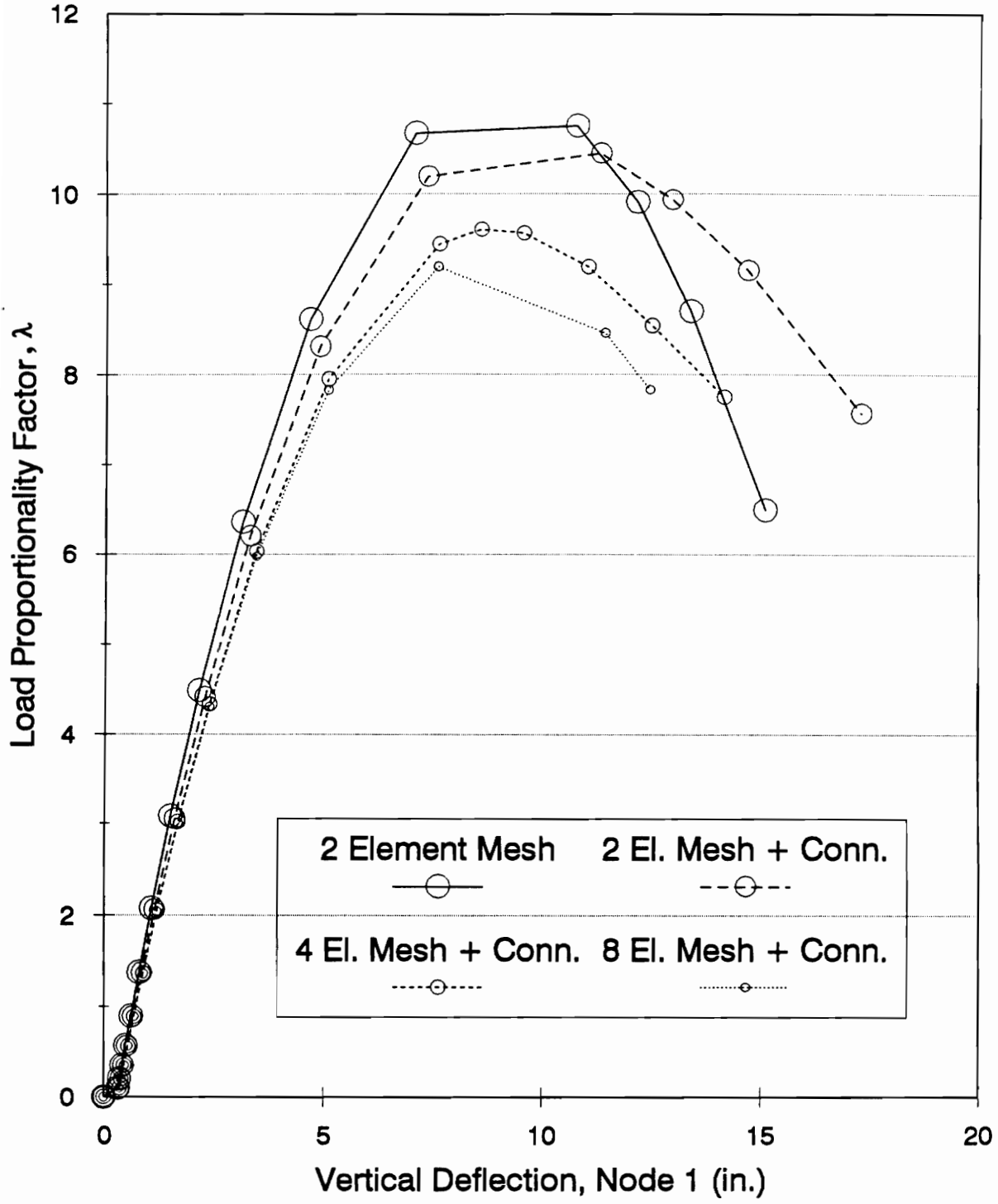


Figure 2.16 Dome Cap Model, Full Snow Load
Refined Mesh Models with Hinge Elements

Table 2.9

Results for the Dome Cap Models with Mesh Refinement, Full Snow Load

Mesh size	Critical L.P.F. (Vertical deflection of node 1 in inches)			
(Full snow)	Linear law 1	Linear law 2	Bilinear law	Nonlinear
2	9.75 (-8.31)	10.87 (-7.10)	10.77 (-7.15)	10.68 (-7.08)
4	8.56 (-8.87)	9.77 (-7.58)	9.65 (-7.66)	9.51 (-7.57)
8	8.26 (-8.89)	9.48 (-7.66)	9.36 (-7.71)	9.20 (-7.61)
16	8.20 (-8.86)	9.41 (-7.64)	9.29 (-7.68)	9.13 (-7.59)
2 + Conn.	9.23 (-8.54)	10.32 (-7.32)	10.23 (-7.39)	10.20 (-7.37)
4 + Conn.	8.49 (-8.86)	9.66 (-7.63)	9.55 (-7.68)	9.45 (-7.63)
8 + Conn.	8.25 (-8.84)	9.45 (-7.63)	9.33 (-7.68)	9.19 (-7.60)

Table 2.10

Results for the Dome Cap Models with Mesh Refinement, Half Snow Load

Mesh size	Critical L.P.F. (Vertical deflection of node 1 in inches)			
(half snow)	Linear law 1	Linear law 2	Bilinear law	Nonlinear
2	9.77 (-8.70)	11.62 (-12.01)	10.76 (-11.94)	9.82 (-6.56)
4	8.79 (-9.15)	10.39 (-12.38)	9.60 (-12.27)	8.94 (-7.04)
8	8.55 (-9.01)	10.15 (-12.16)	9.36 (-12.31)	8.69 (-7.04)
16	8.50 (-8.86)	10.13 (-11.93)	9.35 (-11.91)	8.64 (-6.95)
2 + Conn.	8.94 (-12.62)	11.51 (-10.38)	10.71 (-10.33)	9.67 (-6.30)
4 + Conn.	8.67 (-10.0)	10.53 (-11.30)	9.76 (-11.24)	8.96 (-6.78)
8 + Conn.	8.30 (-6.14)	10.25 (-11.56)	9.47 (-11.56)	8.71 (-6.88)

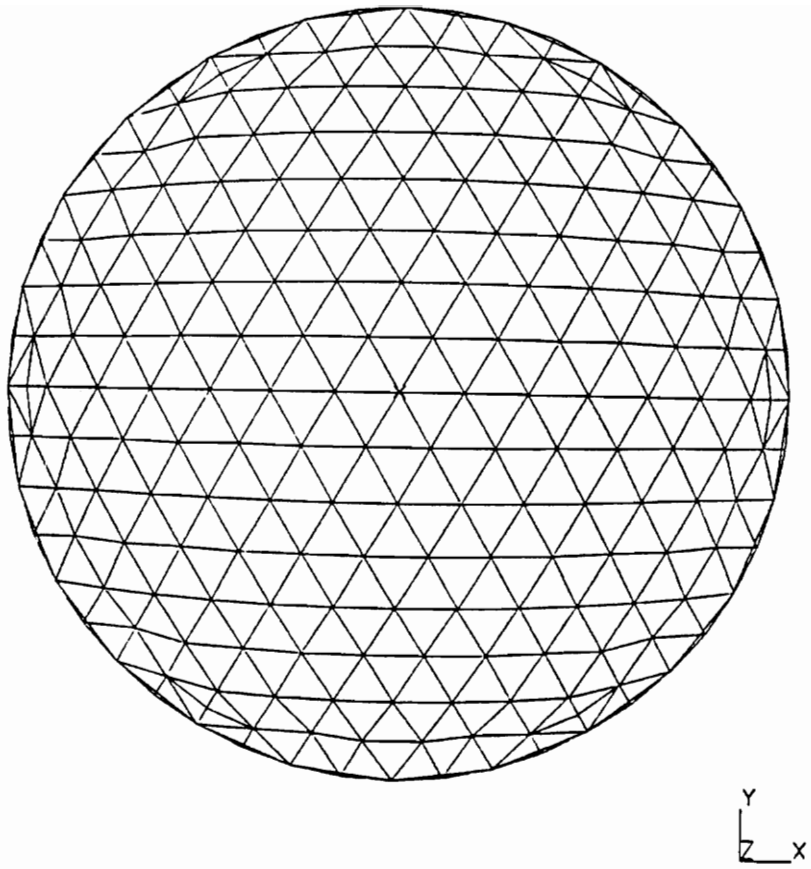
compared to the lesser refined model. For example, the difference between 4 and 8-element mesh models is 3.5 percent of the value for the 4-element mesh model. The corresponding differences in the deflection values are about 7 percent, 1 percent, and 0.3 percent, respectively. For the half snow load condition, these values are slightly less, 10 percent, 3 percent and 0.6 percent, respectively.

The load-deflection paths for node 1 in case of full and half snow load conditions for all the models with uniform mesh refinement and the nonlinear material law (Figure 2.12) are shown in Figure 2.14 and 2.15 respectively, to show the effect of mesh refinement. Figure 2.16 shows the response of models with hinge elements (6 inch length) as compared to the 2-element mesh model with the full snow load.

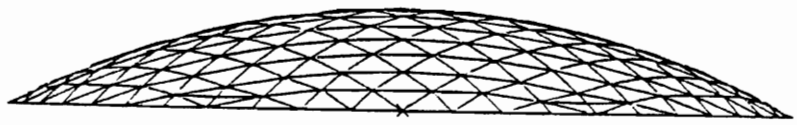
The percent differences in the critical load factors, on an average, for the successive mesh refinements from 2 to 16 elements are 11, 3.5 and 0.75 for the full snow load and 10, 2.8 and 0.60 for the half snow load, each compared to the lesser refined mesh model.. The percent difference in the critical load factors, on an average, between 2 and 16 element mesh models is 15.5 for the full snow load and 12.5 for the half snow load. The percent difference in the critical load factors between 4 and 16 element mesh models are 4.2 and 3.3, respectively.

2.5 Analysis of Full Dome for Full and Half Snow Load Cases

The dome model with truss bracing (Figure 2.17) was analysed by Telang (1992). It was analysed for the full and half snow load conditions with the modifications suggested earlier in this chapter: The nodal coordinates were corrected by adjusting the near-zero values to exact zero values and the Jacobian was modified in user subroutine UMAT for defining the nonlinear material law. The boundary conditions used in the analysis were the same as used by Telang. All perimeter nodes were fixed in the Z-direction and the four nodes at quarter points were alternatively restrained in the X and Y directions to prevent rigid body rotation of the dome. The tolerance values used in the analysis were PTOL = 20, MTOL = 3000. There was no convergence problem experienced in the analysis. The results from the analysis are as follows.



(a)



(b)

Figure 2.17 Dome Model with Truss Bracing a) Plan View, b) Elevation

1. Full Snow Load :

With corrected Jacobian and nodal coordinates:

λ_{cr} = 10.11 U3 (Node 1) = -8.96 in.

λ_{max} = 10.36 U3 (Node 1) = -9.419 in.

With original Jacobian and nodal coordinates:

λ_{cr} = 9.94 U3 (Node 1) = -8.60 in.

2. Half Snow Load Case:

With corrected Jacobian and nodal coordinates:

λ_{cr} = 7.46 U3 (Node 1) = -3.616 in.

λ_{max} = 8.01 U3 (Node 1) = -3.952 in.

With original Jacobian and nodal coordinates:

λ_{cr} = 8.01 U3 (Node 1) = -6.7 in.

The deflected shapes (buckling modes) for full and half snow load are shown in Figures 2.18 and 2.19, respectively.

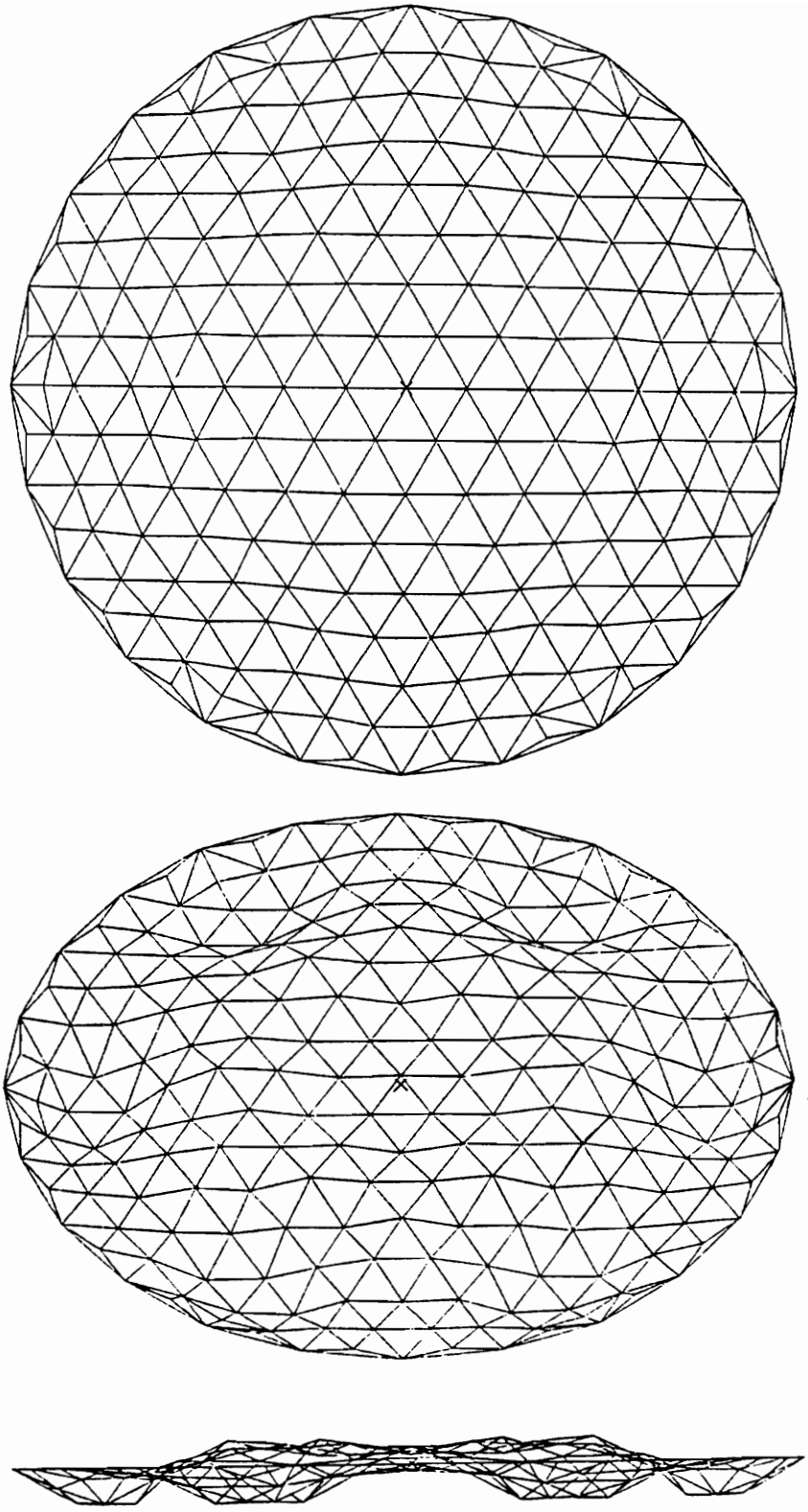


Figure 2.18 Buckling Mode for the Dome Model with Truss Bracing: Full Snow

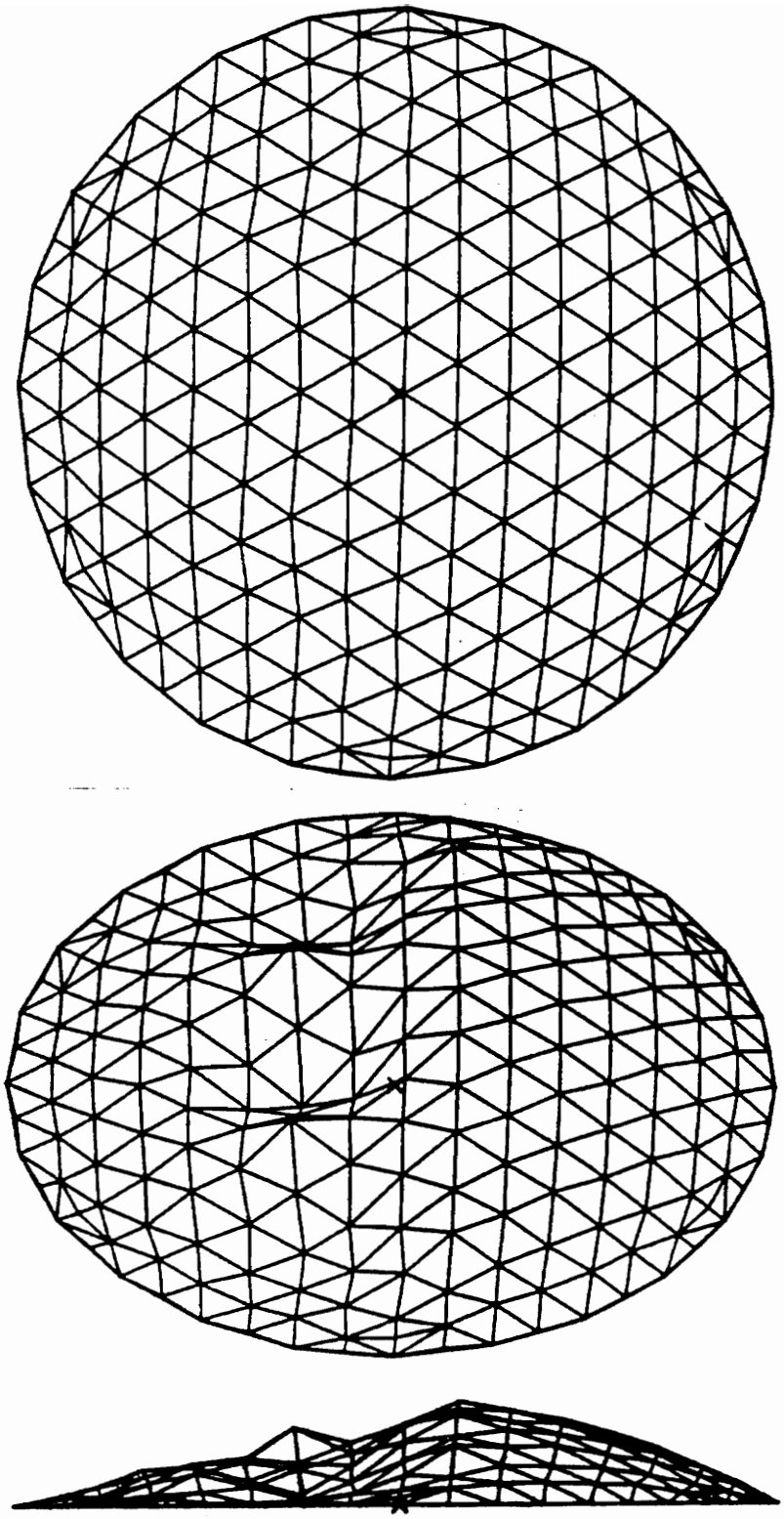


Figure 2.19 Buckling Mode for the Dome Model with Truss Bracing: Half Snow

Chapter 3

Parametric Studies of the Dome Cap Model

3.1 Introduction

The modeling assumptions for the dome cap model analyzed in chapter 2 are similar to those for the full dome model. A dome cap model similar to the actual dome cap in the full dome but with a tension ring is analysed in section 3.2. The decking is modeled by truss bracing as done for the model in Chapter 2. The tension ring is necessary to model the stiffening effect offered by the rest of the dome on the dome cap. The area of tension ring is varied in the analysis of the model used in section 3.2 to study its effect on the dome cap behavior. The results are presented in section 3.3. A sensitivity study of the ultimate load on the dome cap relative to the variation in the value of the ultimate compressive stress is performed in section 3.4. This is done by varying the nonlinear law for wood developed by Connors (1989). Finally, analyses with varying stiffness of the hinge-connector elements is done in section 3.6 to study the effect of joint flexibility on the ultimate load of the dome cap. The modified dome cap model used in section 3.2 is analyzed in chapter 4 using Saint-Venant's torsion solution to study the effect of the warping of the rectangular beam cross section.

3.2 Modified Dome Cap Model

The base beams of dome cap in the real structure are oriented such that their top surface if flush with the top of the vertical main beams I ('meridional beams') and also the surface of dome. They are inclined with respect to the vertical main beams I so that their cross-sectional axis n_1 points towards the center of sphere (Figure A.3b in Appendix A). These beams also are called main beams I in the full dome finite element model, and have same cross section as the vertical main beams, i.e., 11.0" × 6.75". The dome cap model in chapter 2 is modified to take into account the inclined base beams with the same cross section dimension as the main beams. The extra nodes on the base beams in the unrefined (2-element) mesh model lie on the surface of the dome and their coordinates need not be

revised. The direction cosines are modified as explained in Appendix A and the correct dimensions are used in this model of the dome cap. The boundary conditions in the analysis remain same as before. The material laws used in the analyses are the same as given in section 2.4.2.

Figures 3.1 and 3.2 show the response of this modified model with various material laws for full and half snow load, respectively. In case of the analysis with nonlinear material law, the critical load proportionality factors (L.P.F.) for full and half snow load conditions are 10.95 and 11.07, respectively. The vertical deflections of the apex node for the same are 7.04 in. and 6.02 in.

The maximum stresses obtained in the analysis with nonlinear material law are as given below. The dome cap finite element model is shown in Figure 2.8.

Full Snow Load :

Maximum tensile stress	=	5610 psi	(element 5 at node 6)
Maximum compressive stress	=	-8139 psi	(element 44 at node 16)

Half Snow Load :

Maximum tensile stress	=	1.20×10^4 psi	(element 15 at node 8)
Maximum compressive stress	=	-1.00×10^4 psi	(element 16 at node 8)

3.3 Variation in the Area of Tension Ring

The dome cap models analysed so far had a tension ring with a cross section area of 12 $in.^2$, which is the same as the area of the tension ring in the full dome model. However, since the tension ring is used in the dome cap model only to give the stiffening effect offered by the dome, it is necessary to study the effect of the variations in the area of tension ring on the buckling response of the dome cap.

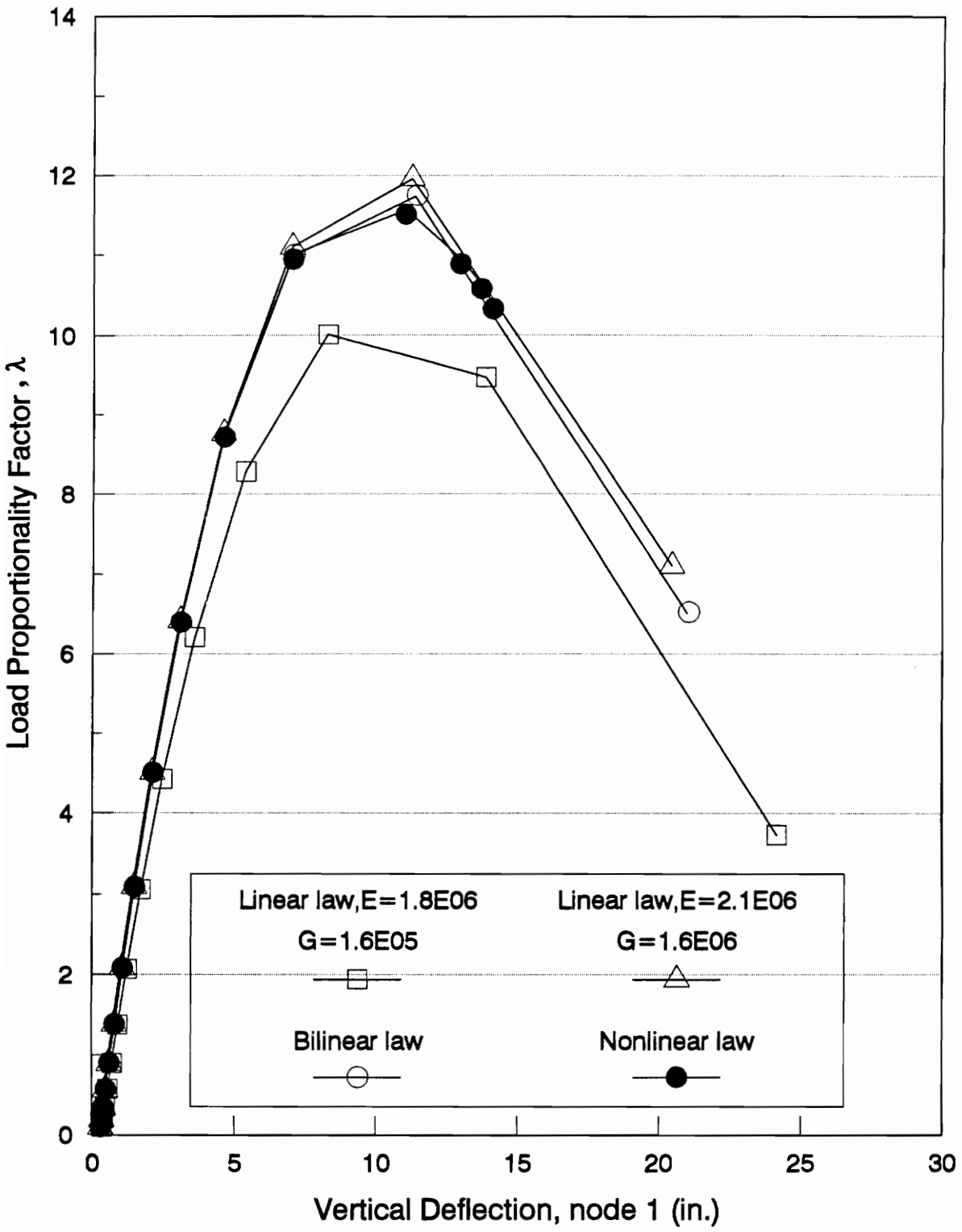


Figure 3.1 Modified Dome Cap Model
Full Snow Load, All Material Laws

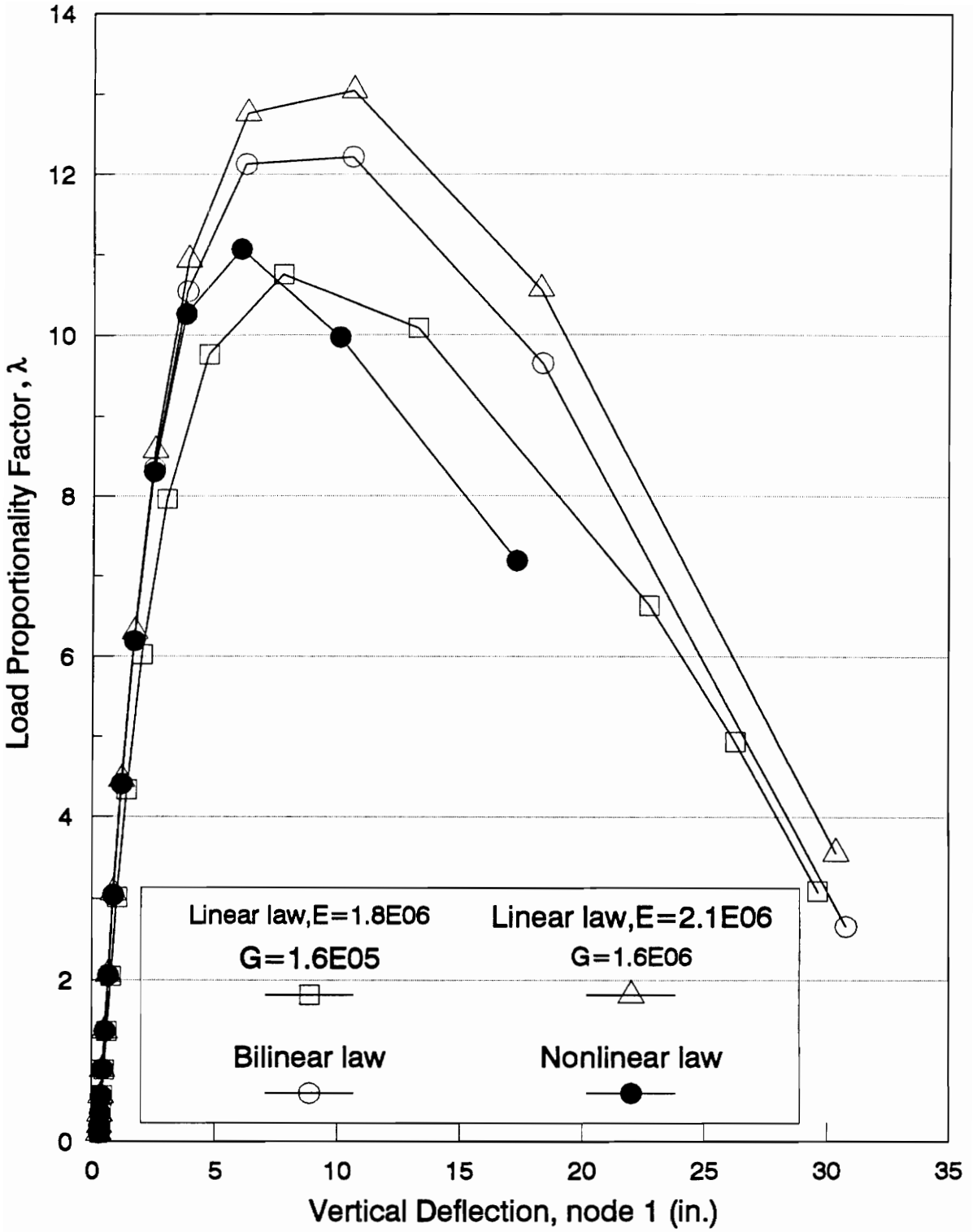


Figure 3.2 Modified Dome Cap Model
Half Snow Load, All Material Laws

Two different areas of tension ring were used. Figure 3.3 shows the response of the 2-element mesh model for full snow load with nonlinear material law and with 8 $in.^2$ and 4 $in.^2$ tension ring area. The same for half snow load is shown in Figure 3.4. It can be seen that the cap model is sensitive to the stiffness of the tension ring. This indicates the important role played by the tension ring in the stability of the dome cap and the full dome. The results obtained from the analysis of these models are as given below. The stresses in the elements can be studied in relation to the stress-strain law for wood shown in Figure 2.12.

Area of tension ring = 8 in^2

Full snow load: λ_{cr} = 10.28, Deflection (node 1) = 8.25 in.
Maximum tensile stress = 6326 psi (element 5 at node 6)
Maximum compressive stress = -8318 psi (element 44 at node 16)
Half snow load: λ_{cr} = 10.84, Deflection (node 1) = 6.82 in.
Maximum tensile stress = 1.20×10^4 psi (element 15 at node 8)
Maximum compressive stress = -1.00×10^4 psi (element 16 at node 8)

Area of tension ring = 4 in^2

Full snow load: λ_{cr} = 8.78, Deflection (node 1) = 11.1 in.
Maximum tensile stress = 7542 psi (element 5 at node 6)
Maximum compressive stress = -8519 psi (element 44 at node 16)
Half snow load: λ_{cr} = 10.31, Deflection (node 1) = 8.74 in.
Maximum tensile stress = 1.30×10^4 psi (element 15 at node 8)
Maximum compressive stress = -9762 psi (element 16 at node 8)

3.4 Variation in the Nonlinear Constitutive Law

A nonlinear material law for softwood (Yellow Poplar) developed by Connors (1989) has been used so far to analyze the dome cap model. It is discussed in detailed and used by Telang (1992) to analyze the dome cap and the dome models. The constitutive model consists of individual segments in tension and compression, each defined by a different mathematical equation containing moisture content (MC) and specific gravity (SG) values for the wood. SG and MC values used in the dome cap models so far are the ones used in Connors' model, i.e., 0.52 and 12 % respectively. The ultimate compressive stress (σ_{cu})

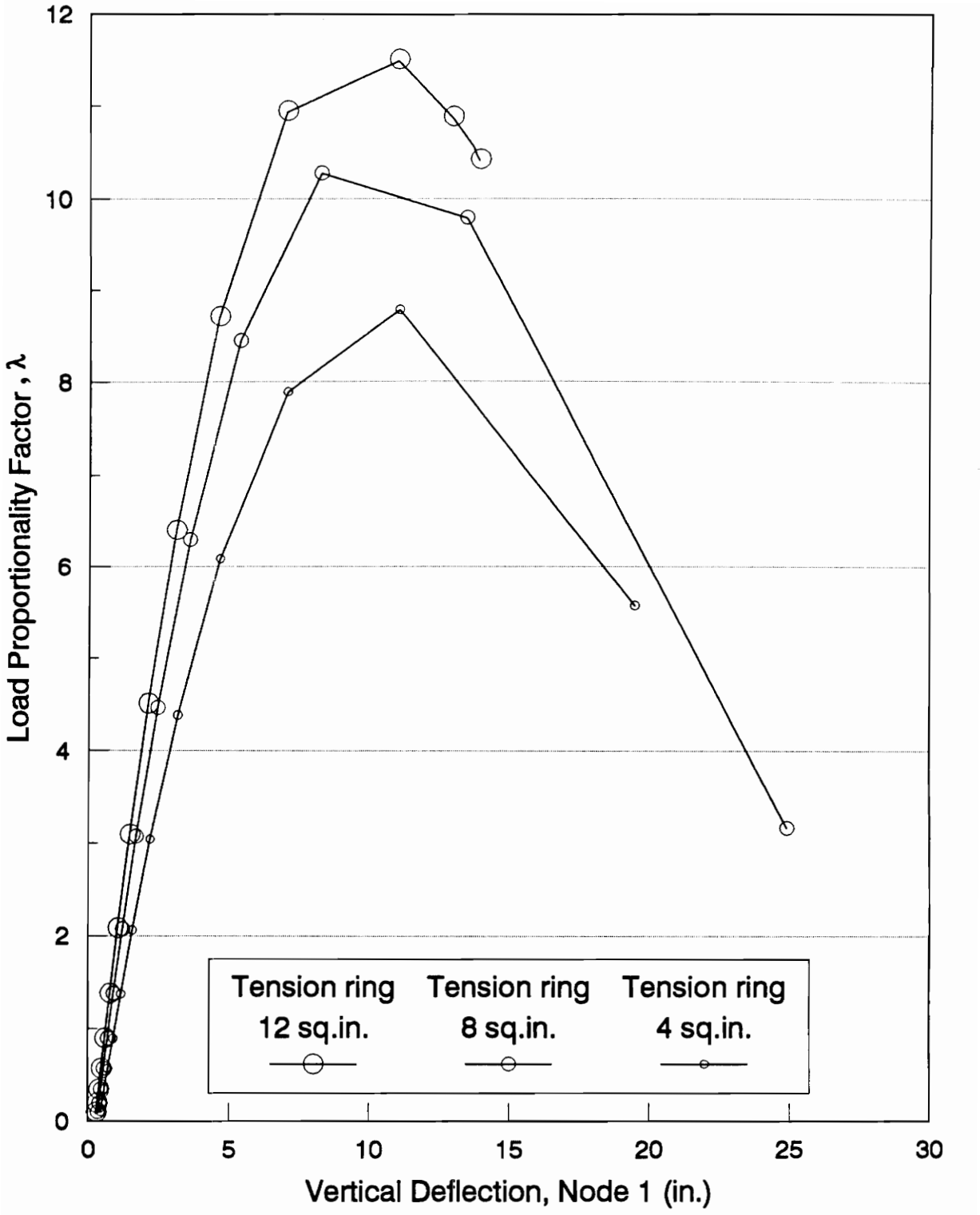


Figure 3.3 Dome Cap Model, Different Areas of Tension Ring, Full Snow Load, Nonlinear Material Law

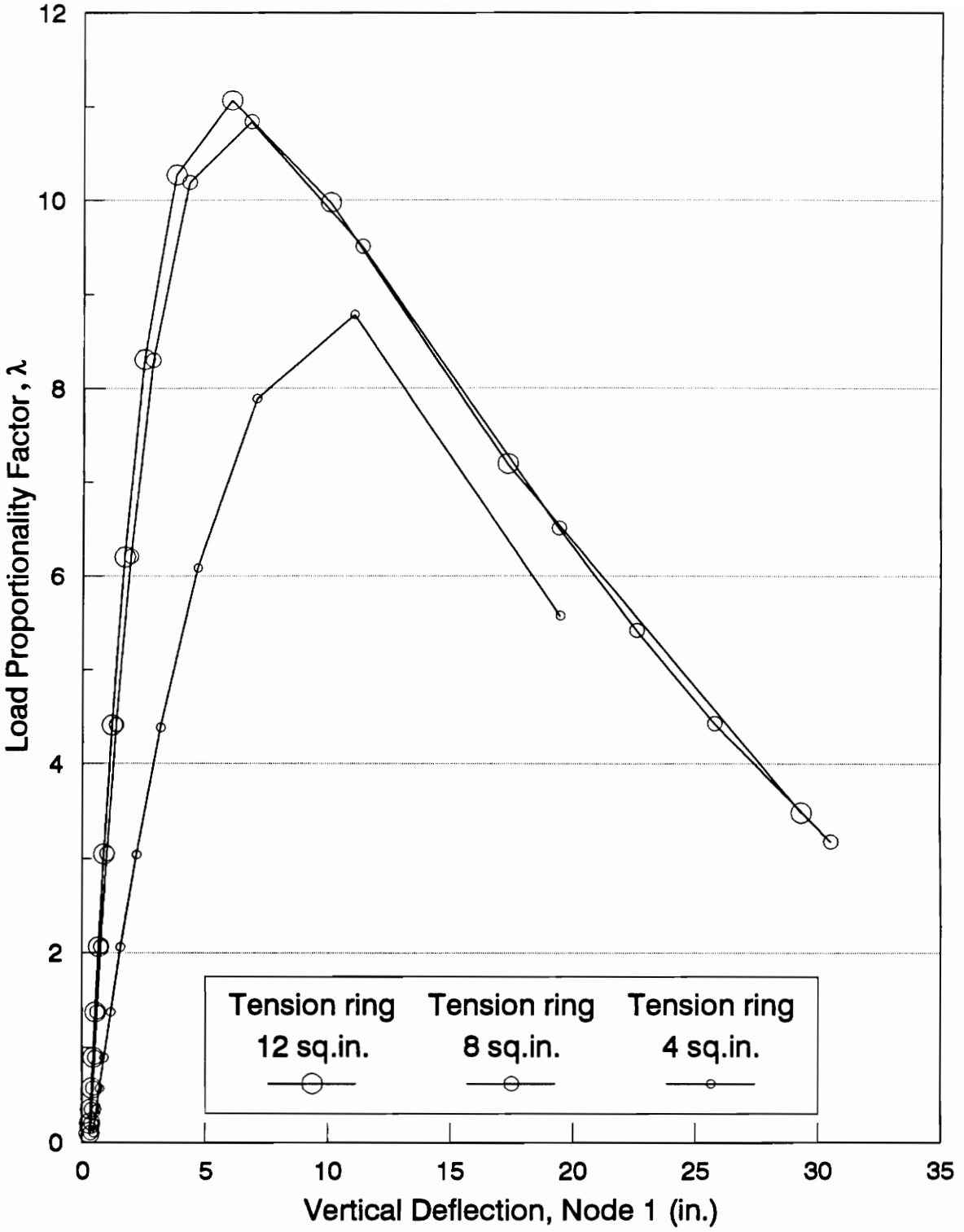


Figure 3.4 Dome Cap Model, Different Areas of Tension Ring, Half Snow Load, Nonlinear Material Law

for these values is 10496 psi. The ultimate tensile stress (σ_{tu}) for Yellow Poplar is taken as 14500 psi, which is the modulus of rupture obtained from static bending tests (Wood Engineering Handbook, 1990, Holzer, Wu, Tissoui, 1992).

The value of σ_{cu} can be varied by varying the values of SG and MC in the nonlinear constitutive equations derived by Connors (1985). The dome cap is analyzed for a varying nonlinear material law with different values for SG and MC. The purpose is to conduct a sensitivity study of the ultimate load relative to the variation in the value of ultimate compressive stress. The effect of the variation in the SG value on the nonlinear curve is shown in the Figures 3.5 and 3.6 for different MC values. It can be seen that the ultimate compressive stress decreases with the increasing MC and decreasing SG. An important point in plotting these curves is that the values of K_{1C} and K_{2C} that mark the boundaries between the three segments of the nonlinear curve in compression change as the MC and SG values are changed. Therefore, appropriate equations must be used for the points in the three different regions of the curve for finding the stress values corresponding to the strain values in these three regions.

Table 3.1 gives the values of proportional limit in compression and tension (corresponding to the strain values of K_{1C} and K_{1T} respectively) and the ultimate compressive stress for some typical values of SG and MC. The ultimate tensile stress is taken as 14500 psi in all cases as recommended in the Wood Engineering Handbook (1992) for long leaf pine. The ultimate compressive stress for long leaf pine wood is 8500 psi based on the maximum crushing strength (Holzer, Wu, Tissoui, 1992). In case of glulam beams, which consist of southern pine wood, the average MC is about 12 percent (Wood Engineering Handbook, 1992, p. 10-10, Timber Construction Manual, 1985, p. 3-72). It can be seen from Table 3.1 that for the values of MC and SG equal to 12 % and 0.48, the ultimate compressive stress is 8223 psi, which is close to the recommended value of 8500 psi. Thus, these values of MC and SG are most appropriate for the analysis of glulam dome using Connors' model.

The dome cap model defined in section 3.1 was analyzed for some of the MC and SG values in Table 3.1, and the results are summarized in Tables 3.2 and 3.3. The load deflection paths for node 1 are shown in Figures 3.7 and 3.8 for full and half snow load cases, respectively. The locations of the maximum stresses in both cases are the same

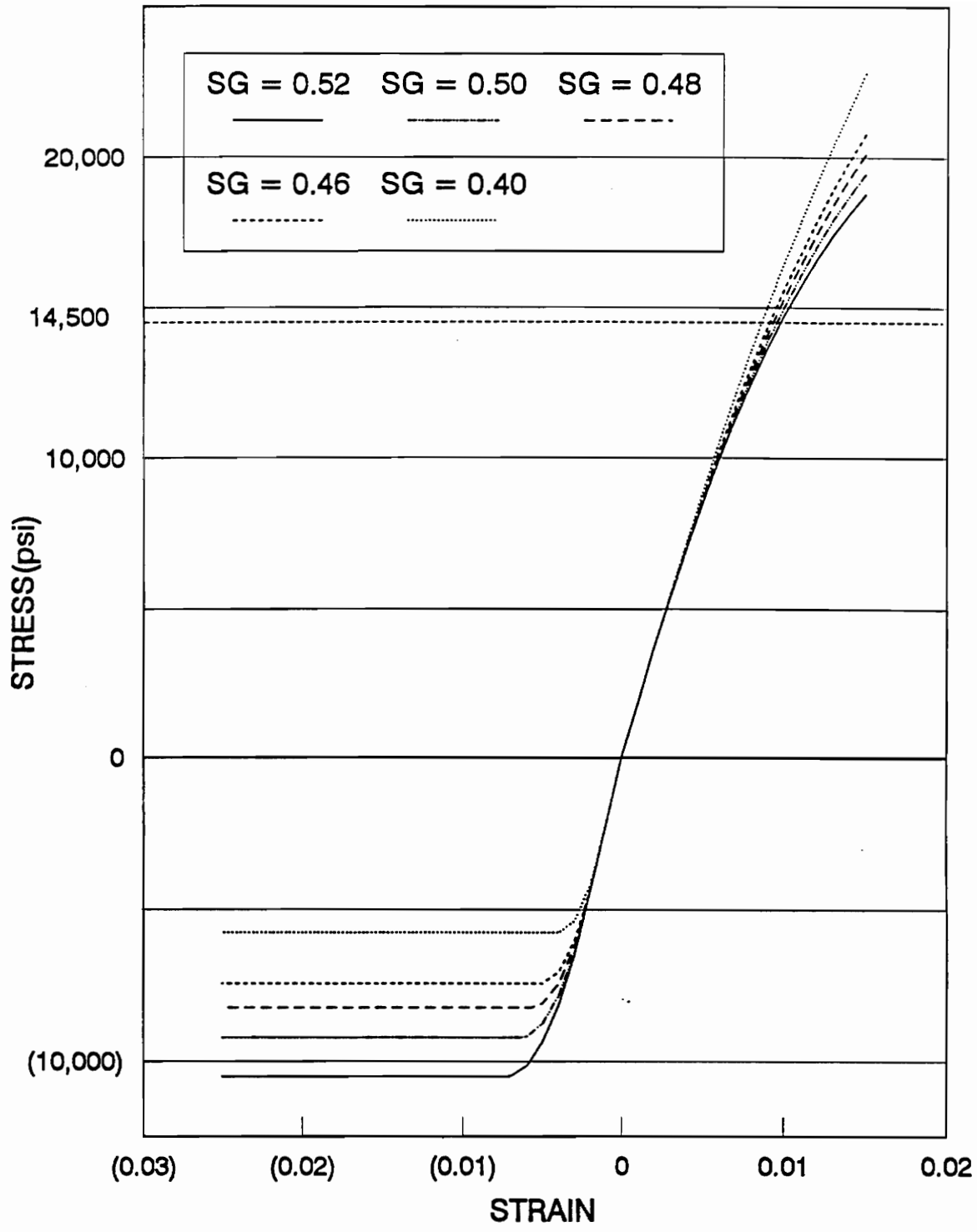


Figure 3.5 Nonlinear material law for wood Connor's segmented model, MC=12%

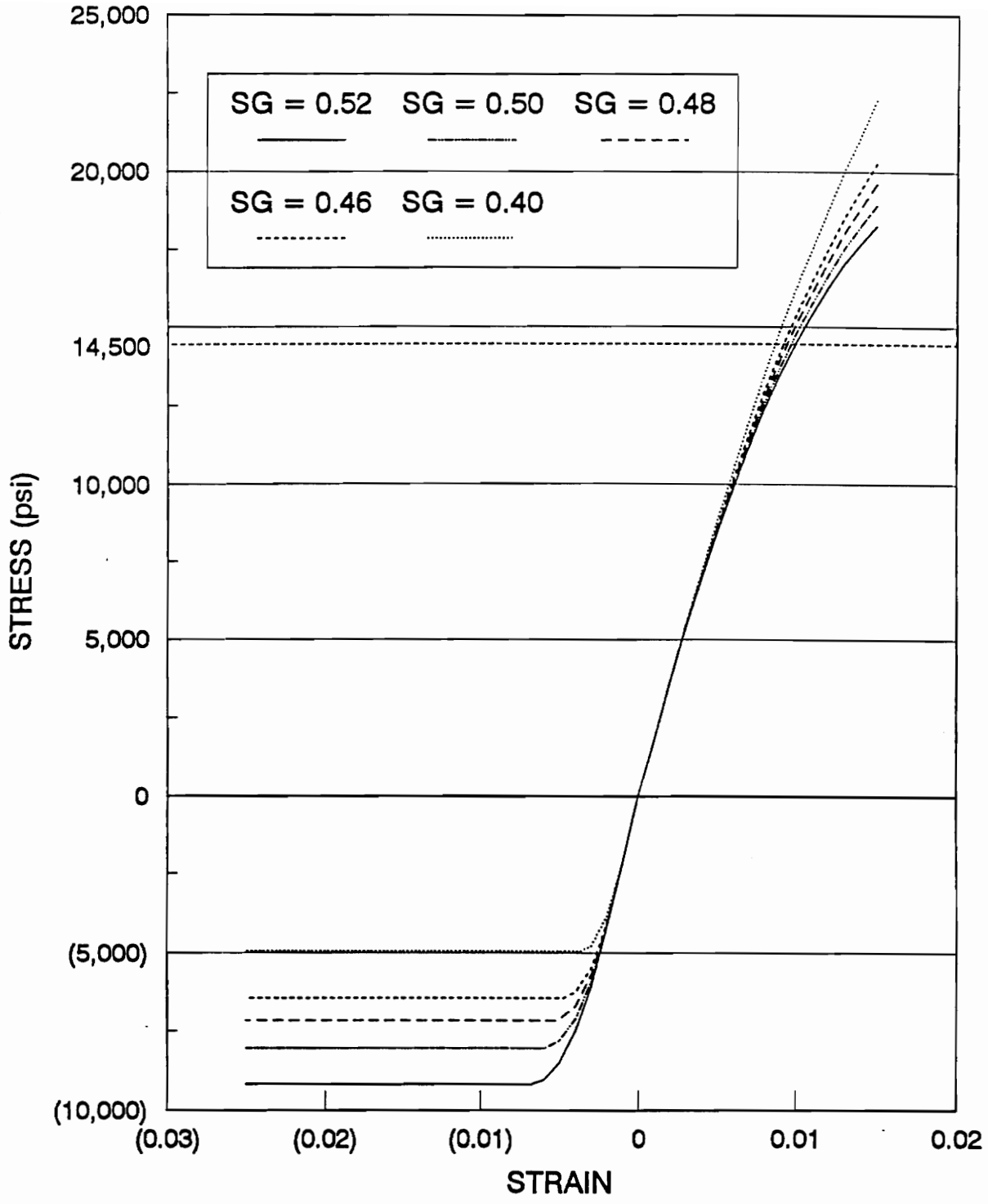


Figure 3.6 Nonlinear material law for wood Connor's segmented model (MC=14%)

as those in sections 3.1 and 3.2. From Tables 3.2 and 3.3 and Figures 3.7 and 3.8, it can be seen that the variation in the material law and consequently the ultimate compressive stress does not affect the critical load factor significantly. The load-deflection paths are similar for different ultimate compressive values up to the critical load, however they differ to some extent in the post-buckling region.

Table 3.1

Proportional Limit and Ultimate Stresses for Nonlinear Material Law

MC	SG	Proportional Limit in Compression (psi)	Proportional Limit in Tension (psi)	Ultimate Compressive Stress (psi)	Ultimate Tensile Stress (psi)
9	0.52	7295	2526	12307	14500
9	0.45	4989	3349	8415	14500
12	0.52	4873	2578	10496	14500
12	0.48	3990	2985	8223	14500
14	0.52	4015	2639	9186	14500
14	0.50	3513	2818	8039	14500
15	0.58	6387	2251	15149	14500
16	0.52	3283	2699	7970	14500

3.6 Effect of Joint Flexibility

All the joints in the dome cap finite element models so far were considered to be fully rigid. This does not, however, reflect the flexibility of real joints. The connections between the beams consist of patented steel hubs as shown in Figure 3.9 (Davalos, 1989; Tissoui, 1991).

One way to model these joints is to use a finite element model with 'hinge' elements. These are beam finite elements of 6 inch length, introduced at the real (beam-to-beam) joints. The cross sectional dimensions of these elements are varied to modify their

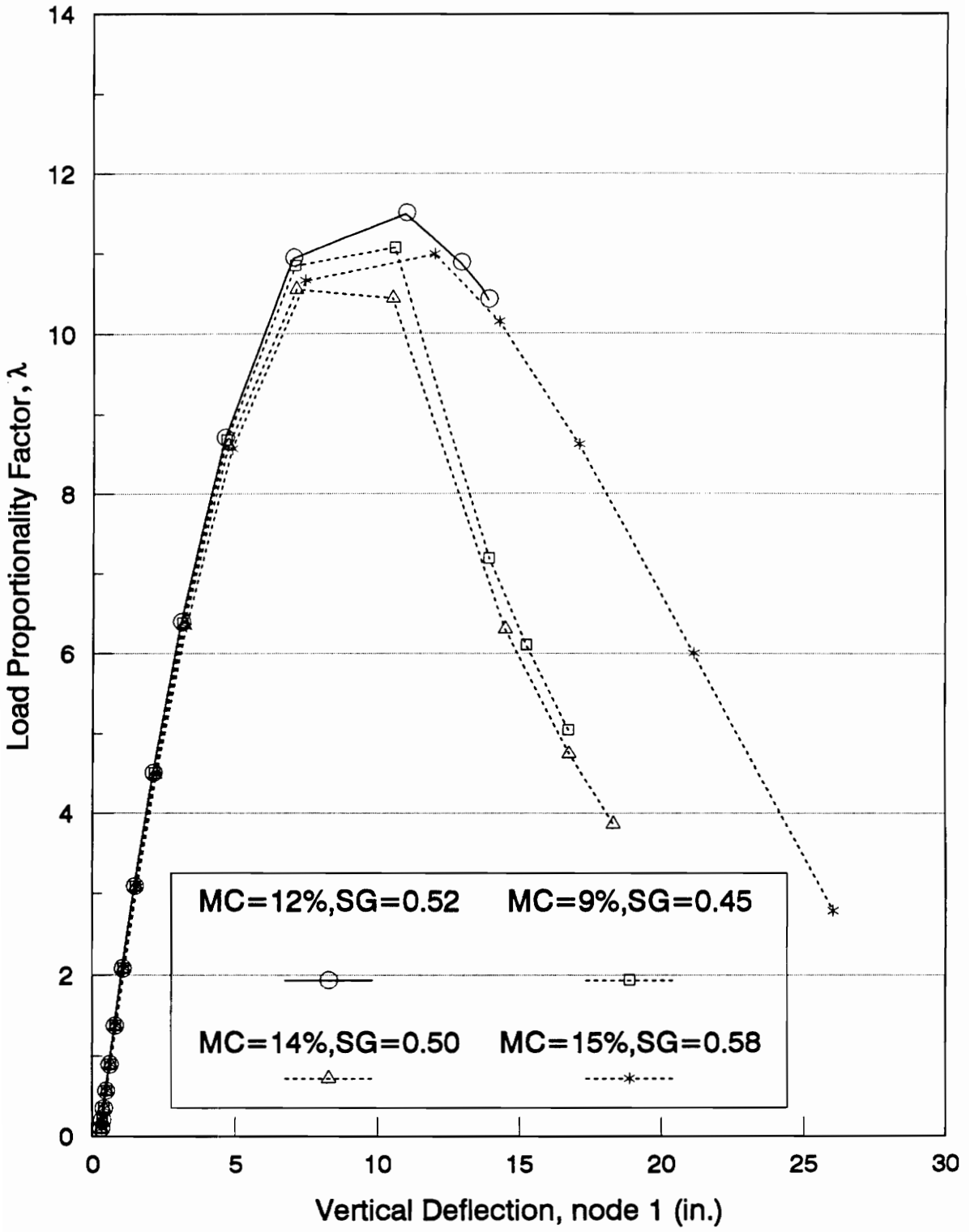


Figure 3.7 Dome Cap Model, Full Snow Load, Variation in Nonlinear Material Law

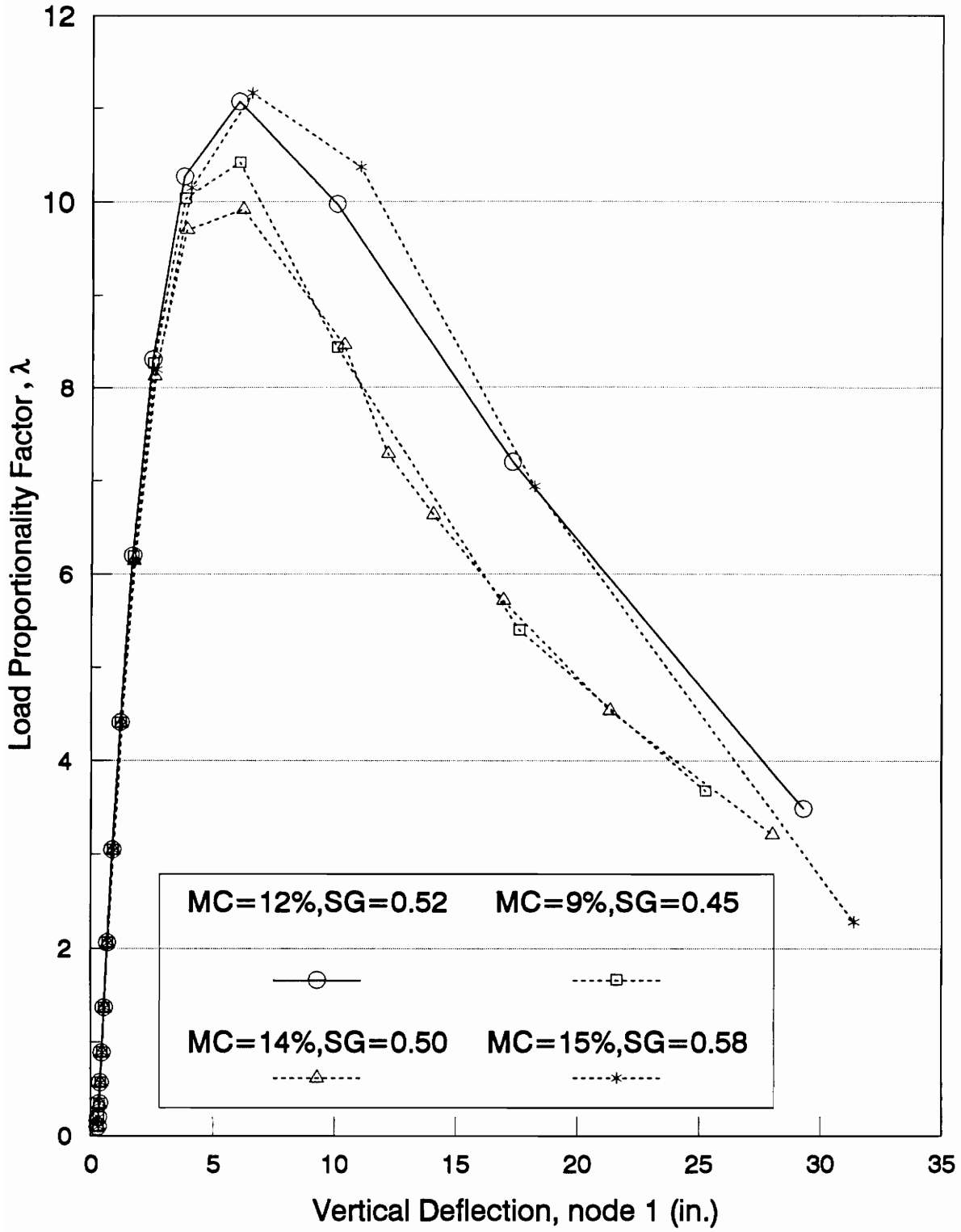


Figure 3.8 Dome Cap Model, Half Snow Load, Variation in Material Law

Table 3.2

Results for Variation in Nonlinear Material Law : Full Snow Load

MC	SG	Ultimate compressive stress (psi)	λ_{cr}	Deflection of node 1 (in.)	Maximum Tensile Stress (psi)	Maximum Compressive Stress (psi)
9	0.45	8415	10.85	7.10	5696	-7793
12	0.52	10496	10.95	7.04	5601	-8139
12	0.48	8223	10.80	6.56	5610	-7629
14	0.50	8039	10.55	7.13	5569	-7470
15	0.58	15149	10.66	7.45	5547	-8321

Table 3.3

Results for Variation in Nonlinear Material Law : Half Snow Load

MC	SG	Ultimate compressive stress (psi)	λ_{cr}	Deflection of node 1 (in.)	Maximum Tensile Stress (psi)	Maximum Compressive Stress (psi)
9	0.45	8415	10.42	6.06	1.17×10^4	-7288
12	0.52	10496	11.07	6.02	1.20×10^4	-1.01×10^4
12	0.48	8223	10.29	5.95	1.13×10^4	-7177
14	0.50	8039	9.92	6.19	1.12×10^4	-7028
15	0.58	15149	10.37	11.04	1.38×10^4	-1.54×10^4

stiffness as described below.

The height and width of the hinge elements are modified by a reduction factor 'c_0' (Figure 3.10) such that their moment of inertia is reduced by a factor of 'c'.

a = original width of beam
b = original height of beam
c_0 = width and height reduction factor
c = stiffness reduction factor
I = original moment of inertia
I' = moment of inertia of the hinge elements

$$I = \frac{ab^3}{12}, \quad I' = \frac{c_0^4 ab^3}{12}; \qquad I' = c\,I, \quad c = c_0^4$$

$$\text{Stiffness reduction (\%)} = \frac{I - I'}{I} \times 100$$

A dome cap model with a 2 element mesh and hinge elements is analyzed in chapter 2 (Figure 2.10). This model is modified as explained in section 3.2 for the 2 element mesh model. The beams in the modified model have dimensions of a = 6.75" and b = 11". This model is analyzed with reduction factors of 100, 75, 50 and 25 %, i.e., the values of c equal to 1.00, 0.75, 0.50, and 0.25, respectively. The nonlinear material law (SG =0.52, MC = 12%) is used in the analysis. Table 3.4 gives the values of various parameters listed above for these reduction factors.

Table 3.4 Hinge Element Dimensions for Reduced Stiffness

Stiffness Reduction (%)	Width & height reduction factor, c_0	Reduced height (in)	Reduced width (in)
0	1.0	11.0	6.75
25	0.931	10.24	6.28
50	0.841	9.25	5.68
75	0.707	7.78	4.77

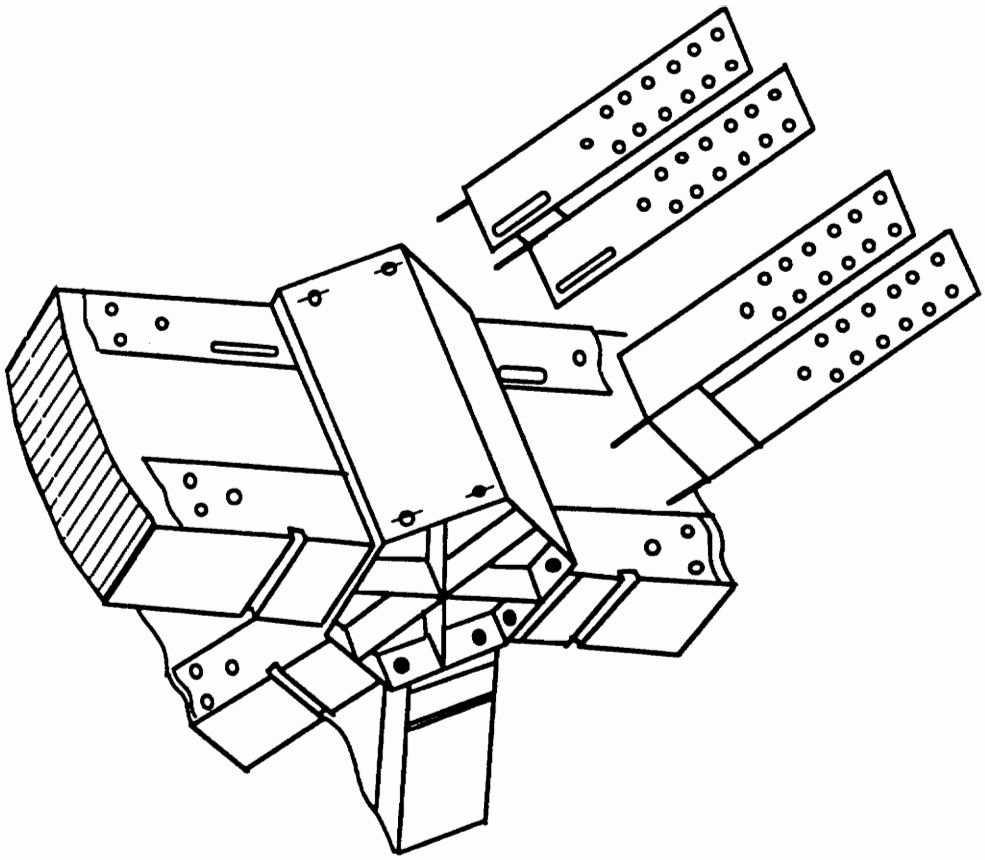


Figure 3.9 Varax Beam-to-beam Joint

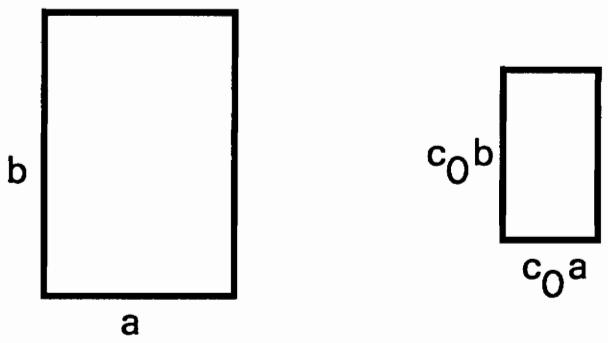


Figure 3.10 Stiffness Reduction of the Hinge Elements

The results of the analysis with the reduced stiffness are shown in Figure 3.11 and 3.12. The nonlinear material law is used. Tables 3.5 and 3.6 give the critical load factors for the different stiffnesses of the hinge elements and percent difference as compared to load factor for no reduction. It can be seen that the results are not very sensitive with respect to joint flexibility.

Table 3.5

Results for Reduced Stiffness for Full Snow

Stiffness Reduction (%)	Width & height reduction factor, c_0 (%)	Load Factor	Change in load factor (%)
0	100.0	10.41	-
25	93.1	10.38	0.29
50	84.1	10.32	0.86
75	70.7	10.06	3.36

Table 3.6

Results for Reduced Stiffness for Half Snow

Stiffness Reduction (%)	Width & height reduction factor, c_0 (%)	Load Factor	Change in load factor (%)
0	100.0	10.74	-
25	93.1	10.71	0.28
50	84.1	10.64	0.93
75	70.7	10.47	2.50

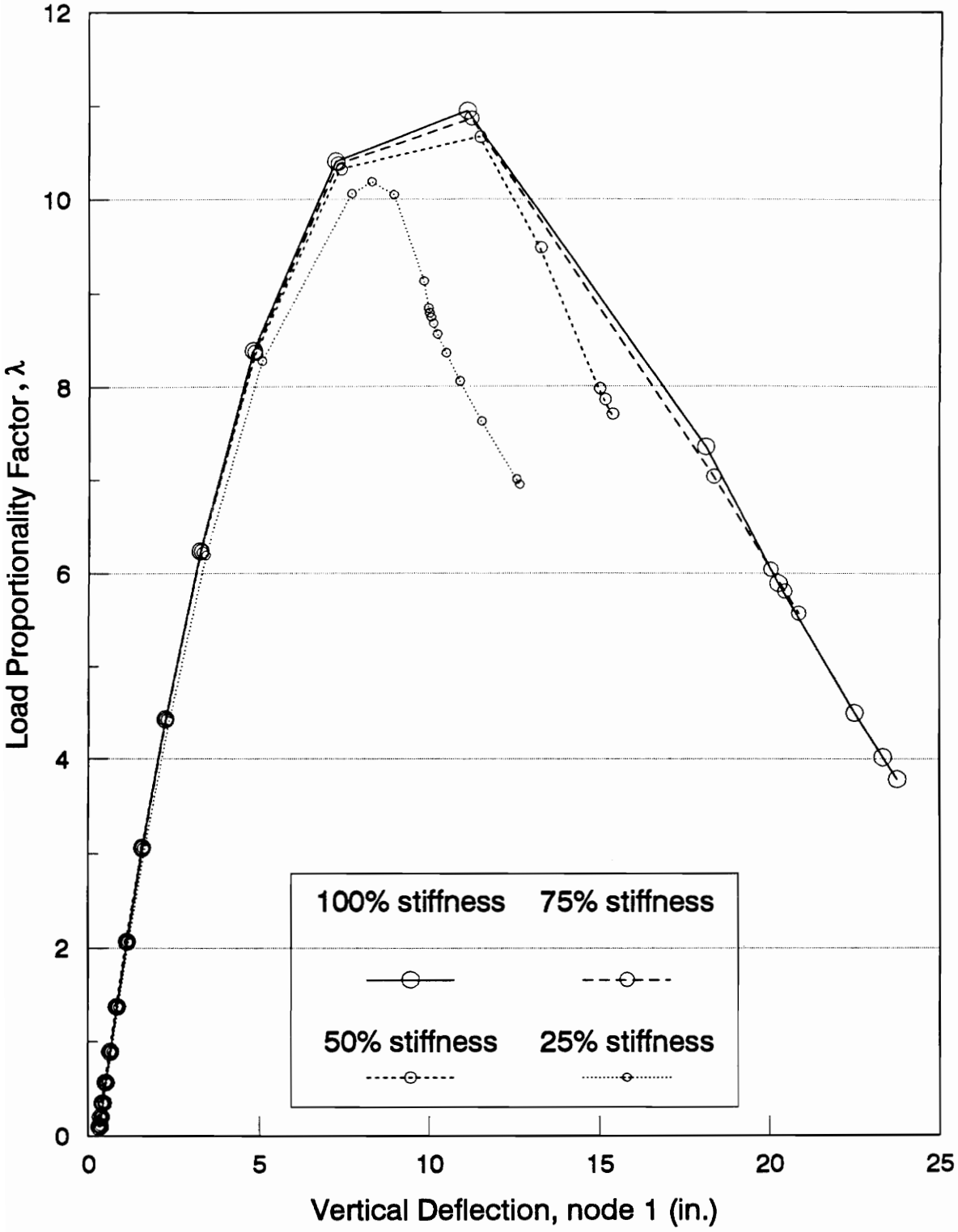


Figure 3.11 Dome Cap Model with Hinge Elements, Full Snow Load, Variation in Stiffness of Hinge Elements

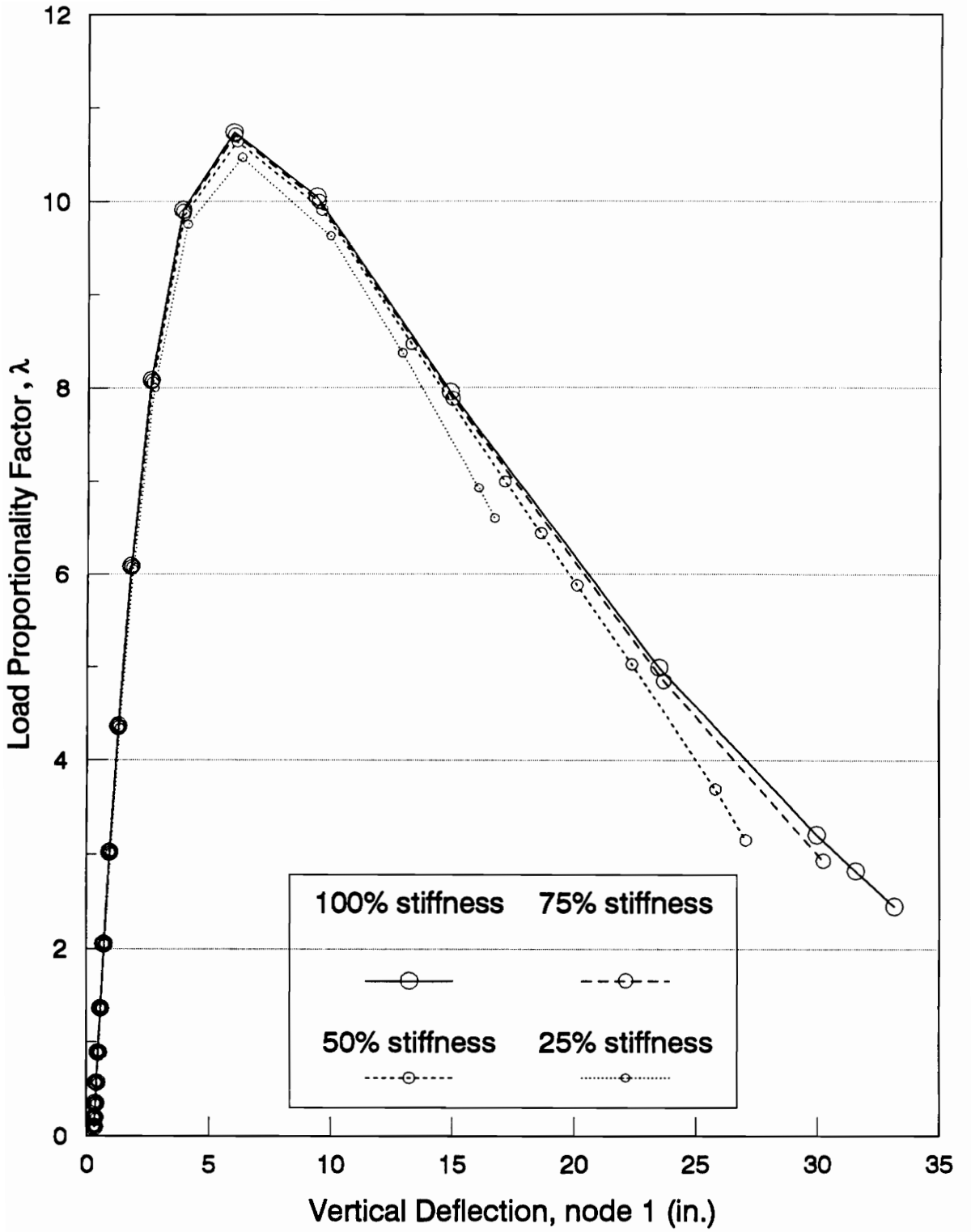


Figure 3.12 Dome Cap Model with Hinge Elements, Half Snow Load, Variation in Hinge Element Stiffness

Chapter 4

Application of Saint-Venant's Torsion Solution in Dome Analysis

4.1 Introduction

The rib and edge members (named as main beams I & II and edge beams) are modeled with beam finite elements in the finite element model of the dome cap and the dome. They consist of rectangular glulam timber members with different sizes of cross sections. In this study they have been modeled as two node space beam elements from the ABAQUS element library, with cubic interpolation of displacements (B33 beam elements). The beam finite elements in ABAQUS do not include the effect of warping of non-circular cross sections. The shear stresses and deflections are calculated according to the linear elastic torsion theory. This chapter describes a method to take into account the warping in the analysis with ABAQUS. The shear modulus is modified for this purpose to take into account the reduced polar moment of inertia of rectangular sections according to Saint-Venant's solution for torsion of rectangular sections. The experimental tests on southern pine glulam beams by Davalos, et al. (1991) showed that they behave transversely isotropic, so that single shear modulus value can be assumed for any cross section of a glulam beam. The tests showed that Saint-Venant's isotropic torsion solution can accurately represent the linear torsional response of southern pine glulam beam.

A brief review of torsion theory is presented in the first section. The method of shear modulus modification is discussed in the second section. The test cases of cantilever beams subjected to torque at free ends are discussed next to verify this method.

4.2 Review of Torsion Theory

The problem of torsion for an elastic circular member was first studied by Coulomb in 1784, in which he developed the first analytical expression for torsion of thin circular

wires (Hsu, 1984). He found that the torsional moment, T, is proportional to the twisting angle of the wire. The theoretical solution for torsion of a solid circular shaft was later derived and published by Navier in 1826.

4.2.1 Navier's Solution for Elastic Circular Sections

A transverse slice of a circular shaft fixed at one end and subjected by a torque, T, at the free end is shown in Figure 4.1a. The deformation of the slice is described by the assumptions of compatibility

1. The shape of the cross section remains unchanged after twisting
2. A plane section perpendicular to the axis remains plane after the torque is applied, i.e., no warping or distortion out of the plane of the slice takes place.

To establish a relation between internal torque and the resulting stresses, the following assumptions in addition to homogeneity of material are necessary (Popov, 1968):

3. The shearing strain γ vary linearly from the central axis
4. The shearing stress is proportional to the shearing strain.

The shearing strain γ at a distance 'r' from the central axis is given by

$$\gamma = \frac{r\, d\phi}{dz} = r\theta \tag{4.1}$$

where $\theta = \frac{d\phi}{dz}$ = angle of twist per unit length of the shaft. The maximum shearing strain occurs at the surface of the shaft at r = R, i.e., $\gamma_{max} = R\,\theta$. Thus, the shearing stress τ at a distance r from the central axis is

$$\tau = G\gamma = Gr\theta \tag{4.2}$$

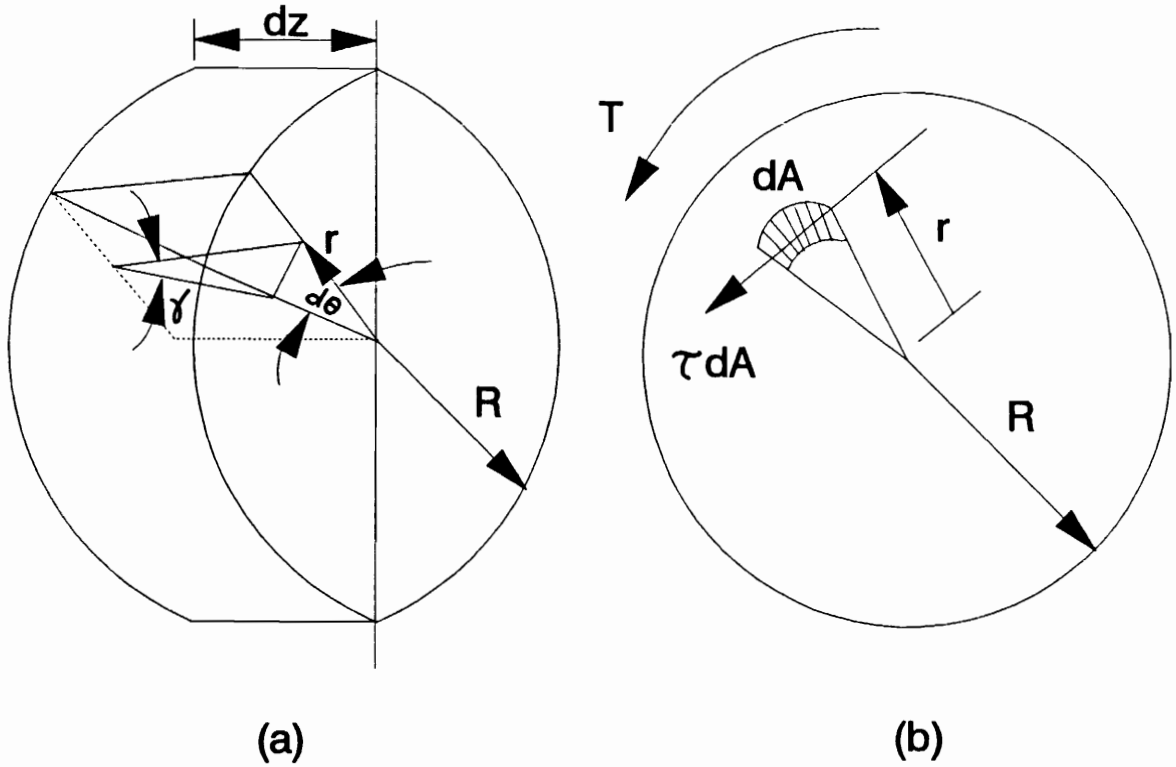


Figure 4.1 Equlibrium and compatibility of a circular shaft

where G = shear modulus. Thus, for a circular cross section, the shear stress is proportional to 'r' and the maximum stress develops at the surface, $\tau_{max} = R\ G\ \theta$. The applied torque, T, is obtained from Figure 4.1b as follows:

$$T = \int_A (\tau\, dA)\, r \tag{4.3}$$

From Eqs. (4.2) and (4.3) we obtain

$$T = G\theta \int_A r^2\, dA = I_p\, G\theta \tag{4.4}$$

where $I_p = \int_A r^2\, dA$ = polar moment of inertia of the cross section. From Eqs. (4.2) and (4.4) we obtain

$$G\theta = \frac{T}{I_p} = \frac{\tau}{r} = \frac{\tau_{max}}{R} \tag{4.5}$$

Eq. (4.5) gives relationship between τ, θ, and T and completely describes the elastic torsion of a circular shaft.

4.2.2 Saint-Venant's Semi-Inverse Method

Navier applied his solution for torsion of circular bars to the bars of non-circular sections and came to the erroneous conclusion that for a given torque, angle of twist is inversely proportional to the polar moment of inertia and that the maximum shear stress occurs at points most remote from the central axis. For example, for rectangular bars, the corners do not distort at all thus developing zero stresses. The distortion on the surface of bars is greatest at the middle of the long sides giving rise to maximum shearing stresses there. Thus, the maximum shearing stresses develop on the surface point closest to the central axis, in contrast to the circular sections.

Navier modified his equations for the circular section to apply for the non-circular sections simply by replacing the polar moment of inertia of the circular section with that of

non-circular sections. The experimental results were, however, not supported by these equations. Obviously, his equations did not take into account the warping of non-circular sections. The problem of torsion of non-circular sections remained unsolved until the famous French elastician B. de Saint-Venant developed the correct solution for such problems in1853 using the necessary mathematical tools undeveloped till then, namely the Fourier series and the theory of elasticity (Hsu, 1984). He invented the 'Semi-inverse method', in which certain assumptions based upon understanding of mechanics of the problem and observation of deformations are introduced first. They are, however, not so specific as to attempt to meet all the requirements of the problem (Sidebottom & Boresi, 1985, Hsu, 1984). Thus the displacement components u, v, w corresponding to rotation of the cross section due to the applied torque, T, (Figure 4.2) are first assumed. These assumptions are then shown to satisfy the equations of equilibrium, the theory of elasticity, and the boundary conditions. From the uniqueness of the solutions of the elasticity equations, it follows that the assumptions made at the start are correct. Thus the solution obtained is the exact solution of the torsion problem. The torques at the ends are applied as shear stresses in exactly the manner required by the solution itself (Timoshenko & Goodier, 1970). The assumptions involved to describe the displacement components for the non-circular section are:

1. The shape of the cross section remains unchanged after the twisting.
2. Warping of the cross section is identical throughout the length of the member.

The following formulation follows the presentation by Sidebottom and Boresi (1985) and Hsu (1984). Consider a point P(x,y,z) in an undeformed non-circular torsion member with the origin of coordinates in an end cross section (Figure 4.2). The member undergoes a rotation of angle θ per unit length of the member about the central axis. The point P is in general displaced by an amount, w, parallel to the z-axis due to warping of the cross section and by amounts, u and v, parallel to the x and y axis, respectively. u and v are caused principally due to rotation of cross section in which point P rotates through an angle β with respect to the cross section at the origin. Then u, v, and w are given by

$$u = \theta z r(\sin\beta) = -\theta z r(y/r) = -\theta z y$$

$$v = \theta z r(\cos\beta) = \theta z r(x/r) = \theta z x \qquad (4.6)$$

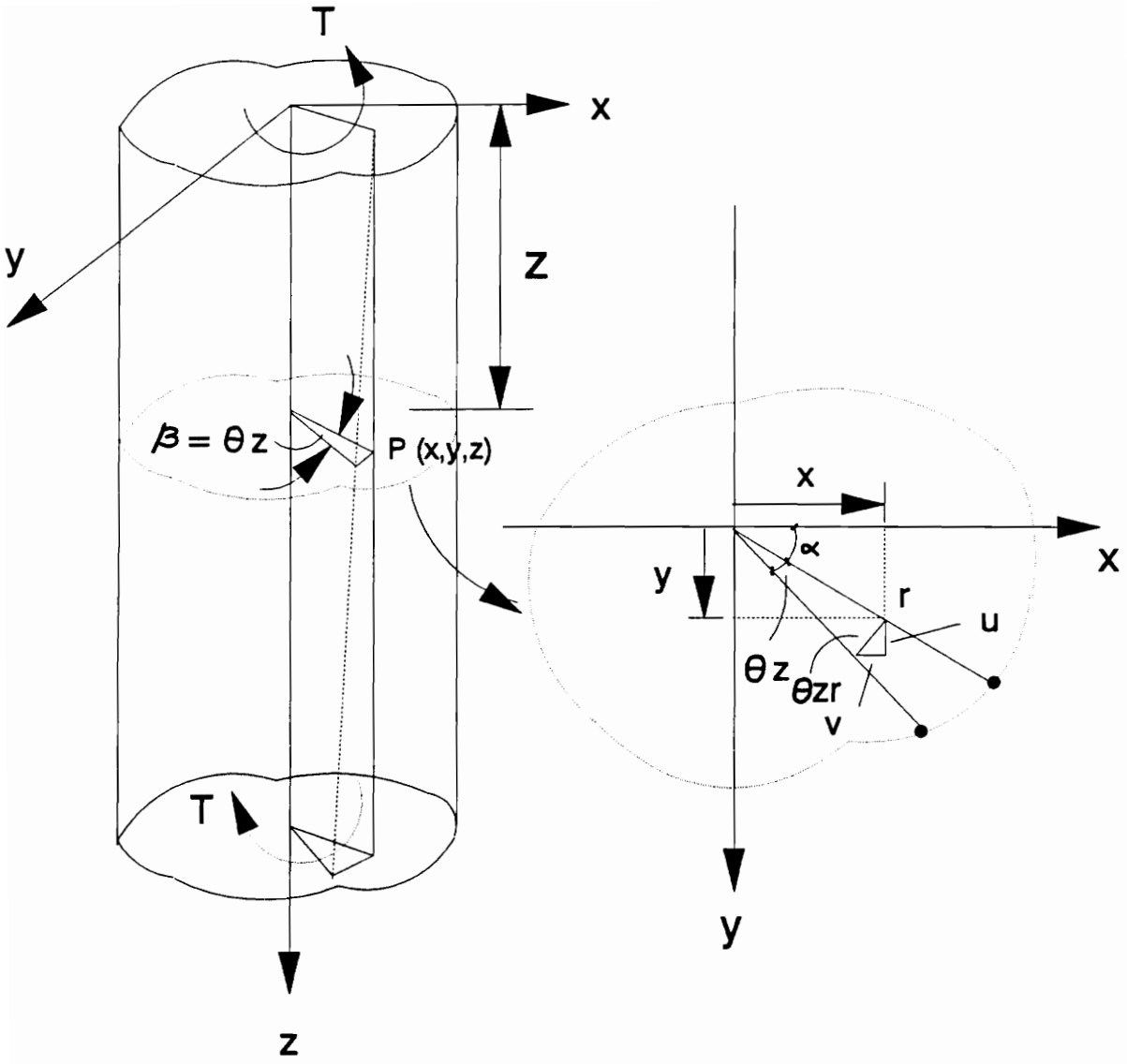


Figure 4.2 Twisting of a shaft with non-circular cross section

$$w = \theta \psi(x,y)$$

where $\psi(x,y)$ is the *warping function* and is not a function of z. It is an unknown and will be determined later so that it satisfies all the equations of the theory of elasticity. Our purpose is to determine if the displacements together with ψ result in a system of stresses compatible with the boundary conditions. The boundary conditions of the problem are pure torsion at the ends and no forces on the lateral surfaces of the torsion member. The strain-displacement relations give

$$\varepsilon_{xx} = \varepsilon_{yy} = \varepsilon_{zz} = 0$$

$$2\varepsilon_{zx} = \gamma_{xz} = \frac{\partial w}{\partial x} + \frac{\partial u}{\partial z} = \theta\left(\frac{\partial \psi}{\partial x} - y\right) \tag{4.7}$$

$$2\varepsilon_{zy} = \gamma_{yz} = \frac{\partial w}{\partial y} + \frac{\partial v}{\partial z} = \theta\left(\frac{\partial \psi}{\partial y} + x\right)$$

The corresponding stress components are given by

$$\sigma_{xx} = \sigma_{yy} = \sigma_{zz} = \tau_{xy} = 0$$

$$\tau_{xz} = G\theta\left(\frac{\partial \psi}{\partial x} - y\right) \tag{4.8}$$

$$\tau_{yz} = G\theta\left(\frac{\partial \psi}{\partial y} + x\right)$$

Assuming body forces to be zero, the equations of equilibrium are as follows.

$$\Sigma F_x = 0, \quad \frac{\partial \sigma_x}{\partial x} + \frac{\partial \tau_{yx}}{\partial y} + \frac{\partial \tau_{zx}}{\partial z} = 0$$

$$\Sigma F_y = 0, \quad \frac{\partial \sigma_y}{\partial y} + \frac{\partial \tau_{zy}}{\partial z} + \frac{\partial \tau_{xy}}{\partial x} = 0 \tag{4.9}$$

$$\Sigma F_z = 0, \qquad \frac{\partial \sigma_z}{\partial z} + \frac{\partial \tau_{xz}}{\partial x} + \frac{\partial \tau_{yz}}{\partial y} = 0$$

Eqs. (4.9) should be satisfied by the warping function ψ. The first two of them are satisfied since τ_{xz} and τ_{yz} are independent of z. However, the third becomes

$$\frac{\partial \tau_{xz}}{\partial x} + \frac{\partial \tau_{yz}}{\partial y} = 0 \tag{4.10}$$

From Eqs (4.8) and (4.10) we obtain

$$\frac{\partial^2 \psi}{\partial y^2} + \frac{\partial^2 \psi}{\partial x^2} = \nabla^2 \psi = 0 \tag{4.11}$$

The lateral surface of bar is free from external forces since only torsional moments are applied at the ends. Therefore, the boundary conditions are $\overline{X} = \overline{Y} = \overline{Z} = 0$, where $\overline{X}$, $\overline{Y}$, and $\overline{Z}$ represent the stress distributions in the direction of X, Y, and Z axes, respectively. Also, the direction cosines with respect to the z-axis, cos (N,z) = n = 0. The equations of equilibrium at the surface of an elastic body are

$$\begin{aligned}
\Sigma F_x = 0: &\quad \sigma_x l + \tau_{yx} m + \tau_{zx} n = \overline{X} \\
\Sigma F_y = 0: &\quad \tau_{xy} l + \sigma_y m + \tau_{zy} n = \overline{Y} \\
\Sigma F_z = 0: &\quad \tau_{xz} l + \tau_{yz} m + \sigma_z n = \overline{Z}
\end{aligned} \tag{4.12}$$

where l, m, n are direction cosines of normal to the surface of the bar relative to the x, y, z axes (Figure 4.3) given by

$$l = \cos(N,x) = \frac{dx}{ds} \quad \text{for the angle between the N and theX-axis}$$

$$m = \cos(N,y) = -\frac{dy}{ds} \quad \text{for the angle between the N and the Y-axis} \tag{4.13}$$

n = cos (N,z) for the angle between the N and the Z-axis

From the boundary conditions and Eqs. (4.12) we obtain

$$\tau_{xz}\, l + \tau_{yz}\, m = 0 \tag{4.14}$$

From Eqs. (4.8) and (4.14) we obtain

$$\left(\frac{\partial \psi}{\partial x} - y\right)\frac{dx}{ds} - \left(\frac{\partial \psi}{\partial y} + x\right)\frac{dy}{ds} = 0 \tag{4.15}$$

On the other two surfaces, i.e., the ends of the bar defined by the planes z = 0 and z = l, the distribution of stresses given by Eqs. (4.8) is equivalent to a torsional couple so that there is no resultant force. Thus, the torsion problem is reduced to finding a function ψ (x,y) satisfying the Eqs. (4.11) and (4.15). These equations are the Saint-Venant's original equations in terms of ψ. Prandtl introduced a *stress function* ϕ(x,y) to give simpler equations for the boundary conditions and for the torsional moment. He defined

$$\tau_{xz} = \frac{\partial \phi}{\partial y}, \qquad \tau_{yz} = -\frac{\partial \phi}{\partial x} \tag{4.16}$$

The Eqs. (4.8), (4.11) and (4.14) thus become

$$\begin{aligned} \frac{\partial \phi}{\partial y} &= G\,\theta\,\left(\frac{\partial \psi}{\partial x} - y\right) \\ -\frac{\partial \phi}{\partial x} &= G\,\theta\,\left(\frac{\partial \psi}{\partial y} + x\right) \end{aligned} \tag{4.17}$$

$$\frac{\partial^2 \phi}{\partial x^2} + \frac{\partial^2 \phi}{\partial y^2} = \nabla^2 \psi = F = -2\,G\,\theta \tag{4.18}$$

and

$$\frac{\partial \phi}{\partial y}\frac{\partial y}{\partial s} + \frac{\partial \phi}{\partial x}\frac{\partial x}{\partial s} = \frac{d\phi}{ds} = 0 \tag{4.19}$$

respectively. Eq. (4.18) is a harmonic differential equation commonly known as the Laplace equation. Eq. (4.19) implies that the stress function ϕ must be constant along the boundary of the cross section and can be chosen as any arbitrary value, which we assume to be zero.

$$\phi = 0 \qquad \text{along the boundary} \tag{4.20}$$

Thus the problem now reduces to finding the function ϕ, satisfying Eqs. (4.18) and (4.19). At the ends of a twisted bar, $l = m = 0$ and $n = \pm 1$, so that from Eqs. (4.12) we obtain

$$\overline{X} = \pm \tau_{xz}, \qquad \overline{Y} = \pm \tau_{yz} \tag{4.21}$$

The resultant torsional moment is given by

$$T = \iint_A (\overline{Y}x - \overline{X}y)\, dxdy$$

$$= G\theta \iint_A (x^2 + y^2 + x\frac{\partial \phi}{\partial y} - y\frac{\partial \phi}{\partial x})\, dxdy$$

$$= GJ\theta \tag{4.22}$$

where

$$J = \iint_A (x^2 + y^2 + x\frac{\partial \phi}{\partial y} - y\frac{\partial \phi}{\partial x})\, dxdy$$

$$= \text{torsional constant} \tag{4.23}$$

Thus, T is proportional to the angle of twist per unit length and the product GJ provides a measure of the stiffness of the bar. Equations (4.22) can also be written as

$$T = -\iint_A (x\frac{\partial \phi}{\partial x} + y\frac{\partial \phi}{\partial y})\, dxdy$$

$$= 2\iint_A \phi\, dxdy \tag{4.24}$$

4.2.3 Torsion of Rectangular Bars

For a rectangular cross section (Figure 4.4), the boundary conditions according to Eq. (4.20) are

$$\begin{aligned} \phi &= 0 \qquad \text{at} \quad y = \pm b \\ \phi &= 0 \qquad \text{at} \quad x = \pm a \end{aligned} \tag{4.25}$$

The function ϕ that satisfies Eqs. (4.18) and (4.25) can be given by the cosine Fourier series

$$\phi = \sum_{n=1,3,5...}^{\infty} b_n \cos\frac{n\pi x}{2a} Y_n(y) \qquad -a < x < a \tag{4.26}$$

where b_n are constants and $Y_n(y)$ are functions of y only. Also, the constant $2G\theta$ can be expressed in terms of the Fourier series

$$-2G\theta = -\sum_{n=1,3,5...}^{\infty} 2G\theta \frac{4}{n\pi}(-1)^{(n-1)/2} \cos\frac{n\pi x}{2a} \tag{4.27}$$

From Eqs. (4.26), (4.27) and (4.18), we obtain a second order differential equation in $Y_n(y)$. From the boundary conditions (4.25), symmetry about x-axis, and considering the expression for ϕ in Eq. (4.26), we obtain the solution of the differential equation as

$$Y_n(y) = \frac{32G\theta a^2}{n^3\pi^3 b_n}(-1)^{(n-1)/2}\left[1 - \frac{\cosh(n\pi y/2a)}{\cosh(n\pi b/2a)}\right] \tag{4.28}$$

Eqs. (4.26) and (4.28) yield

$$\phi = \frac{32G\theta a^2}{\pi^3} \sum_{n=1,3,5...}^{\infty} \frac{1}{n^3}(-1)^{(n-1)/2}\left[1 - \frac{\cosh(n\pi y/2a)}{\cosh(n\pi b/2a)}\right] \tag{4.29}$$

The stress components can now be obtained from Eq. (4.16). For example,

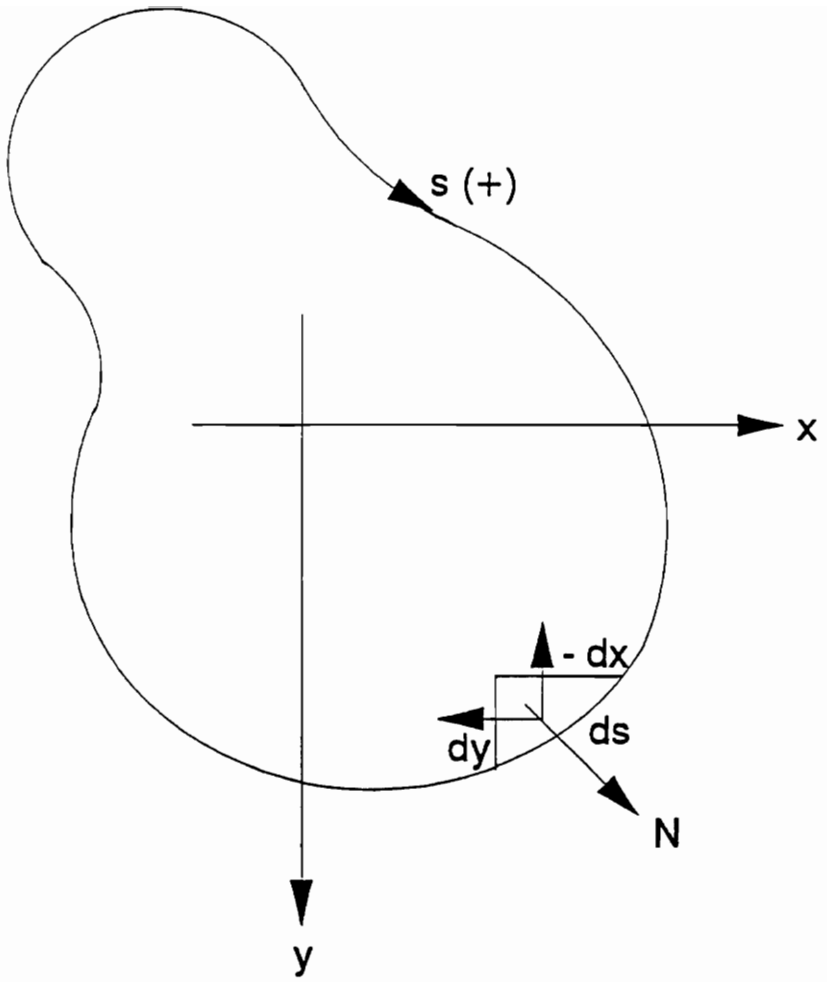


Figure 4.3 Stresses in a cross section of a shaft

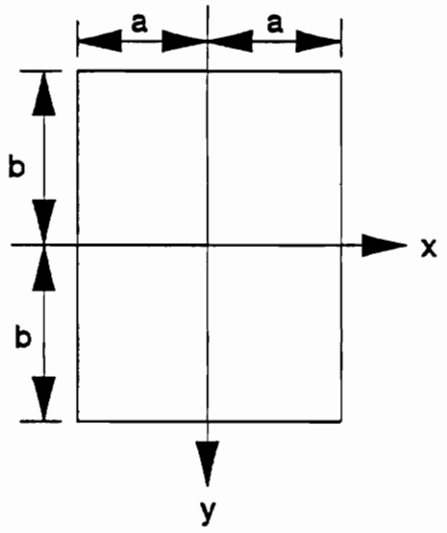


Figure 4.4 Rectangular cross section

$$\tau_{yz} = \frac{16G\theta a}{\pi^2}\sum_{n=1,3,5...}^{\infty}\frac{1}{n^2}(-1)^{(n-1)/2}\left[1-\frac{\cosh(n\pi y/2a)}{\cosh(n\pi b/2a)}\right]\sin\frac{n\pi x}{2a} \qquad (4.30)$$

Assuming b > a

$$\tau_{max} = (\tau_{yz})_{max} \qquad \text{at} \quad x = \pm a,\ y = 0 \quad (\tau_{zx} = 0) \qquad (4.31)$$

Thus, the maximum stress is at the center of the longer side of the rectangle. From Eqs. (4.30) and (4.31) we obtain

$$\tau_{max} = \frac{16G\theta a}{\pi^2}\sum_{n=1,3,5...}^{\infty}\frac{1}{n^2}\left[1-\frac{1}{\cosh(n\pi b/2a)}\right]$$

$$= G\theta(2a)\left[1-\frac{8}{\pi^2}\sum_{n=1,3,5...}^{\infty}\frac{1}{n^2\cosh(n\pi b/2a)}\right]$$

$$= k_1\, G\,\theta\, x \qquad (4.32)$$

where x = 2a = the shorter dimension of the rectangular cross section. The torsional moment T can be calculated from Eq. (4.24) as

$$T = 2\iint_A \phi\, dxdy$$

$$= \frac{32G\theta(2a)^3(2b)^3}{\pi^4}\left[\sum_{n=1,3,5...}^{\infty}\frac{1}{n^4}-\frac{2a}{\pi b}\sum_{n=1,3,5...}^{\infty}\frac{1}{n^5}\tanh\frac{n\pi b}{2a}\right]$$

$$= \frac{G\theta(2a)^3(2b)^3}{3}\left[1-\frac{192a}{\pi^5 b}\sum_{n=1,3,5...}^{\infty}\frac{1}{n^5}\tanh\frac{n\pi b}{2a}\right]$$

$$= k\, x^3\, y\, G\,\theta \qquad (4.33)$$

where y = 2b = the longer dimension of the rectangle. From Eqs. (4.32) and (4.33), we obtain the maximum shearing stress as a function of the torque as follows:

$$\tau_{max} = \frac{T}{k_2 x^2 y} \tag{4.34}$$

Using a similar derivation as above, the maximum shearing stress at the center of shorter face ($y = \pm b$, $a = 0$) can be expressed as

$$\tau_{x,\,max} = \frac{T}{k_3 x y^2} \tag{4.35}$$

The constants k, k_1, k_2, k_3 in the Eqs. (4.33), (4.32), (4.34) and (4.35), respectively, are all functions of the ratio b/a and are tabulated in the Table 4.1 (Timoshenko and Goodier, 1970). Their approximate values for the intermediate values of b/a can be found by linear interpolation. Let us define

$$C = k x^3 y \tag{4.36}$$

The Eq. (4.33) then becomes

$$T = C G \theta \tag{4.37}$$

Comparing Eqs. (4.4) and (4.37), it can be concluded that the polar moment of inertia (I_p) in case of a circular cross section is replaced by the constant 'C' in the torsion equation of the rectangular cross section such that the product CG is the proportionality constant between T and θ. C is called Saint-Venant's torsional constant for the rectangular section. From Eqs. (4.33) and (4.37) C can be expressed as

$$C = J_{sv} = \frac{T}{G\theta} = x^3 y \left[\frac{1}{3} - \frac{64a}{\pi^5 b} \sum_{n=1,3,5\ldots}^{\infty} \frac{1}{n^5} \tanh \frac{n\pi b}{2a} \right]$$

$$= x^3 y k \tag{4.38}$$

Table 4.1

Saint-Venant's Coefficients for Rectangular Sections
(Timoshenko and Goodier, 1970)

b/a	k	k_1	k_2	k_3
1.0	0.1406	0.675	0.208	0.208
1.2	0.166	0.759	0.219	0.196
1.4	0.187	0.822	0.227	0.185
1.5	0.196	0.848	0.231	0.179
1.6	0.204	0.869	0.234	0.174
1.8	0.217	0.904	0.240	0.164
2.0	0.229	0.930	0.246	0.155
2.5	0.249	0.968	0.258	0.135
3.0	0.264	0.985	0.267	0.118
4.0	0.281	0.997	0.282	0.0945
5.0	0.291	0.999	0.291	0.0782
10.0	0.312	1.000	0.312	0.0397
100.0	0.331	1.000	0.331	0.00217
∞	0.333	1.000	0.333	0.000

4.3 Application of Saint-Venant's Solution in Analysis with ABAQUS

The rigorous solution for the torsion of rectangular bars was given in the previous section. As discussed in section 4.1, it is necessary to take into account this theory in the analysis of domes using ABAQUS, since all the beams in the dome are rectangular in cross section. In ABAQUS, the polar moment of inertia of the rectangular section (J_n) as given in Eq. (4.40) below is used, and Navier's solution by the linear elastic theory is applied in the calculations. Thus, it is not possible to directly incorporate the Saint-Venant's torsional constant in Eq. (4.38) in the analysis. This problem can be solved by modifying the value of shear modulus G, provided, through a user subroutine as follows. The general equation for the applied torque is

$$T = J G \theta \tag{4.39}$$

where, θ = Angle of twist per unit length. For rectangular cross section

$$J = \begin{cases} J_n = \dfrac{ab(a^2+b^2)}{12} & \text{(Navier, without warping)} \\ J_{sv} = a^3 b k & \text{(Saint-Venant, with warping)} \end{cases} \tag{4.40}$$

where a, b are the dimensions of the cross section. Our objective is to use J_n in the Eq. (4.39) and to adjust G such that Saint-Venant's torsion theory is satisfied. Thus,

$$J G = J_n G_e = J_{sv} G \tag{4.41}$$

which yields the equivalent shear modulus

$$G_e = \frac{12k}{\left[1+(b/a)^2\right]} G \tag{4.42}$$

The value of the equivalent shear modulus is used in the user subroutine UMAT. For example, for b/a = 2, k = 0.229 (Table 4.1) we obtain

$$G_e = \frac{12}{5} k G = 0.55 G$$

4.4 Test Cases: Steel Cantilever Beams

In order to verify the concept described in the previous section, two types of steel cantilever beams have been analyzed and the results are presented in this section. The first case involves simple rectangular beams of circular and rectangular cross-sections. Figure 4.5 shows a circular cantilever beam of radius 0.571 inch. The radius is chosen so as to have the same polar moment of inertia (Ip) as a rectangular beam of cross-sectional dimensions 1"× 1" as shown in Figure 4.6. A torque of magnitude 10 kip-inch is applied

at the free ends of both the beams. Each of these beams is modeled by one B33 beam element from the ABAQUS library of elements.

The beam cross section in ABAQUS can be specified in *BEAM SECTION or *BEAM GENERAL SECTION options. If the latter option is used, the section behavior is defined by giving the relationships of the axial force and moments on the section as functions of axial strains, curvature changes and twist. In the *BEAM SECTION option, the cross section is integrated numerically to obtain the generalized force-moment/strain-curvature relationship, thus allowing complete generality in the material response.

In the *BEAM GENERAL SECTION option, the geometry of the beam section and the material descriptions are combined so that no *MATERIAL reference is necessary. Thus nonlinear material response, specified in the *USER MATERIAL option cannot be given if this option is used to specify the beam section. For getting the stress and strain outputs, the points in the cross section at which the values of these variables are required should be defined by the user in *SECTION POINTS suboption. The local (x_1,x_2) coordinates of the points in the cross section on the beam local axes n_1 and n_2 should be given. Refer to Appendix A for the definition of beam local axes in ABAQUS. In *BEAM SECTION option, numerical integration over the cross section is used to compute the section response so that the stress or strain output can be asked for at certain integration points in the cross section as given in section 3.3.2 of ABAQUS User's Manual. The *MATERIAL option must be referenced in this case to provide the material description. The linear or nonlinear material response can be specified using the *USER MATERIAL option.

In the case of the cantilever beams described above, both of these options can used as discussed below. However, the *BEAM SECTION option is recommended for more general use owing to the complete user control over the specification of material properties. The material for the beams is assumed to be steel. Only linear material response is used. The material properties are, E = 2.9 E07 psi, $\nu = 0.1$,
$G = E/2(1+\nu) = 1.318$ E07 psi. The geometric properties are

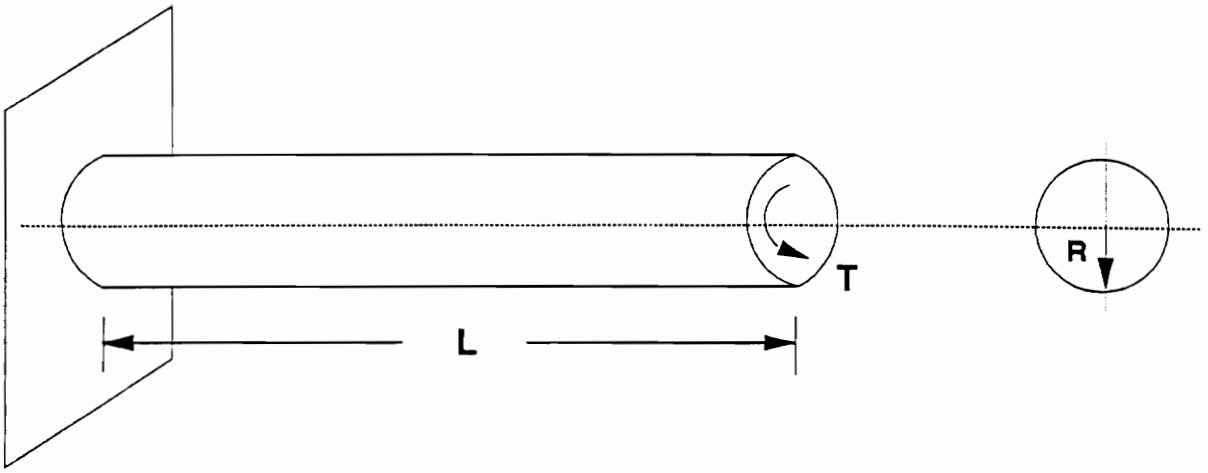


Figure 4.5 Circular cantilever subjected to torque at free end

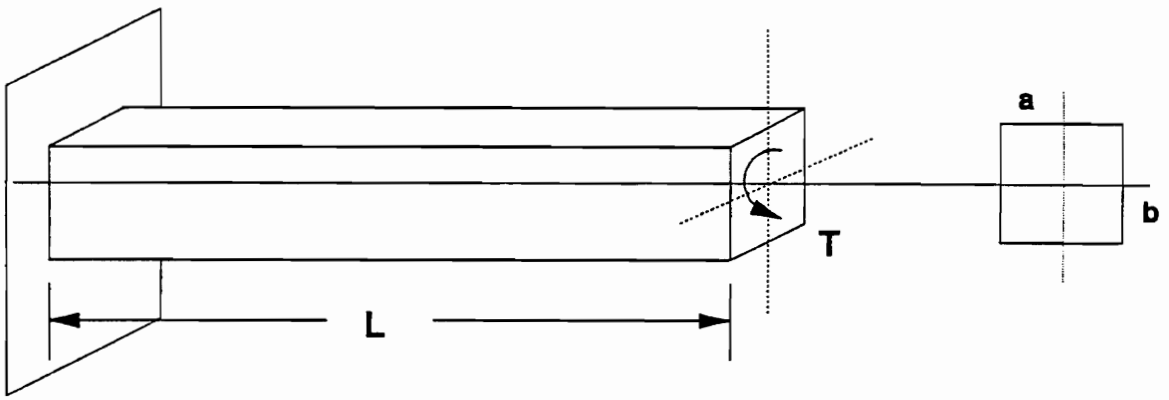


Figure 4.6 Rectangular cantilever subjected to torque at free end

Circular Section	Radius = R = 0.570732 in. Length of the beam = l =10 in. $I_p = \pi R^4/2 = 0.166666$ in.^{4}
Rectangular Section	cross section dimensions, a = 1 in, b = 1 in. Length of the beam = l = 10 in. $I_p = \frac{ab(a^2+b^2)}{12} = 0.16666$ in.^{4}

For the circular beam, the section can be defined as

*BEAM GENERAL SECTION, SECTION = CIRC

0.570732

0, 0, -1

2.9E07, 1.3182E07

As discussed before, the output points for stress and strain values can be defined as follows,

*SECTION POINTS

0., 0.570732, 0., -0.570732, 0.570732, 0., -0.570732, 0.

These are the x_1 and x_2 coordinates of points 7, 15, 11, 3 respectively (Figure 4.7). Alternatively, it can also be specified as

*BEAM SECTION, SECTION = CIRC, MATERIAL = USTEEL

0.0570732

The stress and strain components are printed at the default integration points 3, 7, 11, 15 as shown in Figure 4.7. Note that with this option the *TRANSVERSE SHEAR STIFFNESS card (sec. 6.5.18, ABAQUS) must be used. The material properties are specified by using *USER SUBROUTINE and *USER MATERIAL cards. It is worthwhile to note that

*STEP

*STATIC, LINEAR

can not be used when using the user material option. The file runs only till the preout stage with the error messages saying that this *STEP, LINEAR can not be used with nonlinear materials. This is because a nonlinear analysis is assumed when using the user

material option. In that case, the STEP card with NLGEOM parameter and the appropriate values of force (and moment) tolerances must be specified.

*STEP, NLGEOM
*STATIC, PTOL = , MTOL =

The correction factor for the shear modulus J_{SV}/J_n from Eq. 4.42 is entered as a material constant in the *USER MATERIAL card as follows:
*USER MATERIAL, CONSTANT = 3
**E,ν,J_{SV}/J_n
2.90E07, 0.1, 1.00

The value of the correction factor for the circular section is used as 1.00 since there is no warping. The value of shear modulus in the user subroutine (the Jacobian term J_{22}) is multiplied by this factor.
DDSDDE (2,2) = PROPS (3)*PROPS (1)/(2.*(1+PROPS (2))
STRESS (2) = DDSDDE (2,2)*TT

For an applied torque of 10 k-in, the angle of rotation of the free end and the maximum shear stress is obtained from Eq. (4.5) as follows. These values are confirmed by the analysis with ABAQUS.

$$\text{Angle of rotation} = \theta l = \frac{Tl}{GI_p} = \frac{10 \times 10^3 \times (10)}{1.3182 \times 10^7 \times 0.167} = 0.0455 \text{ rad}$$

$$\tau_{max} = \frac{T\,R}{I_p} = \frac{10 \times 10^3 \times 0.570732}{0.167} = 34.244 \times 10^3 \text{ psi}$$

$$\gamma_{max} = \tau_{max} / G = 2.5978 \times 10^{-3}$$

The rectangular beam can be analyzed in a similar way with the appropriate modifications such as SECTION=RECT in the cards defining the section. Initially, the correction factor value of $J_{SV}/J_n = 1.0$ is used to show that the warping is not taken into account. ABAQUS prints the shear stress/strain values for the space beams by default at

the corner points 1, 5, 21, 25 as shown in Figure 4.8. These points are at a radial distance of $\sqrt{1^2+1^2} = 0.707$ in. from the central axis. Therefore at these points

$$\tau = \frac{T R}{I_p} = \frac{10 \times 10^3 \times 0.707}{0.167} = 42.426 \times 10^3 \text{ psi}$$

$$\gamma = \tau / G = 3.2185 \times 10^{-3}$$

$$\text{angle of rotation} = \theta l = \frac{Tl}{GI_p} \quad 0.0455167 \text{ rad}$$

These values were obtained in the analysis with correction factor of 1.00. This shows that the Navier's torsion equations are used in ABAQUS even for the rectangular beams. From Eq. (4.42), the correction factor is chosen as

$$\frac{J_n}{J_{sv}} = \frac{12k}{\left[1+(b/a)^2\right]} = \frac{12 \times 0.1406}{2} = 0.8436$$

The shear stress values are maximum at the midpoints of the longer sides of the rectangle as discussed in the section 4.2. Thus we need the shear stress/strain output at the (non-default) integration points 3, 23 or 11, 15 (Figure 4.8), depending on whether a or b is bigger. This can be specified in the input file as,

*EL PRINT

3,11,15,23

S,E

From the Eqs. (4.33), (4.34) and (4.35)

$$\text{Angle of rotation} = \frac{Tl}{ka^3bG} = 0.054$$

$$\tau_{max} = \frac{T}{k_2 a^2 b} = 48.08 \text{ ksi}$$

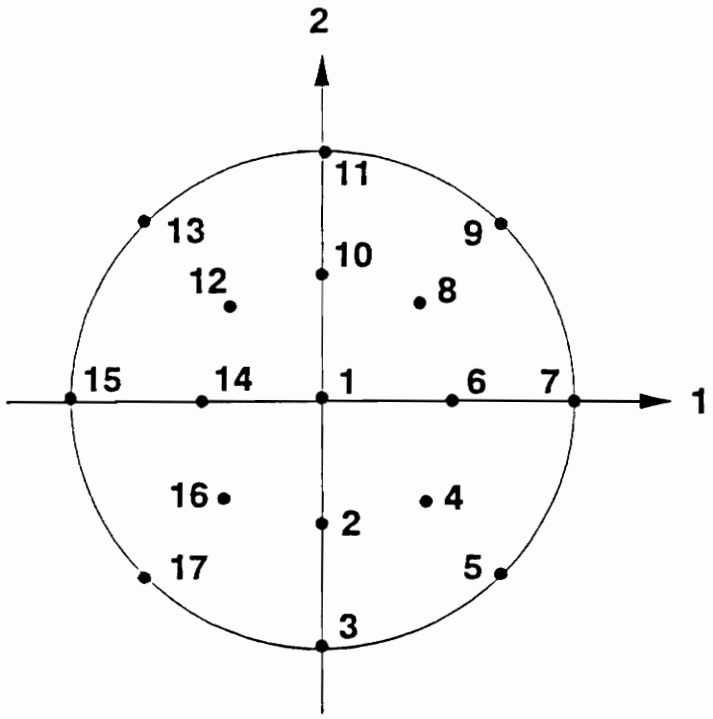


Figure 4.7 Circular beam in space, default integration points

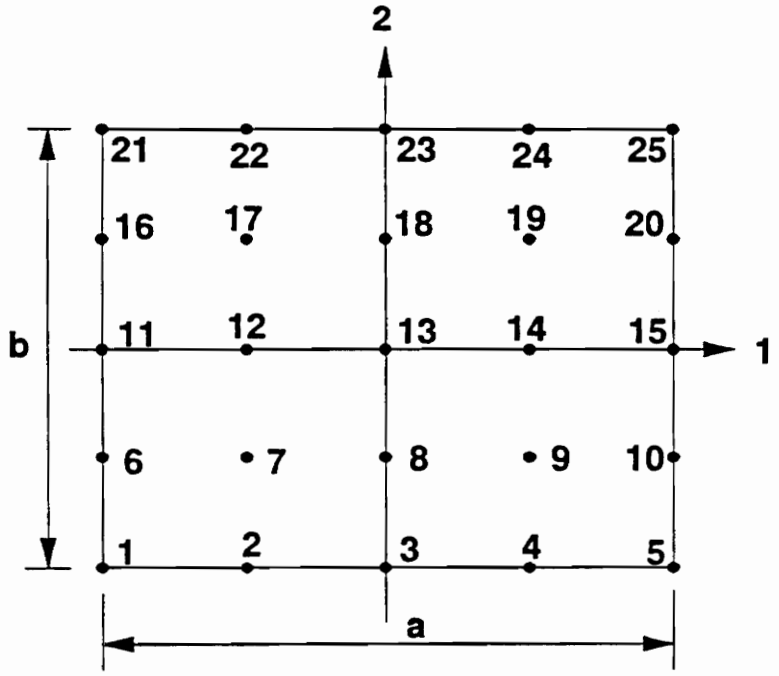


Figure 4.8 Rectangular beam in space, default integration points

$$\tau_{x,\,max} = \frac{T}{k_3 a^2 b} = 48.08 \text{ ksi}$$

The ABAQUS results correctly give the above angle of rotation of the free end, however the shear stress at the points 3, 11, 15, 23 is 30 ksi, which is still obtained by the Navier's equation as

$$\tau_{max} = \frac{T\,R}{I_p} = \frac{10 \times 0.5}{0.167} = 30.00 \text{ ksi}$$

Also, the shear strain is obtained using the modified value of shear modulus. A method to get correct stresses was tried as follows. If τ_{sv} and τ_n are stresses by Saint-Venant and Navier solutions, then

$$\frac{\tau_{sv}}{\tau_n} = \frac{T/k_2 a^2 b}{Tr/I_p} = \frac{I_p}{k_2 a^2 br} = \frac{(a^2+b^2)}{12 k_2 ar} \qquad (4.43)$$

For the maximum stress at r = a/2

$$\frac{(\tau_{sv})_{max}}{(\tau_n)_{max}} = \frac{(a^2+b^2)}{6k_2 a} \qquad (4.44)$$

In case of the cantilever beam under consideration

$$\frac{(\tau_{sv})_{max}}{(\tau_n)_{max}} = \frac{2}{6 \times 0.208} = 1.6026$$

In the user subroutine, the equation for torsional stress can be modified as
STRESS (2,2) = PROPS(4)*DDSDDE(2,2)*TT
where PROPS(4) is the material constant τ_{sv}/τ_n specified in *USER MATERIAL card.

Unfortunately, if the shear stress is defined in this way, no output is obtained since the convergence is not achieved. This is due to the incompatibility between the stress and the Jacobian equation. In chapter 2 the issue of constitutive modeling in the user subroutine

is addressed in detail. Thus there seems to be only one way to obtain the correct shear stresses according to Saint-Venant's solution, which is modifying the maximum shear stresses obtained in the analysis by the correction factor in Eq. (4.44). The stress of 30 ksi in the present example case is, therefore, multiplied by a factor of 1.6026 to get the true stress value of 48.08 ksi.

Cantilever beams with varying cross sections (Figures 4.9 and 4.10) were analyzed next, with the torques of magnitude 10 k-in applied as shown. Once again, the radii of parts of the circular beam are chosen to have the same I_p as the corresponding sections in the rectangular beam. For the circular composite beam, the torque at the fixed end is 20 k-in. Therefore, for L = 10 in and $I_p = 0.8333$ in^4, the angle of rotation at the section between the left and the right portion is 0.0182 rad according to Navier's equations. The maximum shear stress, neglecting the stress concentration at the location of the change of cross section dimension, is at the surface (at R = 0.85344 in), and is equal to 20.48 ksi. For the right portion, the shear stress values are the same as in the first test case (Figure 4.5). The rotation of the free end is the sum of the rotations of the two different portions of the beam in their individual free body diagrams, i.e., the total angle of rotation = 0.0182 + 0.0455 = 0.0637 rad.

For the rectangular beam, the left cross section has the ratio b/a = 2.0. For this, we have from Table 4.1, k = 0.229, $k_2 = 0.246$, $k_3 = 0.155$. Again from Eqs. (4.33), (4.34) (4.35), we get

$$\text{Angle of rotation} = 0.033127 \text{ rad}$$

$$\tau_{max} = 40.65 \text{ ksi}$$

$$\tau_{x,\,max} = 32.26 \text{ ksi}$$

$$\frac{J_n}{J_{sv}} = 0.5496$$

$$\frac{(\tau_{sv})_{max}}{(\tau_n)_{max}} = 3.3875$$

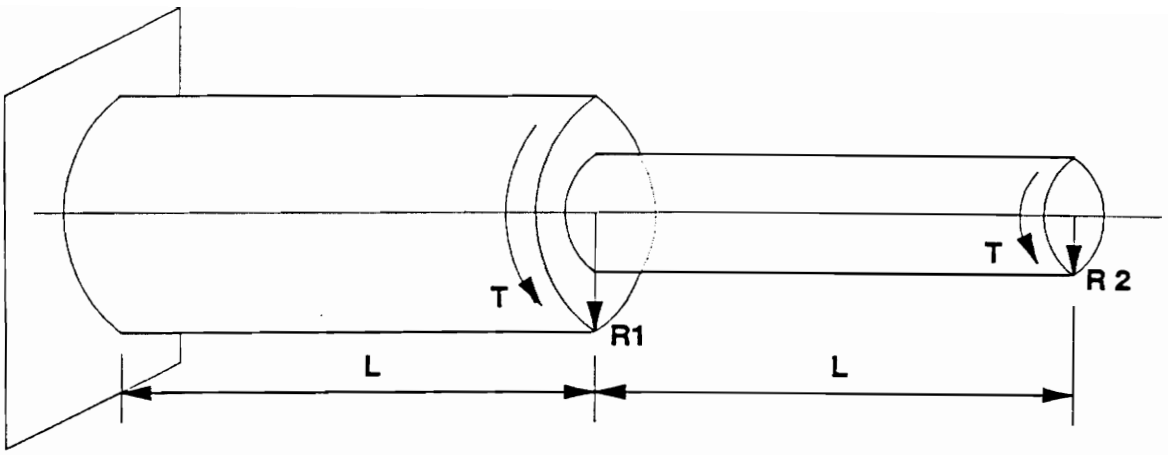


Figure 4.9 Circular beam with varying cross section

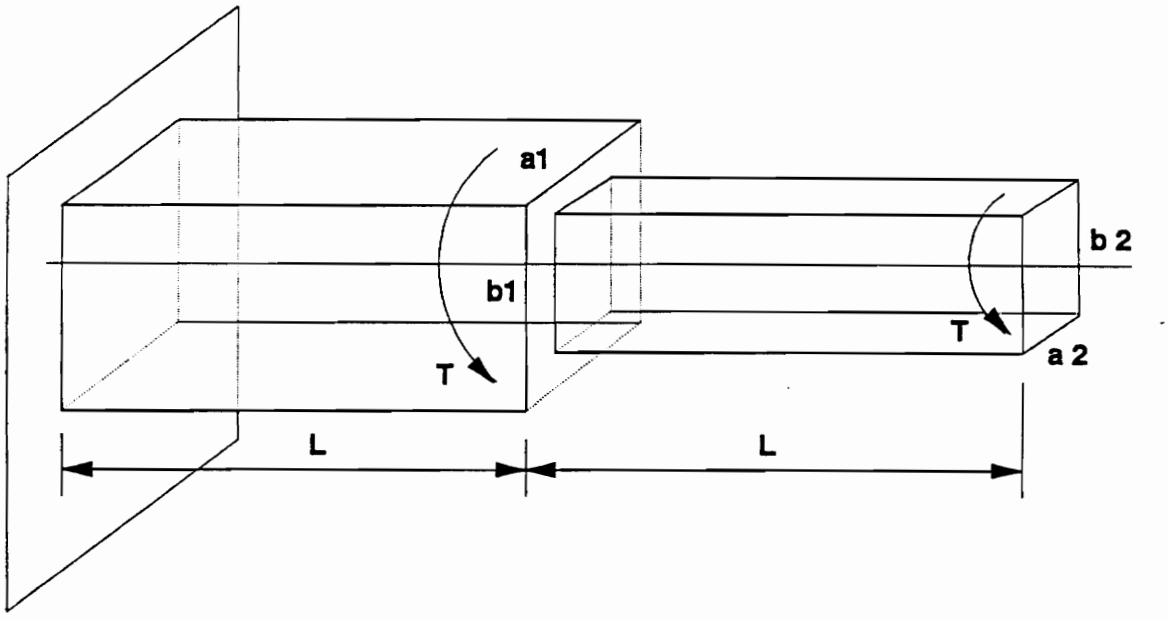


Figure 4.10 Rectangular beam with varying cross section

The stress values for the right portion of the beam remain the same as the earlier case of single rectangular beam. The angle of rotation of the free end = 0.033 + 0.054 = 0.087. All the above values in case of the circular and rectangular beams were verified by the analyses with ABAQUS.

Note that the two portions of the beam have a different b/a ratio. Therefore, different shear correction factors are specified as material constants in two different *USER MATERIAL cards. Consequently, we need to provide two different User Subroutines corresponding to two different user materials. These two materials are denoted by Usteel1 and Usteel2 in the *USER MATERIAL card. Also, these names are used in the User Subroutine as the value for the CMNAME character 'passed in' the subroutine by the main program. The input files for the test case of the composite beams and results for each of them are given in Appendix B.

4.5 Analysis of Dome Cap Model with Warping of Beam Cross sections

A method to include the warping of rectangular cross section in the analysis with ABAQUS is discussed in the earlier sections. The modified dome cap model described in section 3.2 is analyzed to include the warping of the beam elements. The beams in this model have dimensions of a = 6.75" and b = 11.0". For these beam dimensions, we have

$$\frac{b}{a} = \frac{11.0}{6.75} = 1.63$$

From Table 4.1, by linear interpolation, we get k = 0.206.

From Eq. (4.42)

$$G_e = \frac{12k}{\left[1+(b/a)^2\right]}G = 0.676\,G$$

Thus, the shear modulus for the beams needs to be modified by the factor of 0.676 to take into account warping. This is done in the user subroutine UMAT as described in

the previous section. The results obtained in the analysis with nonlinear material law are as follows.

Full snow : λ_{cr} = 9.67, Deflection (node 1) = 5.64 in.
Maximum tensile stress = 4263 psi (element 5 at node 6)
Maximum compressive stress = -7010 psi (element 44 at node 16)
Half snow : λ_{cr} = 8.431, Deflection (node 1) = 2.665 in.
Maximum tensile stress = 6602 psi (element 15 at node 8)
Maximum compressive stress = -9060 psi (element 16 at node 8)

The critical load factor obtained in the analysis with warping is lower than the one obtained in the analysis without considering warping (Tables 4.2 and 4.3). This shows that the cross section warping due to the twisting of the rectangular beams lowers the ultimate load capacity for the dome cap model. This is found to be true in case of all the material laws discussed in chapter 2. The effect of warping is more pronounced for the half snow load case. This is bacause, for half snow loading, the beams are subjected to more twisting about their centroidal axis than for the full snow loading.

Table 4.2

Results for the Dome Cap Model with and without Warping of Beams : Full Snow

	λ_{cr} for analysis without warping G = 1.6 E05 psi	λ_{cr} for analysis with warping G = 1.6 E05 psi	Change in λ_{cr} relative to λ_{cr} for analysis without warping
linear law E = 1.8 E06	10.01	8.76	12.5 %
Bilinear law	11.75	9.68	17.6 %
Nonlinear law	10.95	9.67	11.7 %

Table 4.3

Results for the Dome Cap Model with and without Warping of Beams : Half Snow

	λ_{cr} for analysis without warping G = 1.6 E05 psi	λ_{cr} for analysis with warping G = 1.6 E05 psi	Change in λ_{cr} relative to λ_{cr} for analysis without warping
linear law E = 1.8 E06	10.76	6.87	36.15 %
Bilinear law	12.22	8.48	30.6 %
Nonlinear law	11.07	8.43	23.85 %

4.6 Analysis of Dome with Warping of Beam Cross sections

The dome model consists of beams with three different cross-sectional dimensions.

main beams I	6.75" ×11.0"	b/a = 1.63, k = 0.206
main beams II	5.0" ×11.0"	b/a = 2.20, k = 0.237
edge beams	3.0" ×12.25"	b/a = 4.08, k = 0.281

The effective shear modulus values for these three beam types are 0.676G, 0.487G and 0.1912G, respectively, where G = 1.60 E05 psi. Thus, there is a reduction of 32.4 %, 51.3 % and 80.9 %, respectively in the shear modulus values for these three beams. The modified shear modulus values are G_1 = 1.08 E05 psi, G_2 = 0.78 E05 psi, G_3 = 0.31 E06 psi.

To incorporate warping of the beams in the dome analysis, it is required to provide different user subroutine UMAT for the three beams. The three beam types are defined with the material names UWOOD1, UWOOD2 AND UWOOD3 in their respective *USER MATERIAL cards. In the corresponding user subroutine UMAT, the CMNAME character is assigned with these three names. The shear moduli are modified by the correction factors passed through the variable PROPS(3) as earlier.

The dome model in section 2.5 was analysed for warping of cross section of all beams. Nonlinear material law (Connors' model) is used. The results from the analysis are as follows.

Full snow load : $\lambda_{cr} = \lambda_{max} = 9.90$ U3 (Node 1) = -8.05 in.

Half snow load : $\lambda_{cr} = 7.45$ U3 (Node 1) = -3.62 in.
$\lambda_{max} = 7.97$ U3 (Node 1) = -3.95 in.

The results without shear modification are given in section 2.5. It can be seen that there is 2.1 % and 0.2 % reduction in the ultimate load capacity in the above two load cases as compared to the results in section 2.5. This indicates that there is no significant effect of change in the shear modulus on the behaviour of the dome model with the decking modeled by truss bracing.

Chapter 5

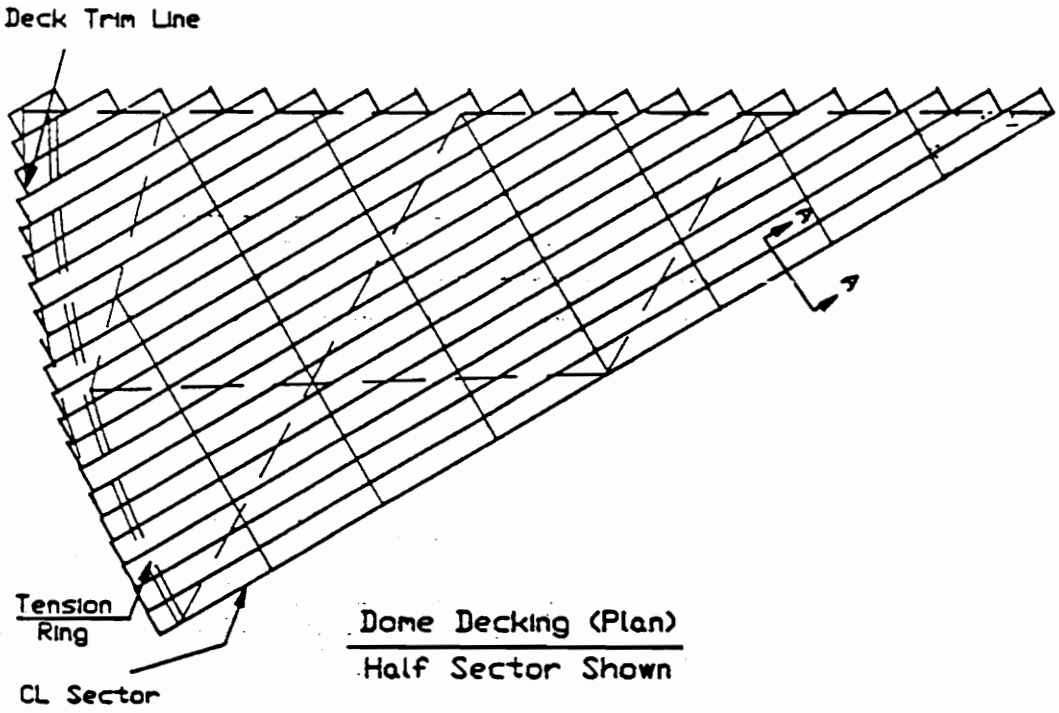
Formulation And Testing Of Nonlinear Beam/Connector Elements

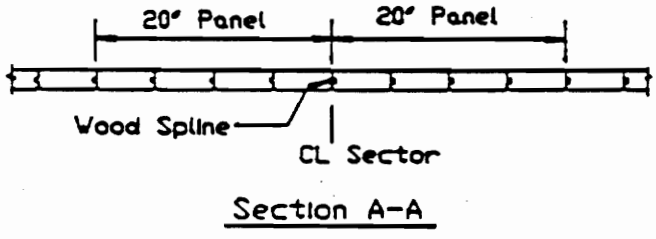
5.1 Introduction

The glulam dome analyzed in this study is covered with a 2" tongue-and-groove wood decking fastened to the beams and purlins with nails (Figure 5.1). In order to take into account the stabilizing effect of the decking on the beams, Wu (1991) and Telang (1992) used a truss bracing to model the decking. A 3-D finite element beam/connector (b/c) element model was formulated and tested by Tsang (1992) for the dome cap model, in order to replace the truss bracing and to model the nailed connections between the decking and the beams. The beam/connector element model in this study is based upon the method used by Dolan (1989). The nails are modeled as spring elements attached to the beam at the locations of the nails in the real structure. The spring element, in general, is called the connector element and does not have any nodes of its own. It uses the nodes and associated degrees of freedom (DOF) of the beam itself, irrespective of the number of connectors attached. This approach of modeling the nails is ideal for analyzing large structures since it saves significant computer time and memory due to reduced number of nodes and DOF in the finite element model of the structure.

The connector elements in the beam/connector model used by Tsang (1992) were linear springs. A constant stiffness value was used by linearizing the load-deflection curve of the nailed joint. This, however, does not truly represent the nonlinear character of the connector load-deformation relationship. The nonlinearity must be taken into account if the designer wants to estimate ultimate loads based upon the connection behavior (Foschi, 1977). For this reason, a nonlinear beam/connector element is developed in this chapter and used for the analysis of the dome cap and the full dome in the following chapter.

The properties assigned to the connector springs must be obtained from experiments on the actual connections used since it is often difficult to calculate the required properties taking into account all the parameters influencing the connection behavior (Foschi, 1977). The load-deflection curve used to assign properties to the nonlinear connector in the beam/connector element, and the experiments done on the nailed





Note: 2-16d face nails thru each 2x6 within the panel @ each support.
1-16d toe nail on the tongue edge of each support.

Figure 5.1 Tongue-and-groove wooden decking of the dome

connections to obtain this curve are discussed in section 5.2. These nailed connections are similar to the connections in the glulam dome analysed in this study.

The formulation of the 2D and 3D connector stiffness matrix based on a constant connector stiffness of connector is reviewed in section 5.3. The nonlinear connector element is defined in the user subroutine UEL for the analysis with ABAQUS. The development of the subroutine UEL used in the geometrically nonlinear analysis of the dome is presented in section 5.4. Numerous test cases were analyzed with 2D and 3D beam/connector elements before the subroutine for the dome analysis was developed. These are discussed and their results are presented in section 5.5.

5.2 Load-deflection Curve for Nails

Nails are commonly used as fasteners in timber structures. The nail size is specified by the pennyweight of the nail (abbreviated by 'd'), which is associated with the length of nail. In the glulam dome at Raleigh, NC, 16-d common wire nails with a diameter of d = 0.162 inch are used as connectors between the wooden decking and the beams. This connection is assumed to be a lateral load connection, since the lateral forces are transmitted to the beams as well as to the nailed joints from the decking (Mohhamad, 1990). The decking restrains the beams laterally, which is its primary function. For this reason, it is necessary to determine the lateral load-deflection relationship of a nailed joint.

A review of nail behavior under lateral loads and a discussion of some earlier theories on load-deflection relationships of nailed joints is presented by Tsang (1992). The empirical equation developed by McLain (1975) to predict the load-slip curve of a nailed connection was used by Tsang (1992) to get the linearized load-deflection curve for the nails. One of the parameters in this empirical formulation is found using an equation derived by Wilkinson (1971) to provide a value of the initial slope of the load-slip curve based on elastic theory. This model, however, was developed for a specific joint configuration using 8-d common wire nails. Also, Wilkinson's equation is valid only up to a proportional limit slip of 0.011 in. and McLain's formula predicts the load-slip curve up to joint slip of 0.1 in. Thus, the model is useful to estimate the initial stiffness of the nail, but it cannot be used to predict the maximum load carrying capacity of the nail (Foschi, 1974). Because of these limitations in McLain's model, it is necessary to obtain a more general formula for the load-deflection curve based on experimental results.

Foschi (1974) developed a nonlinear load-deflection model with three parameters, K_0, K_2, and P_0 to model the monotonic load-displacement curve for a nailed connection. Monotonic loads are non-reversing loads that are applied only in one direction such as a ramp load (Dolan, 1992). Figure 5.2 shows the parameters used to describe the load-displacement curve. Foschi's model was modified by Dolan (1989) for nail deformations greater than Δ_{max}. The capacity of the nail decreases from the maximum load capacity, giving rise to the negative slope $-K_3$.

The load-deflection curve is described by the following equations.

$$F = (P_0 + K_2 \Delta)\left(1 - \exp\left(-\frac{K_0 \Delta}{P_0}\right)\right) \quad \text{..... for } \Delta < \Delta_{max} \qquad (5.1)$$

and

$$F = (P_0 + K_2 \Delta_{max})\left(1 - \exp\left(-\frac{K_0 \Delta_{max}}{P_0}\right)\right) - K_3 (\Delta - \Delta_{max}) \quad \text{..... for } \Delta > \Delta_{max} \qquad (5.2)$$

Eq.(5.2) applies till the load capacity of zero is reached.

To get a good estimate of the above parameters for the nailed connections in the glulam dome at Raleigh, NC, monotonic tests were performed on nailed connections with 16-d common nails and with Douglas Fir and Southern Pine wood. The nailed connection configuration is shown in Figure 5.3. The experimental arrangement for the monotonic loading of the nailed joints is shown in Figure 5.4.

To prepare the nailed connection samples, 3/32" holes were drilled for the 16-d nails. The samples were conditioned for a week at 65 % relative humidity and 20°C (68°F) temperature, in order to get uniform moisture content in all the samples. It also gives wood fibers surrounding the nails time to relax so that the connections in the sample resemble more closely connections in the real structure.

Five samples each with Douglas Fir and southern pine were tested for lateral load capacity. The average MC and SG for the Douglas Fir and southern pine samples were 14 % and 0.52, and 15 % and 0.58, respectively. The southern pine samples showed softer response compared to the Douglas Fir samples. Figure 5.5 shows the load-deflection

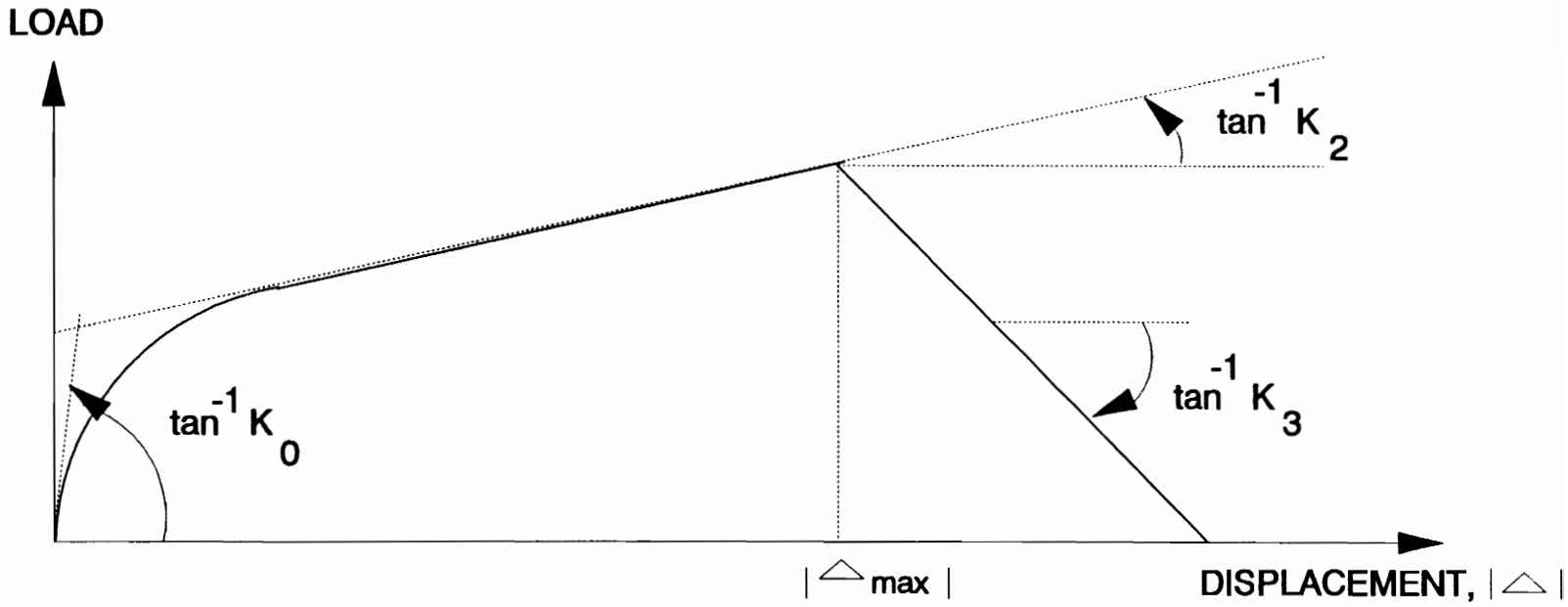


Figure 5.2 Foschi's load-deflection curve

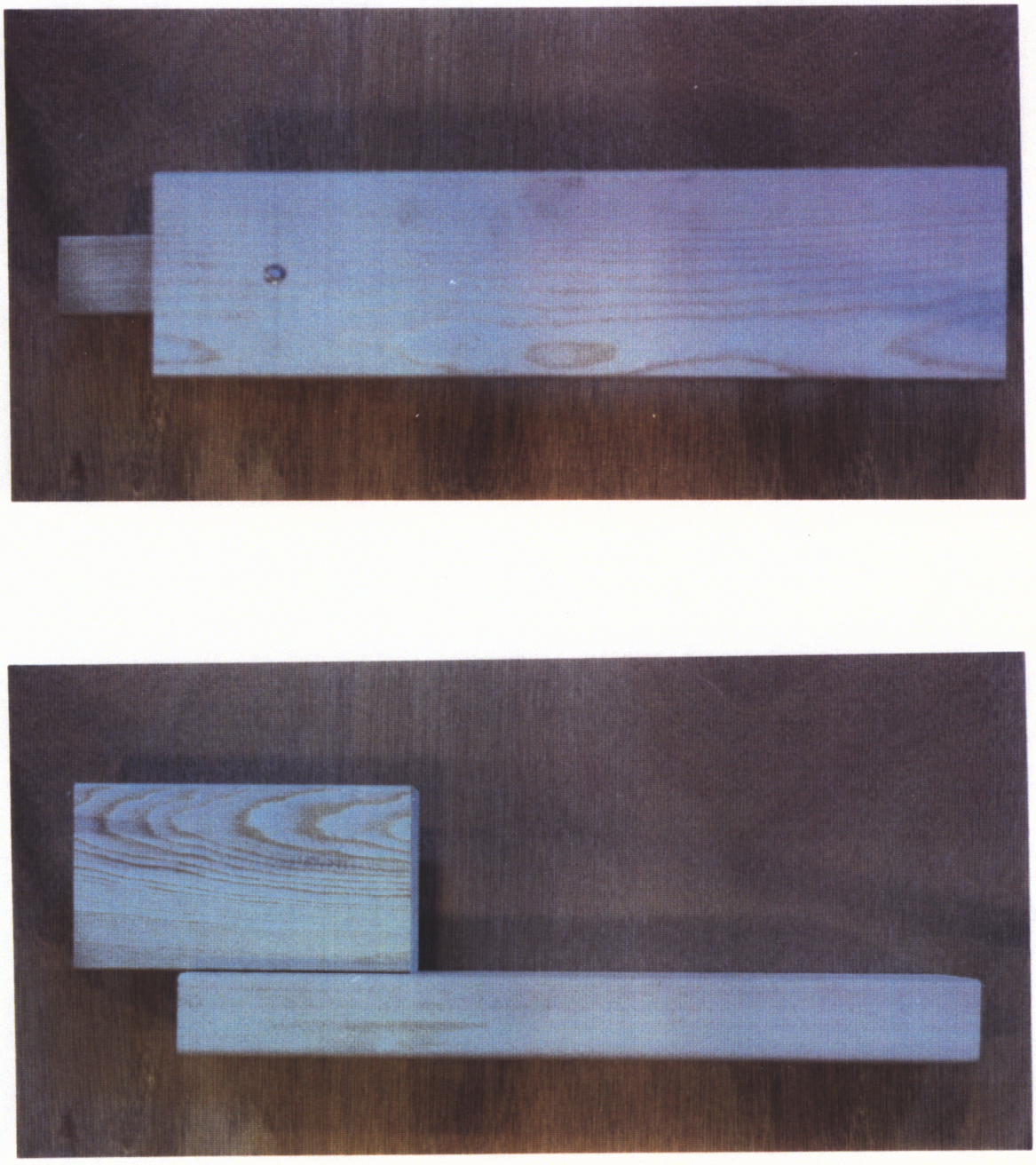


Figure 5.3 (a) Nailed connection for the lateral load tests

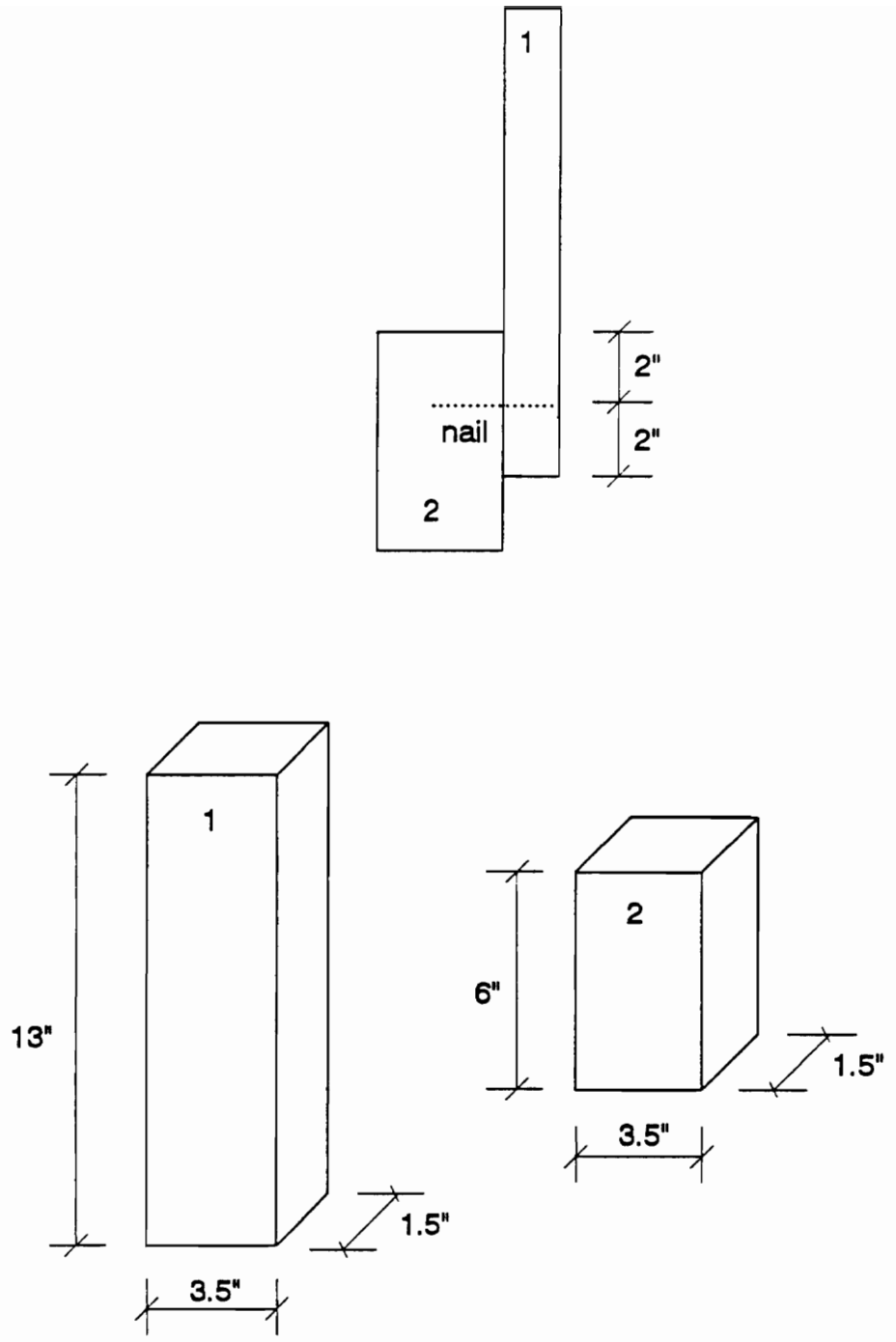


Figure 5.3(b) Dimensions of the wood samples in the tests on the nailed connections

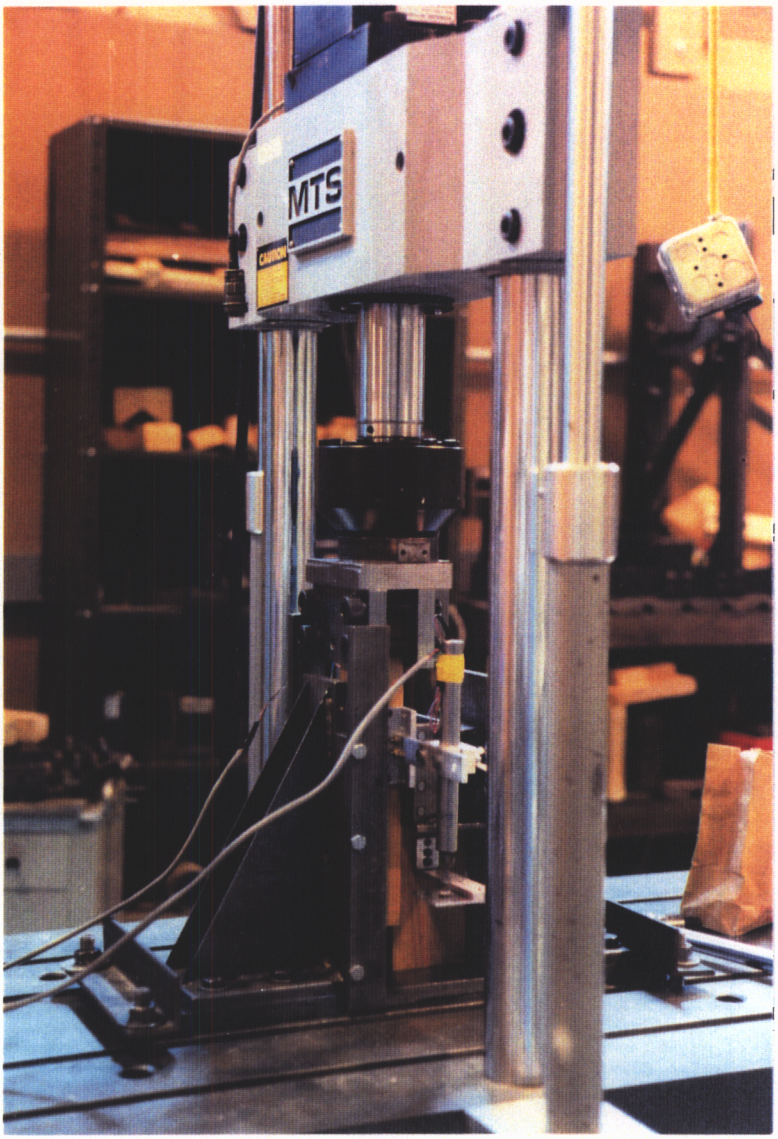


Figure 5.4 Experimental setup for the lateral load tests on the nailed connections

curves obtained for the southern pine samples. The monotonic test data of each sample was analyzed using least square regression method to fit the data into Eq. (5.1). This was done using the program TableCurve (1992). The average values of the various parameters in Foschi's model for the southern pine samples were found to be

$$K_0 = 19800 \text{ lb/in}$$
$$K_2 = 18 \text{ lb/in}$$
$$P_0 = 365 \text{ lb}$$

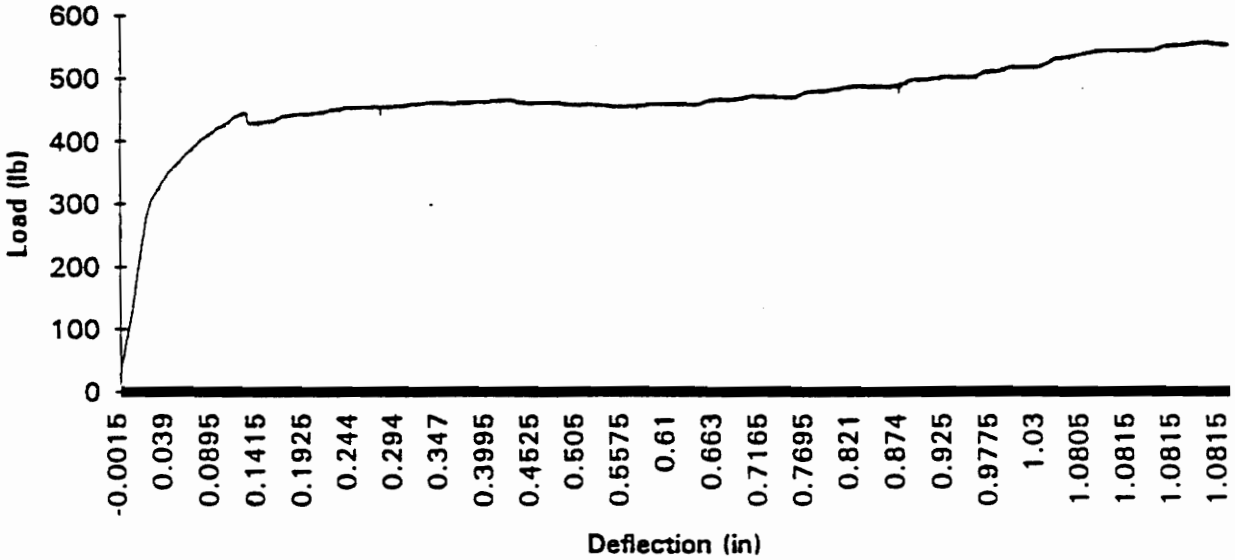
The parameter K_3 was not obtained in the experiments since it is not used in the present study. From Figure 5.5, it can be seen that the lateral load-deflection response of the nailed connection is nearly elastic-perfectly plastic in case of sothern pine wood samples. Based upon the above values, an elastic-perfectly plastic curve as shown in Figure 5.6 can be assumed as the nonlinear load-deflection curve for the connector elements in the b/c models of the dome cap and the full dome. In this case, the bilinear P-Δ curve has the following characteristics.

$$\gamma_1 = 6850 \text{ lb/in}$$
$$\Delta_1 = 0.056"$$
$$\gamma_2 = 0.0 \text{ lb/in}$$
$$\Delta_{max} = 1.0"$$
$$P_0 = 384 \text{ lb/in}$$

The value of $\Delta_{max} = 1.0"$ is the average nail deflection at which the load resisted by the nailed connection (Figure 5.3a) is maximum. The experiments were stopped at the an average nail deflection of 1.10 in. As discussed earlier, the modification by Dolan (1989) suggests a negative slope for the load-deflection curve after Δ_{max}. However, it was decided to disconnect the nail completely when the deflection Δ_{max}, corresponding to the maximum load resisted by the nail in this case, is reached. This is because generally the lateral load capacity of the nailed connection reaches zero rapidly after the nail deflection of Δ_{max}. This is shown in Figure 5.6 by the dotted line at $\Delta = 1.0"$. These values are used in the user subroutine UEL to specify the bilinear lateral load-deflection characteristics of the connectors in the dome cap and full dome models.


Load (lb)
450
400
350
300
250
200
150
100
50
0
0.015
0.059
0.1085
0.1575
0.2055
0.256
0.3055
0.356
0.4065
0.457
0.508
0.559
0.6105
0.6615
0.7135
0.765
0.8165
0.8665
0.9185
0.9675
1.018
1.069
1.0965
1.099
1.099
Deflection (in)


Load (lb)
400
350
300
250
200
150
100
50
0
0
0.0455
0.0965
0.1485
0.201
0.2535
0.3065
0.36
0.413
0.468
0.522
0.576
0.6305
0.685
0.7395
0.7935
0.8475
0.8995
0.9535
1.0065
1.0585
1.1015
1.109
1.109
1.109
Deflection (in)


Load (lb)
600
500
400
300
200
100
0
-0.0015
0.039
0.0895
0.1415
0.1925
0.244
0.294
0.347
0.3995
0.4525
0.505
0.5575
0.61
0.663
0.7165
0.7695
0.821
0.874
0.925
0.9775
1.03
1.0805
1.0815
1.0815
1.0815
Deflection (in)

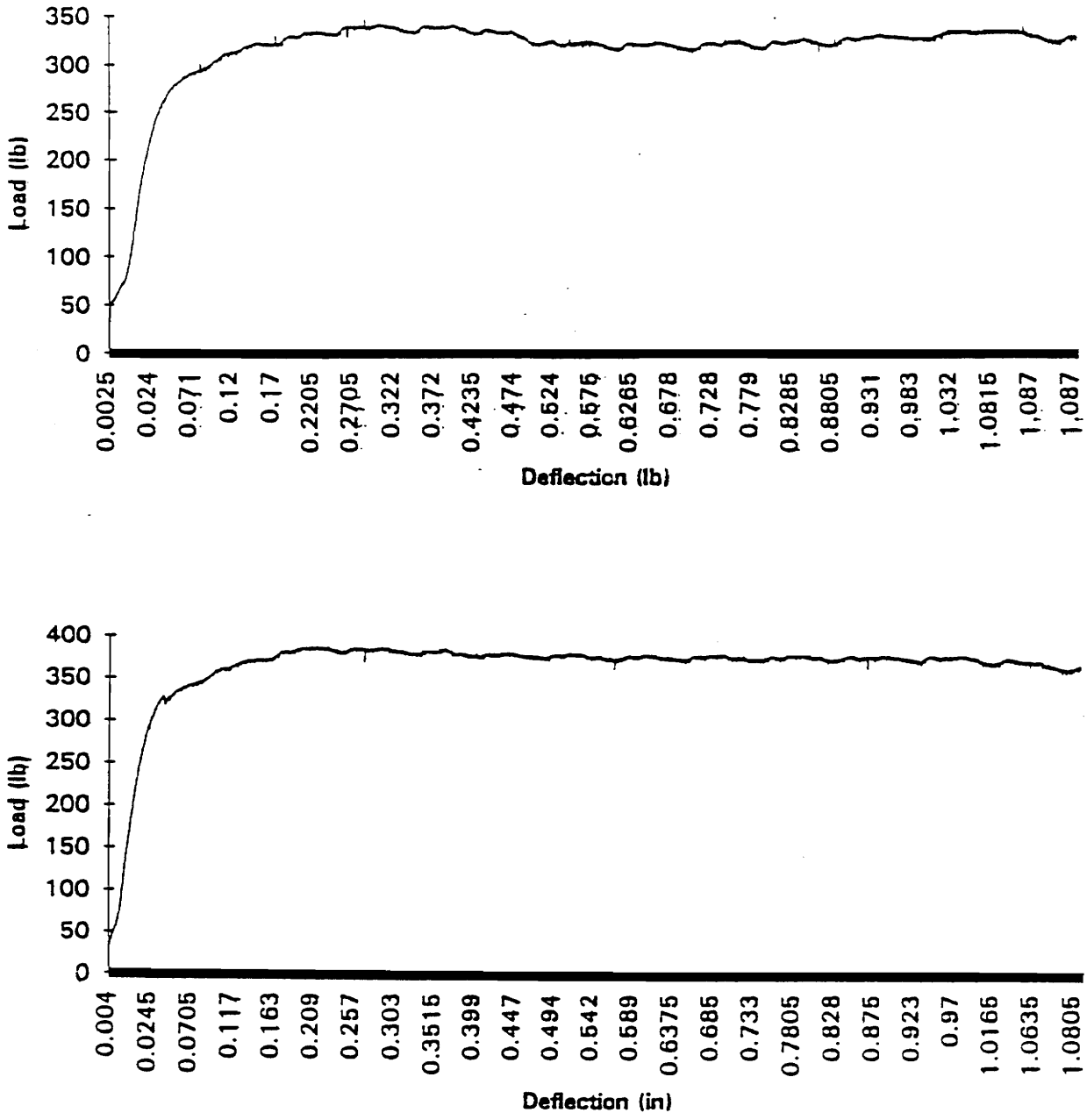


Figure 5.5 Load-deflection curves for the test samples with southern pine wood

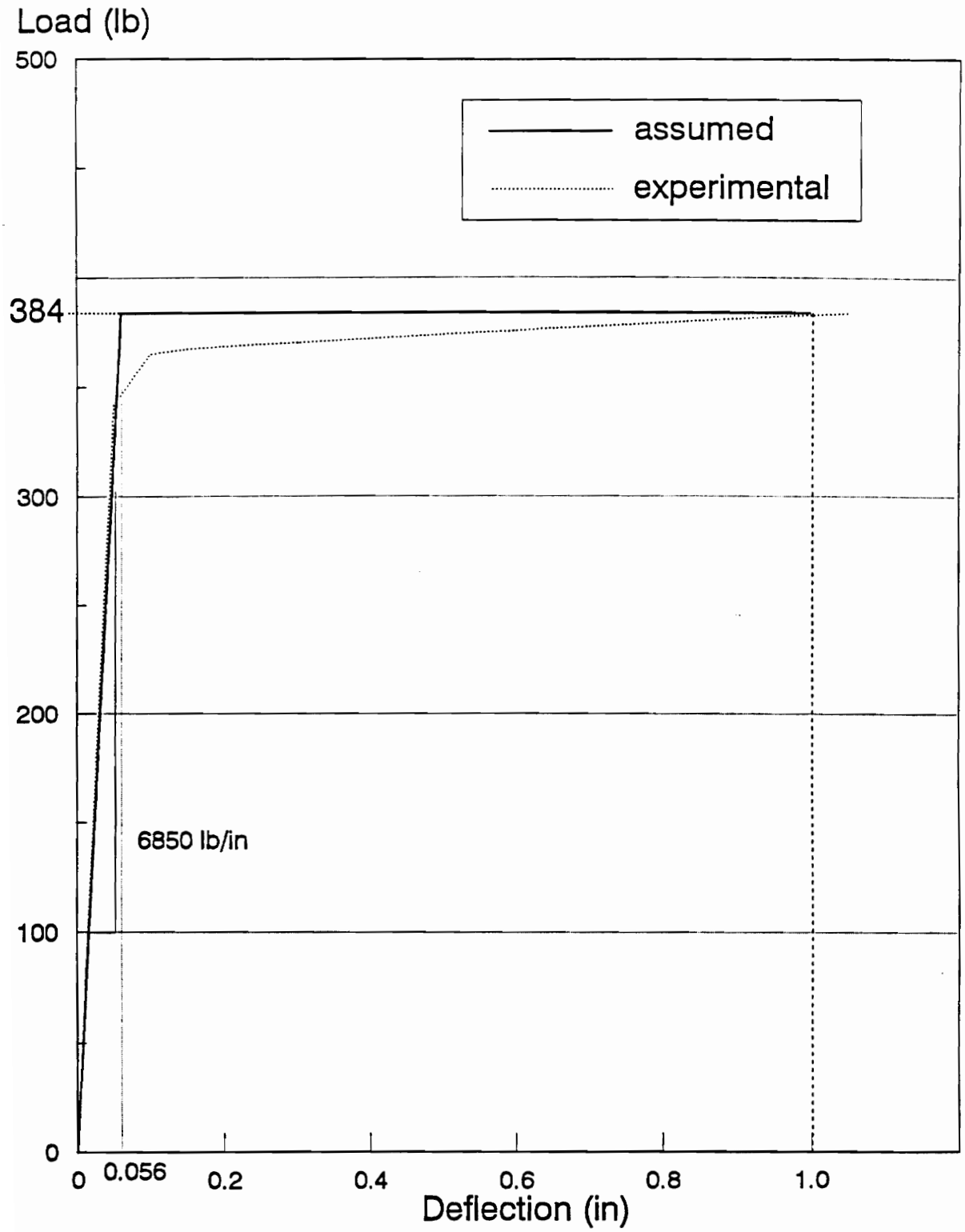


Figure 5.6 Bilinear elastic-plastic load-deflection curve assumed for the 16-d nailed connection in Southern Pine wood

5.3 Formulation of 2D and 3D Connector Stiffness Matrices

The plane (2D) beam element with attached connector (Figure 5.7) has four DOF, namely d_1, d_2, d_3, d_4. The connector element is a nonlinear spring with stiffness of $\gamma(v_s)$, which is a function of the spring deflection v_s. As discussed in the previous section, the nonlinear load-slip curve of a nail is approximated by a bilinear curve. Thus, within a certain deflection range of the spring, a constant stiffness value can be used. For a constant stiffness of γ, the spring energy is

$$Us = \frac{1}{2}\gamma v_s^2 = \frac{1}{2} v_s^T \gamma v_s \tag{5.3}$$

Since the connector element uses the same DOF as the beam element, its deflection can be obtained from beam interpolation functions as (Tsang, 1992)

$$\begin{aligned} v_s(\xi) &= N_1(\xi)\, d_1 + N_2(\xi)\, d_2 + N_3(\xi)\, d_3 + N_4(\xi)\, d_4 \\ &= N_s\, d \end{aligned} \tag{5.4}$$

where

$$\begin{aligned} N_1(\xi) &= 1 - 3\xi^2 + 2\xi^3 \\ N_2(\xi) &= (\xi - 2\xi^2 + \xi^3)\, l \\ N_3(\xi) &= 3\xi^2 - 2\xi^3 \\ N_4(\xi) &= (-\xi^2 + \xi^3)\, l \\ \xi &= \frac{s}{l} \end{aligned} \tag{5.5}$$

and

$$N_s = [N_1 \; N_2 \; N_3 \; N_4]$$

$$d = \begin{bmatrix} d_1 \\ d_2 \\ d_3 \\ d_4 \end{bmatrix}$$

From Eqs. (5.3) and (5.4), the spring energy can be written as

$$U_s = \frac{1}{2} d^T N_s^T \gamma N_s d = \frac{1}{2} d^T k_s d \tag{5.6}$$

k_s is the connector stiffness matrix given by

$$k_s = N_s^T \gamma N_s$$

$$= \gamma \begin{bmatrix} N_1 \\ N_2 \\ N_3 \\ N_4 \end{bmatrix} [N_1 \; N_2 \; N_3 \; N_4]$$

$$= \gamma \begin{bmatrix} g_1 & g_2 & g_4 & g_7 \\ & g_3 & g_5 & g_8 \\ & & g_6 & g_9 \\ \text{sym.} & & & g_{10} \end{bmatrix} \tag{5.7}$$

where

$$\begin{aligned} g_1 &= N_1 N_1 \\ g_2 &= N_1 N_2 \\ g_3 &= N_2 N_2 \\ g_4 &= N_1 N_3 \\ g_5 &= N_2 N_3 \\ g_6 &= N_3 N_3 \\ g_7 &= N_1 N_4 \\ g_8 &= N_2 N_4 \\ g_9 &= N_3 N_4 \\ g_{10} &= N_4 N_4 \end{aligned} \tag{5.8}$$

The total energy of the beam/connector element, composed of the beam and attached spring, is the addition of the internal energy of the beam (U_b) and the spring energy (U_s).

$$U = U_b + U_s = \frac{1}{2} d^T k_b d + \frac{1}{2} d^T k_s d$$

$$= \frac{1}{2} d^T k d \tag{5.9}$$

where

k_b = plane beam stiffness matrix

$k = k_b + k_s$ = beam/connector stiffness matrix

In case of a multiple number of springs attached to the beam at different locations, the total energy of the beam/connector element is

$$U = U_b + \sum_{i=1}^{n} U_s^i$$

$$= \frac{1}{2} d^T (k_b + \sum_{i=1}^{n} k_s^i) d \qquad (5.10)$$

where

U_s^i = energy of the ith spring
k_s^i = stiffness of the ith connector
n = total number of springs

and

$$k = k_b + \sum_{i=1}^{n} k_s^i$$

= stiffness matrix of b/c element with multiple springs

The connector stiffness matrix for a plane frame element can be generated from the same for the beam element (Eq. 5.7) using member code method (Holzer 1985). The member code matrix for doing the above is obtained by comparing the plane beam and plane frame elements in Figure 5.8 and is given below.

$$M = [2 \quad 3 \quad 5 \quad 6] \qquad (5.11)$$

Applying this to the matrix in Eq.(5.7), k_S for plane frame element is found to be

$$k_S = \gamma \begin{bmatrix} 0 & 0 & 0 & 0 & 0 & 0 \\ & g_1 & g_2 & 0 & g_4 & g_7 \\ & & g_3 & 0 & g_5 & g_8 \\ & & & 0 & 0 & 0 \\ & & & & g_6 & g_9 \\ \text{sym.} & & & & & g_{10} \end{bmatrix} \qquad (5.12)$$

This transformation is possible since the connector offers no resistance to the axial deformation of the beam. Thus, 2, 3, 5, and 6 are the only active DOF in the plane frame

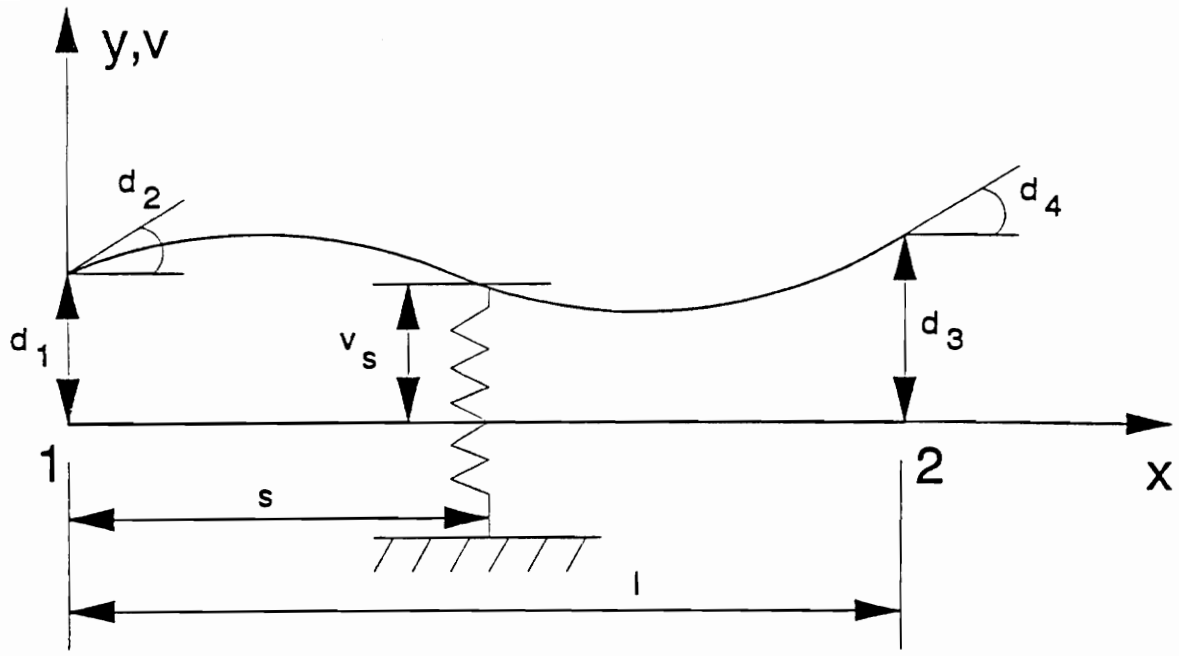


Figure 5.7 Plane beam element with an attached connector

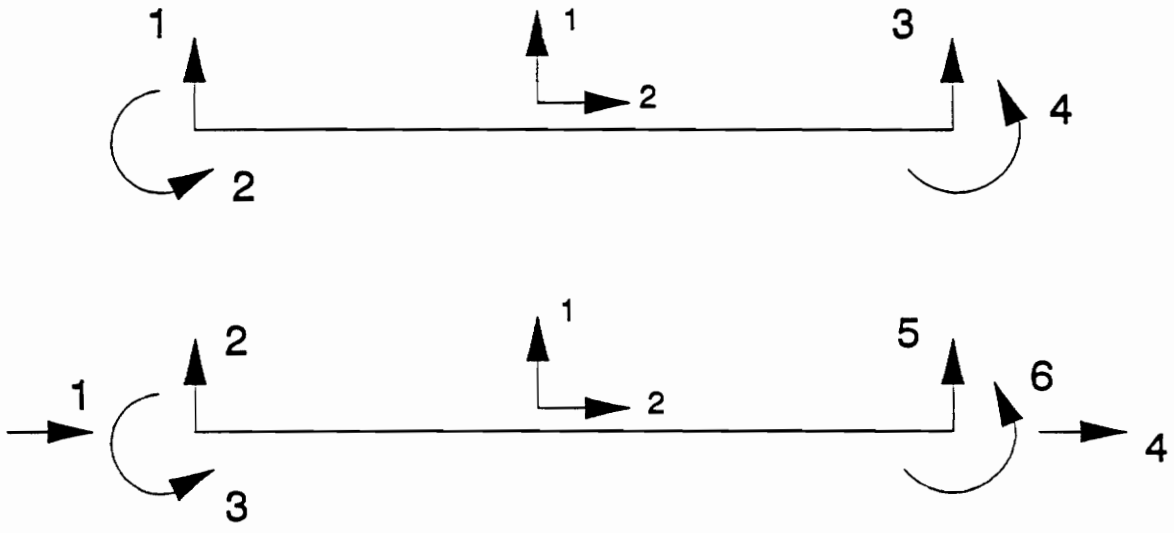


Figure 5.8 DOF for plane beam and plane frame element

element as far as the connector element is concerned. The matrix in Eq.(5.12) is the stiffness matrix for the 2D b/c element and is used in the test cases.

Beam elements in a space frame have a total of 12 DOF, 6 at each node. These are shown in Figure 5.9 for a local space beam element. The beam-connector assembly for a space frame ('3D b/c element') is shown in Figure 5.10. Note that the local axes of the beam element are so chosen as to coincide with global coordinate axes. This is done so that the local and global stiffness matrices of the 3D b/c are the same in the test case described in the next section.

The connector spring is placed horizontally to model the nailed connection in space frame, since we want to model lateral restraint offered by the decking to the beams. The connector in the b/c model deforms laterally when the beam is subjected to nodal load in the 2-direction and moments in the 1 and 2 directions. Thus, at any nail location along the length of the beam only one spring in the direction as shown is sufficient. This is because the nail is assumed to offer only the lateral resistance to beam deformation. The other end of spring is assumed to be fixed since the decking is much stiffer than the nail and is rigid in its surface, and thus does not move. The connector spring is attached to the beam finite element through a rigid link since the nail in the real structure is attached to the top of the beam cross section (Figure 5.11). The axial and transverse DOF of the beam (i.e., DOFs 1, 3, 7, 8, and 9) are not considered for the connector elements because the effect of decking on the beam bending (T-beam action) is ignored.

Thus, the only active DOF of the beam element shared by the connector are 2, 4, 6, 8, 10 and 12 and are denoted by d_1 through d_6 as shown in Figure 5.10. Figure 5.12 shows the relationship between the nail deflection and the deflection of the ends of beam in the direction of active DOF for the connector. The spring deflection is given by

$$v_s(\xi) = w(\xi) - h\,\phi(\xi) \tag{5.13}$$

where

$w(\xi)$ = deflection of beam corresponding to the displacement in the 2-direction and bending about 3-axis

h = rigid link length

$\phi(\xi)$ = rotation of beam subjected to moment (torque) about 1-axis

and

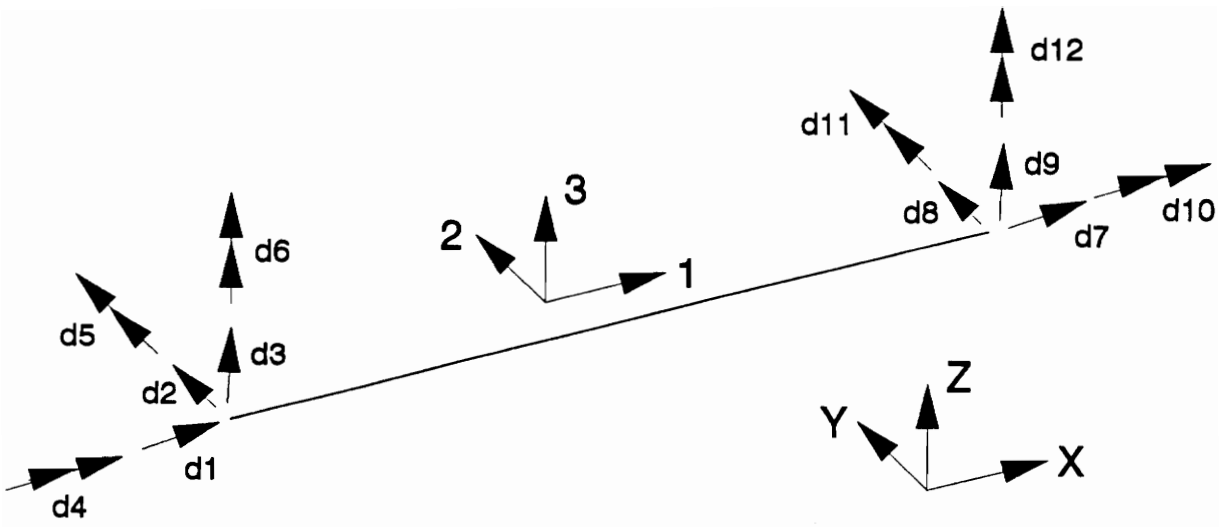


Figure 5.9 Local space beam element

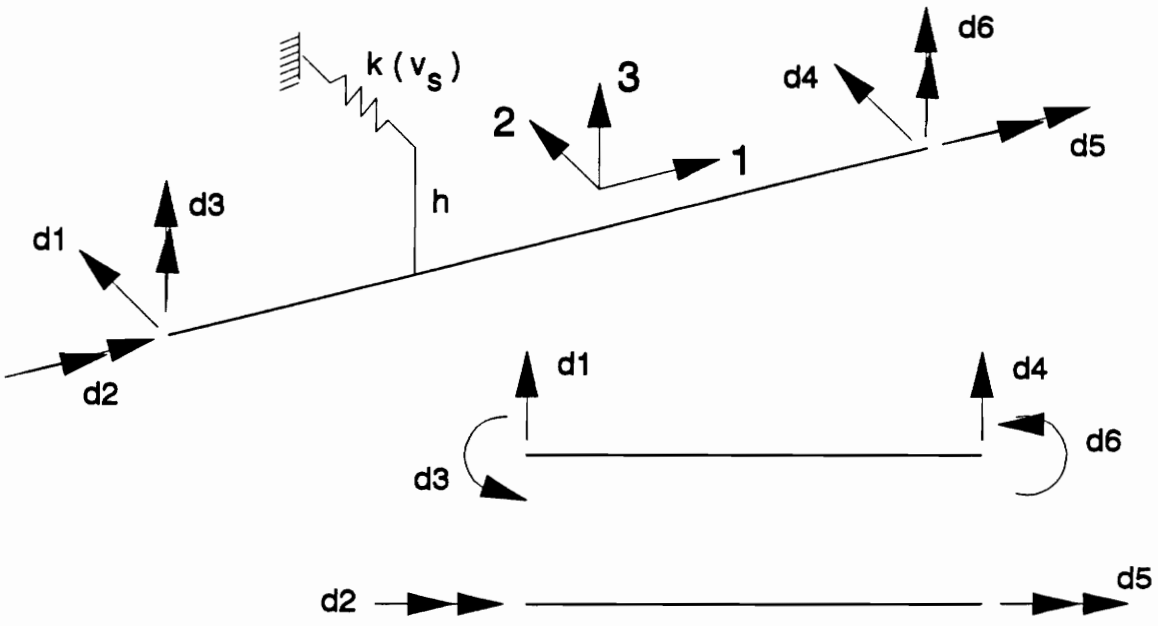


Figure 5.10 3D beam/connector assembly

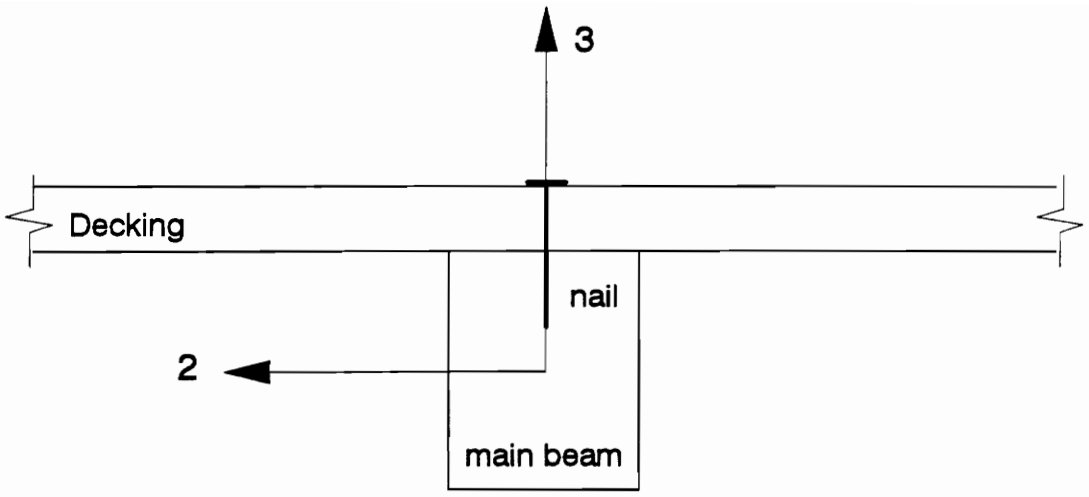


Figure 5.11 Nailed connection between decking and beams

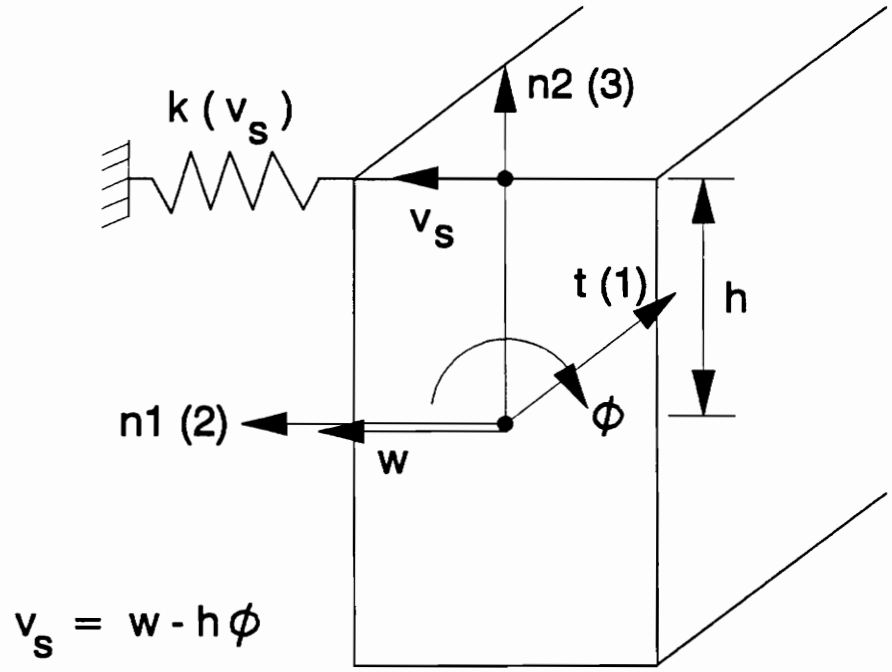


Figure 5.12 Relationship between nail deflection and nodal deflections of the beam

$$\xi = \frac{s}{l}$$

The deflection and the rotation of beam are independent of each other, and are expressed by different interpolation functions as given below.

$$\phi(\xi) = \begin{bmatrix} N_1^1 & N_2^1 \end{bmatrix} \begin{bmatrix} d_2 \\ d_5 \end{bmatrix} \tag{5.14}$$

where

$$N_1^1 = (1 - \xi)$$

and (5.15)

$$N_2^1 = \xi$$

$$w(\xi) = \begin{bmatrix} N_1^2 & N_2^2 & N_3^2 & N_4^2 \end{bmatrix} \begin{bmatrix} d^1 \\ d^2 \\ d^3 \\ d^4 \end{bmatrix} \tag{5.16}$$

where

$$\begin{aligned} N_1^2 &= N_1(\xi) = 1 - 3\xi^2 + 2\xi^3 \\ N_2^2 &= N_2(\xi) = (\xi - 2\xi^2 + \xi^3)\, l \\ N_3^2 &= N_3(\xi) = 3\xi^2 - 2\xi^3 \\ N_4^2 &= N_4(\xi) = (-\xi^2 + \xi^3)\, l \end{aligned}$$

From Eqs.(5.13), (5.14) and (5.16) we obtain

$$\begin{aligned} v_s &= N_1^2 d_1 - hN_1^1 d_2 + N_2^2 d_3 + N_3^2 d_4 - hN_2^1 d_5 + N_4^2 d_6 \\ &= S\, d \end{aligned} \tag{5.17}$$

where

$$S = [S(1)\ S(2)\ S(3)\ S(4)\ S(5)\ S(6)]$$

$$= [N_1^2 \ -hN_1^1 \ N_2^2 \ N_3^2 \ -hN_2^1 \ N_4^2] \tag{5.18}$$

and

$$d = \begin{bmatrix} d_1 \\ d_2 \\ d_3 \\ d_4 \\ d_5 \\ d_6 \end{bmatrix} \tag{5.19}$$

Equations (5.18) and (5.19) represent the interpolation functions and end deflections, respectively for the connector element. These are used in the user subroutine UEL for the 3D b/c element test case for calculating the stiffness matrix of the connector elements. The connector stiffness matrix is obtained as

$$k_s = S^T \gamma S$$

$$= \begin{bmatrix} g_1 & g_2 & g_4 & g_7 & g_{11} & g_{16} \\ & g_3 & g_5 & g_8 & g_{12} & g_{17} \\ & & g_6 & g_9 & g_{13} & g_{18} \\ & & & g_{10} & g_{14} & g_{19} \\ & & & & g_{15} & g_{20} \\ \text{sym} & & & & & g_{21} \end{bmatrix} \tag{5.20}$$

where

$$\begin{aligned} g_1 &= S(1)\,S(1) \\ g_2 &= S(1)\,S(2) \\ g_3 &= S(2)\,S(2) \\ g_4 &= S(1)\,S(3) \\ g_5 &= S(2)\,S(3) \\ g_6 &= S(3)\,S(3) \\ g_7 &= S(1)\,S(4) \\ g_8 &= S(2)\,S(4) \\ g_9 &= S(3)\,S(4) \\ g_{10} &= S(4)\,S(4) \\ g_{11} &= S(1)\,S(5) \\ g_{12} &= S(2)\,S(5) \\ g_{13} &= S(3)\,S(5) \\ g_{14} &= S(4)\,S(5) \\ g_{15} &= S(5)\,S(5) \end{aligned} \tag{5.21}$$

$$
\begin{aligned}
g_{16} &= S(1)\,S(6)\\
g_{17} &= S(2)\,S(6)\\
g_{18} &= S(3)\,S(6)\\
g_{19} &= S(4)\,S(6)\\
g_{20} &= S(5)\,S(6)\\
g_{21} &= S(6)\,S(6)
\end{aligned}
$$

where S(1) through S(6) are as given in Eq.(5.18). Similar to the 2D b/c element, the above stiffness matrix must be transformed into a 12 × 12 matrix to make conform to a stiffness matrix of a connector attached to a space beam. The member code matrix for doing this is given as

$$
M = [2\ 4\ 6\ 8\ 10\ 12] \tag{5.22}
$$

This is assigned to the matrix in Eq.(5.20) to get the connector stiffness matrix of the 3D b/c element as given below.

$$
\begin{bmatrix}
0 & 0 & 0 & 0 & 0 & 0 & 0 & 0 & 0 & 0 & 0 & 0\\
 & g_1 & 0 & g_2 & 0 & g_4 & 0 & g_7 & 0 & g_{11} & 0 & g_{16}\\
 & & 0 & 0 & 0 & 0 & 0 & 0 & 0 & 0 & 0 & 0\\
 & & & g_3 & 0 & g_5 & 0 & g_8 & 0 & g_{12} & 0 & g_{17}\\
 & & & & 0 & 0 & 0 & 0 & 0 & 0 & 0 & 0\\
 & & & & & g_6 & 0 & g_9 & 0 & g_{13} & 0 & g_{18}\\
 & & & & & & 0 & 0 & 0 & 0 & 0 & 0\\
 & & & & & & & g_{10} & 0 & g_{14} & 0 & g_{19}\\
 & & & & & & & & 0 & 0 & 0 & 0\\
 & & & & & & & & & g_{15} & 0 & g_{20}\\
 & & & & & & & & & & 0 & 0\\
\text{sym} & & & & & & & & & & & g_{21}
\end{bmatrix}
\tag{5.23}
$$

The total stiffness matrix of the b/c element is given by Eq. (5.10) as before. This is the local stiffness matrix and it must be transformed into the global stiffness matrix in the analysis of the dome cap and the dome . This is done in the user subroutine UEL as discussed in section 5.4.

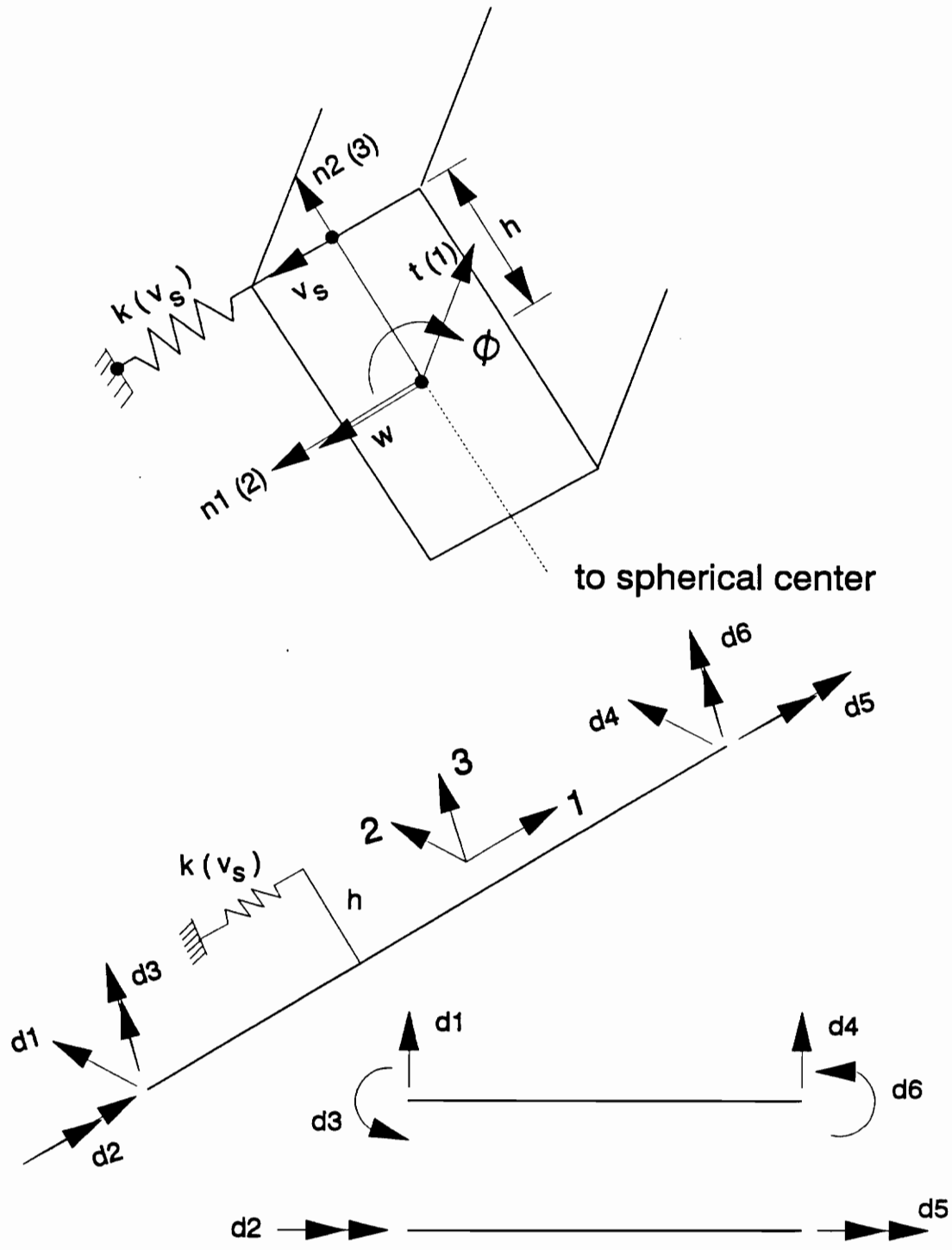


Figure 5.13 3D beam/connector assembly for the inclined main beams of the dome

5.3.1 Connector Stiffness Matrices for the Beams in the Dome

The various beams in the dome are oriented differently so that their local axes are defined in different ways. This is explained in detail in Appendix A. There are 3 types of beams in the dome:

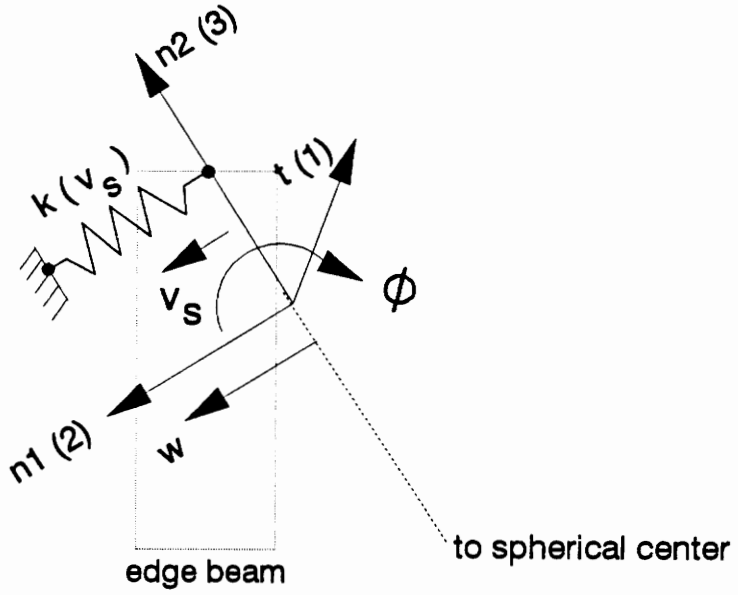
- Main beams with vertical cross section (Fig. A.3a)
- Main beams with inclined cross section (Fig. A.3b)
- Edge beams (Fig. A.4)

The local axes orientation for the vertical main beams is identical to that of the beam axes shown in Figure 5.9. Thus, the stiffness matrix in Eq. (5.23) is the local stiffness matrix for the connectors for main beams with vertical cross sections. The b/c connector assembly for the inclined main beams is shown in Figure 5.13. The interpolation functions S(1) through S(6) for these beams are same as given in Eq. (5.18) due to the identical orientation of the beam local axes. Therefore, the local stiffness matrix of the connectors for the inclined main beams is same as the one given in Eq. (5.23). The b/c assembly for the edge beams is as shown in Figure 5.14. Even though the orientation of local axes for edge beams are different than those for main beams, the nail orientations are same as in case of the inclined main beams. Therefore, the same interpolation functions and local stiffness matrix as used for the main beams are used for the edge beam connectors.

5.4 User Subroutine UEL to Define Nonlinear Connector Elements

The local stiffness matrices for the connector elements with a constant spring stiffness are derived in the previous section. For a segmented load-deflection curve of the nail, the connector stiffness changes for every segment of the curve. There are two ways of defining the nonlinear spring with segmented load-deflection curve in ABAQUS. These are, use of the *SPRING, NONLINEAR option or use of user subroutine UEL to define the nonlinear spring as a user element. However, the user subroutine UEL is preferred for defining the nonlinear connector elements. This is because the use of *SPRING, NONLINEAR option results in significant increase of the system DOF, which is not desirable.

Though the user element defined by subroutine UEL will be used for the dome analysis, the nonlinear spring element will be used in the test cases to check the results of the models with user elements. These test cases are described in section 5.5.



$$v_s = w - h\phi$$

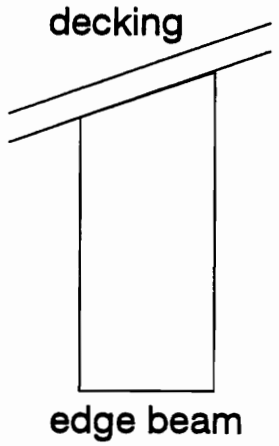


Figure 5.14 3D beam/connector assembly for nails on the edge beams of the dome

5.4.1 Defining the User Elements in ABAQUS

A user can introduce his own finite element types in the analysis with ABAQUS with the option of subroutine UEL. The subroutine will be called each time element calculations are required for each of the element that is a user-defined element type. The user element is introduced in the analysis in the *USER ELEMENT card (ABAQUS, sec. 6.5.20). A purely linear element can be defined in the *MATRIX suboption, whereas a general, nonlinear behavior is defined in UEL. The program will look for one of these depending on the presence or absence of the LINEAR parameter in the *USER ELEMENT option.

The user element defined in UEL may be a finite element in the usual sense of representing a geometric part of the model, or it may be a feedback link supplying forces at some points as a function of nodal variables such as displacement or velocity. In the coding of UEL, any number of parameters may be used to define the element. Numerical values of these parameters are given in the *UEL PROPERTY option (ABAQUS sec. 6.5.19). The number of properties, say n, defined in this option are declared on the *USER ELEMENT card in the PROPERTIES parameter as PROPERTIES = n. In addition to this, the following basic element data for the user element type are defined in this card.

- The element type definition in the form of Un, where n is a positive integer. This identifies the element type uniquely for use in an analysis. The integer part of this is provided in UEL as the values of JTYPE variable so that a user can distinguish different element types.
- The number of nodes associated with the user element.
- The maximum number of coordinates needed at any node of the element
- The list of DOF associated with the user element. These are given for the first node and for the subsequent nodes only if they are different from the first node.

5.4.2 User Subroutine UEL

For a general user element, subroutine UEL must be able to define the force contribution of the element to the model. The subroutine must do the following tasks:

1. Define the contribution of the element to the Jacobian (stiffness) matrix
2. Define the contribution of the element to the residual vector.

3. Update the solution dependent state variables associated with the element. Since there are no such variables present in the b/c finite element model, this will not be required.

The properties of a user element associated with its nodes, such as the nodal coordinates and deflection values, are passed in the UEL in the order of the DOF described above for each consecutive node starting from node 1. For example, for a 2-noded element with DOF of 1, 2, 3 at each node, the arrays of nodal values will be passed in UEL in the order [(1,1); (2,1); (3,1); (1,2); (2,2); (3,2)] where (i,j) means i^{th} DOF at node j. The values defined in the *UEL PROPERTY option are passed in the subroutine in the array PROPS in the same order as they appear in this option.

ABAQUS calls UEL every time, i.e., in each iteration of every increment in the nonlinear analysis, when information about a user defined element is needed. In every iteration, the main program provides the updated nodal data and values of parameters in the *UEL PROPERTY option to the subroutine, which updates the stiffness matrix and the residual vector and passes its values back to the main program. For the b/c model, the following information is passed in the subroutine.

Arrays :

PROPS (I)	Parameter values associated with the element
COORDS (I,J)	Nodal coordinates
U (I)	Current estimates of nodal displacements. These are passed in UEL in the order of DOF for consecutive nodes of the element, starting from the first node

Scalar parameters :

NDOFEL	Number of total DOF in the element
NRHS	Number of load vectors. 1 for most nonlinear problems, 2 for *STATIC, RIKS option
NPROPS	Number of property values associated with the element as defined in the PROPERTIES parameter
NNODE	Number of nodes on the element
JTYPE	The integer value n in Un, given as the TYPE parameter in *USER ELEMENT card

The following arrays must be defined in the UEL.

1. AMATRX (I,J) The contribution of the b/c element to the Jacobian (stiffness) matrix of the overall system of equations. This array contains the global stiffness matrix of the connector elements. The local stiffness matrix for the same, derived in last section, is transformed into the global stiffness matrix using the rotation matrix defined in Appendix A.

In order to verify that the global, and not the local, stiffness matrix should be provided in the *MATRIX card and UEL, a test case as shown in Figure 5.15 is analyzed. The members of the model are defined as C1D2 truss elements and also as user elements, first using local and then using global stiffness matrices supplied in the *MATRIX card.

The local stiffness matrix for each of the truss elements shown in Figure 5.15 is

$$k = \gamma \begin{bmatrix} 1 & 0 & -1 & 0 \\ 0 & 0 & 0 & 0 \\ -1 & 0 & 1 & 0 \\ 0 & 0 & 0 & 0 \end{bmatrix} \tag{5.24}$$

where, $\gamma = EA/L$, $E = 1.8 \times 10^6$ psi, and $A = 1$ in^2

The global stiffness matrix for a truss element is given by (Holzer,1985)

$$K = \gamma \begin{bmatrix} c_1^2 & c_1c_2 & -c_1^2 & -c_1c_2 \\ & c_2^2 & -c_1c_2 & -c_2^2 \\ & & c_1^2 & c_1c_2 \\ & & & c_2^2 \end{bmatrix} \tag{5.25}$$

where c_1 and c_2 are the direction cosines of the local-1 axis of the truss member.

It was found that, the analysis with the global stiffness matrices for the truss members in Figure 5.15 gave the correct results, which were also obtained with C1D2 elements. These are shown in Figure 5.15. The analysis with the local stiffness matrices does not give any results indicating presence of numerical singularity during the analysis. This confirms that the global stiffness matrix must be defined in the user element in the analysis with ABAQUS. The input files for this test case are given in Appendix C.

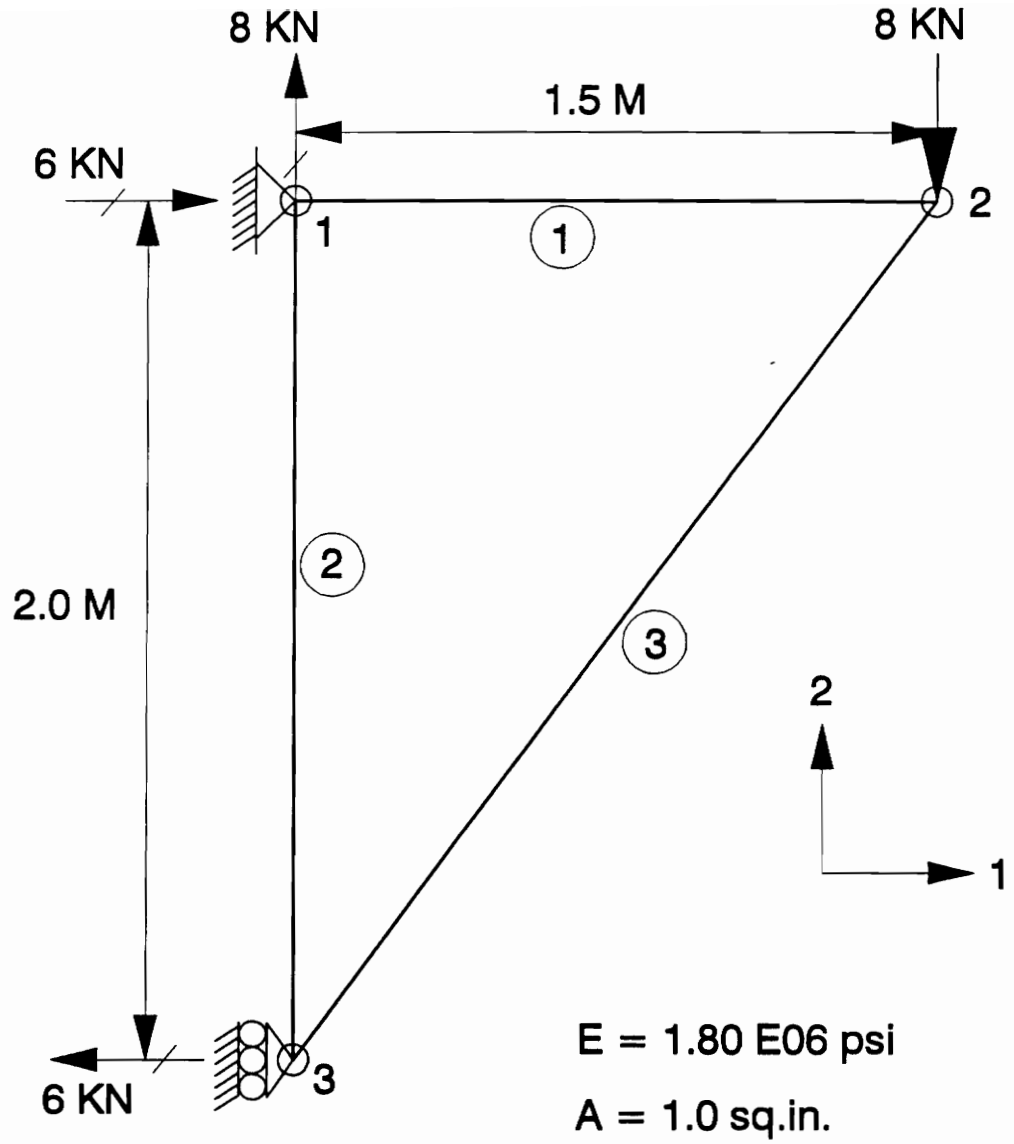


Figure 5.15 Truss model to verify the use of global stiffness matrix in user element option in ABAQUS

2. RHS (I,J) The contribution of the user element to the right-hand-side vectors of the overall system of equations. For most nonlinear problems, NRHS = J = 1 and RHS contains the residual vector. In a static analysis with the RIKS option, NRHS = J = 2, and the first column should contain the residual vector and the second the increments of the external load. RHS (I,J) is the entry for the Ith DOF of the element in the Jth right-hand-side vector.

In order to determine the coding of this array, it is necessary to review the nonlinear solution procedure for the connector elements with a segmented load-deflection path.

5.4.3 Contribution of User Elements Defining b/c Model

There are several algorithms used in the incremental iterative solution of nonlinear problems of which the Newton/Raphson and modified Riks/Wempner methods are commonly used (Holzer and Watson, 1981). They iterate along the equilibrium path with small increments of load. The N/R method traces the response of a nonlinear structural system by the use of piecewise linear stiffness increments. For a single DOF, to trace the equilibrium path in the load-deflection plane (Figure 5.16), the process starts with a known equilibrium point also called as initial configuration denoted by number 0. The desired equilibrium state after a load increment of ΔQ is denoted by letter N, and corresponds to the desired load Q^N. It can be seen that the internal force F^0 falls short of equilibrating the applied load of Q^N. The structure must deform to develop the internal resistance necessary to equilibrate Q^N. This deformation is found by successive iterations. Displacement increments are found for a specific applied load increment and are accumulated until convergence is obtained. In the iteration procedure, the tangent stiffness matrix K_T, which is a linearized approximation of the equilibrium path based on the internal forces occurring in the structure is found and is modified in each iteration. The N/R algorithm is summarized below.

1. Formulate tangent stiffness matrix and find load residual

$$K_T^{k-1} \Delta q^k = (Q^N - F^{k-1}) = R^{k-1} \tag{5.26}$$

2. Compute Δq^k from above and find new trial configuration

$$q^k = q^{k-1} + \Delta q^k \tag{5.27}$$

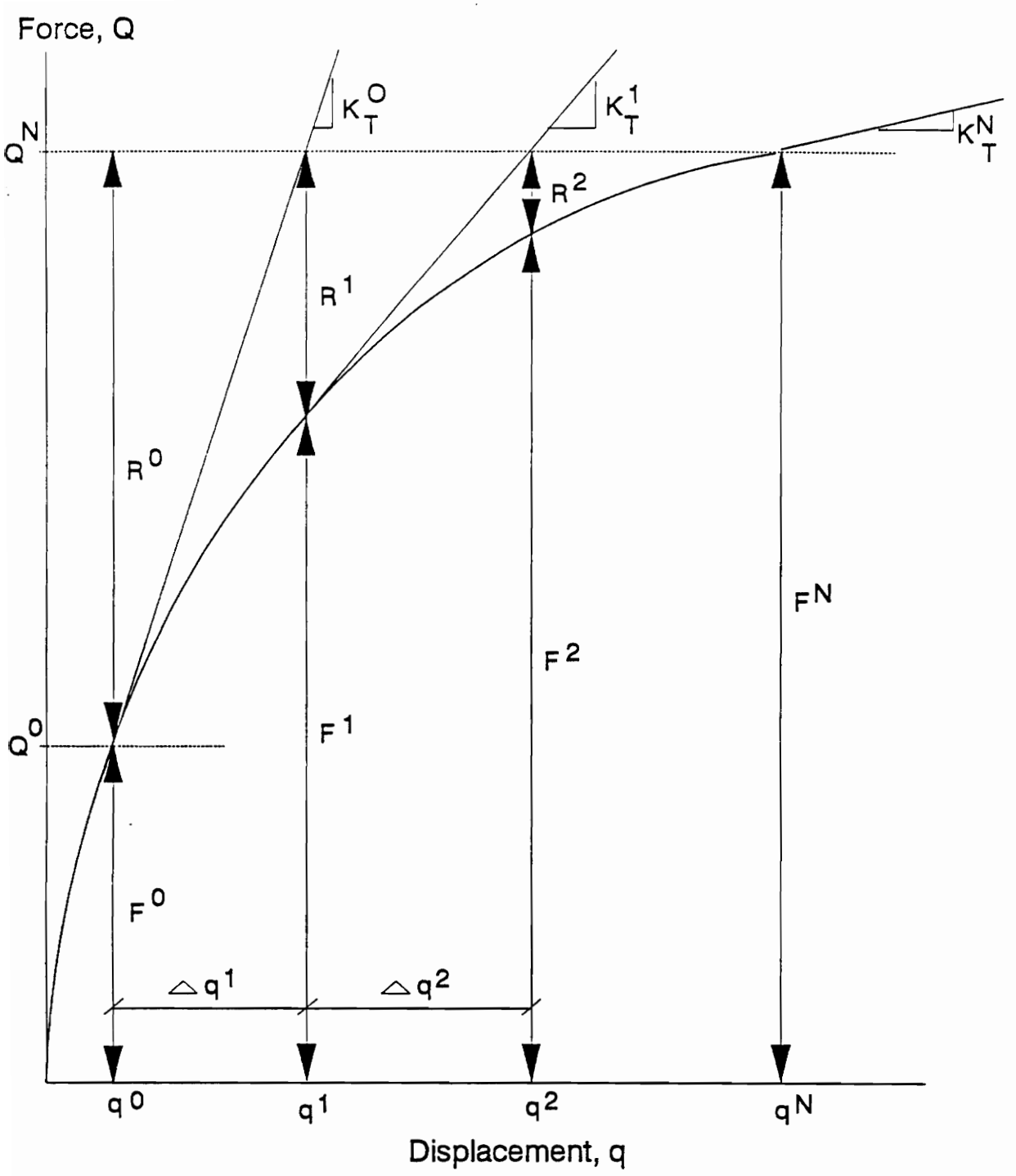


Figure 5.16 Nonlinear analysis : Newton/Raphson method

3. Compute R^k and check for prescribed accuracy. Convergence for the load increment is achieved, for example, if the components of R^k are sufficiently small, as prescribed by the user. The notations used above are as follows.

K_T^{k-1} = tangent stiffness matrix of configuration k-1
Δq^k = displacement increment from configuration k-1 to k
q^{k-1} = displacement of configuration k-1
R^{k-1} = load residual for configuration k-1

In the N/R algorithm, the Δq^k term is the unknown being solved for. In the Riks/Wempner method (Figure 5.17), a generalized arc length Δs is the independent variable that controls progress along the equilibrium path. The new equilibrium point is the intersection of a normal plane to the tangent with the equilibrium path. Iteration proceeds along the normal, with a tangent stiffness matrix formulated for each iteration.

According to section (3.14.1) of ABAQUS User's Manual, the most general mathematical statement of an element's contribution to the model is that it provides forces at its nodes.

$$F^N = F^N(u^M) \tag{5.28}$$

where

F^N = Force contributed by the element to DOF N at a node of the element
u^M = Values of displacement at DOF M

In most procedures, the user subroutine UEL must define F^N, given the variables upon which it depends. If the equivalent nodal forces caused by the distributed loads applied on an element are zero, then F^N is given by

$$F^N = -K^{NM}\, u^M \tag{5.29}$$

where

K^{NM} = Jacobian (stiffness) matrix of the element

$$= \frac{\partial F^N}{\partial u^M} \tag{5.30}$$

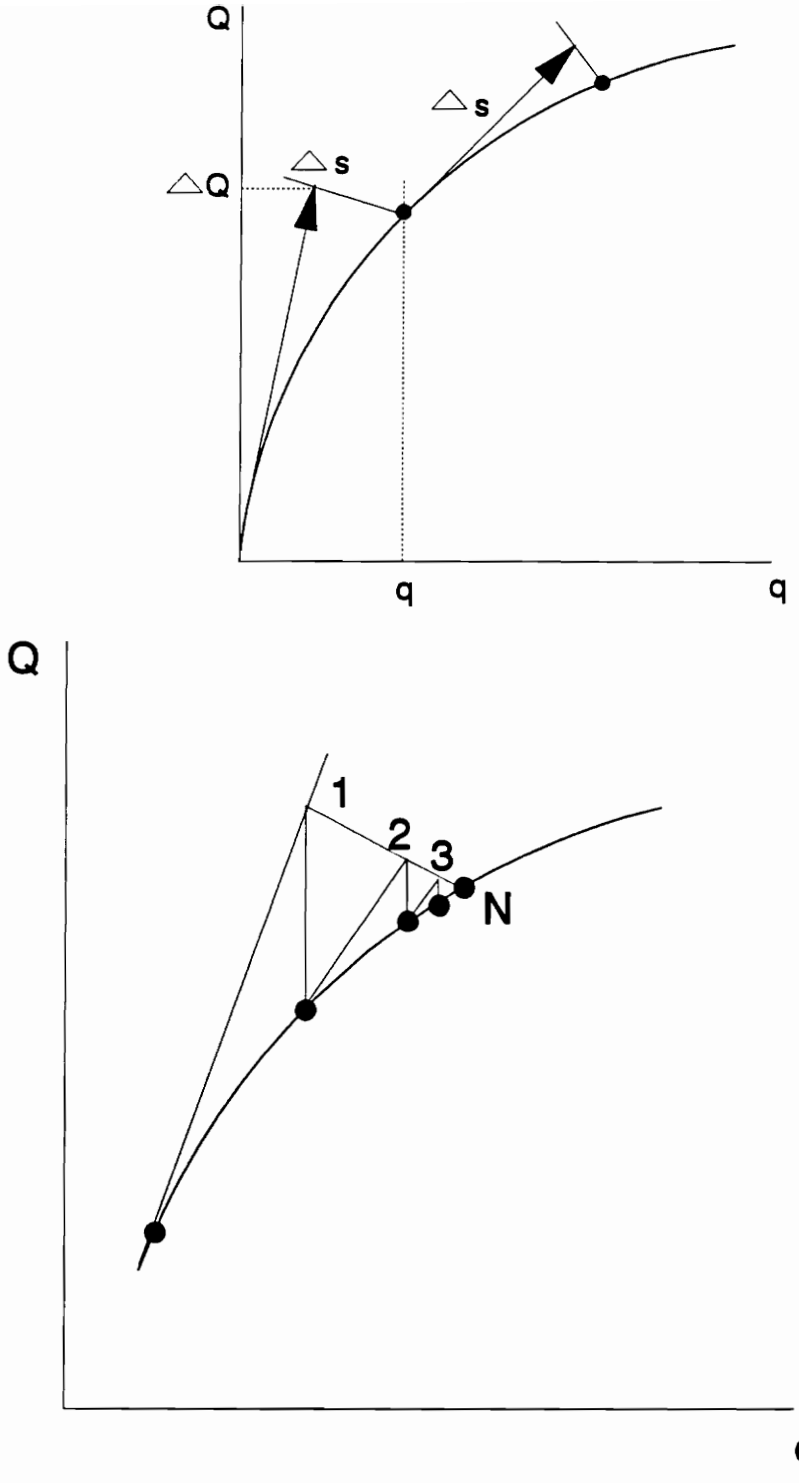


Figure 5.17 Nonlinear Analysis: Riks method

The negative sign in Eq.(5.33) is because the internal forces caused by stresses in the element provide negative nodal force values.

The contribution of the user element, F^N, is thus the nodal force values caused by internal stresses in the element and should be specified in the array RHS(I,J). This is the contribution of the element to the right-hand-side vectors of the overall system of equations or the 'residual vector' as described in ABAQUS User's manual, and it represents the term F^{k-1} in the N/R algorithm. For the connector elements, the internal force in the connector spring is represented by its load-deflection curve itself. Therefore, the contribution of the connectors to the model is given by the equation of the load-deflection curve.

The first column of RHS(I,J) is thus the force in the spring given by the equation of the load-deflection curve. For a segmented load-deflection curve, the tangent stiffness matrix remains constant for a load increment within a segment of the curve, and the desired load increment is achieved in one iteration. A test case described in the next section confirms this. In the analysis with the RIKS option, the external load increment on the element within an analysis increment is zero since there is no more than one iteration. Convergence is achieved in one iteration due to the constancy of the stiffness matrix. The second column of RHS (I,J) in the RIKS option for a segmented load-deflection curve is zero due to this reason. Figure 5.18 shows the N/R scheme for a bilinear load-deflection curve.

5.5 Test Cases for the Nonlinear Connector Element

Test models having nonlinear connectors attached to beams are analyzed in this section to test the user elements' capability in ABAQUS. The nonlinear connectors are modeled by the user elements specified through subroutine UEL. Similar test models using nonlinear spring elements from ABAQUS' element library to model the nonlinear connectors are also analyzed in order to verify the results obtained from the models with user elements.

5.5.1 A Single Nonlinear Spring with Two Nodes

A nonlinear spring with one end fixed and with a load applied at the other end (Figure 5.19a) is analyzed with N/R and Riks options in ABAQUS. The load-deflection path for

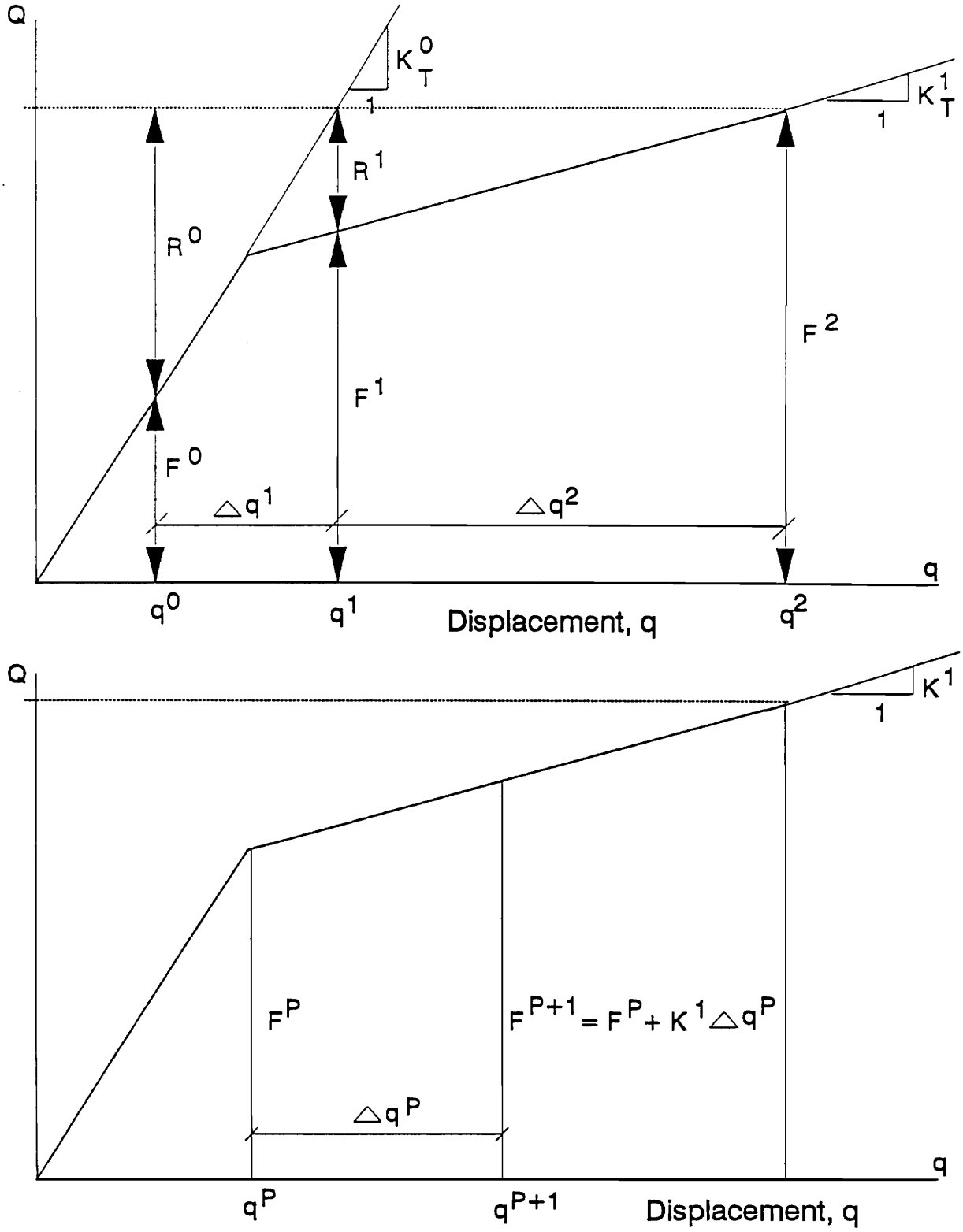


Figure 5.18 N/R scheme for bilinear load-deflection curve

the spring is segmented as shown in Figure 5.19b. This model is assumed to have 2 DOF, one at each node in the direction of the applied force. The stiffness matrix for the spring is

$$K_T = \gamma \begin{bmatrix} 1 & -1 \\ -1 & 1 \end{bmatrix} \tag{5.31}$$

As described in the previous section, the contribution of the element in the array RHS is given by the equation of the load-deflection curve. The RHS terms corresponding to the second element DOF are thus

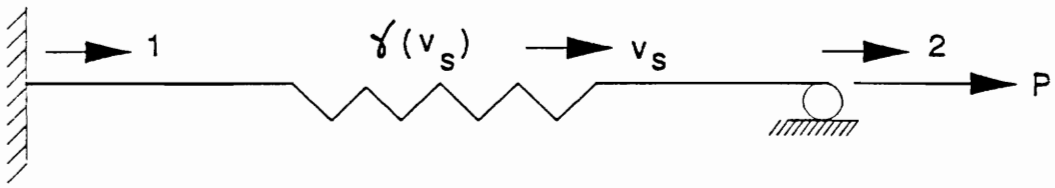
RHS (2,1)	=	-10000. * U(2)	.....	for U(2) < 2.0"
RHS (2,1)	=	-10000. - 5000. * U(2)		
	=	-5000. * (U(2) + 2.0)	.....	for 2.0" < U(2) < 4.0"
RHS (2,1)	=	-20000. - 2500. * U(2)		
	=	-2500. * (U(2) + 8.0)	.....	for 4.0" < U(2) < 8.0"

The input file for this test case is given in Appendix D.

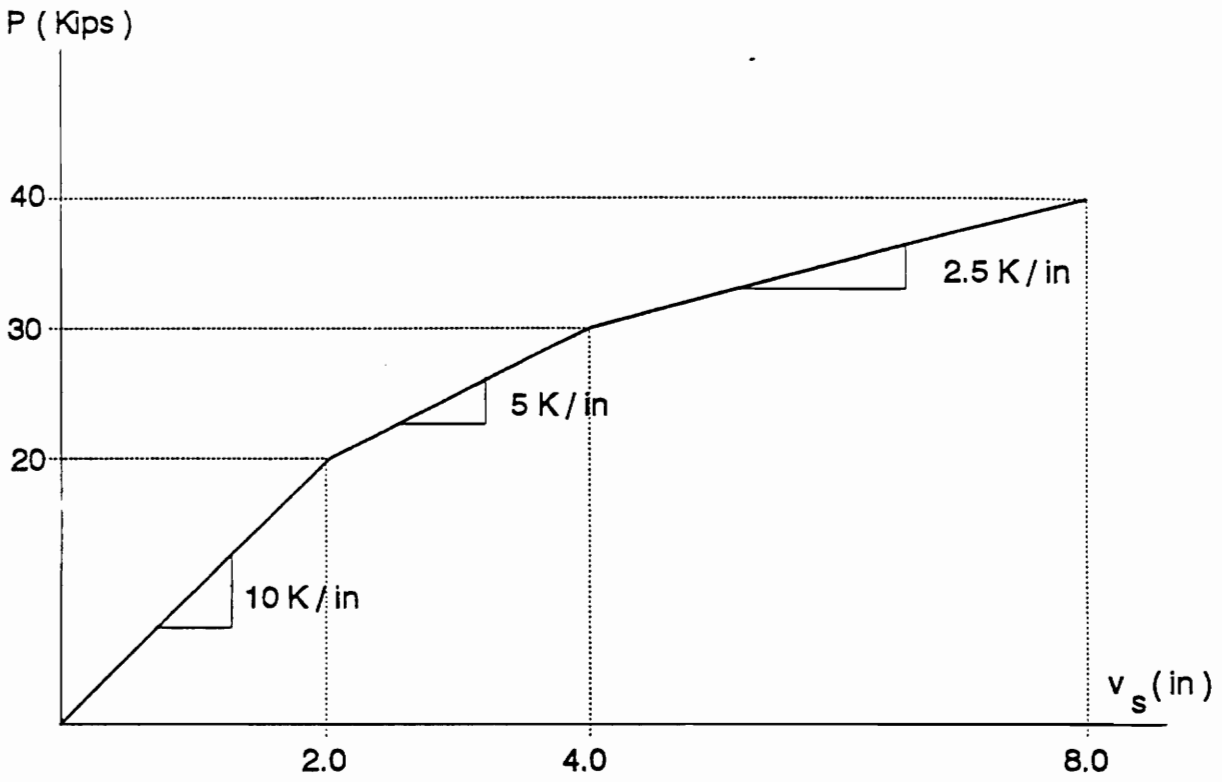
This model was also analyzed with the nonlinear spring element. the nonlinear spring is specified in the input file as follows.

```
*ELEMENT, TYPE=SPRING2, ELSET=SPRING
1,1,2
*SPRING, ELSET=SPRING, NONLINEAR
2,1
-40000., -8.0
-30000., -4.0
-20000., -2.0
0., 0.
20000., 2.0
30000., 4.0
40000., 8.0
```

The analyses with the UEL and the nonlinear spring element gave the same results. As discussed in the previous section, the tangent stiffness matrix for a segment of the P-Δ curve is constant. Therefore, if the load up to 20K is applied with initial time increment of 1.0 (i.e., if the load of 20K is applied in one load increment) in the nonlinear analysis, only



(a)



(b)

Figure 5.19 Test case of a single spring, a) nonlinear spring with 2 DOF, b) load-deflection curve for the spring

one iteration is required to achieve this load level. Similarly, for a load level corresponding to the 2nd and 3rd segmented of the curve, 2 and 3 iterations, respectively are required if the load is applied in one increment as follows.

*STEP, NLGEOM
*STATIC, PTOL=100.
1.0, 1.0
*CLOAD
2, 1, 20000. (or 25000. or 35000.)

Figure 5.20 shows the iterations in the N/R scheme for these three loads.

5.5.2 Testing of 2D Nonlinear b/c Elements

The 2D b/c models were tested by Tsang (1992) using a linearized load-deflection curve for the connectors. He performed linear analysis by defining the connector stiffness matrix in the *MATRIX card. Similar models with nonlinear connector elements are analyzed using N/R and Riks options.

5.5.2.1 Linear Analysis

Before doing the nonlinear analysis, a linear analysis of the models is also performed using SPRING2 elements and the user elements to model the connector. The user elements are defined using two different options, namely *MATRIX as used by Tsang (1992) and the user subroutine UEL. The beams are modeled with the B23 plane beam element. The purpose of the linear analysis is to compare the results obtained in these three different methods. The beam/connector assembly for the linear analysis is shown in Figure 5.21. The geometric and material properties are the same as those of the main beams in the dome cap model. A constant connector stiffness of γ = 14400 lb/in is used in the analysis. The stiffness matrix for the connector attached at the mid-span, from Eq. (5.12), is as follows.

$$k_s = \begin{bmatrix} 0 & 0 & 0 & 0 & 0 & 0 \\ & 3600 & 118800 & 0 & 3600 & -118800 \\ & 0 & 3920400 & 0 & 118800 & -3920400 \\ & & & 0 & 0 & 0 \\ & & & & 3600 & -118800 \\ \text{sym.} & & & & & 3920400 \end{bmatrix}$$

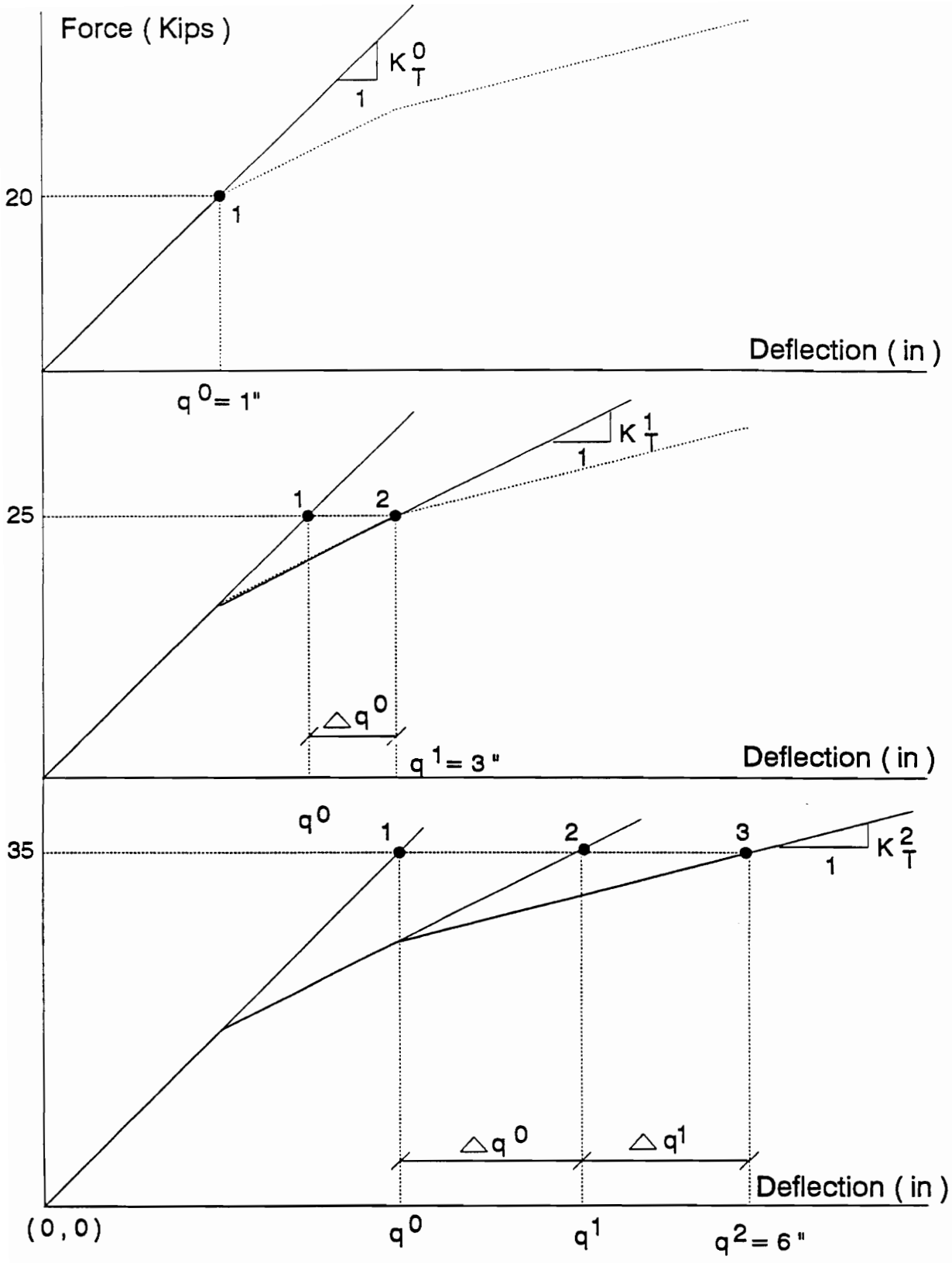


Figure 5.20 N/R iterations for the nonlinear spring model

This is specified in the *MATRIX option as discussed by Tsang (1992) and in subroutine UEL in the array AMATRX (I,J). The contribution of the connector element to the model, specified in the array RHS (I,1), is determined as follows. Consider the spring energy for a constant spring stiffness as shown in Figure 5.22. From Eq.(5.3)

$$U_S = \frac{1}{2} v_s^T \gamma \; v_s$$

$$= \frac{1}{2} d^T N_s^T \gamma \; N_s d$$

$$= \frac{1}{2} d^T k_s d \tag{5.32}$$

$$\therefore \quad \delta U_S = \frac{1}{2} \delta d^T k_s d \tag{5.33}$$

The external work done by the spring is given by

$$\delta W_{es} = (\delta W_S - \delta U_S) = \delta d^T F_S \tag{5.34}$$

where, F_S is the force contribution of the spring. Since there is no external force acting on the spring, $\delta W_S = 0$. From Eqs.(5.33) and (5.34)

$$\delta d^T F_S = -\delta U_S = -\delta d^T k_s d$$

$$\therefore \; F_S = -k_S d \tag{5.35}$$

This is the same as the expression of the force contribution given by Eq.(5.29), and the vector d is as given in the previous section. Note that k_S is given in AMATRX (I,J) array and d is passed in the subroutine in U(J) array. From Eq. (5.35), the contribution of the connector can be coded in UEL as

RHS (I,J) = RHS (I,1) - AMATRX (I,J) * U(J)

The ABAQUS input file for this model is as given below.

*HEADING

B23 WITH ONE DISCRETE CONNECTOR(USER ELEMENT)

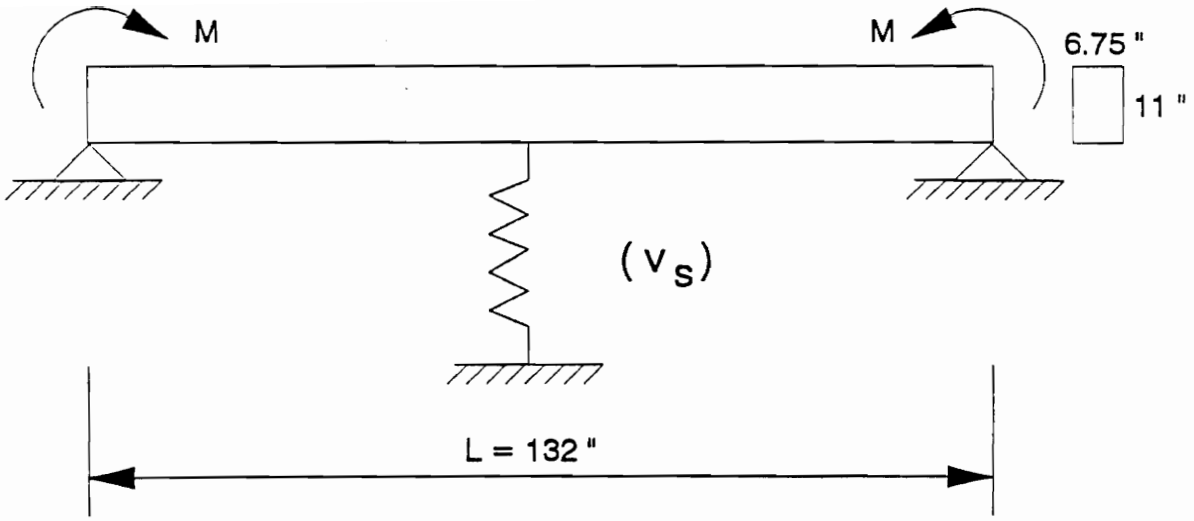


Figure 5.21 2D b/c assembly for linear analysis

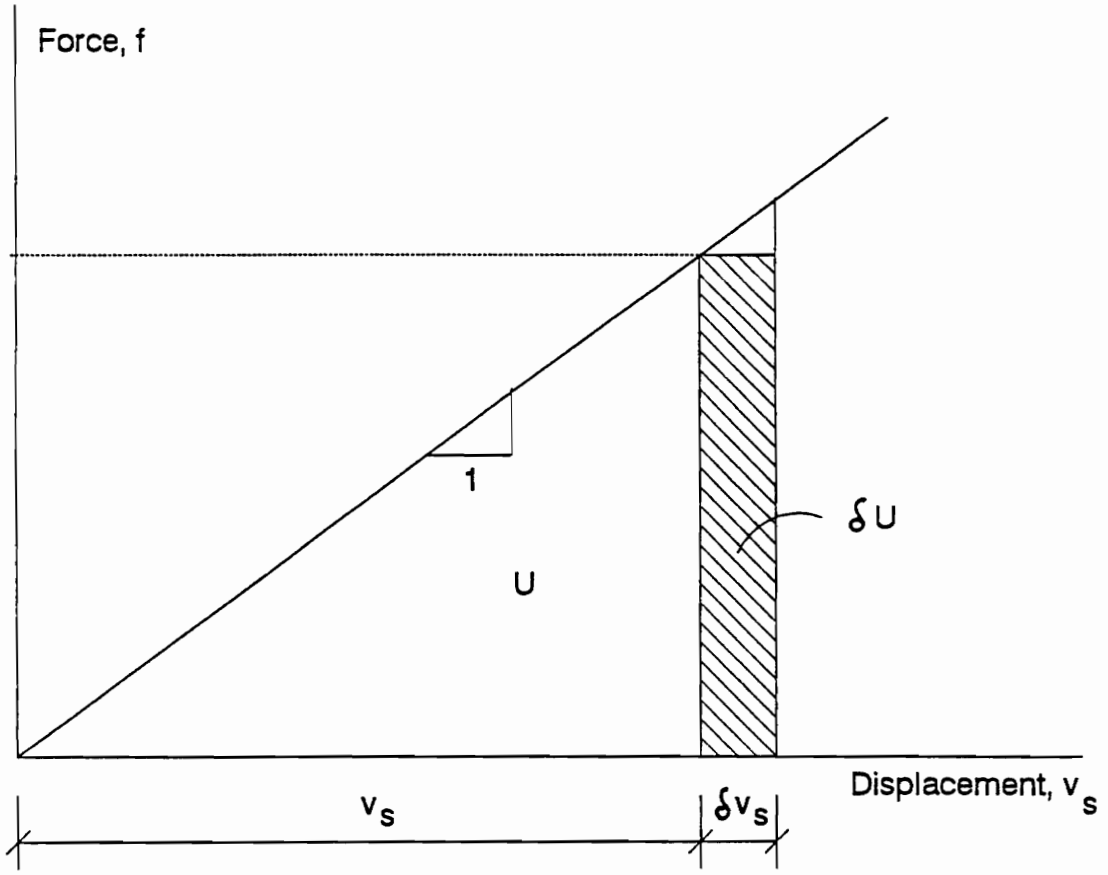


Figure 5.22 Spring energy for a constant spring stiffness

```
** UNITS: INCH, KIPS    , KS = 14.4 K/IN
*NODE
 1,0.,0.
 2,132.,0.
*NSET,NSET=NOUT
 1,2
*ELEMENT,TYPE=B23,ELSET=BEAM
 1,1,2
*BEAM SECTION,SECTION=RECT,ELSET=BEAM,MATERIAL=WOOD
 6.75,11.0
*MATERIAL,NAME=WOOD
*ELASTIC
 1.8E06
*USER ELEMENT,NODES=2,TYPE=U1,COORDINATES=3
 1,2,6
*ELEMENT,TYPE=U1,ELSET=C1
 2,1,2
*UEL PROPERTY,ELSET=C1
*USER SUBROUTINES
CC
CC*************************************************************
CC      USER SUBROUTINE TO DEFINE CONNECTOR ELEMENT U1
CC        SANDEEP KAVI                                  JANUARY 1993
CC*************************************************************
CC
      SUBROUTINE UEL(RHS,AMATRX,SVARS,ENERGY,JLINES,XVAL,
     1 NDOFEL,NRHS,NSVARS,PROPS,NPROPS,COORDS,MCRD,NNODE,
     2 U,DU,V,A,JTYPE,TIME,DTIME,KSTEP,KINC,JELEM,PARAMS,
     3 NDLOAD,JDLTYP,ADLMAG,PREDEF,NPRED,LFLAGS)
C
      IMPLICIT REAL*8(A-H,O-Z)
C
      DIMENSION RHS(NDOFEL,NRHS),AMATRX(NDOFEL,NDOFEL),
     1 SVARS(1),ENERGY(6),JLINES(1),XVAL(1),PROPS(1),
     2 COORDS(MCRD,NNODE),U(NDOFEL),DU(NDOFEL),V(NDOFEL),
     3 A(NDOFEL),TIME(7),DTIME(7),PARAMS(1),JDLTYP(NDLOAD,NRHS),
```

```
     4 ADLMAG(NDLOAD,NRHS,2),PREDEF(2,NPRED,NNODE),LFALGS(4)
C
      DO 10 I=1,NDOFEL
       DO 20 J=1,NDOFEL
        AMATRX(I,J)=0.0
20     CONTINUE
10    CONTINUE
C
        AMATRX(2,2)=3600.0
        AMATRX(2,3)=118800.0
        AMATRX(3,3)=3920000.0
        AMATRX(2,5)=3600.0
        AMATRX(3,5)=118800.0
        AMATRX(5,5)=3600.0
        AMATRX(2,6)=-118800.0
        AMATRX(3,6)=-3920000.0
        AMATRX(5,6)=-118800.0
        AMATRX(6,6)=3920000.0
C
      DO 30 I=1,NDOFEL
       DO 40 J=1,NDOFEL
        IF(I.GT.J) AMATRX(I,J)=AMATRX(J,I)
40     CONTINUE
30    CONTINUE
C
      DO 50 I=1,NDOFEL
       DO 60 J=1,NDOFEL
       RHS(I,1)=RHS(I,1)-AMATRX(I,J)*U(J)
60     CONTINUE
50    CONTINUE
      RETURN
      END
**********************************************************************
*BOUNDARY
1,1,2
2,1,2
```

```
*STEP,LINEAR
*STATIC
*CLOAD
 1,6,-10000.
 2,6,10000.
*EL PRINT,SUMMARY=NO
 S
*NODE PRINT,NSET=NOUT,SUMMARY=NO
 U
*NODE PRINT,NSET=NOUT,SUMMARY=NO
 CF
*NODE PRINT,NSET=NOUT,SUMMARY=NO
 RF
*END STEP
```

The results of the analysis were found to be exactly same as those obtained with the user element and the *MATRIX and UEL options. These results and those for the model with SPRING2 elements are given in the thesis by Tsang (1992).

5.5.2.2 Nonlinear Analysis

Bilinear load-deflection curve shown in Figure 5.23 is used in the nonlinear analysis of the 2D b/c elements. The geometric and material properties used are the same as those of the previous section. The beams are modeled as B23 beam elements. Three different models with different numbers of connector elements are analyzed. Figures 5.21 and 5.24 show the arrangement of beam and connectors in these models. The number of connector elements used in these are 1, 3, and 15. Each model is analyzed using the SPRING2 elements and the user elements to model the connectors. Note that, the *MATRIX option can not be used in this case due to the nonlinearity of the springs.

The connector stiffness matrix k_s given by Eq.(5.12) is defined in the array AMATRX (I,J). In case of the models with user elements, the individual spring deflection is checked using the interpolation of end deflections. If the deflection is less than 1.0", the spring stiffness of γ = 1000 lb/in is used in defining AMATRX (I,J). If the deflection exceeds

1.0", γ = 500 lb/in is used. The various parameters used in the subroutine are passed in through the *UEL PROPERTY option as follows.

*UEL PROPERTY, ELSET=C1

2,132.,1000.,500.,1.0,3.0,500.

These parameters are passed in the array PROPS (I) and are described below.

PROPS (1) = 2 = Number of springs + 1

PROPS (2) = 132. = Length of the beam element (in.)

PROPS (3) = 1000. = Initial stiffness, γ_1 (lb/in)

PROPS (4) = 500. = Reduced stiffness, γ_2 (lb/in)

PROPS (5) = 1.0 = Spring deflection, Δ_1 (in.)

PROPS (6) = 3.0 = Spring deflection, Δ_2, (in.)

PROPS (7) = 500. = Lateral load 'c' (lb.), where the second segment of the bilinear load-deflection curve intersects Y-axis of P-Δ curve (Figure 5.25)

The contribution of the nonlinear connector can be determined as discussed in the previous section. In the first segment of the bilinear curve, the contribution is given by

RHS (I,1) = RHS (I,1) - AMATRX1 (I,J) * DM1 (J)

where DM(J) are the end deflections corresponding to the active DOF (refer to sec.5.3), and AMATRX1 (I,J) represents the stiffness matrix for the particular connector being considered. Since the connectors are arranged in parallel, their individual contribution can be added arithmetically, as given above. AMATRX (I,J) is the array of cumulative spring stiffnesses. It represents the cumulative Jacobian stiffness matrix for the connectors considered till that point in an iteration.

The contribution of the connectors in the second segment of the bilinear curve is determined as follows. From Figure 5.25, the total spring energy for the stiffness γ_S in the second segment of the load-deflection curve is given by

$$U_S = c\, v_s^T + \frac{1}{2} v_s^T \gamma\ v_s - \frac{1}{2} c\, \Delta_1$$

$$= c\,(Nd)^T + \frac{1}{2} d^T N^T \gamma\ N d - \frac{1}{2} c\, \Delta_1$$

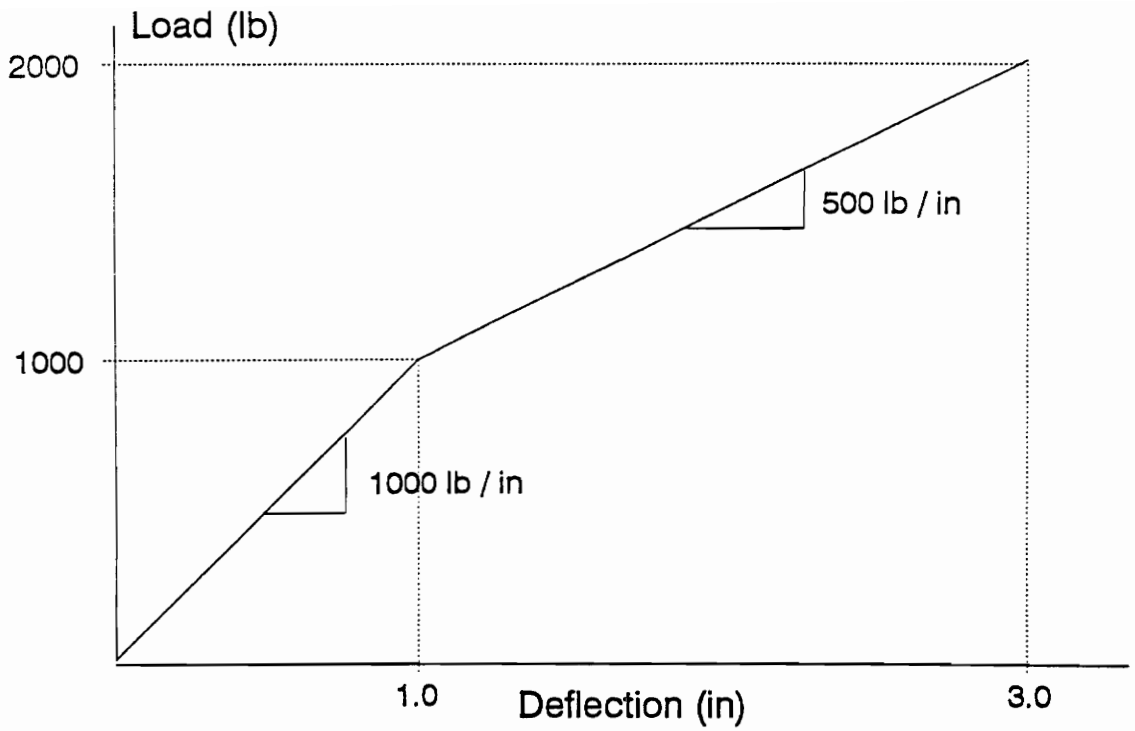


Figure 5.23 Bilinear load-deflection curve for 2D and 3D b/c test cases

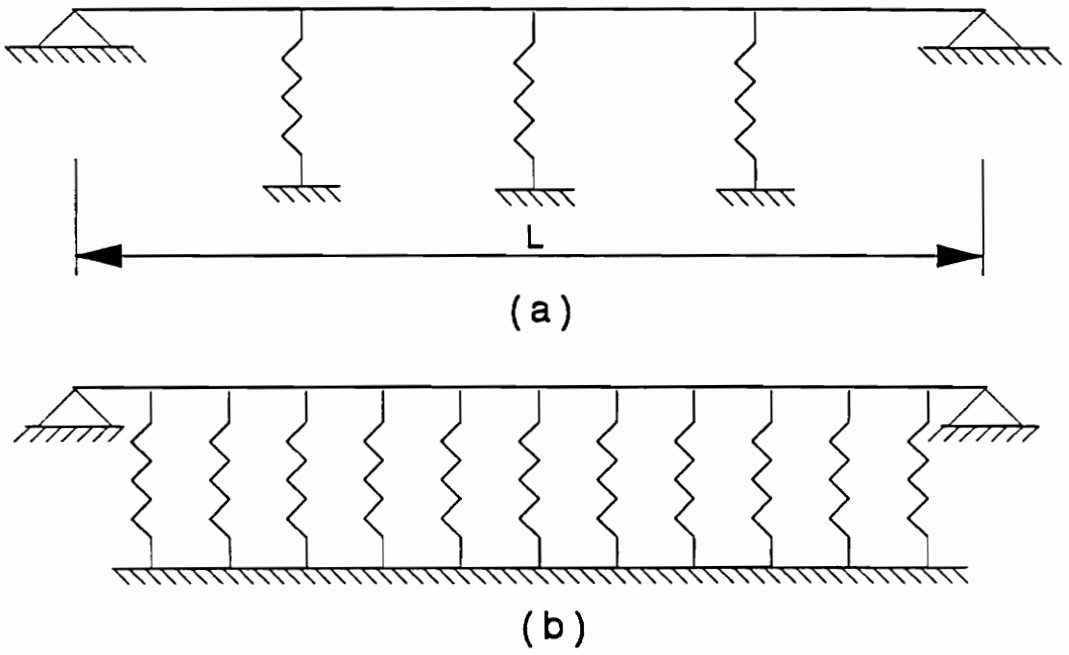


Figure 5.24 2D b/c assemblies with a) 3 and b) 15 connectors

$$= c\,d^T N^T + \frac{1}{2} d^T k_s d - \frac{1}{2} c \Delta_1 \tag{5.36}$$

$$\delta U_S = c\,\delta d^T N^T + \frac{1}{2} \delta d^T k_s d$$

$$= \delta d^T (cN^T + k_S d) \tag{5.37}$$

From Eqs. (5.36) and (5.39)

$$F_S = -(cN^T + k_S d) \tag{5.38}$$

To implement this in the subroutine, first we add the $k_S d$ term for the nth spring to the cumulative contribution of (n-1) springs considered so far, as done in case of the first segment of the load-deflection curve. Once $k_S d$ of all the springs has been added, then the term cN^T is added to the array RHS as follows. If the spring deflection is positive (i.e., if the spring is stretched), then the load 'c' is positive. It is negative if the spring deflection is negative. In the test model of 2D b/c elements, all the springs are compressed due to the particular direction of the end-moments, and c is negative. Therefore, we have to add the term cN^T (subtract $-cN^T$) as follows.

```
RHS (2,1)  =  RHS (2,1) + PROPS(7) * S(1)
RHS (3,1)  =  RHS (3,1) + PROPS(7) * S(2)
RHS (5,1)  =  RHS (5,1) + PROPS(7) * S(3)
RHS (6,1)  =  RHS (6,1) + PROPS(7) * S(4)
```

For the positive value of c, the negative sign should be used in the above equation. For the three models in Figure 5.24, end moments of 2.0×10^6 lb-in as shown are applied incrementally. The end rotations, reaction forces at end nodes, and the deflection of the middle connector for the three models are given in Table 5.1. The nail deflections for the model with user elements are found using a FORTRAN program SDISP2D, which is similar to the one given in Appendix E for 3D b/c elements. The nail deflections are found in this program using Eq.(5.4).

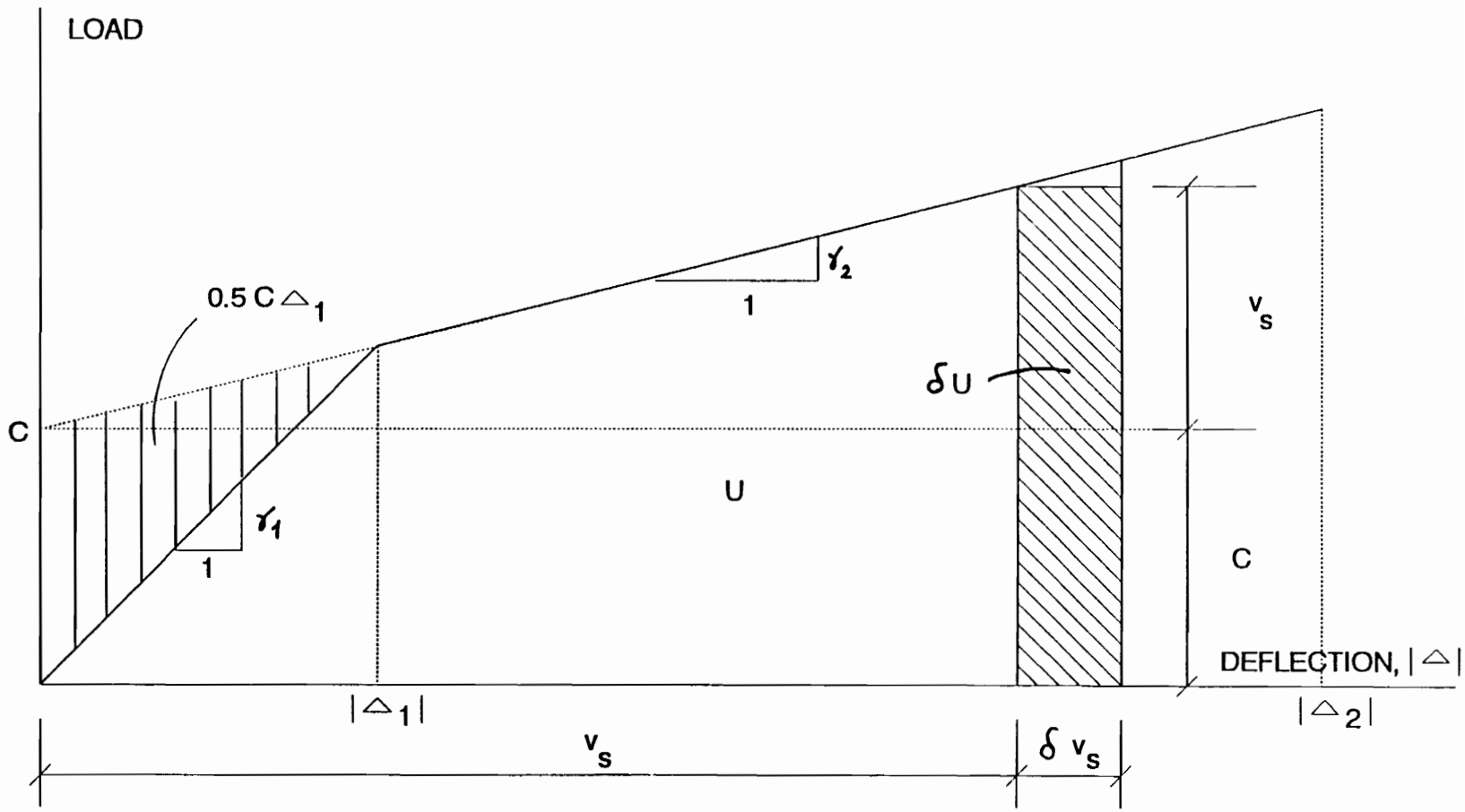


Figure 5.25 Spring energy for the second segment of bilinear load-deflection curve

5.5.3 Testing of 3D Nonlinear b/c Elements

The local stiffness matrix of the 3D b/c element has been derived in section 5.3 (Eq. 5.23). The local beam axes for this element are set to coincide with the global axes so that the local and global stiffness matrices are the same for test models analyzed in this section. Similar to the 2D b/c models, linear and nonlinear analyses are performed on the 3D b/c models. B33 space frame elements are used to model the beams, and SPRING2 and user elements are used to model the connectors. The beam used in the model had a circular cross section with a radius of 5.0". The material properties are those of the beams in the dome cap model, i.e., E = 1.8E06 psi and G = 1.6E05 psi. The 3D b/c assembly with one connector and also the equivalent model with the nonlinear SPRING2 element are shown in Figure 5.26. For the SPRING2 elements, the rigid link between the spring and the beam elements is achieved using MPC (Multi Point Constraint) number 7. The *MPC option (ABAQUS, sec. 6.8.4) allows constraints to be imposed between different DOF of a model. MPC 7 provides a rigid beam between nodes, with identical rotations of the two nodes.

5.5.3.1 Linear Analysis

The models in Figure 5.26 are analyzed with a constant connector stiffness of 14400 lb/in. The *MATRIX and the user element options are used as earlier. The user subroutine is similar to the one used in the linear analysis of the 2D b/c models except that the interpolation functions and the connector stiffness matrix for the 3D b/c elements is used. The user element has 6 DOF at each node, of which 2, 4, 6 are the DOF that activate the springs. The connector stiffness matrix for the spring stiffness of γ_S = 14400 lb/in is calculated from Eq.(5.23).

For the applied moments of 4×10^2 lb-in at the ends, the models with the user element specified by *MATRIX and the user subroutine option gave same results. These and the results for the model with SPRING2 elements are shown in Figure 5.26.

Table 5.1

Results for the 2D b/c Test Models

Connector type	End Moment (lb-in)	End Rotation ($\times 10^{-2}$)	Deflection of the middle spring (in)	RF1 at end nodes (lb) ($\times 10^{5}$)	RF2 at end nodes (lb)
Number of connectors = 1					
SPRING2	2.0×10^{6}	-8.3425	-2.635	-1.4790	-908.7
User Element	2.0×10^{6}	-8.2550	-2.7153	-1.5432	-922.0
Difference	-	1.05 %	3.05 %	4.34 %	1.45 %
Number of connectors = 3					
SPRING2	2.0×10^{6}	-8.2339	-2.5910	-1.4269	-2381
User Element	2.0×10^{6}	-8.1341	-2.6843	-1.4983	-2428
Difference	-	1.21 %	3.60 %	5.00 %	1.97 %
Number of connectors = 15					
SPRING2	2.0×10^{6}	-7.6318	-2.3390	-1.1791	-9847
User Element	2.0×10^{6}	-7.4859	-2.4703	-1.2685	-10101
Difference	-	1.92 %	5.61 %	7.58 %	2.58 %

5.5.3.2 Special Case

The spring was attached in the middle of the beam in the previous section. A model with 2 beams and one connector attached to the end of one of the beams is analyzed in this section. This model was analyzed by Tsang (1992) using the *MATRIX option. It is analyzed with the UEL option to compare with the model having SPRING2 elements. The purpose is to check if the results in the two cases are the same; there are no approximations involved by the interpolation when the spring is attached to the end of the beam.

The same results were obtained with the user elements using subroutine UEL as with the SPRING2 elements. They agree with those given by Tsang (1992) for the user element using the *MATRIX option..

5.5.3.3 Nonlinear Analysis

The connector elements with the bilinear load-deflection curve are used in the nonlinear analysis of the 3D b/c models. Models with 1, 3, and 15 connectors are analyzed using SPRING2 elements and the user elements specified through UEL. The model with one connector is shown in Figure 5.26. Figure 5.27 shows the models with 3 and 15 connectors.

Two different boundary conditions are used in two different sets of test cases (Figure 5.28).

- B. C. #1 : DOF 1,2,3,5,6 fixed with applied moment CM1
- B. C. #2 : DOF 1,2,3,4,5 fixed with applied moment CM3

The purpose is to test the user subroutine by activating different DOF such as 4 or 6 while suppressing the others. Similar to the 2D b/c models, the function of UEL is to check the deflection of the individual connector in each iteration and modify the Jacobian stiffness matrix AMATRX and also the cumulative contribution of the connector elements in RHS. The input files for the models with SPRING2 and user elements with UEL option (15 connectors) for the B. C. #1 are given in Appendix E. An additional parameter

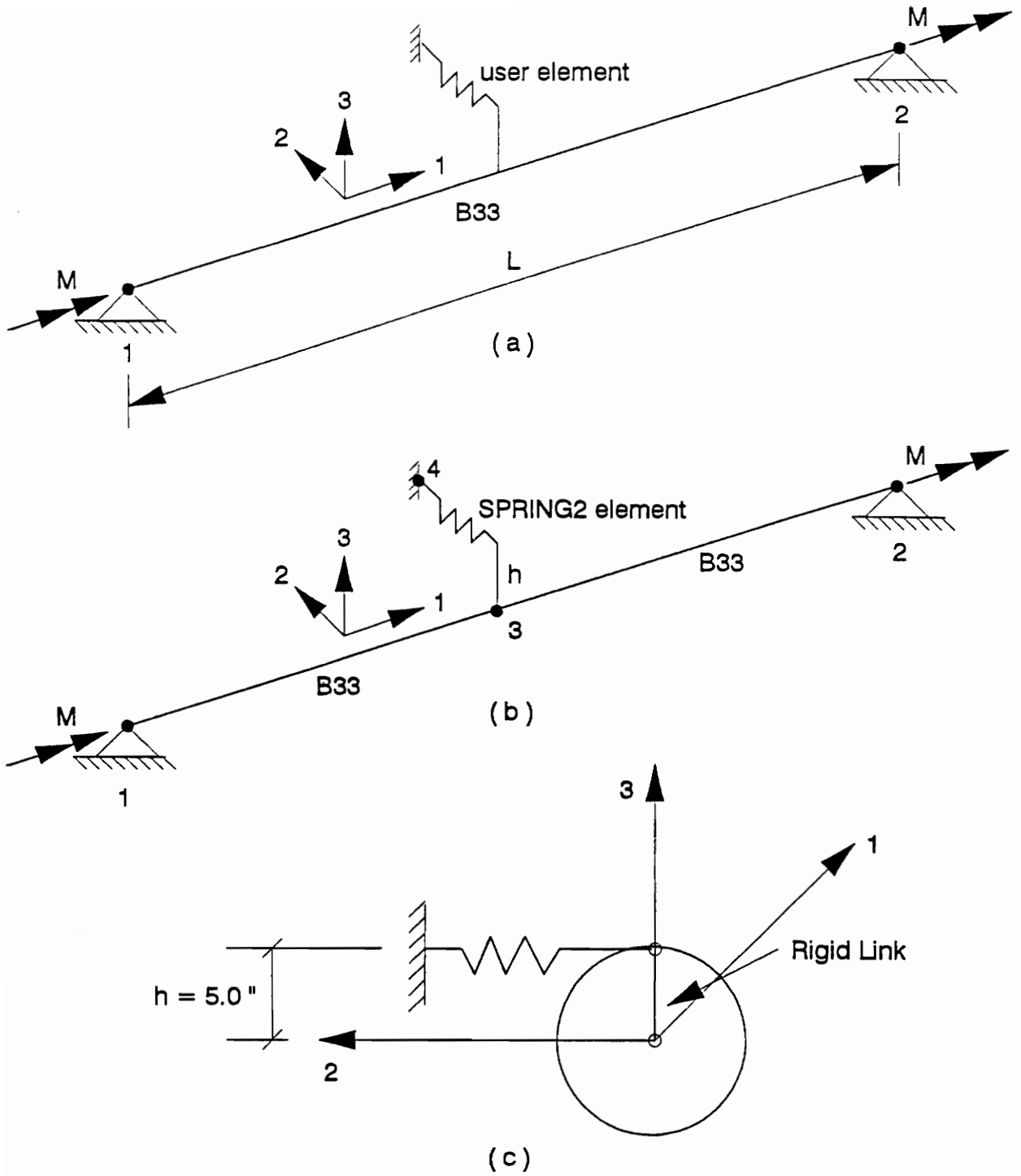


Figure 5.26 3D beam/connector assembly, a) with user element, b) with SPRING2 elements for the connector; c) beam cross section

to supply the rigid link length h = 5.0" is given as the eighth property in the *UEL PROPERTY option.

The results for the tests on the 3D b/c models are summarized in Tables 5.2 and 5.3. The nail deflections for the model with user elements are obtained by Eq. (5.17) using a FORTRAN program SDISP3D, which is given in Appendix E.

5.5.4 Subroutine UEL for the Dome Cap and Dome Models

The 3D b/c models in the previous section were analyzed with the connector elements having the same local and global stiffness matrices. However, in a general structure such as dome cap model, the beams are oriented arbitrarily in space. Therefore, the stiffness matrices of the connector elements need to be transformed into global stiffness matrices. This is done in user subroutine UEL using the rotation matrix R discussed in Appendix A. The nodal coordinates are passed in the subroutine UEL in the array COORDS (I,J). These are used in the calculation of the rotation matrix. The user subroutine UEL for the analysis of the dome cap and the full dome models is given in Appendix F. Note that another subroutine AMATRH is given at the end of UEL. It is used to calculate the AMATRX and RH arrays. RH contains the contributions of the connector elements in the beam local frame of reference. The contributions in the global frame of reference are calculated in UEL using the rotation matrix R as follows:

$$F = R^T f \tag{5.39}$$

where

F = global force vector
f = local force vector
R = rotation matrix (refer to Appendix A)

The test models in the previous sections were analyzed using UEL for the dome cap to check its accuracy. A small modification is required in the input files of the 3D b/c models for doing this. Since the normalized position vectors (vectors with reference to the origin, 0., 0., 0.) of the nodes of the beam elements are used in the calculation of the rotation matrix, coordinates of node 1 are changed from 0., 0., 0. to 0., 10., 0. This is necessary because the length of the position vector is zero if node 1 is the origin itself, causing

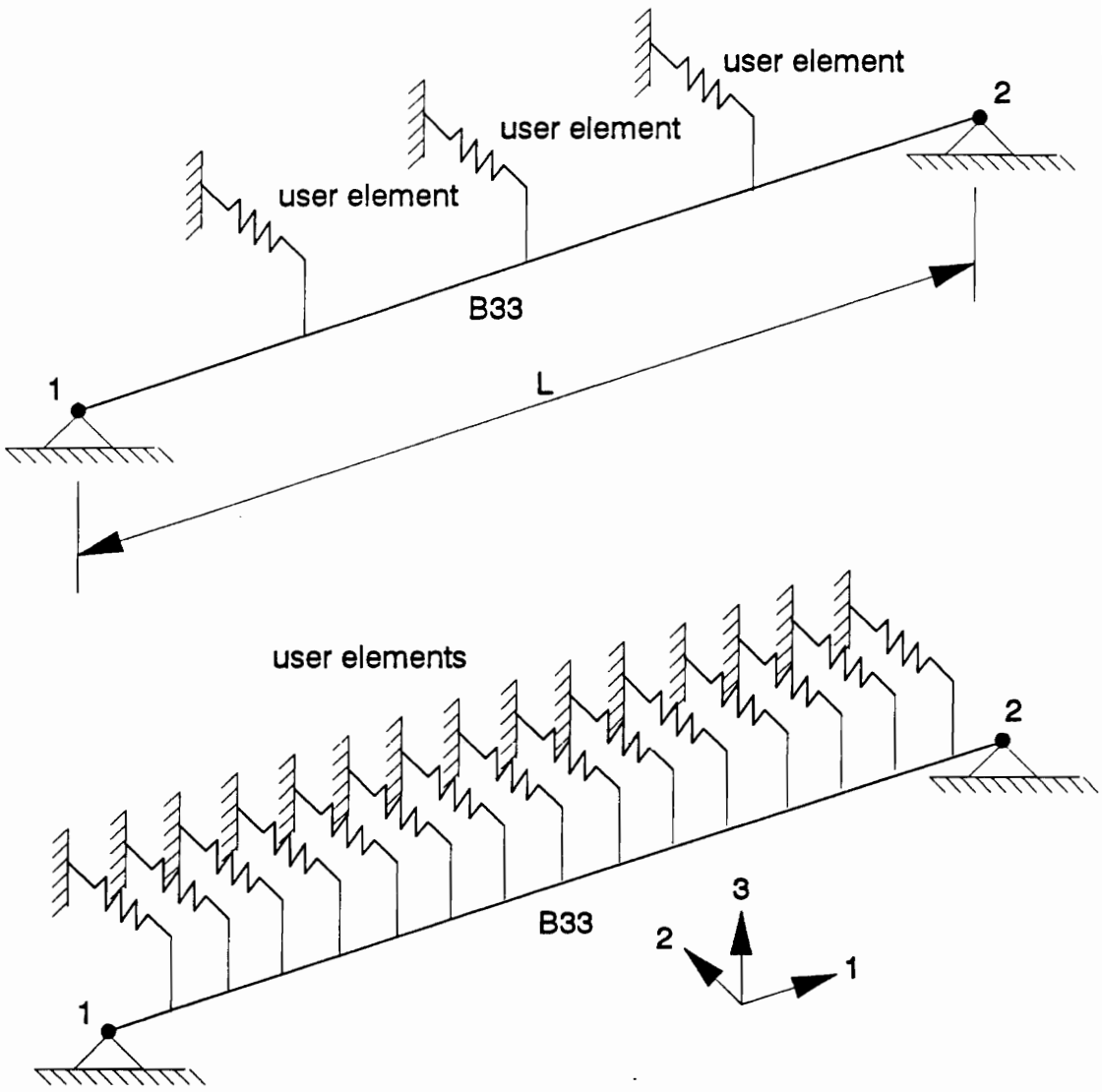


Figure 5.27 3D beam/connector assembly, a) 3 connectors, b) 15 connectors

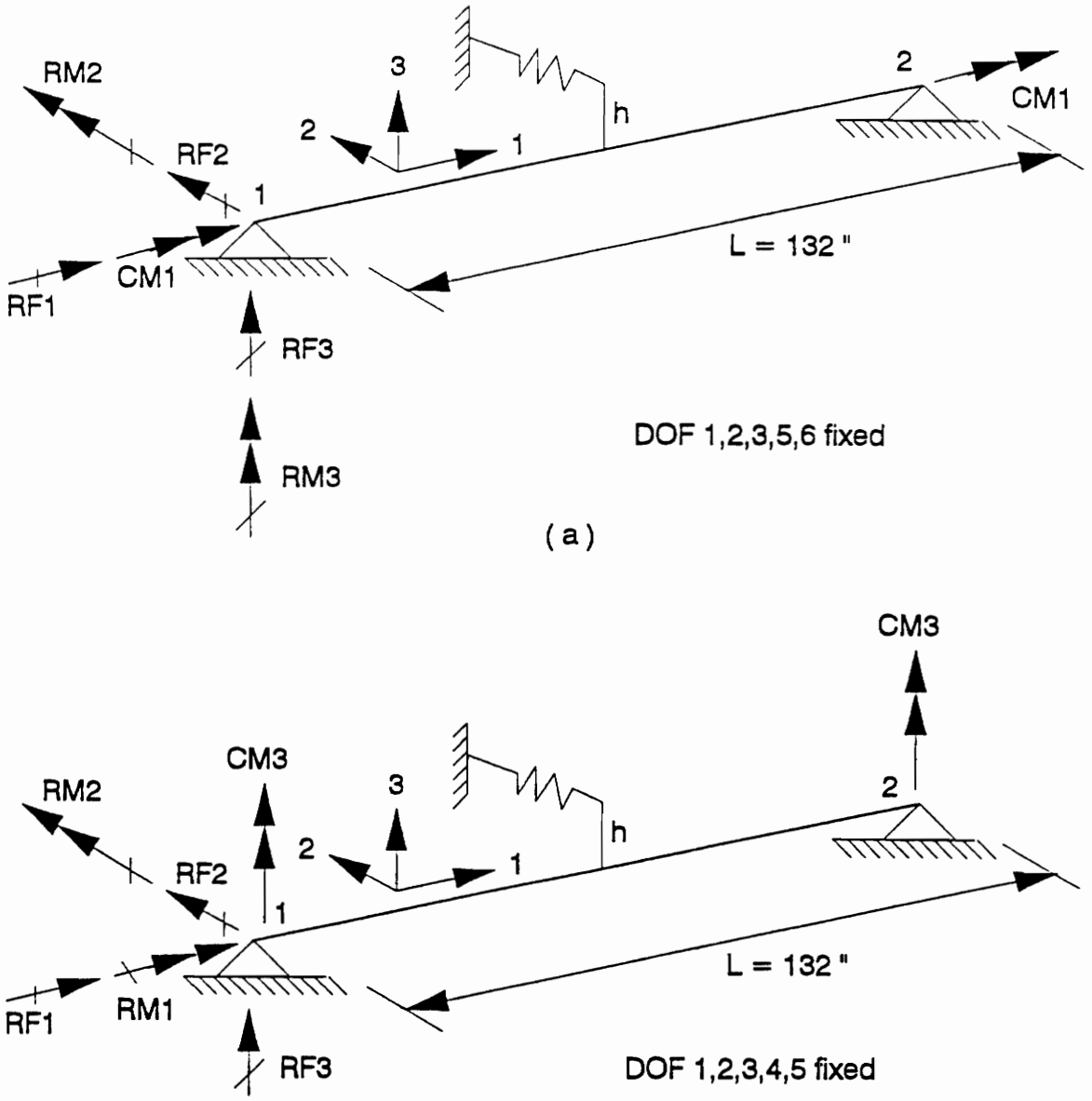


Figure 5.28 Different boundary conditions used in the test cases on 3D b/c element

Table 5.2

Results for the 3D b/c Test Models : B. C. #1

Connector type	End Moment (lb-in)	End Rotation	Deflection of the middle spring (in)	RF2 at end nodes (lb)	RM3 at end nodes (lb) ($\times 10^4$)
Number of connectors = 1					
SPRING2	3500	0.4288	-2.079	-769.7	-2.54
User Element	3500	0.3600	-1.800	-700.0	-2.31
Difference	-	16.0 %	13.4 %	9.06 %	9.06 %
Number of connectors = 3					
SPRING2	1.05×10^4	0.4288	-2.079	-2309	-6.35
User Element	1.05×10^4	0.3600	-1.800	-2100	-5.77
Difference	-	16.0 %	13.4 %	9.05 %	9.1 %
Number of connectors = 15					
SPRING2	5.25×10^4	0.4290	2.079	-11546	-26.99
User Element	5.25×10^4	0.3600	1.80	-10500	-24.54
Difference	-	16.0 %	13.4 %	9.06 %	9.08 %

Table 5.3

Results for the 3D b/c Test Models : B. C. #2

Connector type	End Moment (lb-in)	End Rotation ($\times 10^{-2}$)	Deflection of the middle spring (in)	RF1 at end nodes (lb) ($\times 10^{4}$)
Number of connectors = 1				
SPRING2	9.0×10^{5}	6.415	1.94	-8.13
User Element	9.0×10^{5}	6.57	2.02	-8.196
Difference	-	2.44 %	4.1 %	0.80 %
Number of connectors = 3				
SPRING2	9.0×10^{5}	5.68	1.787	-7.149
User Element	9.0×10^{5}	5.83	1.927	-8.115
Difference	-	2.64 %	7.83 %	13.5 %
Number of connectors = 15				
SPRING2	9.0×10^{5}	5.415	1.593	-5.27
User Element	9.0×10^{5}	5.584	1.843	-7.42
Difference	-	3.12 %	15.67 %	40.8 %

division by 0 in the calculations of the rotation matrix. The coordinates of node 2 are changed accordingly to 132., 10., 0. The results of the analysis using the UEL for the dome cap model were found to be exactly the same as those obtained in the previous section. To further confirm the accuracy of UEL for the dome cap, a model obtained by rotating the beam through 90 degrees (Figure 5.29) is tested with SPRING2 elements and also this subroutine. Note that the local and the global stiffness matrices for the connector elements in this case are different and the subroutine used in the previous section cannot be used. The two models gave the same results, indicating that the local to global transformation of the connector stiffness matrix performed in the subroutine UEL for the dome cap is correct.

In the models tested so far, only one user element was used. However, in case of the dome cap and the dome models, more than one user element is present. This is because there is one user element, which defined the cumulative effect of all the connectors on the beam, for every beam in those models. For this reason, more than one *USER ELEMENT card is required, one for every user element in the model. All of these elements refer to the same subroutine UEL during the analysis. To test this, a b/c test model with 2 beam elements and 2 associated user elements is analyzed. Figure 5.30 shows the assembly of these two models. A similar model with SPRING2 elements is also analyzed to compare the results. The same kind of nonlinear connectors as used in the previous sections on the 2D and 3D b/c models are used.

The results of the analysis of these two models were found to be identical. This shows that the user subroutine UEL is capable of supporting more than one user element in a model, provided all of them have the same element properties.

This completes the formulation and testing of the nonlinear beam/connector user elements and the user subroutine UEL used for specifying them in the nonlinear analysis with ABAQUS. The user subroutine UEL developed in this chapter for the dome cap model will be used in the next chapter for the analysis of the dome cap model with nonlinear b/c elements.

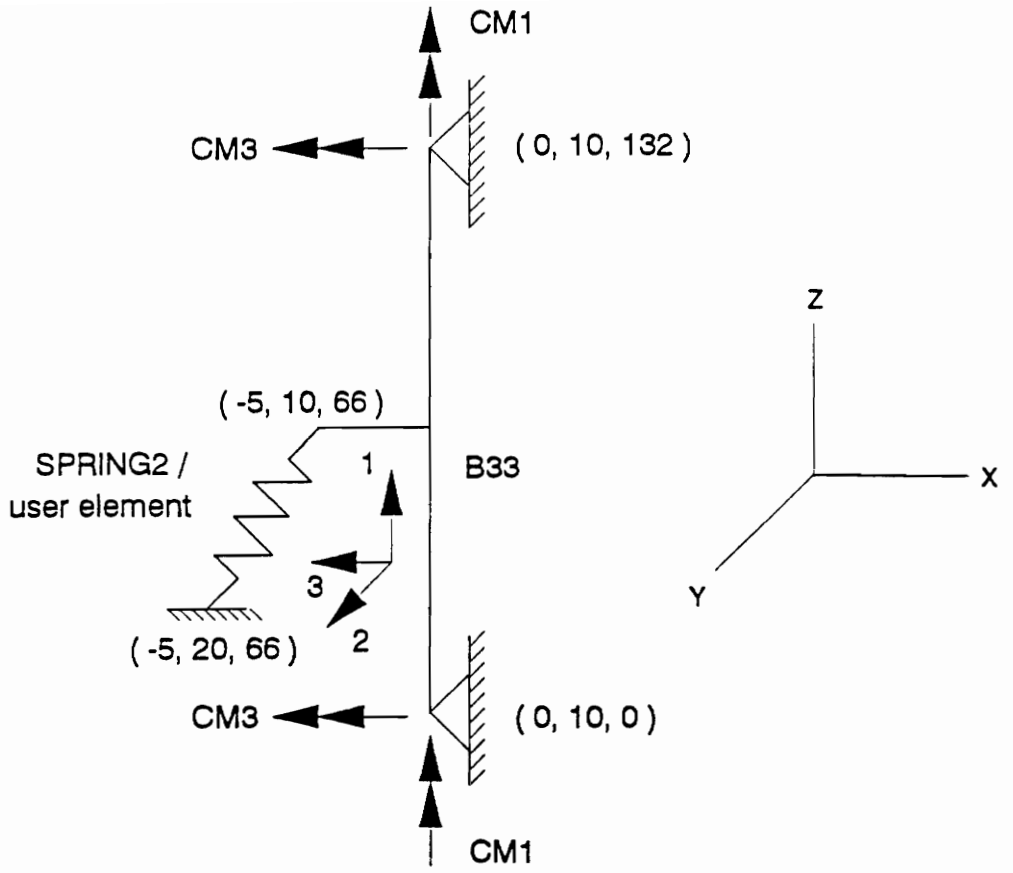


Figure 5.29 3D b/c model with vertical beam

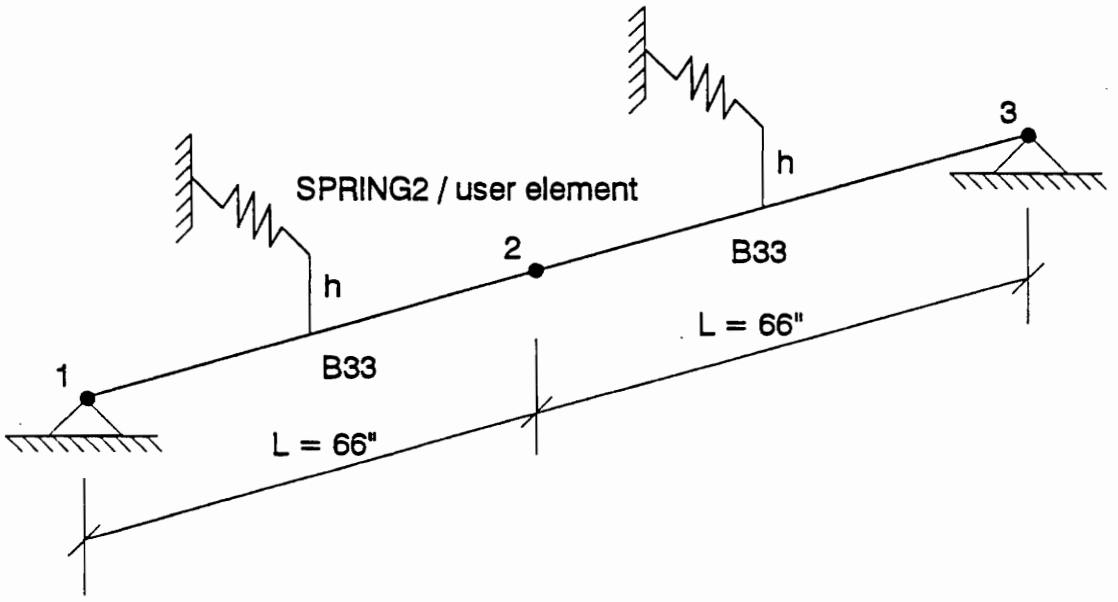


Figure 5.30 3D b/c model with two b/c elements

Chapter 6

Analysis of Dome Cap and Dome with 3D b/c Elements

6.1 Introduction

The significance of the 3D b/c finite element model in the analysis of the Crafts Pavilion Glulam Dome is discussed in section 5.1. The user subroutine UEL for use in dome cap and dome models was tested for a few test problems and is given in Appendix F.

The dome cap and dome models are analyzed in this chapter for full and half snow load cases. Results for the following three models are presented.

- Model without truss bracing or b/c elements (i.e., the decking is not modeled)
- Model with truss bracing (decking modeled by truss bracing)
- Model with 3-D b/c elements having nonlinear connectors (decking modeled by b/c elements) but no truss bracing

The linear material law 1 (section 2.4.2) with E = 1.80E06 psi and G = 1.60E05 psi is used in all the models. The purpose is to check if the stresses at bifurcation or limit point remain below the proportional limit, especially in the model with b/c elements. The dome is analyzed later with nonlinear material law, since the stresses were found to exceed the proportional limits in tension and compression in the analyses with the linear material law.

6.2 Modification in the Input File for the Model with b/c Elements

The input file for the dome model with truss bracing is given by Telang (1992, Appendix A). The C1D2 truss elements are removed from this input file for the model without truss bracing. For the models with b/c elements, the input deck for truss bracing is replaced by the *USER ELEMENT cards and the user subroutine UEL is given at the end of the input file. To create the *USER ELEMENT cards for the input files for the dome cap and the dome, the FORTRAN programs SUEL1, SUEL2, SUEL3 are used. These programs write the input data cards for b/c elements corresponding to the main beams I & II and the edge beams, respectively. The program SUEL1 is given in Appendix

G. The output created by this program is the input data deck for b/c elements of main beams I and is given below. Note that the nail properties in *UEL PROPERTY cards are the same as those discussed in section 5.2.

```
**----------------------------------MAIN BEAMS-I : B/C ELEMENTS
*USER ELEMENT,NODES=2,TYPE=U 1001,COORDINATES=3,PROPERTIES=7
1,2,3,4,5,6
*ELEMENT,TYPE=U 1001,ELSET=C1001
 911,  1,  28
*UEL PROPERTY,ELSET=C1001
16,5.500,6850.00,    0.00,0.0560,1.0000,384.00
   :    :     :     :     :     :     :
   :    :     :     :     :     :     :
   :    :     :     :     :     :     :
   :    :     :     :     :     :     :
*USER ELEMENT,NODES=2,TYPE=U 1179,COORDINATES=3,PROPERTIES=7
1,2,3,4,5,6
*ELEMENT,TYPE=U 1179,ELSET=C1179
1089,  2,  72
*UEL PROPERTY,ELSET=C1179
16,5.500,6850.00,    0.00,0.0560,1.0000,384.00
```

6.3 Analysis of Dome Cap Models

The 2 element mesh dome cap model (Figure 2.8) with inclined base beams, used in chapter 3, is analyzed for the three models described in section 6.1. The results for the model with truss bracing are given in section 3.2. The results for the three models are summarized in table 6.1. The element stresses for the model without truss bracing or b/c elements are not presented, since this model is not realistic as it does not model the decking. In case of the model with b/c elements, 16 connectors (nails) are used for every finite element and are attached at the top of the beam cross section (h = 5.5"). Note that there are 2 nails present at each location of the connector. Therefore, the nail stiffness of $2\gamma_1$ = 13700 lb/in is used in the analyses of the dome cap and the dome models (section 6.4). The load-deflection paths for the two load cases are shown in Figures 6.1 and 6.2.

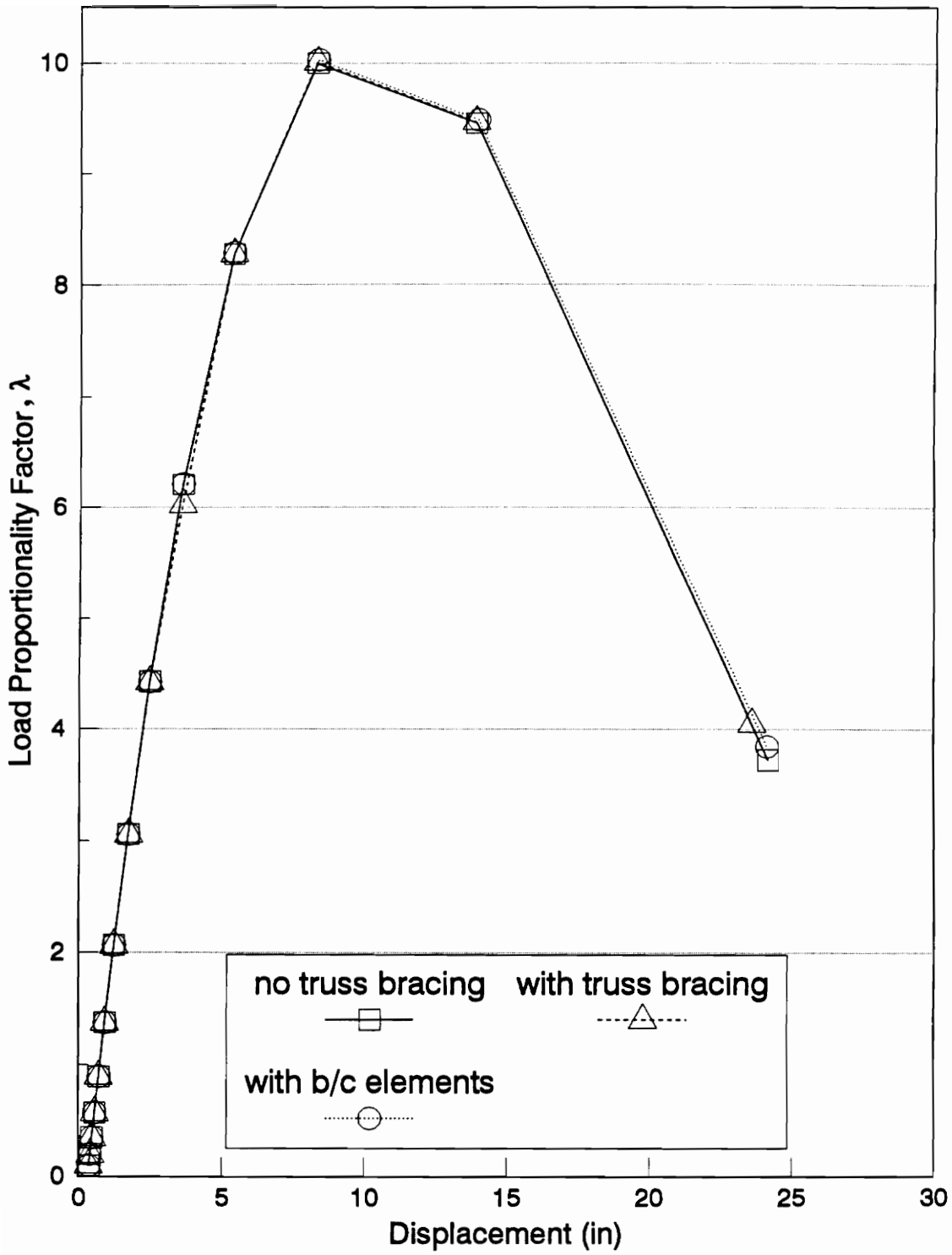


Figure 6.1 Load-deflection paths for cap models with, and without truss bracing, and with b/c elements: full snow load

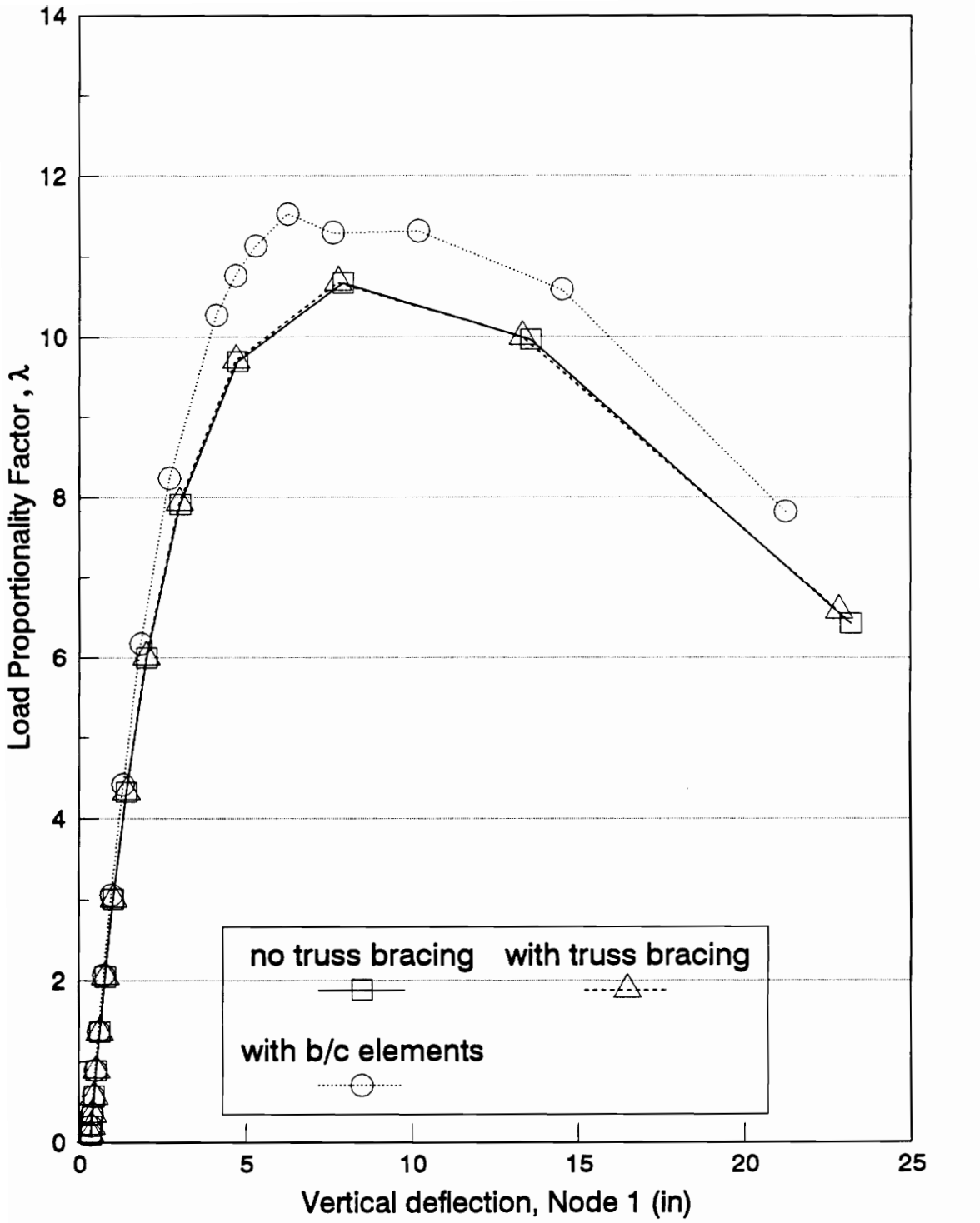


Figure 6.2 Load-deflection paths for cap models with, and without truss bracing, and with b/c elements: half snow load

Table 6.1

Results for the Different Dome Cap Models

	λ_{cr}	Vertical deflection (node 1)	Max. tensile stress (psi)	Max. compressive stress (psi)
Full Snow				
No Truss Bracing	8.274	-5.373	--	--
With Truss Bracing	10.01	-8.279	5858 (El. 59, Node 18)	-8095 (El. 44, Node 16)
With b/c Elements	10.03	-8.318	4644 (El. 59, Node 18)	-7540 (El. 44, Node 16)
Half Snow				
No Truss Bracing	10.67	-7.923	--	--
With Truss Bracing	10.68	-7.776	14190 (El. 15, Node 8)	-18090 (El. 16, Node 8)
With b/c Elements	11.31	-10.20	15160 (El. 15, Node 8)	-19200 (El. 16, Node 8)

For the model without truss bracing, $\lambda_{cr} < \lambda_{max}$, indicating a bifurcation point. It can be observed that the b/c element model shows stiffer response in the half snow load case. The stresses in the elements are higher corresponding to the higher live load present at the limit point. For the full snow load case, the models with truss bracing and b/c elements have the same load carrying capacity; however, the element stresses in the b/c element model are significantly lower. This is because the beam is supported continuously by the connectors in the b/c model, whereas, it is supported only at the ends by the purlins or the truss bracing in the model with truss bracing. Note that the stresses in both the cases exceed the proportional limit for wood (Table 6.2) significantly; thus, the assumption of linear material law is not valid. The nonlinear material law is used for the dome model in next section for this reason.

Table 6.2

Proportional Limit and Ultimate Stresses for different material laws (Telang, 1992)

	Proportional limit in compression (psi)	Proportional limit in tension (psi)	Ultimate compressive stress (psi)	Ultimate tensile stress (psi)
Linear law	5900	5900	8500	14500
nonlinear law	4873	2578	10496	14500

For the b/c element model, it is possible to monitor the status of the nails on the main beams by post-processing the results. The end deflections of the beams are obtained in the analysis and are used as input data for the FORTRAN program SCAP3D, given in Appendix G. Following maximum deflections of the nails are obtained.

Full Snow Load :
0.3713 in. beams 33, 34 at node 12, Beams 59, 60 at node 18.
0.2950 in. beams 2, 16, 32, 46 at nodes 5, 8, 11, 15, respectively.

Half Snow Load :
1.606 in. beams 19 near node 9, Beams 48 near node 17.
1.138 in. beams 45, 46 near node 15.
1.03 in. beams 15, 16 at node 8.

It can be seen that the nails are more severely stressed in the half snow load case as compared to the full snow load case. This is because the twist buckling of the beams is more prominent in the half snow load due to its asymmetric nature. Note that the nail deflections above are found by interpolating the deflections of end nodes of the beams and they simply represent the displacement in space of the point where nail is present. The nail is cut-off after deflection of 1.0 in., and is not physically present for deflections greater than 1.0 in.

6.4 Analysis of Full Dome Models

In addition to the three models described in section 6.1, the dome was also analyzed for the following cases.

- Nails (connectors) at all nodes on the dome (Nail stiffness = $2\gamma_1$)
- Nails at bracing points only (Figure 6.3)

  Nail stiffness = $2\gamma_1$, $5\gamma_1$, $10\gamma_1$

The nail stiffness mentioned above is the initial nail stiffness, where γ_1 = 6850 lb./in (Figure 5.6). Linear material law 1 (E = 1.80E06 psi, G = 1.60E05 psi) and full and half snow load conditions were used in all the cases. In the above cases, the nails are attached to the centroid of beam cross section, so that h = 0.0. This is to simulate the truss bracing model in which the truss bracing is attached to beams at their centroids. Following tolerance values were used in the analyses.

PTOL = 100 (lb.), MTOL = 15000 (lb-in)

The PTOL and MTOL values of 30 lb. and 3000 lb-in, respectively were used in the earlier analyses. The PTOL value is required to be relaxed to 100 lb. for the analysis of the b/c model. The relaxed value of MTOL of 15000. lb-in is obtained approximately as follows. The average maximum stresses in the beam elements are 15000 psi. For the beam cross section dimensions of b = 5" and d = 11", the section modulus, Z, is about 100 in^3. The maximum moment for these values is M = stress × Z = 1.5×10^6 lb-in. The MTOL is taken as 10^{-2} times this value of the maximum moment.

The 2-element mesh model is used in all analyses since the model with b/c elements is relatively expensive and needs large disk space for the output files, even for this mesh size. Telang (1992) has done a limited study on the refined mesh models of dome with truss bracing and with bilinear and nonlinear material laws. The results from the analyses of the above models are given in Table 6.3. For half snow load, only the relevant results are given. The load-deflection paths of node 1 for the important models are shown in Figures 6.5 and 6.6.

For the b/c model with 16 nails for every beam finite element, two different models are analyzed. The connector elements are used only for the main beams I and II, i.e., excluding the edge beams in the first model ('16 nails, main beams'). The second model

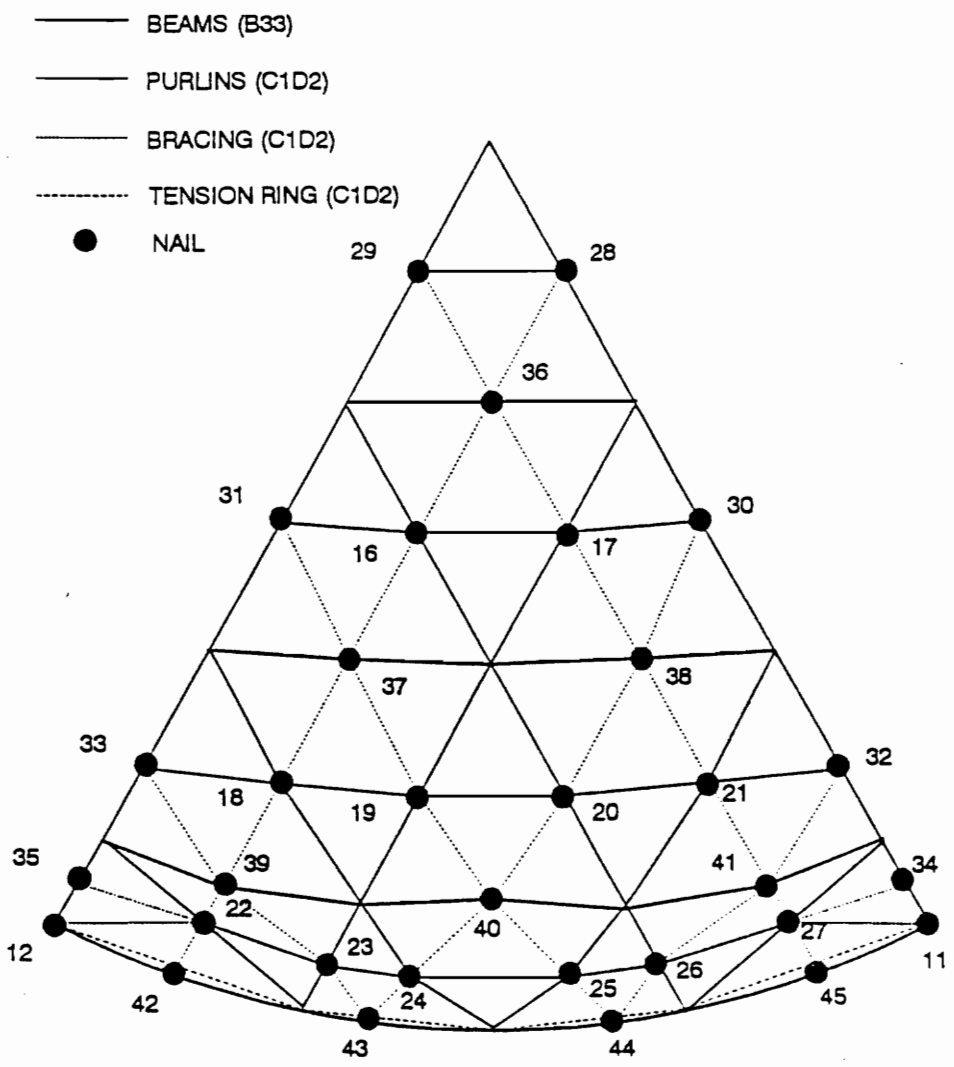


Figure 6.3 Dome Sector: Nails at bracing points

('16 nails, all beams') consists of connector elements for all the beams. The maximum element stresses in the models with truss bracing and b/c elements at the critical loads are given below. Refer to Figure 6.4 for the locations of the elements.

Full Snow Load:				
Maximum tensile stress :	2426 psi	El. 31	.....	No truss bracing
	3876 psi	El. 31, 36	.....	Truss bracing model
	2437 psi	El. 31, 36	.....	b/c element model (16 nails, main beams)
	2487 psi	El. 31,36	.....	b/c element model (16 nails, all beams)
Maximum Compressive stress :	-3803 psi	El. 37	.....	No truss bracing
	-10920 psi	El. 20, 30	.....	Truss bracing model
	-5935 psi	El. 20, 30	.....	b/c element model (16 nails, main beams)
	--6607 psi	El. 20, 30	.....	b/c element model (16 nails, all beams)
Half Snow Load:				
Maximum tensile stress :	1.21 E04 psi	El. 32	.....	No truss bracing
	9059 psi	El. 11, 12	.....	Truss bracing model
	5552 psi	El. 11, 12	.....	b/c element model (16 nails, main beams)
	1.05 E04 psi	El. 11, 12	.....	b/c element model (16 nails, all beams)
Maximum Compressive stress :	-1.59 E04 psi	El. 32	.....	No truss bracing
	-1.78 E04 psi	El. 11, 12	.....	Truss bracing model
	-1.18 E04 psi	El. 11, 12	.....	b/c element model (16 nails, main beams)
	-1.89 E04 psi	El. 11, 12	.....	b/c element model (16 nails, All beams)

In the model with b/c elements, the status of the nails on main beams is checked by post-processing nodal deflections at the critical point. This is done using program

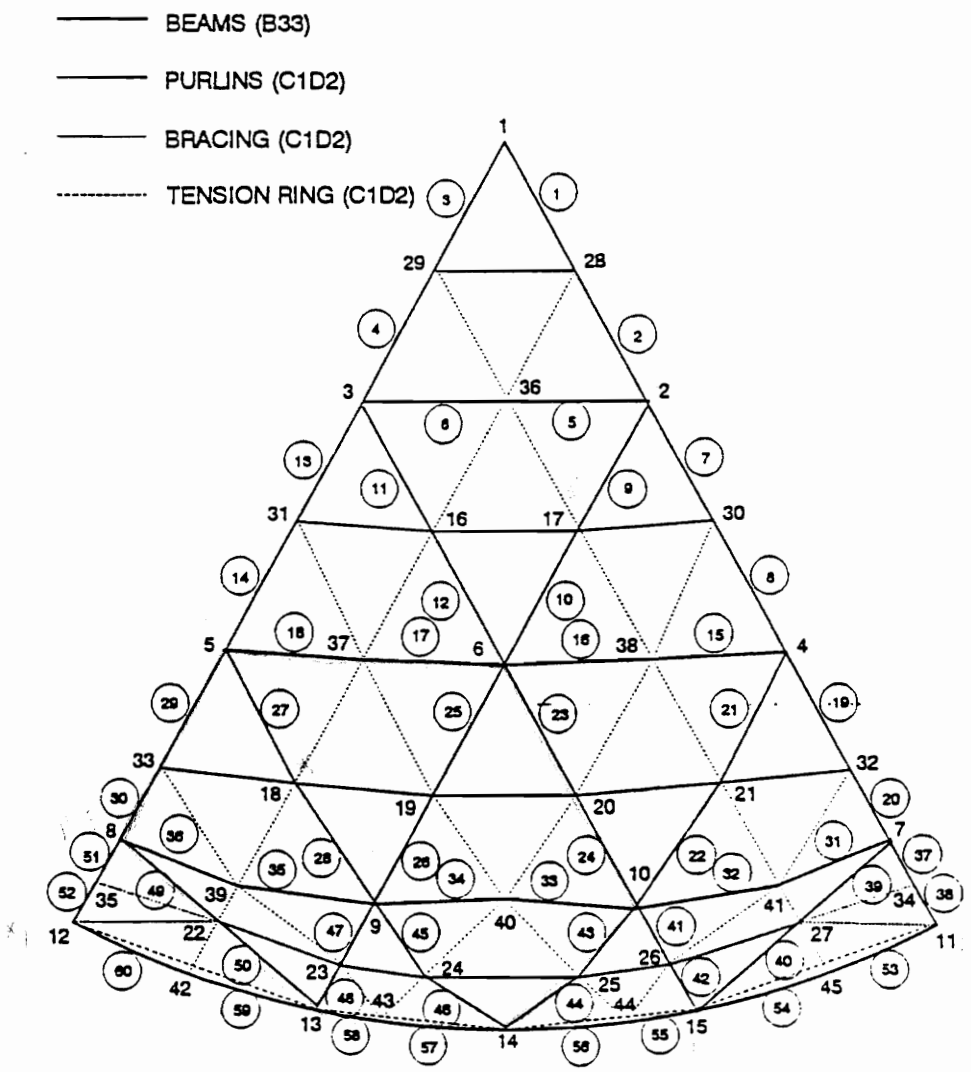


Figure 6.4 Sector of the Dome

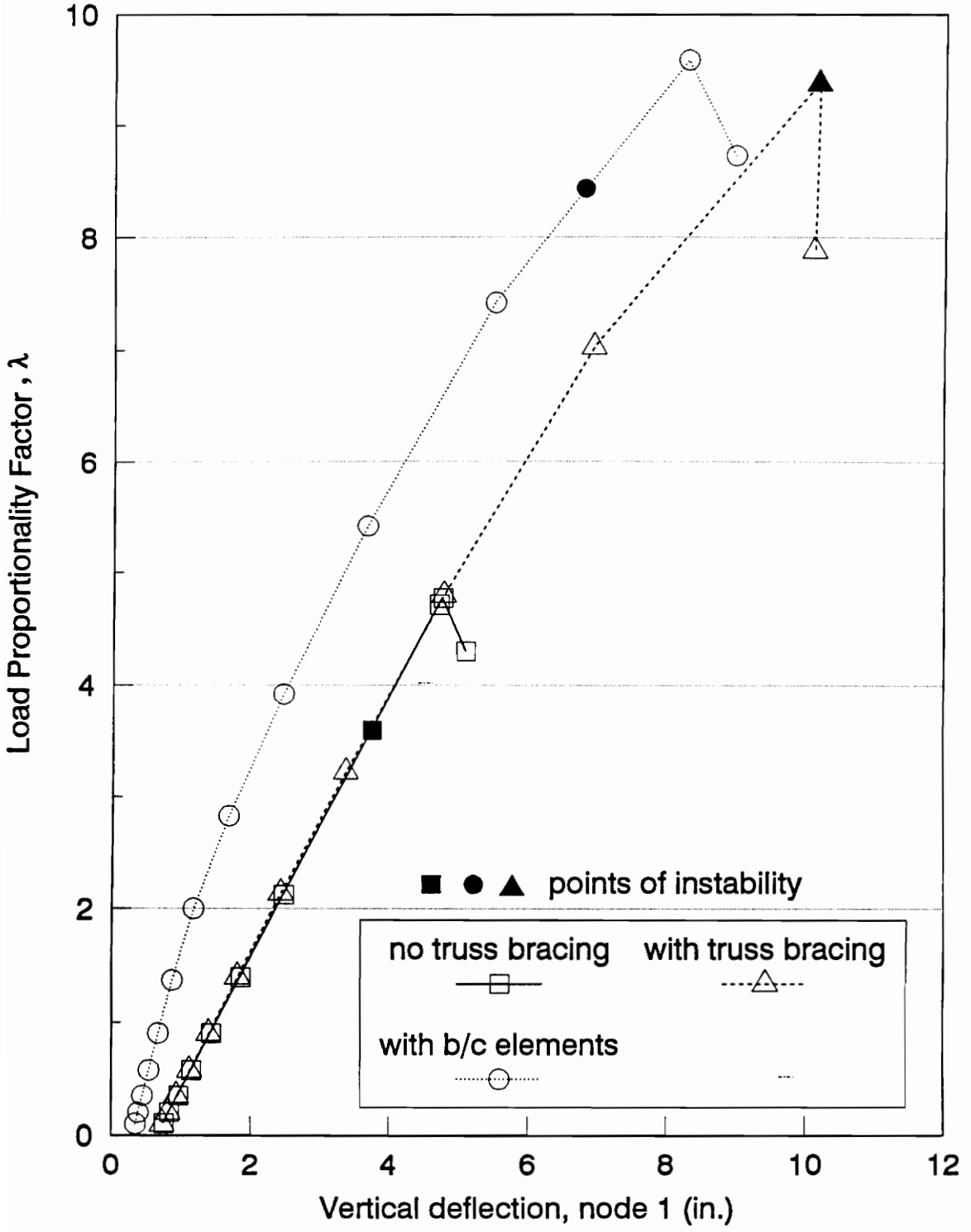


Figure 6.5 Load-deflection paths for various dome models, Full snow load

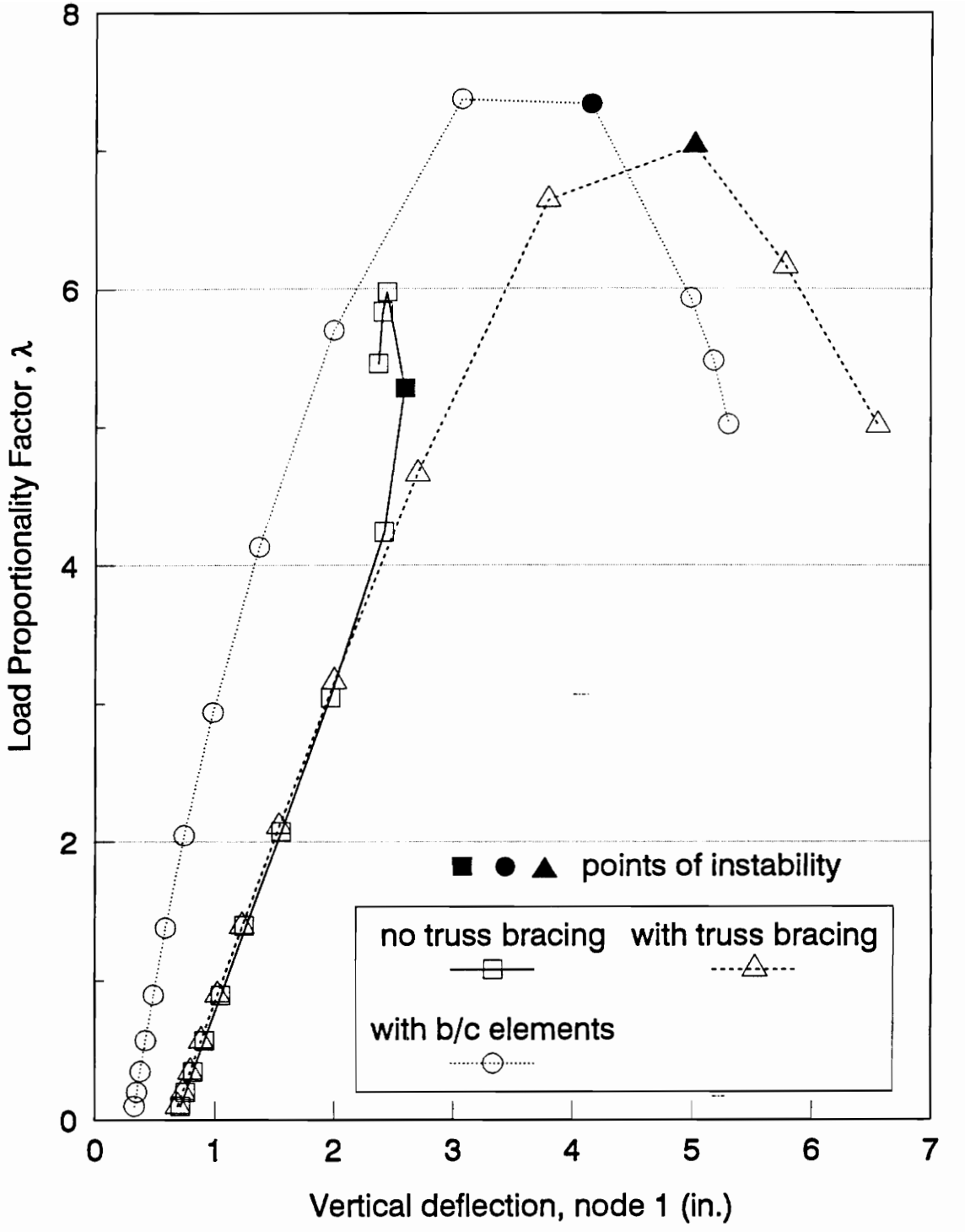


Figure 6.6 Load-deflection paths for various dome models, Half snow load

SECT3D, which is similar to SCAP3D given in Appendix G. The maximum nail deflections are given in Tables 6.4 and 6.5. Note that the stresses exceed proportional limits in tension and compression (Table 6.2) in the analyses with linear material law. For this reason, nonlinear material law for wood by Connors (1989) is used in the next section for the analyses of the dome models.

Table 6.3

Results for Different Dome Models, Linear Material Law

	Full Snow		Half Snow	
MODEL	λ_{cr}	**Vertical deflection node 1, (in.)**	λ_{cr}	**Vertical deflection node 1, (in.)**
No Truss Bracing	3.58	-3.74	5.26	2.59
With Truss Bracing	9.26	-10.03	7.20	-4.70
With B/C Elements				
Nails at all nodes ($2\gamma_1$, h= 0.0)	6.171	-5.91	--	--
Nails at bracing points				
($2\gamma_1$, h= 0.0)	4.77	-4.70	5.19	-2.59
($5\gamma_1$, h= 0.0)	6.07	-5.74	--	--
($10\gamma_1$, h= 0.0)	5.92	-5.50	--	--
16 nails for all main beams ($2\gamma_1$, h= d/2)	7.73	-5.95	7.39	-3.15
16 nails for all beams ($2\gamma_1$, h= d/2)	8.517	-6.64	7.55	-3.82

6.5 Analysis of the Dome Model with Nonlinear Material Law

The dome models with and without truss bracing and with 16 nailed joints for every beam finite element are analyzed using the nonlinear material law. The critical load factors

Table 6.4

Locations of Maximum Nail Deflections in Dome : Full Snow, Linear Material Law

	Beam #	Node	Deflection (in.)
Nails at bracing points ($2\gamma_1$)	52	12	0.918
	15	38	0.825
	18	37	0.644
16 Nails per main beam	35	39	1.15
	36	39	1.13
	52	12	0.88
16 Nails for all beams	35, 36	39	1.36
	28	18	1.06
	52	12	0.992

Table 6.5

Locations of Maximum Nail Deflections in Dome : Half Snow, Linear Material Law

	Beam #	Node	Deflection (in.)
Nails at bracing points ($2\gamma_1$)	32	41	2.23
	15	38	2.04
	19, 23, 27	32, 20, 18	1.70
	18, 21, 25, 29	37, 21, 19, 33	1.30
16 Nails per main beam	33, 34	40	1.24
	16, 17	6	1.01
	23, 24; 25, 26	20; 19	1.003
16 Nails for all beams	33, 34	40	1.51
	23, 24	20	1.37
	6, 11, 13	3	1.20
	17, 25	6	1.12

and nodal deflections for these models are given in Table 6.6. The nail deflections for the model with b/c elements are given in Table 6.7. The maximum stresses obtained in the analyses are as follows.

Full snow load :

Maximum tensile stress:	2698 psi	El. 31	..... No truss bracing
	3329 psi	El. 31, 36	..... Truss bracing model
	2631 psi	El. 36, 36	..... b/c element model (16 nails, all beams)
Maximum compressive stress:	-4853 psi	El. 37	..... No truss bracing
	-9759 psi	El. 37	..... Truss bracing model
	-7107 psi	El. 37	..... b/c element model (16 nails, all beams)

Half snow load:

Maximum tensile stress:	-1.16 E04 psi	El. 32	..... No truss bracing
	6619 psi	El. 39, 40	..... Truss bracing model
	5962 psi	El. 39, 40	..... b/c element model (16 nails, All beams)
Maximum compressive stress:	-1.05 E04 psi	El. 32	..... No truss bracing
	-1.05 E04 psi	El. 11, 12	..... Truss bracing model
	-1.03 E04 psi	El. 11, 12	..... b/c element model (16 nails, All beams)

Following observations can be made from the results of dome models with truss bracing and with b/c elements.

1. For models with nails attached at beam centroids at truss bracing points, the increase in the nail stiffness increases the critical load factor up to a certain level. It does not increase further with increase in nail stiffness. This is due to two reasons. First, the nails offer resistance to the twisting of beams in one direction only, whereas the truss bracing offers resistance in a plane. Second, the nail stiffness becomes zero after a small deflection of 0.056 in. and it offers only a constant resistance of 384 lb. up to Δ_{max}.

2. The model with 16 connectors (nails) for only the main beams I and II, and with 16 connectors for all beams show softer response compared to the truss bracing model for the

Table 6.6

Results for Dome Models with Nonlinear Material Law

	Full Snow		Half Snow	
MODEL	λ_{cr}	**Vertical deflection node 1, (in.)**	λ_{cr}	**Vertical deflection node 1, (in.)**
No Truss Bracing	4.38	-3.89	5.89	-2.20
With Truss Bracing	9.90	-8.74	7.75	-3.79
With B/C Elements 16 nails for all beams	9.02	-6.04	8.29	-3.10

Table 6.7

Maximum Nail Deflections in Dome : Nonlinear Material Law

	Beam #	Node	Deflection (in.)
Full Snow Load			
16 Nails for all beams	35, 36	39	1.30
	28	18	1.01
	52	35	0.996
Half Snow Load			
16 Nails for all beams	33, 34	40	1.25
	23, 24	20	1.10
	16, 25	6	1.05

full snow load condition. However, they show stiffer response than the truss bracing model for half snow load.

3. The element stresses are lower in the model with nails only on the main beams as compared with the truss bracing model in both loading cases. This is corresponding to the lesser load (lower load factor) present on the dome at critical point for this model. The element stresses in the model with nails on all beams are lower than those of the truss bracing model for full snow load, but are higher for half snow load.

4. The response of the b/c model with nails on all beams is in between the models without and with truss bracing for full snow load. It is closer to the truss bracing model because the decking is modeled in both cases. This confirms the significant role of decking in the ultimate load carrying capacity of the dome.

5. The absence of nails on the edge beams has noticeable effect on the capacity of the dome in the full snow load case only. It does not have any effect on the dome capacity in the half snow load condition. This may be due to the fact that the maximum stresses and locations of the maximum nail deflections are near the base beams in the full snow load case, whereas for the half snow load case the critical region is near the center portion of the dome.

6. The dome models with truss bracing and the b/c elements (nails on all beams) are comparable to each other to a certain extent as far as the critical load factor, corresponding nodal deflections and the element stresses are concerned. The b/c model has shows much lower critical load factor and element stresses for full snow load, but marginally higher stresses for half snow load compared to truss bracing model. This trend is also observed for the analyses with nonlinear material law with the exception of lower stresses for b/c model, for both full and half snow load.

The buckling modes for the dome models without truss bracing, and with the beam/decking connectors (b/c elements) for full and half snow load are shown in Figures 6.7 through 6.10. The summary of results of the dome analyses is given in Appendix H.

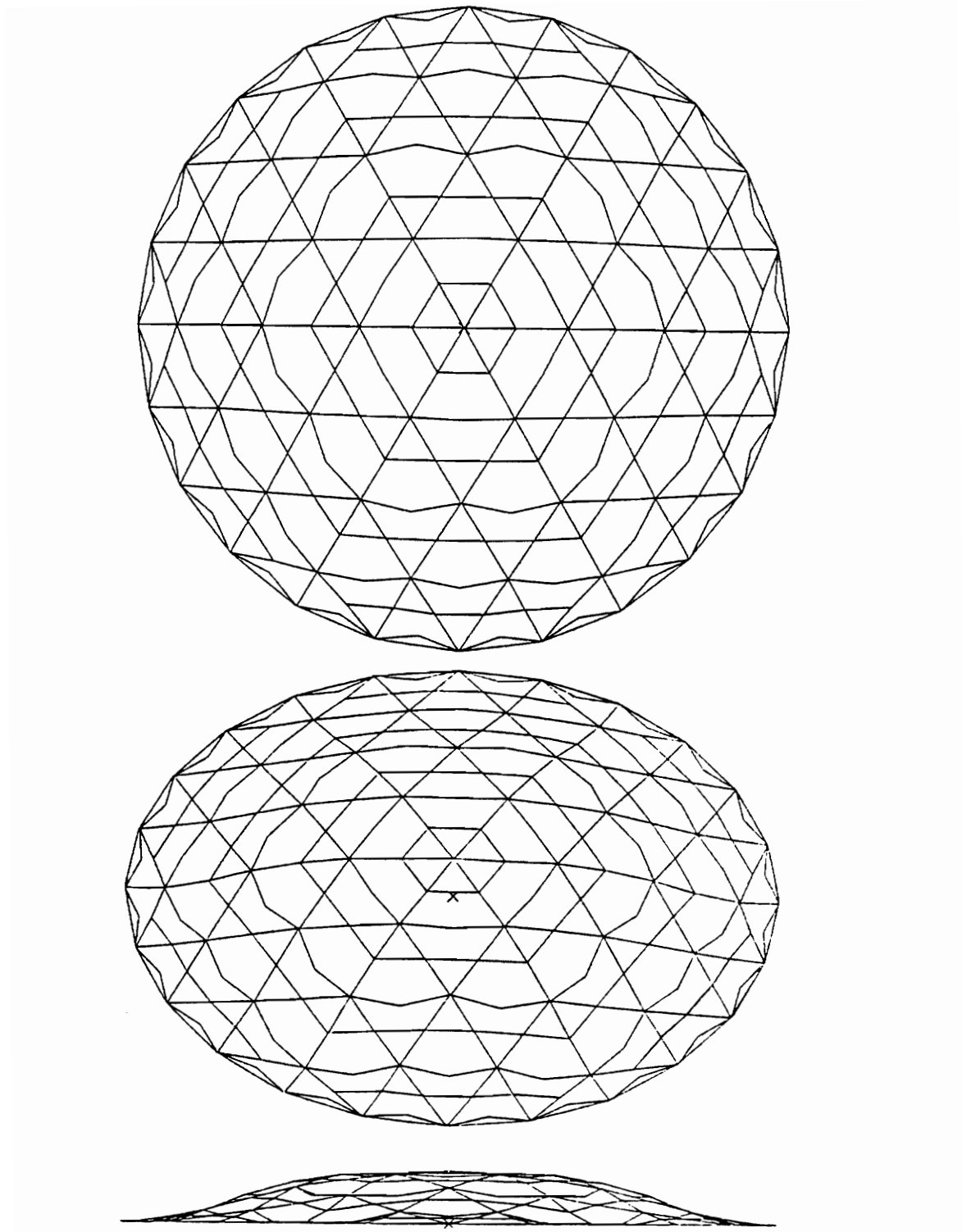


Figure 6.7 Buckling mode for the dome model without truss bracing: full snow

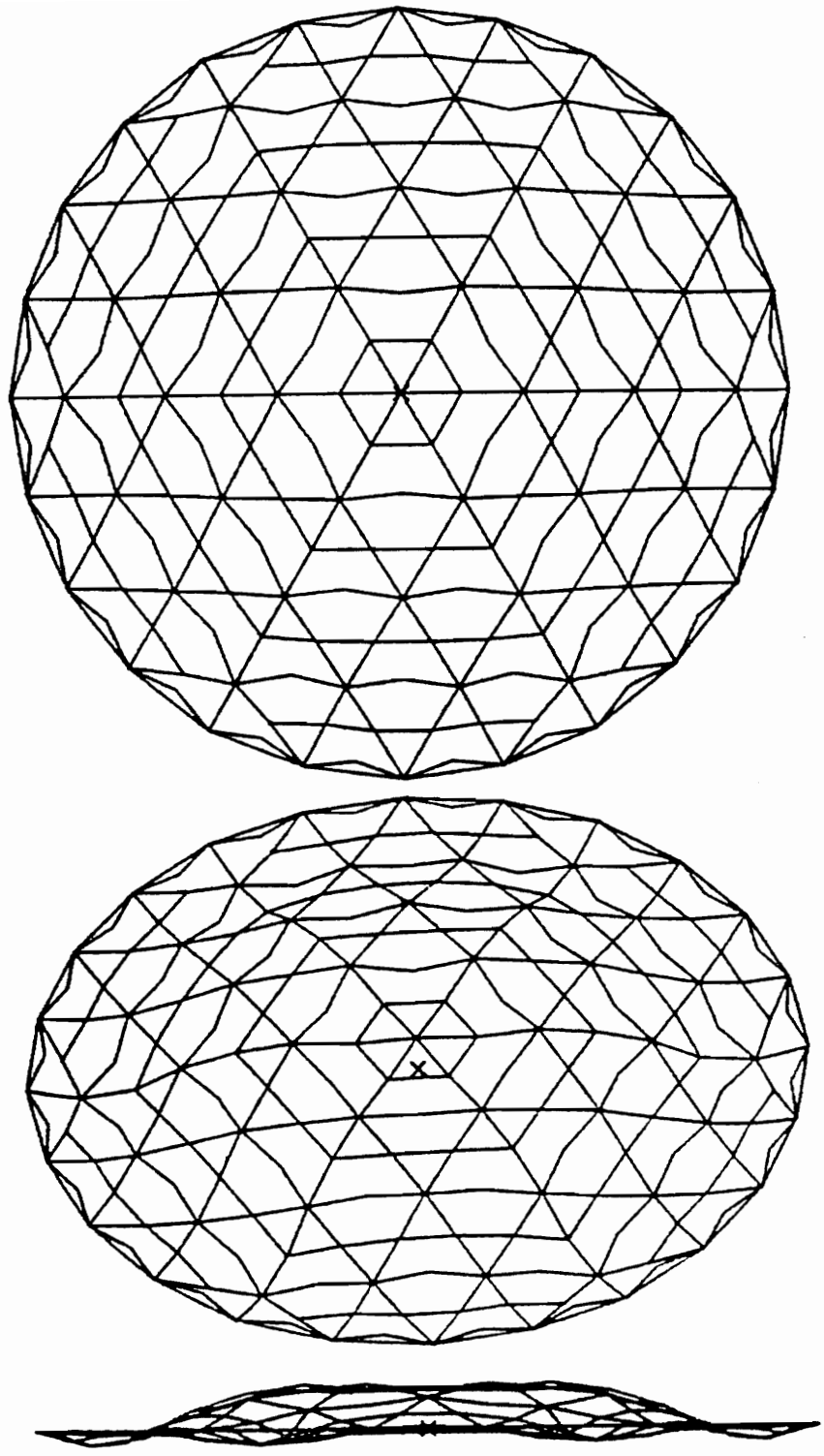


Figure 6.8 Buckling mode for the dome model with b/c elements: full snow

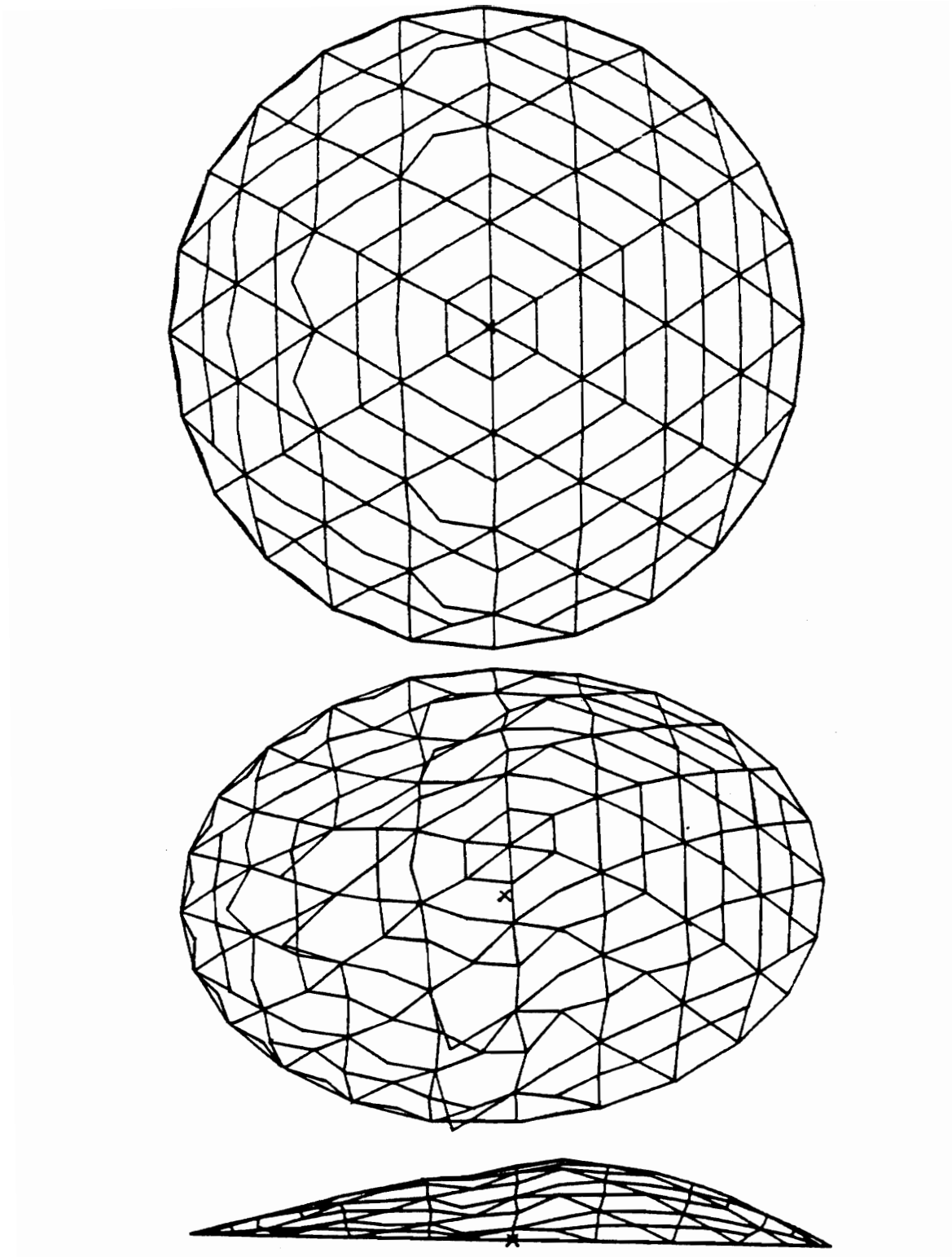


Figure 6.9 Buckling mode for the dome model without truss bracing: half snow

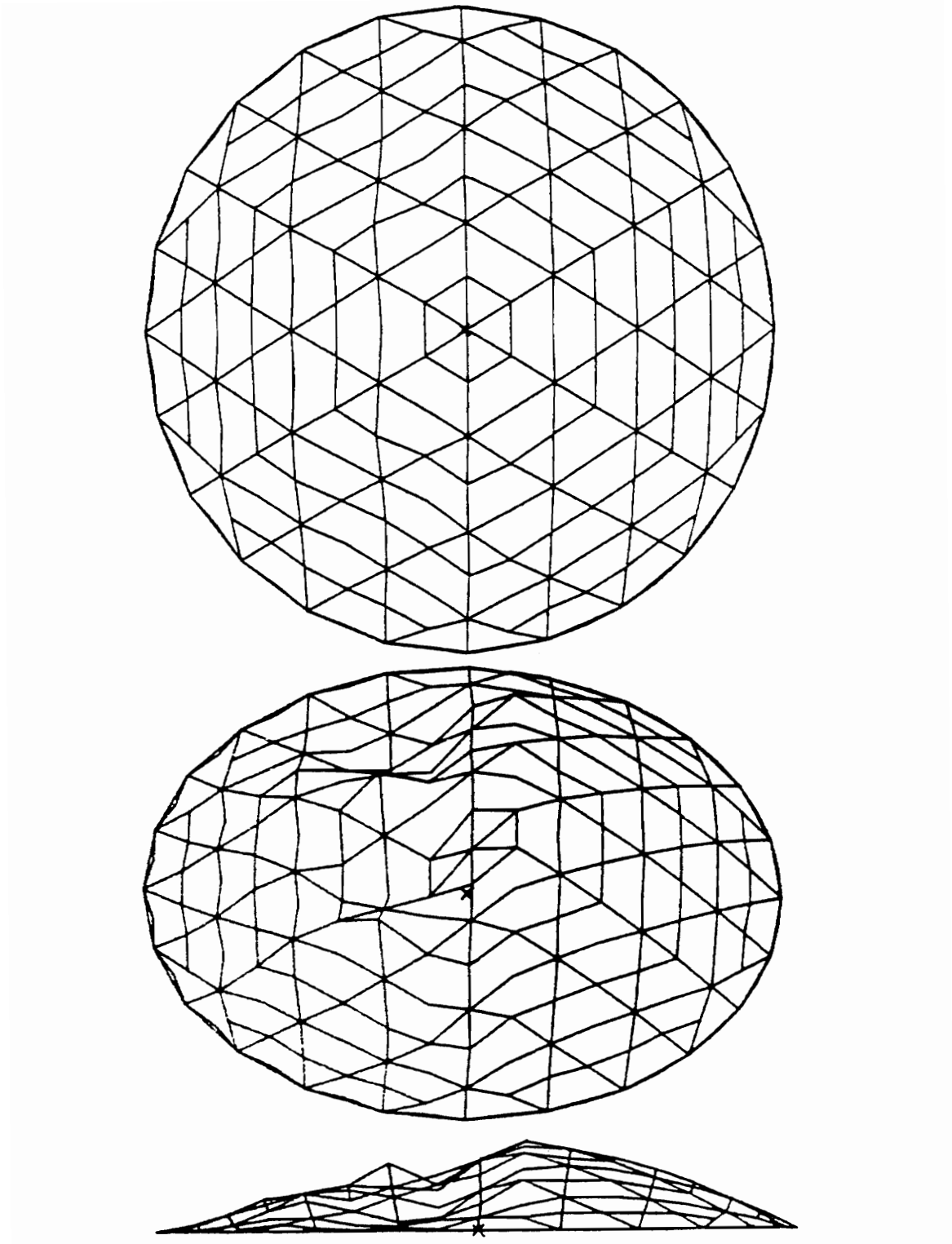


Figure 6.10 Buckling mode for the dome model with b/c elements: half snow

Chapter 7

Conclusions and Recommendations

7.1 Conclusions

The following conclusions can be drawn from the studies conducted in this research:

1. The convergence of solutions with the Riks method in ABAQUS is affected by the accuracy of constitutive modeling in the user subroutine UMAT, tolerance specifications for PTOL and MTOL, and the degree of mesh refinement. The convergence is more difficult to achieve for a highly refined mesh.

2. Accuracy in the formulation of the Jacobian matrix of the constitutive equations is found to be important for rapid convergence in the nonlinear analysis using Newton-Raphson or Riks option in ABAQUS. A potential cause of the convergence problem in the analysis of the dome done by Telang (1992) using nonlinear material law was the error in the expression for the Jacobian. The convergence problem was not encountered after the modification in the Jacobian. The error in the Jacobian was found to have no appreciable effect on the accuracy of the solution, since the stress-strain equations are coded correctly.

3. Various arrangements of shell elements can be tried to obtain equivalent nodal distribution of the uniformly distributed dead and live loads. However, assemblies with unrestrained nodes produce reaction forces at one or some of the nodes in the opposite direction to the expected direction of equivalent loads. This does not happen if the extra nodes are restrained.

4. Variations in the area of the tension ring has significant effect on the critical load capacity of the dome cap. However, variations in nonlinear material law produced by changing MC and SG values within a limited range and reduction in stiffness of the hinge (connector) elements does not have appreciable effect on the critical load capacity.

5. Saint-Venant's torsion solution can be successfully incorporated in the analysis with ABAQUS to model warping of the rectangular cross section of the beams. The shear modulus value should be modified for this purpose.

6. The modification in the value of shear modulus has considerable effect on the response of the dome cap model. However, the full dome model shows negligible reduction in the critical load capacity for shear modulus modification. This may be because the full dome model is much bigger and contains large number of elements so that the warping does not affect its load capacity significantly.

7. The beam/connector elements with nonlinear connectors can be successfully modeled and incorporated in the finite element program ABAQUS by the user subroutine UEL option.

8. The global stiffness matrix must be specified for the user elements in the subroutine UEL.

9. The truss bracing and the b/c models for the dome cap show close agreement in the response for full snow load, whereas b/c model is stiffer for the half snow load case. The nail deflections are higher in the half snow load case.

10. The response of the b/c model with nailed joints at truss bracing points for the full dome remains much softer than the truss bracing model, regardless of the magnitude of the nail stiffness.

11. The b/c model of the dome with 16 nailed joints on all beams shows softer response than the truss bracing model for full snow load but stiffer response for half snow load, both for the linear and the nonlinear material laws.

12. The maximum element stresses in the b/c model are much lower than in the truss bracing model for full snow load and are marginally higher for the half snow load in the analysis with linear material law (E = 1.8 E06 psi). However, for nonlinear material law, the stresses for b/c model are lower than in the truss bracing model for both the loading

conditions. The maximum stresses are found to exceed proportional limits in tension and compression in all the models and for both the loading conditions, however, by much greater margin for half snow load than full snow load. For b/c model, stresses are very close to the proportional limits in tension and compression for full snow load.

7.1 Recommendations

1. The material law modeled in this research is for small clear timber (Yellow Poplar). Experimental tests must be conducted on the glulam beams to formulate the stress-strain relationships for the same. This material law should then be coded in the subroutine UMAT.

2. The purlins can be modeled as beam elements, so that extra nodes can be created on them in refined mesh models. Better arrangement of shell elements are possible in this case for finding the equivalent nodal loads for the uniformly distributed dead and snow loads. Moreover, a comparison of nodal loads should be done when all DOF at a node are constrained rather than only the vertical DOF.

3. The effect of imperfections on the behavior of the dome must be studied. Material and geometric imperfections such as support settlements, fabrication and construction errors may have an effect on the ultimate load capacity of the glulam dome.

4. Experimental tests should be conducted to obtain the load-deflection curve for the nailed joint in glulam beams.

5. The response of the dome model in this study must be evaluated for various other load conditions like snow concentrations, special hanging loads and earthquake loads to determine the most critical load combination.

6. An experiment to test the ultimate load capacity for a scaled glulam model is necessary for the verification of analytical results; it is possible that the contribution of decking in the present models with truss bracing and b/c elements is overestimated.

7. The method of combined linear and nonlinear buckling prediction method should be used to study its applicability in the buckling analysis of the dome models in this study.

9. A selective mesh refinement study of the dome model with b/c elements should be performed to study the effect of reduction in the stiffness of hinge-connector elements on the response of the dome.

REFERENCES

1. ABAQUS, **General Purpose Finite Element System,** Hibbitt, Karlsson and Sorensen, Inc., 1080 Main Street, Pawtucket, RI 02906.

2. American Institute of Timber Construction (1985). **Timber Construction Manual,** Third Edition, John Wiley and Sons, Inc., New York, NY.

3. Bathe (1982). **Finite Element Procedures in Engineering analysis,** Prentice Hall, Englewood Cliffs, NJ.

4. Boresi, A.P., O.M. Sidebottom (1985). **Advanced Mechanics of Materials,** Third Edition, John Wiley and Sons, New York, NY.

5. Connors T.E. (1989). **Segmented Models for Stress-Strain Diagrams,** Wood Science and Technology, Vol. 23, pp.65-73.

6. Davalos J.F. (1989). **Geometrically Nonlinear Finite Element Analysis of a Glulam Timber Dome,** Ph.D. Dissertation, Virginia Polytechnic Institute and State University, Blacksburg, VA 24061.

7. Davalos J.F., J.R. Loferski, S.M. Holzer, and V. Yadama (1991). **Transverse Isotropy Modeling of 3-D Glulam Beams,** Journal of materials in Civil Engineering, ASCE, Vol. 3, No. 7, pp 125-139.

8. Dolan J.D. (1989). **The Dynamic Response of Timber Shear Walls,** Ph.D. Dissertation, University of British Columbia, Vancouver, Canada.

9. Dolan J.D., B. Madsen (1992). **Monotonic and Cyclic Nail Connection Test,** Canadian J. of Civil Engineering, Vol. 19, pp. 97-104.

10. Foschi R.O. (1974). **Load-Slip Characteristics of Nails,** Wood Science, Vol. 7, No. 1, pp.69-76.

11. Foschi R.O. (1977). **Analysis of Wood Diaphragms and Trusses. Part II - Truss-Plate Connections,** Canadian J. of Civil Engineering, Vol. 4, pp. 353-362.

12. Holzer, S.M., L.T. Watson (1981). **Stability Analysis of Lamella Domes,** Long Span Roof Structures, Proceedings of Symposium held at 1981 Annual Convention and Exhibit, St. Louis, Missouri.

13. Holzer S.M. (1985). **Computer Analysis of Structures, Matrix Structural Analysis Structured Programming,** Elsevier Science Publishing Co., Inc., New York.

14. Holzer S. M., J. R. Loferski (1987). **Background for research on glulam lattice domes,** Proceedings of the sixth Annual Structures Congress, ASCE Structural Division, Orlando, FL, pp. 305-318.

15. Holzer S. M., J. F. Davalos and C. Y. Huang (1990). **A review of Finite Element Stability Investigations of Spatial Wood Structures,** Bulletin of International Association for Shell and Spatial Structures, Vol. 31, No. 3, pp. 161-171.

16. Holzer S.M., C.H. Wu and J. Tissoui (1992). **Finite element Stability Analysis of a Glulam Dome,** International Journal of Space Structures, Vol. 7, No. 4, pp.353-361.

17. Hsu, T.T.C. (1984). **Torsion of Reinforced Concrete,** Van Nostrand Reinhold Company, Inc., New York 10020.

18. I-DEAS, **Engineering Analysis, Model Solution and Optimization,** Macneal-Schwnedler, Structural Dynamics Corporation, 2000 Eastman Drive, Milford, OH.

19. McLain, T.E. (1975). **Curvilinear Load-Slip Relations in Laterally Loaded Nailed Joints,** Ph.D. Dissertation, Colorado State University, Fort Collins, Colorado.

20. Meek J. L., S. Loganathan (1989). **Geometrically Non-linear Behaviour of Space Frame Structures,** Computers and Structures, Vol. 31, No. 1, pp. 35-45.

21. Mohammad, H. (1990). **Modeling the roof Deck and Determining its Effect on the Stability of a Glulam Timber Dome,** M.E. Project, Virginia Polytechnic Institute and State University, Blacksburg, VA 24061.

22. Popov E.P. (1968). **Introduction to Mechanics of Solids,** Prentice Hall, NJ.

23. TableCurve (1992). **Jandel Scientific TableCurve,** Version 3.10, 1992 AISN Software.

24. Telang, N.M. (1992). **Stability analysis of a Glulam Dome with Nonlinear Material Law,** M.S. Thesis, Virginia Polytechnic Institute and State University, Blacksburg, VA 24061.

25. Timoshenko, S.P., J.N. Goodier (1970). **Theory of Elasticity,** Third Edition, Mc-Graw Hill Book Company, New York, NY.

26. Tissoui, J. (1991). **Stability Analysis of the Church of the Nazarene Varax Dome,** M.S. Thesis, Virginia Polytechnic Institute and State University, Blacksburg, VA

27. Tsang, M.T. (1992). **3-D Finite Element Beam/Connector Model for a Glulam Dome Cap,** M.S. Thesis, Virginia Polytechnic Institute and State University, Blacksburg, VA 24061.

28. U.S. Forest Product Laboratory (1990). **Wood Engineering Handbook,** Second Edition, Prentice Hall, Englewood Cliffs, NJ.

29. Wilkinson T.L. (1971). **Theoretical Lateral Resistance of Nailed Joints,** Journal of Structural Division, ASCE, Vol. 97 (ST5), pp. 1381-1398.

30. Wu, C.H. (1991). **Modeling and Stability Investigation of a Glulam Dome,** M.S. Thesis, Virginia Polytechnic Institute and State University, Blacksburg, VA 24061.

Appendix A

The purpose of this appendix is to present a comprehensive review of the geometry of the Crafts Pavilion Triax Dome in Raleigh, North Carolina, which is analyzed in this study, and to discuss the orientations of the beam elements in space. Also, the rotation matrix used in transforming the stiffness matrix of the connector element in the user-supplied subroutine from local to global coordinates is presented.

A.1 Dome Geometry

The Crafts Pavilion Triax Dome consists of part of a sphere (Figure A.1) with a radius of 1600 inches (133.33 feet). The base of the dome lies 1387.66 inches (115.64 feet) above the center of the sphere; thus the height of the dome is 212.34 inches (17.70 feet).

R = radius of the dome = 1600 inches.
h = height of the dome = 1600 - 1387.66 = 212.34 inches.

The span of the dome can be calculated as follows:

$$(R-h)^2 + (s/2)^2 = R^2 \qquad (A.1)$$

Thus

$$(1387.66)^2 + (s/2)^2 = (1600)^2$$

and

$$s = 1593 \text{ inches } (132.75 \text{ feet})$$

In the finite element model of the dome created with I-DEAS and analyzed using ABAQUS, the origin of the frame of reference is at the base of the dome as shown in Figure A.1, thus the center of the sphere has global coordinates of 0.0, 0.0 and

-1387.66 inches denoted by X_0, Y_0 and Z_0, respectively.

A.2 Beam orientation

Since the members of the dome (beams and purlins) lie on great circles of the sphere, all the nodes in the finite element model of the dome lie on the surface of the sphere. Thus, all the main beams in the dome are oriented such that they lie in planes passing through the center of the sphere. The eve purlins, also called the edge (or base) beams, lie in the plane defined by the tension ring.

In the ABAQUS input file, the * BEAM SECTION option is used for specifying the beam cross section. For the beams in space, the directions of the beam cross section axes must be defined in this input data by specifying the direction cosines of a unit vector in the direction of the first cross section axis (n_1) of the beam. Axis n_1 is part of the local right-handed (n_1, n_2, t) system in ABAQUS (Figure A.2), which are the local 1, 2 and 3 axes of the beam.

Note that the beam cross-section dimensions a, b, specified in this order in the *BEAM SECTION option, are in the n_1 and n_2 directions respectively (Figure A.2). For example, for the vertical main beams I, the n_1 axis lies perpendicular to the vertical planes passing through the center of the sphere (discussed below in detail) and thus the n_2 axis lies in vertical planes (Figure A.3a). Therefore, the depth of 11.0" must be assigned to the 'b' dimension of the beam, i.e., a = 6.75", b = 11.0". The inclined main beams I (base beams of the dome cap) have the local axes orientation as shown in Figure A.3b. In this case also a = 6.75", b = 11.0". The above is true also for the main beams II, for which a = 5.0", b = 11.0". For the edge beams of the dome, however, the n_1 axis is vertical, so that the depth of 12.25" is assigned to the 'a' dimension of the beam, i.e. a = 12.25", b = 3.0" (Figure A.4).

A FORTRAN program DIRCOS, written for calculating direction cosines of the unit vectors which vary from beam to beam, is given at the end of this section. The local n_1 axis of the main beams is defined as discussed below. Since a typical main

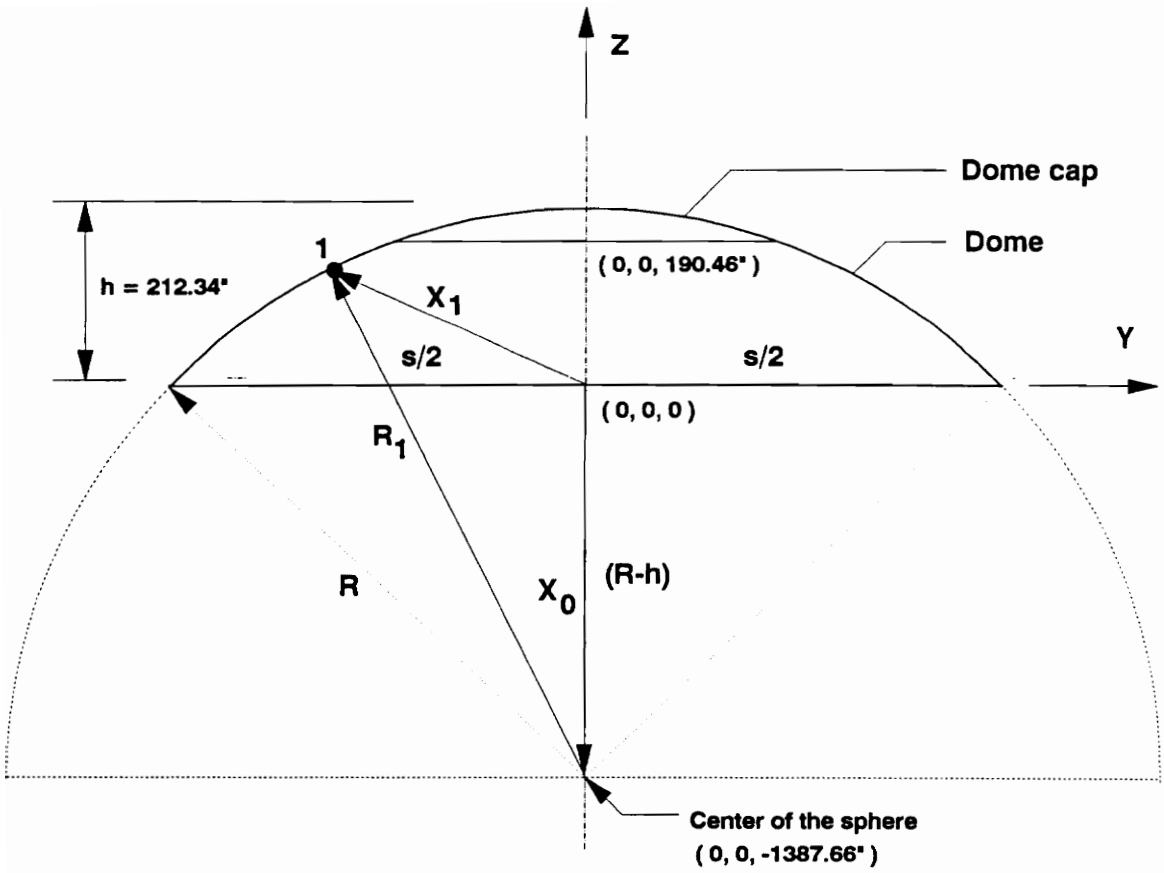


Figure A.1 Geometry of the dome

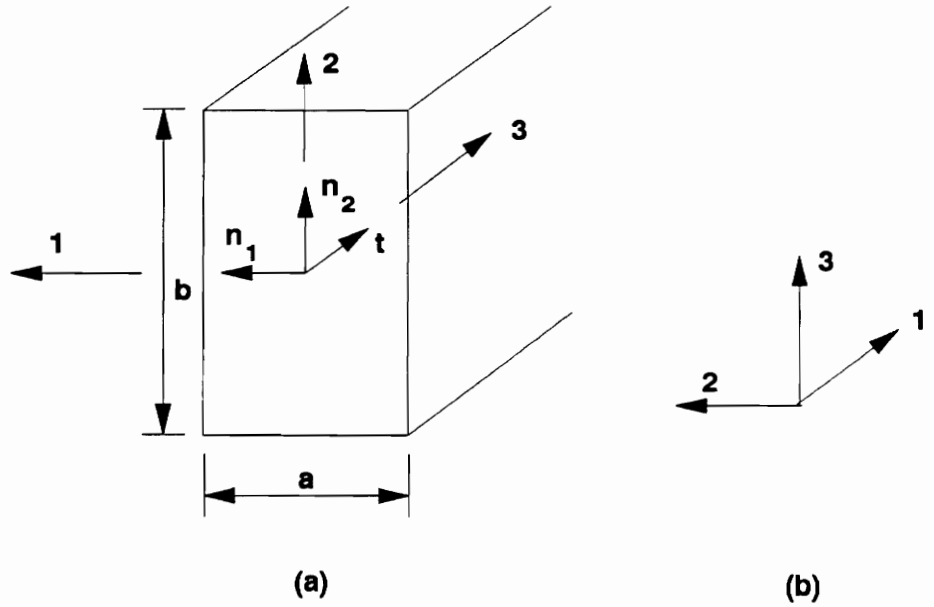


Figure A.2 Convention for local axes: (a) beam in ABAQUS (b) connector

beam lies on a plane passing through the center of the sphere, the n_1 axis (local 1) is perpendicular to this plane. A vector $\mathbf{N_1}$ in n_1 (local 1) direction can be computed as follows (Figures A.3a and b):

$$\mathbf{N_1} = \mathbf{R_1} \times \mathbf{R_2} \tag{A.2}$$

where $\mathbf{R_1}$ and $\mathbf{R_2}$ are the radial vectors (Figure A.1) or the joint coordinate vectors (Holzer, 1985, p. 396) of node 1 and node 2 with respect to the spherical center (X_0, Y_0, Z_0). If the nodal coordinates of nodes 1 and 2 are (X(1),Y(1),Z(1)) and (X(2),Y(2),Z(2)) respectively, $\mathbf{R_1}$ and $\mathbf{R_2}$ are given by (Figure A.1)

$$\begin{aligned} \mathbf{R_1} &= = \mathbf{X_1 - X_0} = \begin{pmatrix} R_1^1 & R_1^2 & R_1^3 \end{pmatrix} \\ \mathbf{R_2} &= = \mathbf{X_2 - X_0} = \begin{pmatrix} R_2^1 & R_2^2 & R_2^3 \end{pmatrix} \end{aligned} \tag{A.3}$$

where

$$\begin{aligned} \mathbf{X_0} &= (X_0, Y_0, Z_0) = (0, 0, -1387.66") \\ \mathbf{X_1} &= (X(1), Y(1), Z(1)) \\ \mathbf{X_2} &= (X(2), Y(2), Z(2)) \end{aligned}$$

Thus

$$\begin{aligned} R_1^1 &= X(1) - X_0 = X(1) & R_2^1 &= X(2) - X_0 = X(2) \\ R_1^2 &= Y(1) - Y_0 = Y(1) & R_2^2 &= Y(2) - Y_0 = Y(2) \\ R_1^3 &= Z(1) - Z_0 = Z(1) + 1387.66 & R_2^3 &= Z(2) - Z_0 = Z(2) + 1387.66 \end{aligned} \tag{A.4}$$

The vector $\mathbf{N_1}$ defined by Eq.(A.2) is obtained as (Holzer, 1985, Appendix C)

$$\mathbf{N_1} = \mathbf{R_1} \times \mathbf{R_2} = \begin{bmatrix} I_1 & I_2 & I_3 \\ R_1^1 & R_1^2 & R_1^3 \\ R_2^1 & R_2^2 & R_2^3 \end{bmatrix} \tag{A.5}$$

Thus

$$\begin{aligned} \mathbf{N_1} = \mathbf{I_1} &[R_1^2 R_2^3 - R_1^3 R_2^2] \\ &- \mathbf{I_2} [R_1^1 R_2^3 - R_1^3 R_2^1] \end{aligned}$$

$$+ \mathbf{I_3} \left[R_1^1 \, R_2^2 - R_1^2 \, R_2^1 \right]$$

$$= \left(N_1^1 \quad N_1^2 \quad N_1^3 \right) \tag{A.6}$$

where

$$\begin{aligned} N_1^1 &= R_1^2 \, R_2^3 - R_1^3 \, R_2^2 \\ N_1^2 &= R_1^1 \, R_2^3 - R_1^3 \, R_2^1 \\ N_1^3 &= R_1^1 \, R_2^2 - R_1^2 \, R_2^1 \end{aligned} \tag{A.7}$$

I_1, I_2 and I_3 are unit vectors on the global axes, also called the basis vectors.

The direction cosines of n_1 axis (local 1) are thus given by normalizing the $\mathbf{N_1}$ vector as follows:

$$\mathbf{n_1} = \frac{N_1}{|N_1|} = \frac{\left(N_1^1 \quad N_1^2 \quad N_1^3 \right)}{\sqrt{(N_1^1)^2 + (N_1^2)^2 + (N_1^3)^2}} = \left(n_1^1 \quad n_1^2 \quad n_1^3 \right) \tag{A.8}$$

For the edge beams of the dome, which lie on in the horizontal plane defined by the tension ring, the n_1 axis is perpendicular to this plane. Thus the $\mathbf{N_1}$ vector is parallel to the global 3 axis. The direction cosines of the unit vectors in the n_1 direction of the edge beams, therefore, are (0 0 ±1). This is obtained in the FORTRAN program, given at the end of this appendix, by modifying the above procedure of finding vector $\mathbf{N_1}$ for the main beams as follows. The position vectors of the beam nodes are found with respect to the dome center in the same horizontal plane as the edge beams (Figure A.4), instead of the center of the sphere as in the case for the main beams (Figure A.3a and b). Thus

$$\mathbf{N_1} = \mathbf{X_1} \times \mathbf{X_2} \tag{A.9}$$

The center of dome model has coordinates, $X_0 = 0.0$, $Y_0 = 0.0$, $Z_0 = 0.0$. Therefore

$$X_n^1 = X(n) - X_0 = X(n)$$

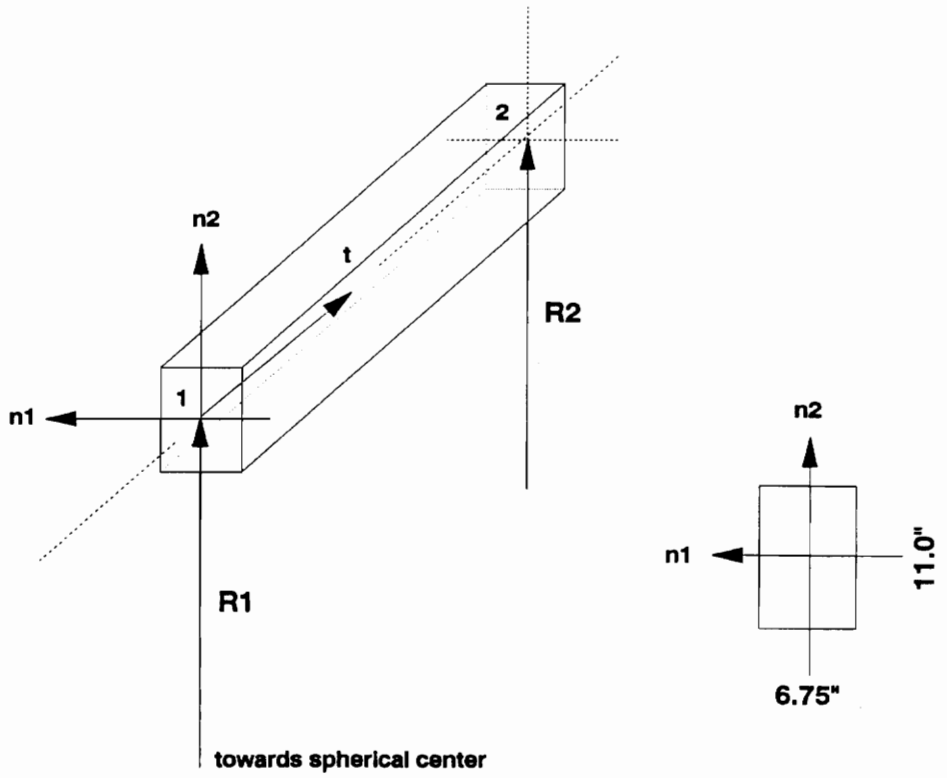


Figure A.3a The local axes orientation for the vertical main beams

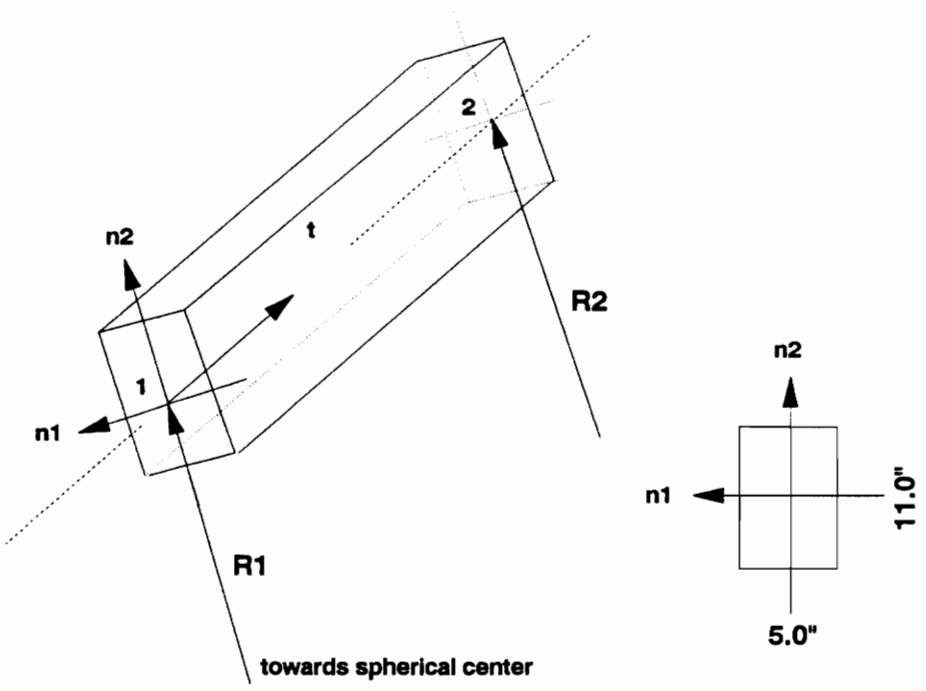


Figure A.3b The local axes orientation for the inclined main beams

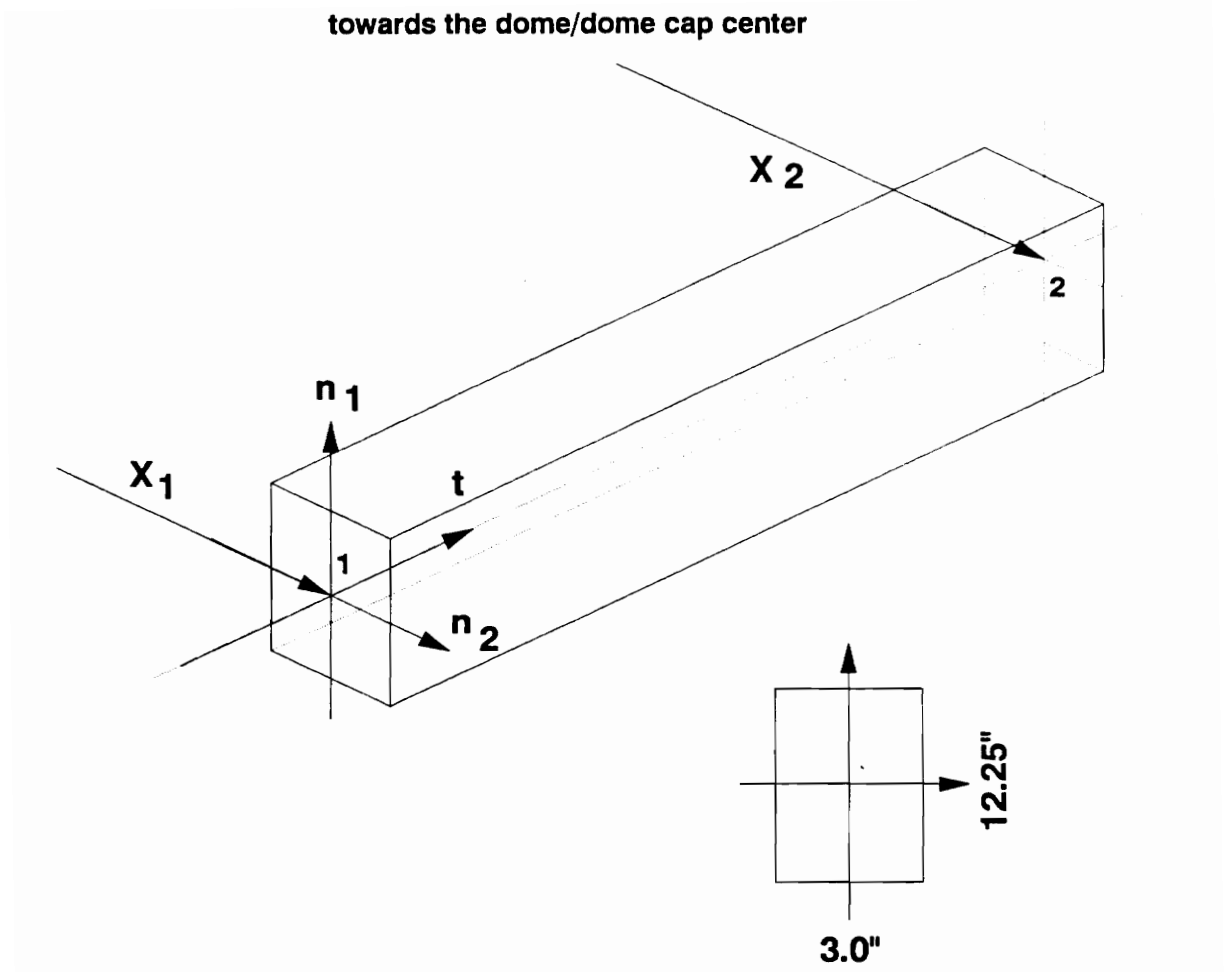


Figure A.4 The local axes orientation for the edge (base) beams

$$X_n^2 = Y(n) - Y_0 = Y(n)$$
$$X_n^3 = Z(n) - Z_0 = Z(n) \qquad (A.10)$$

The remaining procedure remains the same as given in Eqs.(A.2) through (A.8). Comparing Eqs.(A.4) and (A.10), the third component is different for the edge beams, and is changed in the program DIRCOS to find the direction cosines for the edge beams. If the base beams of the dome cap model have vertical cross sections similar to the edge beams of the full dome (refer to Chapter 2), the reference point is the dome cap center, i.e., $X_0 = 0.0$, $Y_0 = 0.0$, $Z_0 = 190.46$ and

$$X_n^1 = X(n) - X_0 = X(n)$$
$$X_n^2 = Y(n) - Y_0 = Y(n) \qquad (A.11)$$
$$X_n^3 = Z(n) - Z_0 = Z(n) - 190.46$$

The FORTRAN program DIRCOS to calculate the direction cosines for the main beams I and the edge beams, and to create the corresponding cards in the input file is given below.

```
CC   PROGRAM TO COMPUTE THE DIRECTION COSINES OF THE BEAM ELEMENTS
CC   AND TO WRITE THE SECTION PROPERTIES AND ELEMENT SETS IN THE
CC   PROPER FORMAT FOR ABAQUS INPUT FILE
CC   THE PROGRAM REQUIRES DATA FILES AS NAMED IN THE COMMENT
CC   STATEMENTS
CC   THE OUTPUT IS GIVEN IN 1)EL AND 2)SEC (OUT) FILES
CC
     REAL R1(500),R2(500),R3(500),R1C(500),R2C(500),R3C(500),
    1    R1CC(500),R2CC(500),R3CC(500),X3(500)
     OPEN(UNIT=55,STATUS='OLD')
     OPEN(UNIT=60,STATUS='OLD')
     OPEN(UNIT=70,STATUS='OLD')
     OPEN(UNIT=88,STATUS='UNKNOWN')
     OPEN(UNIT=98,STATUS='UNKNOWN')
CC
CC   READ NODES FROM, SNODE DAT A
     DO 10 I=1,19
       READ (55,*) N, X, Y, Z
        R1(I) = X
        R2(I) = Y
        R3(I) = Z+1387.66
```

```
CC
CC   X3(I) = Z FOR VERTICAL EDGE BEAMS IN FULL DOME.
CC   X3(I)= Z+1387.66 FOR INCLINED BASE BEAMS IN DOME CAP.
CC   X3(I) = Z-190.46 FOR VERTICAL BASE BEAMS IN DOME CAP.
CC
        X3(I) = Z+1387.66
10    CONTINUE
CC
CC   READ MAIN BEAMS-I    6.75X11, SBEM1 DAT A
     WRITE(88,350)
     WRITE(98,350)
     DO 20 J=1,12
       READ (60,*) NE, N1, N2
       R1C(NE) =  R2(N1) * R3(N2) - R3(N1) * R2(N2)
       R2C(NE) = -(R1(N1) * R3(N2) - R3(N1) * R1(N2))
       R3C(NE) =   R1(N1) * R2(N2) - R2(N1) * R1(N2)
       XNORM = (R1C(NE)**2+R2C(NE)**2+R3C(NE)**2) ** 0.5
       R1CC(NE) = R1C(NE) / XNORM
       R2CC(NE) = R2C(NE) / XNORM
       R3CC(NE) = R3C(NE) / XNORM
       WRITE (88,200) NE
       WRITE (88,220) NE, N1, N2
       WRITE (98,230) NE
       WRITE (98,240)
       WRITE (98,300) R1CC(NE),R2CC(NE),R3CC(NE)
       WRITE (98,310)
       WRITE (98,320)
20    CONTINUE
CC SIMILAR CARDS AS ABOVE FOR THE MAIN BEAMS-II
CC
CC   READ EDGE BEAMS 12.25X3.0, SEBEM DAT A
     WRITE(88,370)
     WRITE(98,370)
     DO 40 K=1,12
      READ (70,*) NE, N1, N2
      R1C(NE) = R2(N1) * X3(N2) - X3(N1) * R2(N2)
      R2C(NE) = -(R1(N1) * X3(N2) - X3(N1) * R1(N2))
      R3C(NE) = R1(N1) * R2(N2) - R2(N1) * R1(N2)
      XNORM = (R1C(NE)**2+R2C(NE)**2+R3C(NE)**2) ** 0.5
      R1CC(NE) = R1C(NE) / XNORM
      R2CC(NE) = R2C(NE) / XNORM
      R3CC(NE) = R2C(NE) / XNORM
      WRITE (88,200) NE
      WRITE (88,220) NE, N1, N2
      WRITE (98,230) NE
      WRITE (98,250)
```

```
      WRITE (98,300) R1CC(NE),R2CC(NE),R3CC(NE)
      WRITE (98,310)
      WRITE (98,320)
40    CONTINUE
CC    SIMILAR CARDS AS ABOVE FOR THE CORRESPONDING HINGE ELEMENTS
200   FORMAT (T1,'*ELEMENT,TYPE=B33,ELSET=E',T26,I4)
220   FORMAT (1X,I4,',',I4,',',I4)
230   FORMAT (T1,'*BEAM SECTION,SECTION=RECT,MATERIAL=UWOOD,ELSET=E',
     1              T50,I4)
235   FORMAT (T1,'*BEAM SECTION,SECTION=RECT,MATERIAL=UWOOD,ELSET=E',
     1              T50, I4)
240   FORMAT (2X,'6.75, 11.0')
250   FORMAT (2X,'12.25, 3.0')
300   FORMAT (1X,F8.4,',',F8.4,',',F8.4)
310   FORMAT ('*TRANSVERSE SHEAR STIFFNESS')
320   FORMAT (2X,'9972128.26, 9972128.26')
350   FORMAT ('**',50('-'),'MAIN BEAMS 1')
370   FORMAT ('**',50('-'),'EDGE BEAMS')
      END
```

A.3 Rotation Matrix (Λ)

The local stiffness matrix of the user elements, which model the nails in the beam-decking connection, is transformed into the global stiffness matrix. It is supplied in the *MATRIX data card (Tsang, 1992), and is also used to define the stiffness matrix array AMATRX(I,J) in the user subroutine UEL (see Appendix D). The transformation into global is achieved by

$$K = \Lambda^{-1} k \Lambda \tag{A.12}$$

where

K = Global stiffness matrix

k = Local stiffness matrix

and

$$\Lambda = \begin{bmatrix} \lambda & 0 & 0 & 0 \\ 0 & \lambda & 0 & 0 \\ 0 & 0 & \lambda & 0 \\ 0 & 0 & 0 & \lambda \end{bmatrix} \tag{A.13}$$

where

λ = Rotation matrix for the connector element

The rotation matrix for the connector elements in the dome is calculated as follows. The local 1,2, and 3 axes of the connector element are as shown in Figure 5.10. Note that these are oriented differently than those for the beam (B33) element in ABAQUS (Figure A.2). Since the global stiffness matrices of the beam and the connector elements are added in the analysis with ABAQUS, the different orientations of the local axes for the beam and the connector elements are allowable. The rotation matrix can be partitioned as (Holzer, 1985, Appendix C),

$$\lambda = \begin{bmatrix} \mathbf{i}_1 \\ \mathbf{i}_2 \\ \mathbf{i}_3 \end{bmatrix} = \begin{bmatrix} \lambda_{11} & \lambda_{12} & \lambda_{13} \\ \lambda_{21} & \lambda_{22} & \lambda_{23} \\ \lambda_{31} & \lambda_{32} & \lambda_{33} \end{bmatrix} \tag{A.14}$$

where $\mathbf{i}_1$, $\mathbf{i}_2$, $\mathbf{i}_3$ are unit vectors in the direction of local 1, 2, 3 axes of the connector element respectively (Figure A.2), defined relative to the global coordinate system. The unit vector $\mathbf{i}_2$ for the connector is in the direction of the n_1 axis of the beam element, and is equal to vector $\mathbf{n}_1$ as calculated in the previous section. From Eq.(A.8) we obtain

$$\begin{aligned} \mathbf{i}_2 &= (\lambda_{21} \ \lambda_{22} \ \lambda_{23}) \\ &= \left(n_1^1 \ \ n_1^2 \ \ n_1^3\right) \end{aligned} \tag{A.15}$$

The vector **T** in the direction of t axis for the beam element is given by

$$\mathbf{T} = \mathbf{R}_2 - \mathbf{R}_1 \tag{A.16}$$

Thus

$$\begin{aligned} \mathbf{T} &= [\,(X(2)-X(1)) \ \ (Y(2)-Y(1)) \ \ (Z(2)-Z(1))\,] \\ &= (T^1 \ T^2 \ T^3) \end{aligned} \tag{A.17}$$

The unit vector $\mathbf{i}_1$ for the connector is in the t direction of the beam element, and is given by normalizing the vector **T** as follows:

$$\mathbf{i_1} = \frac{\mathbf{T}}{|\mathbf{T}|} = \frac{[\,(X(2)-X(1))\;\;(Y(2)-Y(1))\;\;(Z(2)-Z(1))\,]}{\sqrt{(X(2)-X(1))^2+(Y(2)-Y(1))^2+(Z(2)-Z(1))^2}}$$

$$= (\lambda_{11}\;\lambda_{12}\;\lambda_{13}) \qquad \text{(A.18)}$$

The unit vector $\mathbf{i_3}$ for the connector is in the n_2 direction of the beam element, and can be calculated in either of the following two ways. Using the right-handed property of the local coordinate system, the $\mathbf{N_2}$ vector in the n_2 direction is given by

$$\mathbf{N_2} = \mathbf{T} \times \mathbf{N_1} = \begin{bmatrix} I_1 & I_2 & I_3 \\ T^1 & T^2 & T^3 \\ N_1^1 & N_1^2 & N_1^3 \end{bmatrix} = \begin{pmatrix} N_2^1 & N_2^2 & N_2^3 \end{pmatrix} \qquad \text{(A.19)}$$

The $\mathbf{i_3}$ vector is obtained by normalizing $\mathbf{N_2}$ in Eq.(A.19) as follows:

$$\mathbf{i_3} = \frac{\mathbf{N_2}}{|\mathbf{N_2}|} = \frac{\begin{pmatrix} N_2^1 & N_2^2 & N_2^3 \end{pmatrix}}{\sqrt{(N_2^1)^2+(N_2^2)^2+(N_2^3)^2}}$$

$$= (\lambda_{31}\;\lambda_{32}\;\lambda_{33}) \qquad \text{(A.20)}$$

Alternatively, it can be found by

$$\mathbf{i_3} = \mathbf{i_1} \times \mathbf{i_2} \qquad \text{(A.21)}$$

$$= \begin{bmatrix} I_1 & I_2 & I_3 \\ \lambda_{11} & \lambda_{12} & \lambda_{13} \\ \lambda_{21} & \lambda_{22} & \lambda_{23} \end{bmatrix}$$

$$= \mathbf{I_1}\,(\lambda_{12}\lambda_{23} - \lambda_{13}\lambda_{22}) - \mathbf{I_2}\,(\lambda_{11}\lambda_{23} - \lambda_{13}\lambda_{21}) + \mathbf{I_3}\,(\lambda_{11}\lambda_{22} - \lambda_{12}\lambda_{21})$$

$$= (\lambda_{31}\;\lambda_{32}\;\lambda_{33}) \qquad \text{(A.22)}$$

where

$$\lambda_{31} = \lambda_{12}\lambda_{23} - \lambda_{13}\lambda_{22}$$

$$\lambda_{32} = \lambda_{13}\lambda_{21} - \lambda_{11}\lambda_{23} \qquad \text{(A.23)}$$
$$\lambda_{33} = \lambda_{11}\lambda_{22} - \lambda_{12}\lambda_{21}$$

This completes the definition of the rotation matrix. It is used to calculate the global stiffness matrix for the connector elements, which model the beam/decking connections, in the user subroutine UEL.

Appendix B

The ABAQUS input files for the test cases on torsion of steel beams with varying cross sections (Figures 4.9 and 4.10) are given below.

A.1 Circular Beam

```
*HEADING
TEST CASE # 2 : COMPOSITE CIRCULAR STEEL CANTILEVER WITH B33'S
**  EQUIVALENT VALUE OF'G'= 1.0*G USED
*NODE,NSET=NALL
1,0.,0.
2,10.,0.
3,20.,0.
*ELEMENT,TYPE=B33,ELSET=BEAM1
1,1,2
*ELEMENT,TYPE=B33,ELSET=BEAM2
2,2,3
*BEAM SECTION,SECTION=CIRC,ELSET=BEAM1,MATERIAL=USTEEL1
0.85344
*TRANSVERSE SHEAR STIFFNESS
10000.,10000.
*BEAM SECTION,SECTION=CIRC,ELSET=BEAM2,MATERIAL=USTEEL2
0.570732
*TRANSVERSE SHEAR STIFFNESS
10000.,10000.
*MATERIAL,NAME=USTEEL1
*USER MATERIAL,CONSTANT=3
**E,NU,JSV/JN
2.90E+07,0.1,1.00
*MATERIAL,NAME=USTEEL2
*USER MATERIAL,CONSTANT=3
**E,NU,JSV/JN
2.90E+07,0.1,1.00
*BOUNDARY
1,ENCASTRE
*STEP
*STATIC,PTOL=0.1,MTOL=.1
*CLOAD
2,4,10000.
3,4,10000.
*NODE PRINT,NSET=NALL,SUMMARY=NO
U
*NODE PRINT,NSET=NALL,SUMMARY=NO
RF
```

```
*NODE PRINT,NSET=NALL,SUMMARY=NO
CF
*EL PRINT,SUMMARY=NO
S,E
*END STEP
*USER SUBROUTINE
**SUBROUTINE TO TEST USER SUBROUTINE UMAT
C
      SUBROUTINE UMAT(STRESS,STATEV,DDSDDE,SSE,SPD,SCD,
     1 RPL,DDSDDT,DRPLDE,DRPLDT,
     2 STRAN,DSTRAN,TIME,DTIME,TEMP,DTEMP,PREDEF,DPRED,CMNAME,
     3 NDI,NSHR,NTENS,NSTATV,PROPS,NPROPS,COORDS,DROT)
C
      IMPLICIT REAL*8(A-H,O-Z)
C
       CHARACTER*8 USTEEL1
C
      DIMENSION STRESS(NTENS),STATEV(NSTATV),
     1 DDSDDE(NTENS,NTENS),
     2 DDSDDT(NTENS),DRPLDE(NTENS),
     3 STRAN(NTENS),DSTRAN(NTENS),PREDEF(1),DPRED(1),
     4 PROPS(NPROPS),COORDS(3),DROT(3,3)
C     DIMENSION DSTRES(2)
C
      DO 20 I=1,NTENS
        DO 10 J=1,NTENS
          DDSDDE(I,J)=0.0
10      CONTINUE
20    CONTINUE
C
C       *LONGITUDINAL STRESS*
C
      TS=0.0
      TS=STRAN(1) + DSTRAN(1)
C
C       *TENSION ZONE*
C
       DDSDDE(1,1)=PROPS(1)
       STRESS(1)=DDSDDE(1,1)*TS
C
C       *TORSIONAL SHEAR STRESS*
C
      TT=0.0
      TT=STRAN(2) + DSTRAN(2)
C
       DDSDDE(2,2)=PROPS(3)*DDSDDE(1,1)/(2.*(1+PROPS(2)))
       STRESS(2)=DDSDDE(2,2)*TT
C
     RETURN
     END
```

```
*USER SUBROUTINE
C
      SUBROUTINE UMAT(STRESS,STATEV,DDSDDE,SSE,SPD,SCD,
     1 RPL,DDSDDT,DRPLDE,DRPLDT,
     2 STRAN,DSTRAN,TIME,DTIME,TEMP,DTEMP,PREDEF,DPRED,CMNAME,
     3 NDI,NSHR,NTENS,NSTATV,PROPS,NPROPS,COORDS,DROT)
C
      IMPLICIT REAL*8(A-H,O-Z)
C
      CHARACTER*8 USTEEL2
C
      DIMENSION STRESS(NTENS),STATEV(NSTATV),
     1 DDSDDE(NTENS,NTENS),
     2 DDSDDT(NTENS),DRPLDE(NTENS),
     3 STRAN(NTENS),DSTRAN(NTENS),PREDEF(1),DPRED(1),
     4 PROPS(NPROPS),COORDS(3),DROT(3,3)
C     DIMENSION DSTRES(2)
C
      DO 20 I=1,NTENS
        DO 10 J=1,NTENS
          DDSDDE(I,J)=0.0
10      CONTINUE
20    CONTINUE
C
C       *LONGITUDINAL STRESS*
C
      TS=0.0
      TS=STRAN(1) + DSTRAN(1)
C
C       *TENSION ZONE*
C
      DDSDDE(1,1)=PROPS(1)
      STRESS(1)=DDSDDE(1,1)*TS
C
C       *TORSIONAL SHEAR STRESS*
C
     TT=0.0
     TT=STRAN(2) + DSTRAN(2)
C
      DDSDDE(2,2)=PROPS(3)*DDSDDE(1,1)/(2.*(1+PROPS(2)))
      STRESS(2)=DDSDDE(2,2)*TT
C
    RETURN
    END
```

A.2 Rectangular Beam

```
*HEADING
TEST CASE # 2 : COMPOSITE RECTANGULAR STEEL CANTILEVER WITH B33'S
**----------EQUIVALENT VALUE OF'G'= 0.5496*G USED FOR BEAM1
```

```
**----------EQUIVALENT VALUE OF'G'= 0.8436*G USED FOR BEAM2
*NODE,NSET=NALL
1,0.,0.
2,10.,0.
3,20.,0.
*ELEMENT,TYPE=B33,ELSET=BEAM1
1,1,2
*ELEMENT,TYPE=B33,ELSET=BEAM2
2,2,3
*BEAM SECTION,SECTION=RECT,ELSET=BEAM1,MATERIAL=USTEEL1
1.,2.
*TRANSVERSE SHEAR STIFFNESS
10000.,10000.
*BEAM SECTION,SECTION=RECT,ELSET=BEAM2,MATERIAL=USTEEL2
1.,1.
*TRANSVERSE SHEAR STIFFNESS
10000.,10000.
*MATERIAL,NAME=USTEEL1
*USER MATERIAL,CONSTANT=3
**E,NU,JSV/JN
2.90E+07,0.1,0.5496
*MATERIAL,NAME=USTEEL2
*USER MATERIAL,CONSTANT=3
**E,NU,JSV/JN
2.90E+07,0.1,0.8436
*BOUNDARY
1,ENCASTRE
*STEP
*STATIC,PTOL=0.1,MTOL=.1
*CLOAD
2,4,10000.
3,4,10000.
*NODE PRINT,NSET=NALL,SUMMARY=NO
U
*NODE PRINT,NSET=NALL,SUMMARY=NO
RF
*NODE PRINT,NSET=NALL,SUMMARY=NO
CF
*EL PRINT,SUMMARY=NO
3,11,15,23
S,E
*END STEP
```

The same user subroutines as used in case of circular beams follow the *END STEP card above.

Appendix C

The input files for the test case (section 5.4.2) to verify the use of global stiffness matrix in the user element option in ABAQUS are given below.

C.1 Model with C1D2 truss elements

```
*HEADING
*NODE
1,0.,2.
2,1.5,2.
3,0.,0.
*NSET,NSET=SUPP
1,3
*ELEMENT,TYPE=C1D2,ELSET=TRUSS
1,1,2
2,1,3
3,2,3
*SOLID SECTION,MATERIAL=STEEL
1.
*MATERIAL,NAME=STEEL
*ELASTIC
1.8E3
*BOUNDARY
1,1,2
3,1
*STEP,LINEAR
*STATIC
*CLOAD
2,2,-8.0
*EL PRINT,ELSET=TRUSS,SUMMARY=NO
S,E
*NODE PRINT,SUMMARY=NO
U
*NODE PRINT,SUMMARY=NO
CF
*NODE PRINT,SUMMARY=NO
RF
*END STEP
```

C.2 Model with user elements (local stiffness matrices)

```
*HEADING
```

```
*NODE
1,0.,2.
2,1.5,2.
3,0.,0.
*NSET,NSET=SUPP
1,3
**ELEMENT,TYPE=C1D2,ELSET=TRUSS
**1,1,2
**2,1,3
**3,2,3
*SOLID SECTION,MATERIAL=STEEL
1.
*MATERIAL,NAME=STEEL
*ELASTIC
1.8E3
*USER ELEMENT,NODES=2,TYPE=U1,LINEAR
1,2
*ELEMENT,TYPE=U1,ELSET=E1
1,1,2
*MATRIX,TYPE=STIFFNESS
1200.
0.,0.
-1200.,0.,1200.
0.,0.,0.,0.
*UEL PROPERTY,ELSET=E1
*USER ELEMENT,NODES=2,TYPE=U2,LINEAR
1,2
*ELEMENT,TYPE=U2,ELSET=E2
2,1,3
*MATRIX,TYPE=STIFFNESS
900.
0.,0.
-900.,0.,900.
0.,0.,0.,0.
*UEL PROPERTY,ELSET=E2
*USER ELEMENT,NODES=2,TYPE=U3,LINEAR
1,2
*ELEMENT,TYPE=U3,ELSET=E3
3,2,3
*MATRIX,TYPE=STIFFNESS
720.
0.,0.
-720.,0.,720.
0.,0.,0.,0.
*UEL PROPERTY,ELSET=E3
*ELSET,ELSET=TRUSS
1,2,3
*BOUNDARY
1,1,2
3,1
*STEP,LINEAR
```

```
*STATIC
*CLOAD
2,2,-8.0
*EL PRINT,ELSET=TRUSS,SUMMARY=NO
S,E
*NODE PRINT,SUMMARY=NO
U
*NODE PRINT,SUMMARY=NO
CF
*NODE PRINT,SUMMARY=NO
RF
*END STEP
```

C.3 Model with user elements (gloal stiffness matrices)

```
*HEADING
*NODE
1,0.,2.
2,1.5,2.
3,0.,0.
*NSET,NSET=SUPP
1,3
**ELEMENT,TYPE=C1D2,ELSET=TRUSS
**1,1,2
**2,1,3
**3,2,3
*SOLID SECTION,MATERIAL=STEEL
1.
*MATERIAL,NAME=STEEL
*ELASTIC
1.8E3
*USER ELEMENT,NODES=2,TYPE=U1,LINEAR
1,2
*ELEMENT,TYPE=U1,ELSET=E1
1,1,2
*MATRIX,TYPE=STIFFNESS
1200.
0.,0.
-1200.,0.,1200.
0.,0.,0.,0.
*UEL PROPERTY,ELSET=E1
*USER ELEMENT,NODES=2,TYPE=U2,LINEAR
1,2
*ELEMENT,TYPE=U2,ELSET=E2
2,1,3
*MATRIX,TYPE=STIFFNESS
0.
0.,900.
```

```
0.,0.,0.
0.,-900.,0.,900.
*UEL PROPERTY,ELSET=E2
*USER ELEMENT,NODES=2,TYPE=U3,LINEAR
1,2
*ELEMENT,TYPE=U3,ELSET=E3
3,2,3
*MATRIX,TYPE=STIFFNESS
259.2
345.6,460.8
-259.2,-345.6,259.2
-345.6,-460.8,345.6,460.8
*UEL PROPERTY,ELSET=E3
*ELSET,ELSET=TRUSS
1,2,3
*BOUNDARY
1,1,2
3,1
*STEP,LINEAR
*STATIC
*CLOAD
2,2,-8.0
*EL PRINT,ELSET=TRUSS,SUMMARY=NO
S,E
*NODE PRINT,SUMMARY=NO
U
*NODE PRINT,SUMMARY=NO
CF
*NODE PRINT,SUMMARY=NO
RF
*END STEP
```

Appendix D

```
*HEADING
SPRING(TRUSS) ELEMENT : SEGMENTED LOAD-DEFLECTION CURVE
** CONCENTRATED LOAD AT ONE END.(UNITS : LB, IN)
** SANDEEP KAVI .....953 0409
*NODE,NSET=NALL
1,0.
2,10.
*USER ELEMENT,NODES=2,TYPE=U1,COORDINATES=1
1
*ELEMENT,TYPE=U1,ELSET=C1
1,1,2
*UEL PROPERTY,ELSET=C1
*USER SUBROUTINES
CC************************************************************
CC       USER SUBROUTINE TO DEFINE CONNECTOR ELEMENT U1
CC       SANDEEP KAVI                JANUARY 1993
CC************************************************************
      SUBROUTINE UEL(RHS,AMATRX,SVARS,ENERGY,JLINES,XVAL,
     1 NDOFEL,NRHS,NSVARS,PROPS,NPROPS,COORDS,MCRD,NNODE,
     2 U,DU,V,A,JTYPE,TIME,DTIME,KSTEP,KINC,JELEM,PARAMS,
     3 NDLOAD,JDLTYP,ADLMAG,PREDEF,NPRED,LFLAGS)
C
      IMPLICIT REAL*8(A-H,O-Z)
C
      DIMENSION RHS(NDOFEL,NRHS),AMATRX(NDOFEL,NDOFEL),
     1 SVARS(1),ENERGY(6),JLINES(1),XVAL(1),PROPS(1),
     2 COORDS(MCRD,NNODE),U(NDOFEL),DU(NDOFEL),V(NDOFEL),
     3 A(NDOFEL),TIME(7),DTIME(7),PARAMS(1),JDLTYP(NDLOAD,NRHS),
     4 ADLMAG(NDLOAD,NRHS,2),PREDEF(2,NPRED,NNODE),LFALGS(4)
C
      DO 10 I=1,NDOFEL
       DO 20 J=1,NDOFEL
        AMATRX(I,J)=0.0
20     CONTINUE
10    CONTINUE
C
      IF(U(2).LT.2.0)THEN
          AMATRX(1,1)= 10000.0
          AMATRX(1,2)= -10000.0
          AMATRX(2,2)= 10000.0
      ELSEIF(U(2).GE.2.0.AND.U(2).LT.4.0)THEN
          AMATRX(1,1)= 5000.0
          AMATRX(1,2)= -5000.0
          AMATRX(2,2)= 5000.0
      ELSE
```

```
        AMATRX(1,1)= 2500.0
        AMATRX(1,2)= -2500.0
        AMATRX(2,2)= 2500.0
      ENDIF
C     ** LOWER TRIANGULAR MATRIX **
       DO 30 I=1,NDOFEL
        DO 40 J=1,NDOFEL
         IF(I.GT.J) AMATRX(I,J)=AMATRX(J,I)
40       CONTINUE
30      CONTINUE
      DO 50 I=1,NDOFEL
       DO 60 J=1,NRHS
        RHS(I,J)=0.0
60     CONTINUE
50    CONTINUE
       IF(U(2).LT.2.0)THEN
         RHS(2,1) = -10000.*U(2)
       ELSEIF(U(2).GE.2.0.AND.U(2).LT.4.0)THEN
         RHS(2,1) = -5000.*(U(2)+2.0)
       ELSE
         RHS(2,1) = -2500.*(U(2)+8.0)
       ENDIF
      RETURN
      END
**********************************************************************
*BOUNDARY
1,1
***----------------------N/R STEP
*STEP,NLGEOM,INC=100
*STATIC,PTOL=100.,DIRECT
0.02,1.,,,,2,1,8.
*CLOAD
2,1,100000.
*PRINT,RESIDUAL=NO
*NODE FILE
CF,U
*EL PRINT,SUMMARY=NO
S,E
*NODE PRINT,SUMMARY=NO
U
*NODE PRINT,SUMMARY=NO
CF,RF
*END STEP
```

Appendix E

E.1 Input File for 3D Test Model with 15 SPRING2 Connectors

```
*HEADING
BEAM WITH NONLINEAR SPRING ELEMENT (SPRING2) >>>> 3D CASE
3 SPRINGS, S=1000..500LB/IN
*NODE
1,0.,0.,0.
17,132.,0.,0.
18,8.25,0.,5.
32,123.75,0.,5.
33,8.25,10.,5.
47,123.75,10.,5.
*NGEN,NSET=NBOT
1,17
*NGEN,NSET=NTOP
18,32
*NGEN,NSET=NFIX
33,47
*NSET,NSET=NBC
1
17
*ELEMENT,TYPE=B33
1,1,2
*ELGEN,ELSET=BEAM
1,16,1,1
*BEAM SECTION,SECTION=CIRC,ELSET=BEAM,MATERIAL=WOOD
5.0
*TRANSVERSE SHEAR STIFFNESS
1000000.,1000000.
*MATERIAL,NAME=WOOD
*ELASTIC
2.1E08,0.1
*ELEMENT,TYPE=SPRING2,ELSET=SPRING
17,18,33
*ELGEN,ELSET=SPRING
17,31,1,1
*SPRING,ELSET=SPRING,NONLINEAR
2,2
-2000.,-3.
-1000.,-1.
0.,0.
1000.,1.
2000.,3.
*MPC
```

```
7,2,18
7,3,19
7,4,20
7,5,21
7,6,22
7,7,23
7,8,24
7,9,25
7,10,26
7,11,27
7,12,28
7,13,29
7,14,30
7,15,31
7,16,32
*BOUNDARY
NBC,1,3
NBC,5,6
NFIX,2
*STEP,NLGEOM,INC=100
*STATIC,PTOL=1.,MTOL=10.
0.1,1.,,,,
*CLOAD
NBC,4,1.E05
*PRINT,RESIDUAL=NO
*NODE FILE
CF,RF,U
*EL PRINT,SUMMARY=NO
S,E
*NODE PRINT,NSET=NTOP,SUMMARY=NO
U
*NODE PRINT,NSET=NBC,SUMMARY=NO
CF
*NODE PRINT,NSET=NBC,SUMMARY=NO
RF
*END STEP
```

E.2 Input File for 3D b/c Element Test Model with 15 Connectors

```
*HEADING
BEAM WITH NONLINEAR BEAM/CONN. ELEMENT  >>>> 3D CASE
*NODE,NSET=NBC
1,0.,0.,0.
2,132.,0.,0.
*ELEMENT,ELSET=BEAM,TYPE=B33
1,1,2
*BEAM SECTION,SECTION=CIRC,ELSET=BEAM,MATERIAL=STEEL
5.0
```

```
*TRANSVERSE SHEAR STIFFNESS
1000000.,1000000.
*MATERIAL,NAME=STEEL
*ELASTIC
2.1E08,0.1
*USER ELEMENT,NODES=2,TYPE=U1,COORDINATES=3,PROPERTIES=8
1,2,3,4,5,6
*ELEMENT,TYPE=U1,ELSET=C1
2,1,2
*UEL PROPERTY,ELSET=C1
16,132.,1000.,500.,1.0,3.0,500.,5.0
*BOUNDARY
NBC,1,3
NBC,5,6
*STEP,NLGEOM,INC=100
*STATIC,PTOL=1.,MTOL=10.
0.02,1.,,,,
*CLOAD
NBC,4,5.E04
*PRINT,RESIDUAL=NO
*NODE FILE
CF,RF,U
*EL PRINT,ELSET=BEAM,SUMMARY=NO
S,E
*NODE PRINT,SUMMARY=NO
U
*NODE PRINT,SUMMARY=NO
CF
*NODE PRINT,SUMMARY=NO
RF
*END STEP
*USER SUBROUTINES
CC*****************************************************************
CC  USER SUBROUTINE TO DEFINE *3D* NONLINEAR BEAM/CONNECTOR ELEMENT
CC          SANDEEP KAVI  .....  APRIL 1993
CC*****************************************************************
      SUBROUTINE UEL(RHS,AMATRX,SVARS,ENERGY,JLINES,XVAL,
     1 NDOFEL,NRHS,NSVARS,PROPS,NPROPS,COORDS,MCRD,NNODE,
     2 U,DU,V,A,JTYPE,TIME,DTIME,KSTEP,KINC,JELEM,PARAMS,
     3 NDLOAD,JDLTYP,ADLMAG,PREDEF,NPRED,LFLAGS)
C
      IMPLICIT REAL*8(A-H,O-Z)
C
      DIMENSION RHS(NDOFEL,NRHS),AMATRX(NDOFEL,NDOFEL),
     1 SVARS(1),ENERGY(6),JLINES(1),XVAL(1),PROPS(NPROPS),
     2 COORDS(MCRD,NNODE),U(NDOFEL),DU(NDOFEL),V(NDOFEL),
     3 A(NDOFEL),TIME(7),DTIME(7),PARAMS(1),JDLTYP(NDLOAD,NRHS),
     4 ADLMAG(NDLOAD,NRHS,2),PREDEF(2,NPRED,NNODE),LFALGS(4)
      DIMENSION DM(6),S(6),DISP(15),DM1(12),AMATRX1(12,12)
C
CC ** INITIALIZATION OF ARRAYS/MATRICES **
```

```
C
      DO 10 I=1,NDOFEL
       DO 20 J=1,NDOFEL
        AMATRX(I,J)=0.0
        AMATRX1(I,J)=0.0
        DM1(I)=0.0
20     CONTINUE
10    CONTINUE
C
      DO 30 I=1,NDOFEL
       DO 40 J=1,NRHS
        RHS(I,J)=0.0
40     CONTINUE
30    CONTINUE
C
      DO 50 I=1,6
         DM(I)=0.0
          S(I)=0.0
50    CONTINUE
C
CC FIND EACH NAIL DISPLACEMENT ACCORDING TO ITS LOCATION ON THE BEAM &
CC DEFINE THE CONNECTOR STIFFNESS MATRIX ACCORDINGLY.
C
CC PUT THE NODE DISPLACEMENTS OF THE BEAM THAT ACTIVATE THE
CC NAIL DISPLACEMENT INTO DM & DM1.
C
        H=PROPS(8)
C
       DM(1)=H*U(4)
       DM(2)=H*U(10)
       DM(3)=U(2)
       DM(4)=U(6)
       DM(5)=U(8)
       DM(6)=U(12)
C
       DM1(2)= U(2)
       DM1(4)= U(4)
       DM1(6)=U(6)
       DM1(8)=U(8)
       DM1(10)= U(10)
       DM1(12)=U(12)
C
        NS = IDINT(PROPS(1))
        SPACE = PROPS(2)/PROPS(1)
      DO 60 L=1,(NS-1)
C
CC INTERPOLATION FUNCTIONS
C
       XI=SPACE*L/PROPS(2)
       S(1)=-(1-XI)
       S(2)=-XI
```

```
      S(3)=1.-3.*XI**2.+2.*XI**3.
      S(4)=(XI-2.*XI**2.+XI**3.)*PROPS(2)
      S(5)=3.*XI**2.-2.*XI**3.
      S(6)=(XI**3.-XI**2.)*PROPS(2)
C
    DISP(L) = 0.0
    D = 0.0
C
CC COMPUTE THE NAIL DISPLACEMENT BY INTERPOLATION FUNCTIONS
CC MULTIPLY S WITH DM
C
      DO 70 J=1,6
       D=D+S(J)*DM(J)
70     CONTINUE
C
    DISP(L) = ABS(D)
C
      G1=S(3)*S(3)
      G2=H*S(3)*S(1)
      G3=H*H*S(1)*S(1)
      G4=S(3)*S(4)
      G5=H*S(1)*S(4)
      G6=S(4)*S(4)
      G7=S(3)*S(5)
      G8=H*S(1)*S(5)
      G9=S(4)*S(5)
      G10=S(5)*S(5)
      G11=H*S(3)*S(2)
      G12=H*H*S(1)*S(2)
      G13=H*S(4)*S(2)
      G14=H*S(5)*S(2)
      G15=H*H*S(2)*S(2)
      G16=S(3)*S(6)
      G17=H*S(1)*S(6)
      G18=S(4)*S(6)
      G19=S(5)*S(6)
      G20=H*S(2)*S(6)
      G21=S(6)*S(6)
C
    IF(DISP(L).LT.PROPS(5))THEN
C
      C1 = PROPS(3)
C
CC THE GLOBAL STIFFNESS MATRIX OF THE CONNECTORS
CC ASSIGN VALUES TO UPPER TRIANGLE MATRIX ENTRIES
C
      AMATRX1(2,2)=C1*G1
      AMATRX1(2,4)=C1*G2
      AMATRX1(4,4)=C1*G3
      AMATRX1(2,6)=C1*G4
      AMATRX1(4,6)=C1*G5
```

```
      AMATRX1(6,6)=C1*G6
      AMATRX1(2,8)=C1*G7
      AMATRX1(4,8)=C1*G8
      AMATRX1(6,8)=C1*G9
      AMATRX1(8,8)=C1*G10
      AMATRX1(2,10)=C1*G11
      AMATRX1(4,10)=C1*G12
      AMATRX1(6,10)=C1*G13
      AMATRX1(8,10)=C1*G14
      AMATRX1(10,10)=C1*G15
      AMATRX1(2,12)=C1*G16
      AMATRX1(4,12)=C1*G17
      AMATRX1(6,12)=C1*G18
      AMATRX1(8,12)=C1*G19
      AMATRX1(10,12)=C1*G20
      AMATRX1(12,12)=C1*G21
C
      AMATRX(2,2)=AMATRX(2,2)+C1*G1
      AMATRX(2,4)=AMATRX(2,4)+C1*G2
      AMATRX(4,4)=AMATRX(4,4)+C1*G3
      AMATRX(2,6)=AMATRX(2,6)+C1*G4
      AMATRX(4,6)=AMATRX(4,6)+C1*G5
      AMATRX(6,6)=AMATRX(6,6)+C1*G6
      AMATRX(2,8)=AMATRX(2,8)+C1*G7
      AMATRX(4,8)=AMATRX(4,8)+C1*G8
      AMATRX(6,8)=AMATRX(6,8)+C1*G9
      AMATRX(8,8)=AMATRX(8,8)+C1*G10
      AMATRX(2,10)=AMATRX(2,10)+C1*G11
      AMATRX(4,10)=AMATRX(4,10)+C1*G12
      AMATRX(6,10)=AMATRX(6,10)+C1*G13
      AMATRX(8,10)=AMATRX(8,10)+C1*G14
      AMATRX(10,10)=AMATRX(10,10)+C1*G15
      AMATRX(2,12)=AMATRX(2,12)+C1*G16
      AMATRX(4,12)=AMATRX(4,12)+C1*G17
      AMATRX(6,12)=AMATRX(6,12)+C1*G18
      AMATRX(8,12)=AMATRX(8,12)+C1*G19
      AMATRX(10,12)=AMATRX(10,12)+C1*G20
      AMATRX(12,12)=AMATRX(12,12)+C1*G21
C
CC ASSIGN VALUES TO THE LOWER TRIANGLE ENTRIES IN MATRIX
C
     DO 80 I=1,NDOFEL
       DO 90 J=1,NDOFEL
        IF(I.GT.J) AMATRX1(I,J) = AMATRX1(J,I)
        IF(I.GT.J) AMATRX(I,J) = AMATRX(J,I)
90     CONTINUE
80     CONTINUE
C
CC *** THE RIGHT-HAND-SIDE VECTOR ***
C
     DO 100 I=1,NDOFEL
```

```
      DO 110 J=1,NDOFEL
       RHS(I,1) = RHS(I,1) - AMATRX1(I,J)*DM1(J)
110    CONTINUE
100    CONTINUE
C
C
     ELSEIF(DISP(L).GE.PROPS(5).AND.DISP(L).LT.PROPS(6))THEN
C
       C2 = PROPS(4)
C
CC THE GLOBAL STIFFNESS MATRIX OF THE CONNECTORS
CC ASSIGN VALUES TO UPPER TRIANGLE MATRIX ENTRIES
C
       AMATRX1(2,2)=C2*G1
       AMATRX1(2,4)=C2*G2
       AMATRX1(4,4)=C2*G3
       AMATRX1(2,6)=C2*G4
       AMATRX1(4,6)=C2*G5
       AMATRX1(6,6)=C2*G6
       AMATRX1(2,8)=C2*G7
       AMATRX1(4,8)=C2*G8
       AMATRX1(6,8)=C2*G9
       AMATRX1(8,8)=C2*G10
       AMATRX1(2,10)=C2*G11
       AMATRX1(4,10)=C2*G12
       AMATRX1(6,10)=C2*G13
       AMATRX1(8,10)=C2*G14
       AMATRX1(10,10)=C2*G15
       AMATRX1(2,12)=C2*G16
       AMATRX1(4,12)=C2*G17
       AMATRX1(6,12)=C2*G18
       AMATRX1(8,12)=C2*G19
       AMATRX1(10,12)=C2*G20
       AMATRX1(12,12)=C2*G21
C
       AMATRX(2,2)=AMATRX(2,2)+C2*G1
       AMATRX(2,4)=AMATRX(2,4)+C2*G2
       AMATRX(4,4)=AMATRX(4,4)+C2*G3
       AMATRX(2,6)=AMATRX(2,6)+C2*G4
       AMATRX(4,6)=AMATRX(4,6)+C2*G5
       AMATRX(6,6)=AMATRX(6,6)+C2*G6
       AMATRX(2,8)=AMATRX(2,8)+C2*G7
       AMATRX(4,8)=AMATRX(4,8)+C2*G8
       AMATRX(6,8)=AMATRX(6,8)+C2*G9
       AMATRX(8,8)=AMATRX(8,8)+C2*G10
       AMATRX(2,10)=AMATRX(2,10)+C2*G11
       AMATRX(4,10)=AMATRX(4,10)+C2*G12
       AMATRX(6,10)=AMATRX(6,10)+C2*G13
       AMATRX(8,10)=AMATRX(8,10)+C2*G14
       AMATRX(10,10)=AMATRX(10,10)+C2*G15
       AMATRX(2,12)=AMATRX(2,12)+C2*G16
```

```
      AMATRX(4,12)=AMATRX(4,12)+C2*G17
      AMATRX(6,12)=AMATRX(6,12)+C2*G18
      AMATRX(8,12)=AMATRX(8,12)+C2*G19
      AMATRX(10,12)=AMATRX(10,12)+C2*G20
      AMATRX(12,12)=AMATRX(12,12)+C2*G21
C
CC ASSIGN VALUES TO THE LOWER TRIANGLE ENTRIES IN MATRIX
C
     DO 120 I=1,NDOFEL
      DO 130 J=1,NDOFEL
      IF(I.GT.J) AMATRX1(I,J) = AMATRX1(J,I)
      IF(I.GT.J) AMATRX(I,J) = AMATRX(J,I)
130    CONTINUE
120   CONTINUE
C
CC *** THE RIGHT-HAND-SIDE VECTOR ***
C
     DO 140 I=1,NDOFEL
      DO 150 J=1,NDOFEL
       RHS(I,1) = RHS(I,1) - AMATRX1(I,J)*DM1(J)
150    CONTINUE
140   CONTINUE
C
     RHS(2,1) = RHS(2,1) + PROPS(7)*S(3)
     RHS(4,1) = RHS(4,1) + PROPS(7)*H*S(1)
     RHS(6,1) = RHS(6,1) + PROPS(7)*S(4)
     RHS(8,1) = RHS(8,1) + PROPS(7)*S(5)
     RHS(10,1) = RHS(10,1) + PROPS(7)*H*S(2)
     RHS(12,1) = RHS(12,1) + PROPS(7)*S(6)
C
    ENDIF
60   CONTINUE
    RETURN
    END
```

E.3 Program SDISP3D to Calculate Spring Deflections in Case of 3D b/c Element Test Model

```
C
C PROGRAM TO COMPUTE NAIL DEFLECTIONS : 3D MODEL.
C  WRITTEN BY : SANDEEP KAVI
C
C    THE PROGRAM REQUIRES SD3D1 & 2 DAT,SDISP3D EXEC FILES
C    THE OUTPUT IS WRITTEN TO SD3D OUT FILE
C
    IMPLICIT REAL*8(A-H,O-Z)
    DIMENSION U1(2),U2(2),U3(2),RM1(2),RM2(2),RM3(2),
   1 DM(6),S(6),DISP(16)
```

```
C
      OPEN(UNIT=10,STATUS='OLD')
      OPEN(UNIT=20,STATUS='OLD')
      OPEN(UNIT=30,STATUS='UNKNOWN')
CC ######### READ FROM SD3D1 DAT
      READ (10,*) P1,P2,H
CC ######### READ FROM SD3D2 DAT
      DO 10 I=1,2
       READ (20,*) N,D1,D2,D3,D4,D5,D6
        U1(I)=D1
        U2(I)=D2
        U3(I)=D3
        RM1(I)=D4
        RM2(I)=D5
        RM3(I)=D6
10    CONTINUE
C
      DO 20 I=1,6
        DM(I)=0.0
        S(I)=0.0
20    CONTINUE
C
       DM(1)=U2(1)
       DM(2)=RM1(1)
       DM(3)=RM3(1)
       DM(4)=U2(2)
       DM(5)=RM1(2)
       DM(6)=RM3(2)
C
      SPACE=P2/P1
      DO 30 L=1,(P1-1)
       XI=SPACE*L/P2
        S(1)=1.-3.*XI**2.+2.*XI**3.
        S(2)=-(1.-XI)*H
        S(3)=(XI-2.*XI**2.+XI**3.)*P2
        S(4)=3.*XI**2.-2.*XI**3.
        S(5)=-XI*H
        S(6)=(XI**3.-XI**2.)*P2
       DISP(L)=0.0
       D=0.0
      DO 40 J=1,6
        D=D+S(J)*DM(J)
40    CONTINUE
       DISP(L)=D
      WRITE(30,50) L,SPACE*L,DISP(L)
30    CONTINUE
50    FORMAT('**DISPL. OF NAIL #',I2,' LOCATED AT',
     1F6.2,'IN. FROM LEFT END ==>',F8.4,' IN.')
      END
```

Appendix F

User Subroutine UEL for the b/c Elements in Dome Cap & Dome Models

```
************************************************************
** USER SUBROUTINE TO DEFINE 3D NONLINEAR B/C ELEMENT
** WRITTEN BY : SANDEEP A. KAVI                MAY 1993
************************************************************
      SUBROUTINE UEL(RHS,AMATRX,SVARS,ENERGY,JLINES,XVAL,
     1 NDOFEL,NRHS,NSVARS,PROPS,NPROPS,COORDS,MCRD,NNODE,
     2 U,DU,V,A,JTYPE,TIME,DTIME,KSTEP,KINC,JELEM,PARAMS,
     3 NDLOAD,JDLTYP,ADLMAG,PREDEF,NPRED,LFLAGS)
C
      IMPLICIT REAL*8(A-H,O-Z)
C
      DIMENSION RHS(NDOFEL,NRHS),AMATRX(NDOFEL,NDOFEL),
     1 SVARS(1),ENERGY(6),JLINES(1),XVAL(1),PROPS(NPROPS),
     2 COORDS(MCRD,NNODE),U(NDOFEL),DU(NDOFEL),V(NDOFEL),
     3 A(NDOFEL),TIME(7),DTIME(7),PARAMS(1),JDLTYP(NDLOAD,NRHS),
     4 ADLMAG(NDLOAD,NRHS,2),PREDEF(2,NPRED,NNODE),LFALGS(4)
      DIMENSION A(12,12),TA(12,12),DM(12),R1(6,6),GDM1(6),GDM2(6),
     1 DM1(6),DM2(6),DM3(6),S(6),DISP(16),RH(12,2)
C
CC INITIALIZATION OF MATRICES
CC*** ROTATION MATRIX IS DENOTED BY 'A' AND TRANSPOSE OF
CC*** ROTATION MATRIX IS DENOTED BY 'TA'.
C
      DO 5 I=1,NDOFEL
       DO 10 J=1,NDOFEL
        AMATRX(I,J)=0.0
10     CONTINUE
5     CONTINUE
      DO 15 I=1,NDOFEL
       DO 20 J=1,NRHS
        RHS(I,J)=0.0
20     CONTINUE
15    CONTINUE
      DO 25 I=1,12
       DO 30 J=1,12
         A(I,J)=0.0
         TA(I,J)=0.0
         DM(I)=0.0
30     CONTINUE
25    CONTINUE
      DO 35 I=1,6
```

```
      DO 40 J=1,6
        A1(I,J)=0.0
        GDM1(I)=0.0
        GDM2(I)=0.0
        DM1(I)=0.0
        DM2(I)=0.0
        DM3(I)=0.0
        S(I)=0.0
40    CONTINUE
35    CONTINUE
C
CC DEFINING THE ROTATION MATRIX
CC  NODAL COORDINATES
C
        XCOS1 = COORDS(1,1)
        YCOS1 = COORDS(2,1)
        XCOS2 = COORDS(1,2)
        YCOS2 = COORDS(2,2)
        ZCOS1 = COORDS(3,1)+1387.66
        ZCOS2 = COORDS(3,2)+1387.66
C
        T1 = XCOS2 - XCOS1
        T2 = YCOS2 - YCOS1
        T3 = ZCOS2 - ZCOS1
        TNORM = (T1**2+T2**2+T3**2)**0.5
        A11 = YCOS1*ZCOS2 - ZCOS1*YCOS2
        A12 = -(XCOS1*ZCOS2 - ZCOS1*XCOS2)
        A13 = XCOS1*YCOS2 - YCOS1*XCOS2
        A1NORM = (A11**2+A12**2+A13**2)**0.5
        A21 = T2*R13-T3*R12
        A22 = T3*R11-T1*R13
        A23 = T1*R12-T2*R11
        A2NORM = (A21**2+A22**2+A23**2)**0.5
C
CC ROTATION MATRIX FOR STIFFNESS CALCULATION (R).
C
      DO 45 I=1,10,3
        A(I,I) = T1/TNORM
        A(I,I+1)=T2/TNORM
        A(I,I+2)=T3/TNORM
        A(I+1,I)=A11/A1NORM
        A(I+1,I+1)=A12/A1NORM
        A(I+1,I+2)=A13/A1NORM
        A(I+2,I)=A21/A2NORM
        A(I+2,I+1)=A22/A2NORM
        A(I+2,I+2)=A23/A2NORM
C ALTERNATIVELY >>
C       A(I+2,I)=A(1,2)*A(2,3)-A(2,2)*A(1,3)
C       A(I+2,I+1)=A(2,1)*A(1,3)-A(1,1)*A(2,3)
C       A(I+2,I+2)=A(1,1)*A(2,2)-A(1,2)*A(2,1)
45    CONTINUE
```

```
C
CC TRANSPOSE OF ROTATION MATRIX
C
    DO 50 I=1,12
     DO 55 J=1,12
      TA(I,J) = A(J,I)
55    CONTINUE
50   CONTINUE
C
CC ROTATION MATRIX FOR DISPLACEMENT CALCULATION (R1).
C
    DO 60 I=1,4,3
      A1(I,I) = T1/TNORM
      A1(I,I+1)=T2/TNORM
      A1(I,I+2)=T3/TNORM
      A1(I+1,I)=A11/A1NORM
      A1(I+1,I+1)=A12/A1NORM
      A1(I+1,I+2)=A13/A1NORM
      A1(I+2,I)=A21/A2NORM
      A1(I+2,I+1)=A22/A2NORM
      A1(I+2,I+2)=A23/A2NORM
60   CONTINUE
C
CC PUT GLOBAL NODAL DISPLACEMENT OF NODE #1 INTO GDM1
C
    DO 65 I = 1,6
     GDM1(I)=U(I)
65   CONTINUE
C
CC PUT GLOBAL NODAL DISPLACEMENT OF NODE #2 INTO GDM2
C
    DO 70 I = 7,12
     GDM2(I-6)=U(I)
70   CONTINUE
C
CC TRANSFORM NODAL DISPLACEMENTS FROM GLOBAL TO LOCAL FOR
CC NODE #1 AND #2, AND PUT THE LOCAL DISPLACEMENT INTO DM1 AND DM2
C
    DO 75 I=1,6
      DO 80 J=1,6
        DM1(I)=DM1(I)+A1(I,J)*GDM1(J)
        DM2(I)=DM2(I)+A1(I,J)*GDM2(J)
80     CONTINUE
75   CONTINUE
C
CC PUT THE NODE DISPLACEMENTS OF THE BEAM THAT ACTIVATE THE
CC NAIL DISPLACEMENT INTO DM3, ACCORDING TO ORIENTATION OF THE
CC LOCAL AXES OF THE BEAMS (REFER TO MCODE OF BEAMS)
C
      DM3(1)=DM1(2)
      DM3(2)=DM1(4)
```

```
      DM3(3)=DM1(6)
      DM3(4)=DM2(2)
      DM3(5)=DM2(4)
      DM3(6)=DM2(6)
C
CC LOCAL DISPLACEMENTS OF THE TWO NODES CONNECTING THE ELEMENT
C
       DM(2) = DM1(2)
       DM(4) = DM1(4)
       DM(6) = DM1(6)
       DM(8) = DM2(2)
       DM(10) = DM2(4)
       DM(12) = DM2(6)
C
CC **FIND EACH NAIL DISPLACEMENT ACCORDING TO ITS LOCATION ON **
CC **THE BEAM AND DEFINE THE CONNECTOR ELEMENT ACCORDINGLY   **
C
    NS = IDINT(PROPS(1))
    SPACE = TNORM/PROPS(1)
C
    DO 85 L=1,NS
     DO 90 I=1,NDOFEL
      DO 95 J=1,NRHS
       RH(I,J) = 0.0
95     CONTINUE
90    CONTINUE
C
CC INTERPOLATION FUNCTIONS
C
      XI=SPACE*L/TNORM
      H = PROPS(2)
C
      S(1)=1.-3.*XI**2.+2.*XI**3.
      S(2)=-(1.-XI)*H
      S(3)=(XI-2.*XI**2.+XI**3.)*TNORM
      S(4)=3.*XI**2.-2.*XI**3.
      S(5)=-XI*H
      S(6)=(XI**3.-XI**2.)*TNORM
C
    DISP(L) = 0.0
    D = 0.0
    C = 0.0
C
CC COMPUTE THE NAIL DISPLACEMENT BY INTERPOLATION FUNCTIONS
CC MULTIPLY S WITH DM3
C
      DO 100 J=1,6
       D=D+S(J)*DM3(J)
100     CONTINUE
    DISP(L) = ABS(D)
C
```

```
CC *** TO DEFINE THE CONNECTOR F.E. MODEL ***
C
CC THE GLOBAL STIFFNESS MATRIX OF THE CONNECTORS
C
C  THE CONNECTOR STIFFNESS MATRIX IS IN THE LOCAL FRAME OF REFERENCE.
C  WE NEED TO FIND THE GLOBAL STIFFNESS MATRIX. THE ROTATION MATRIX
C  FOR THE BEAMS AND ITS TRANSPOSE IS USED FOR THIS PURPOSE.
C  THE TRANSFORMATION FROM THE LOCAL TO THE GLOBAL IS OBTAINED BY
C  PRE-MULTIPLYING THE LOCAL STIFFNESS MATRIX (SM) BY THE TRANSPOSE
C  OF ROTATION MATRIX (TR) AND THEN POST-MULTIPLYING THE PRODUCT BY
C  THE ROTATION MATRIX (R).
C
CC ASSIGN VALUES TO UPPER TRIANGLE MATRIX ENTRIES
C
      G1=S(1)*S(1)
      G2=S(1)*S(2)
      G3=S(2)*S(2)
      G4=S(1)*S(3)
      G5=S(2)*S(3)
      G6=S(3)*S(3)
      G7=S(1)*S(4)
      G8=S(2)*S(4)
      G9=S(3)*S(4)
      G10=S(4)*S(4)
      G11=S(1)*S(5)
      G12=S(2)*S(5)
      G13=S(3)*S(5)
      G14=S(4)*S(5)
      G15=S(5)*S(5)
      G16=S(1)*S(6)
      G17=S(2)*S(6)
      G18=S(3)*S(6)
      G19=S(4)*S(6)
      G20=S(5)*S(6)
      G21=S(6)*S(6)
C
    IF (DISP(L).LT.PROPS(5)) THEN
C
      C = PROPS(3)
C
    CALL AMATRH(A,TA,AMATRX,DM,RH,G1,G2,G3,G4,G5,G6,G7,G8,G9,G10,
   1 G11,G12,G13,G14,G15,G16,G17,G18,G19,G20,G21,C,NDOFEL,JTYPE)
C
    ELSEIF (DISP(L).GE.PROPS(5).AND.DISP(L).LT.PROPS(6)) THEN
C
      C = PROPS(4)
C
    CALL AMATRH (A,TA,AMATRX,DM,RH,G1,G2,G3,G4,G5,G6,G7,G8,G9,G10,
   1 G11,G12,G13,G14,G15,G16,G17,G18,G19,G20,G21,C,NDOFEL,JTYPE)
C
      IF(D.GT.0.0)THEN
```

```
        RH(2,1) = RH(2,1) - PROPS(7)*S(1)
        RH(4,1) = RH(4,1) - PROPS(7)*S(2)
        RH(6,1) = RH(6,1) - PROPS(7)*S(3)
        RH(8,1) = RH(8,1) - PROPS(7)*S(4)
        RH(10,1) = RH(10,1) - PROPS(7)*S(5)
        RH(12,1) = RH(12,1) - PROPS(7)*S(6)
      ELSE
        RH(2,1) = RH(2,1) + PROPS(7)*S(1)
        RH(4,1) = RH(4,1) + PROPS(7)*S(2)
        RH(6,1) = RH(6,1) + PROPS(7)*S(3)
        RH(8,1) = RH(8,1) + PROPS(7)*S(4)
        RH(10,1) = RH(10,1) + PROPS(7)*S(5)
        RH(12,1) = RH(12,1) + PROPS(7)*S(6)
      ENDIF
C
    ENDIF
C
CC **THE RIGHT-HAND-SIDE VECTOR
C
CC CONTRIBUTION OF ELEMENT IN GLOBAL FRAME OF REFERENCE (RHS)
CC PRE-MULTIPLY (RH) BY THE TRANSPOSE OF ROTATION MATRIX (TA).
C
     DO 105 I=1,12
       DO 110 J=1,12
         RHS(I,1) = RHS(I,1) + TA(I,J)*RH(J,1)
110    CONTINUE
105   CONTINUE
85   CONTINUE
    RETURN
    END
*************************************************************************
    SUBROUTINE AMATRH (A,TA,AMATRX,DM,RH,G1,G2,G3,G4,G5,G6,G7,G8,G9,
   1 G10,G11,G12,G13,G14,G15,G16,G17,G18,G19,G20,G21,C,NDOFEL,JTYPE)
C
    IMPLICIT REAL*8(A-H,O-Z)
C
    DIMENSION R(12,12),TR(12,12),AMATRX(NDOFEL,NDOFEL),DM(12),
   1 RH(12,2)
    DIMENSION DSM1(12,12),DSM(12,12)
C
    DO 5 I=1,12
     DO 10 J=1,12
       DSM(I,J) = 0.0
       DSM1(I,J) = 0.0
10    CONTINUE
5    CONTINUE
C
CC STIFFNESS MATRIX (LOCAL) OF L(TH) NAIL.
C
      DSM(2,2)=C*G1
      DSM(2,4)=C*G2
```

```
      DSM(4,4)=C*G3
      DSM(2,6)=C*G4
      DSM(4,6)=C*G5
      DSM(6,6)=C*G6
      DSM(2,8)=C*G7
      DSM(4,8)=C*G8
      DSM(6,8)=C*G9
      DSM(8,8)=C*G10
      DSM(2,10)=C*G11
      DSM(4,10)=C*G12
      DSM(6,10)=C*G13
      DSM(8,10)=C*G14
      DSM(10,10)=C*G15
      DSM(2,12)=C*G16
      DSM(4,12)=C*G17
      DSM(6,12)=C*G18
      DSM(8,12)=C*G19
      DSM(10,12)=C*G20
      DSM(12,12)=C*G21
C
C
CC ASSIGN VALUES TO THE LOWER TRIANGLE ENTRIES IN MATRIX
C
      DO 15 I=1,12
       DO 20 J=1,12
        IF(I.GT.J) DSM(I,J) = DSM(J,I)
20      CONTINUE
15     CONTINUE
C
CC PRE-MULTIPLYING STIFFNESS MATRIX FOR THE USER ELEMENT BY THE
CC TRANSPOSE OF THE ROTATION MATRIX.(TA X SM = SM1)
C
    DO 25 I=1,12
     DO 30 J=1,12
     DO 35 K=1,12
       DSM1(I,J) = DSM1(I,J) + TA(I,K)*DSM(K,J)
35     CONTINUE
30    CONTINUE
25   CONTINUE
C
CC **THE TANGENT (JACOBIAN) STIFFNESS MATRIX**
CC POST-MULTIPLYING THE ABOVE OBTAINED MATRIX BY
CC THE ROTATION MATRIX.(SM1 X A = AMATRX).
C
    DO 40 I=1,12
     DO 45 J=1,12
      DO 50 K=1,12
       AMATRX(I,J) = AMATRX(I,J) + DSM1(I,K)*A(K,J)
50     CONTINUE
45    CONTINUE
40   CONTINUE
```

```
C
CC CONTRIBUTION OF ELEMENT IN BEAM LOCAL FRAME OF REFERENCE (RH).
C
      DO 55 I=1,NDOFEL
       DO 60 J=1,NDOFEL
        RH(I,1) =  RH(I,1) - DSM(I,J)*DM(J)
60      CONTINUE
55     CONTINUE
    RETURN
    END
```

Appendix G

G.1 Program to write Input Deck for B/C User Elements

```
CC  PROGRAM TO WRITE THE ELEMENT DEFINITION CARDS FOR THE USER ELEMENT
CC  IN ABAQUS INPUT FILE HAVING USER SUBROUTINE UEL.
CC          ***** MAIN BEAMS I *****
CC  WRITTEN BY : SANDEEP A. KAVI
CC  GLULAM DOME RESEARCH.   APRIL 1993.
C
    OPEN(UNIT=10,STATUS='OLD')
    OPEN(UNIT=20,STATUS='OLD')
    OPEN(UNIT=30,STATUS='UNKNOWN')
C
CC OUTPUT WRITTEN IN SBEM1 OUT FILE
CC THE BEAM TYPE
C
    WRITE(30,105)
C
CC READ FROM SUEL1 DAT
C
    READ (10,*) NS,H,S1,S2,D1,D2,Y1,NMAX,NELEM,NUM
C
C    NMAX = MAXIMUM NUMBER OF ELEMENTS IN THE MODEL.
C    NNODE = TOTAL NUMBER OF NODES
C    NELEM = TOTAL NUMBER OF ELEMENTS
C    NUM = 1000 .....FOR MAIN BEAMS
C        = 1000 .....FOR EDGE BEAMS (HORIZONTAL NAILS)
C        = 2000 .....FOR EDGE BEAMS (INCLINED NAILS)
C
CC READ FROM SBEM1 DAT
CC MAIN BEAMS-I 6.75X11
C
    DO 100 N=1,NELEM
      READ (20,*) NE, N1, N2
C
C    NE = THE ELEMENT NUMBER.
C    N1,N2 = NODES OF THE ELEMENT
C
CC WRITE ABAQUS COMMAND LINES TO SBEM1 OUT
C
    WRITE(30,110) NE+NUM
    WRITE(30,115)
    WRITE(30,120) NE+NUM,NE+NUM
    WRITE(30,125)NE+NMAX,N1,N2
    WRITE(30,130) NE+NUM
    WRITE(30,135) NS,H,S1,S2,D1,D2,Y1
100  CONTINUE
105  FORMAT ('**',35('-'),'MAIN BEAMS-I : B/C ELEMENTS')
```

```
110   FORMAT ('*USER ELEMENT,NODES=2,TYPE=U',I5,',COORDINATES=3,',
     1'PROPERTIES=7')
115   FORMAT ('1,2,3,4,5,6')
120   FORMAT ('*ELEMENT,TYPE=U',I5,',ELSET=C',I5)
125   FORMAT (I4,',',I4,',',I4)
130   FORMAT ('*UEL PROPERTY,ELSET=C',I5)
135   FORMAT (I2,',',F5.3,',',2(F8.2,','),F6.4,',',F6.4,',',F6.2)
      END
```

G.2 Program to Find the Nail Deflections in the Dome Cap Model with B/C Elements

```
C PROGRAM TO COMPUTE NAIL DEFLECTIONS : DOME CAP
CC  WRITTEN BY : SANDEEP KAVI
CC  GLULAM DOME RESEARCH.    AUGUST 1993.
C
C THE PROGRAM REQUIRES CAP1, 2 & SNODE DAT,SCAP3D EXEC FILES
C THE OUTPUT IS WRITTEN TO SECTOR OUT FILE
C
      IMPLICIT REAL*8(A-H,O-Z)
      DIMENSION U1(19),U2(19),U3(19),RM1(19),RM2(19),RM3(19),
     1 DM(6),S(6),DISP(16),X(19),Y(19),Z(19),J(24),N1(24),N2(24)
C
      OPEN(UNIT=10,STATUS='OLD')
      OPEN(UNIT=20,STATUS='OLD')
      OPEN(UNIT=30,STATUS='OLD')
      OPEN(UNIT=40,STATUS='UNKNOWN')
C
CC ######### READ FROM SCAP1 DAT
      DO 5 I=1,24,1
       READ (10,*) J(I),N1(I),N2(I),NS,H
5     CONTINUE
CC
CC    J(L)= ELEMENT NUMBER
CC    N1(L) = NODE #1
CC    N2(L) = NODE #2
CC    NS = NUMBER OF SPRINGS
CC    H = RIGID LINK LENGTH
CC
C
CC ######### READ FROM SCAP2 DAT
      DO 20 I=1,19,1
       READ (30,*) N,D1,D2,D3,D4,D5,D6
        U1(I)=D1
        U2(I)=D2
        U3(I)=D3
        RM1(I)=D4
        RM2(I)=D5
        RM3(I)=D6
20    CONTINUE
C
CC ######### READ FROM SNODE DAT
      DO 10 I=1,19,1
```

```
      READ (20,*) N,X(I),Y(I),Z(I)
10    CONTINUE
C
      DO 15 L=1,24,1
        M=J(L)
        M1=N1(L)
        M2=N2(L)
C
        T1 = X(M2) - X(M1)
        T2 = Y(M2) - Y(M1)
        T3 = Z(M2) - Z(M1)
        TNORM = (T1**2+T2**2+T3**2)**0.5
C
CC      TNORM = LENGTH OF BEAM
C
      DO 30 I=1,6
         DM(I)=0.0
         S(I)=0.0
30    CONTINUE
C
        DM(1)=U2(M1)
        DM(2)=RM1(M1)
        DM(3)=RM3(M1)
        DM(4)=U2(M2)
        DM(5)=RM1(M2)
        DM(6)=RM3(M2)
C
      WRITE(40,60) M
C
      SPACE = TNORM/NS
      DO 40 K=1,NS
       XI=SPACE*K/TNORM
        S(1)=1.-3.*XI**2.+2.*XI**3.
        S(2)=-(1.-XI)*H
        S(3)=(XI-2.*XI**2.+XI**3.)*TNORM
        S(4)=3.*XI**2.-2.*XI**3.
        S(5)=-XI*H
        S(6)=(XI**3.-XI**2.)*TNORM
       DISP(K)=0.0
       D=0.0
      DO 50 I=1,6
        D=D+S(I)*DM(I)
50    CONTINUE
        DISP(K)=D
      WRITE(40,70) K,SPACE*K,DISP(K)
40    CONTINUE
15    CONTINUE
60    FORMAT('**BEAM NUMBER #',I3,' >>>>>>>>>>')
70    FORMAT('**DISPL. OF NAIL #',I2,'  LOCATED AT',
     1F6.2,'IN. FROM LEFT END ==>',F8.4,' IN.')
      END
```

Appendix H

Summary of the Dome Results:

Table H.1

Critical Pressure on the Dome

		Full Snow	Half Snow
Material Law	**Decking Model**	$p_{cr} = p_D + \lambda_{cr} p_L$	
	None	3.58	5.26
Linear	*Truss Bracing*	9.26	7.20
	Beam/connector	8.52	7.55
Bilinear	*None*	4.38	6.53
	Truss Bracing	10.31	8.59
	Beam/connector	9.03	8.90
Nonlinear	*None*	4.38	5.89
	Truss Bracing	10.19	7.74
	Beam/connector	9.02	8.29

Table H.2

Stresses in the Beam Elements and Nail Deflections at Critical Pressures: Full Snow

Material Law	Decking Model	Maximum σ_t (psi)	Maximum σ_c (psi)	Maximum Δ (in.)
		σ_{pt} = 2578 psi, σ_{pc} = 4873 psi		
	None	2426 (el. 31)	-3803 (el. 37)	-
Linear	*Truss Bracing*	3872 (el. 31)	-1.1E04 (el. 20)	-
	Beam/connector	2487 (el.31)	-6607 (el. 20)	1.36 (node 39)
Bilinear	*None*	-	-	-
	Truss Bracing	3588 (el. 31)	-1.1E04 (el.20)	-
	Beam/connector	2627 (el. 31)	-7292 (el. 20)	1.30 (node 39)
Nonlinear	*None*	2698 (el. 31)	-4853 (el. 37)	-
	Truss Bracing	4476 (el. 31)	-1.1E04 (el.20)	-
	Beam/connector	2631 (el. 31)	-7107 (el. 20)	1.30 (node 39)

Table H.3

Stresses in the Beam Elements and Nail Deflections at Critical Pressures: Half Snow

Material Law	Decking Model	Maximum σ_t (psi)	Maximum σ_c (psi)	Maximum Δ (in.)
		σ_{pt} = 2578 psi, σ_{pc} = 4873 psi		
	None	1.2E04 (el. 32)	1.6E04 (el. 32)	-
Linear	*Truss Bracing*	9059 (el. 11)	-1.8E04 (el. 11)	-
	Beam/connector	1.1E04 (el. 11)	-1.9E04 (el. 11)	1.50 (node 40)
Bilinear	*None*	-	-	-
	Truss Bracing	7838 (el. 39)	-1.7E04 (el. 11)	-
	Beam/connector	9161 (el. 11)	-2.0E04 (el. 11)	1.25 (node 40)
Nonlinear	*None*	1.2E04 (el.32)	-1.1E04 (el. 32)	-
	Truss Bracing	9819 (el. 11)	-1.1E04 (el. 11)	-
	Beam/connector	5962 (el. 40)	-1.1E04 (el. 11)	1.25 (node 40)

VITA

Sandeep A. Kavi was born in Bombay, India in June of 1968. He graduated in First Class with the Bachelor of Technology degree from Indian Institute of Technology, Powai, Bombay. He worked in Bombay, India for two years as structural design engineer before he started his studies towards the Master of Science degree in Civil Engineering in August 1991 at Virginia Polytechnic Institute & State University. He is planning to work as a Civil Engineer in the U. S. A. after he graduates.

